UNIVERSIDAD DE CANTABRIA
UNIVERSIDAD DEL PAÍS VASCO

PROGRAMA DE DOCTORADO EN INGENIERÍA AMBIENTAL

TESIS DOCTORAL

Aplicación de la Dinámica de Fluidos Computacional a la simulación y optimización de biorreactores multi-ambiente para tratamiento de aguas residuales

PhD THESIS

Application of Computational Fluid Dynamics to the simulation and optimization of multi-environment bioreactors for wastewater treatment

---

RICARDO BLANCO AGUILERA

Directores:
RUBÉN DÍEZ MONTERO
JUAN IGNACIO TEJERO MONZÓN

Escuela de Doctorado de la Universidad de Cantabria
Santander, junio de 2020

UNIVERSIDAD DE CANTABRIA

ESCUELA TÉCNICA SUPERIOR DE INGENIEROS DE CAMINOS, CANALES Y PUERTOS

DPTO. DE CIENCIAS Y TÉCNICAS DEL AGUA Y DEL MEDIO AMBIENTE

TESIS DOCTORAL

APLICACIÓN DE LA DINÁMICA DE FLUIDOS COMPUTACIONAL A LA SIMULACIÓN Y OPTIMIZACIÓN DE BIORREACTORES MULTI-AMBIENTE PARA TRATAMIENTO DE AGUAS RESIDUALES

APPLICATION OF COMPUTATIONAL FLUID DYNAMICS TO THE SIMULATION AND OPTIMIZATION OF MULTI-ENVIRONMENT BIOREACTORS FOR WASTEWATER TREATMENT

RICARDO BLANCO AGUILERA

SANTANDER, JUNIO DE 2020

DIRECTORES:

RUBÉN DÍEZ MONTERO

JUAN IGNACIO TEJERO MONZÓN

"Al igual que todos los jóvenes,

me proponía ser un genio, pero

afortunadamente intervino la risa."

Lawrence Durrell, *Clea (1960).*

"Aprended a distinguir los valores falsos de los verdaderos

y el mérito real de las personas bajo toda suerte de disfraces.

Un [individuo] mal vestido, pobre y desdeñado

puede ser un sabio, un héroe, un santo;

el birrete de un doctor puede cubrir el cráneo de un imbécil."

Antonio Machado, *Homenaje a Antonio Pérez de la Mata (1910).*

"La ciencia no está cimentada sobre roca: por el contrario, podríamos decir

que la atrevida estructura de sus teorías se eleva sobre un terreno pantanoso,

es como un edificio sobre pilotes. Éstos se introducen desde arriba en la ciénaga,

pero en modo alguno hasta alcanzar ningún basamento natural o 'dado'.

Cuando interrumpimos nuestros intentos de introducirlos hasta un estrato

más profundo, ello no se debe a que hayamos topado con terreno firme:

paramos simplemente porque nos basta que tengan firmeza suficiente

para soportar la estructura, al menos por el momento."

Karl Popper, *La lógica de la investigación científica (1962).*

Agradecimientos

El desarrollo de esta tesis doctoral ha llevado mi cuerpo y mi mente al más absoluto de los límites. A pesar de que uno siente haber recorrido el camino demasiado solo, es justo levantar la cabeza para recordar que el ser totalmente aislado jamás culmina satisfactoriamente ningún viaje. Y es que, tal y como escribía una vez el filósofo Javier López Alós, "*la soledad tiene también declinaciones no individuales*". Sirvan las siguientes líneas para agradecer a todas aquellas personas que han hecho posible que hoy esté poniendo punto y final a este intenso tránsito.

En primer lugar, quisiera agradecer a mis directores de tesis el haberme dado la oportunidad de realizar este trabajo de investigación. A Iñaki Tejero, por recibirme en el grupo que fundó hace ya más de tres decenios, y confiar en todo momento en mi capacidad. A Rubén Díez, por descubrirme el mundo académico cuando aún ni siquiera me había graduado como Ingeniero de Caminos, pero, sobre todo, por su supervisión, ayuda y valiosas aportaciones a lo largo de estos complicados años.

A mis directores *no oficiales* del Instituto de Hidráulica Ambiental, sin los cuales esta tesis doctoral jamás hubiera llegado a buen puerto. Al profesor Javier López Lara por su generosidad al tratarme como un doctorando suyo más, por su guía, y por todo el tiempo que ha invertido en este proyecto más allá de su responsabilidad. A Gabriel Barajas, Gabi, por estar siempre disponible, por su incalculable paciencia con un principiante y por enseñarme todo lo que sé de OpenFOAM®; pero también por todos los buenos momentos, las risas y esas conversaciones sobre filosofía política.

Al Grupo de Computación Avanzada de la Universidad de Cantabria (IFCA-CSIC), por darme acceso al Supercomputador Altamira de la Red Española de Supercomputación para poder llevar a cabo las simulaciones numéricas. En especial a los investigadores que allí me han atendido, Álvaro López y Aida Palacio, por toda la ayuda brindada, su disponibilidad incondicional y la excesiva paciencia que han mostrado con todo un dummy de la computación paralela.

Special thanks to the Professor Joel Ducoste for his hospitality and very useful lessons during my research stay in the Department of Civil, Construction and Environmental Engineering at North Carolina State University.

A la Universidad de Cantabria primero (PRE03, CVE-2016-11670), y al Ministerio de Educación, Cultura y Deporte del Gobierno de España después (FPU16-05036), por proporcionarme mediante beca la financiación necesaria para la consecución de esta tesis doctoral.

Durante estos años, también he tenido la gran oportunidad de ejercer la docencia dentro del Departamento de Ciencias y Técnicas del Agua y del Medio Ambiente de la Universidad de Cantabria. Mi agradecimiento al resto de profesores con los que he compartido asignaturas y otros menesteres por sus enseñanzas: Amaya Lobo, Ramón Collado, Carlos Rico, Lorena Esteban. De forma particular a la profesora Ana López, que, además de todo, me ha querido, cuidado y apoyado como una madre, algo que jamás olvidaré.

A mis compañeras de despacho que han ido y venido durante estos tres años, y que han hecho más liviano el devenir de los días: María, Gloria, María Fernanda, Nuria, Jose, Chus, Mercedes. En especial a Eli, que compartió conmigo todos los días y todas las horas de aquellos dos primeros años tan duros; y a Mónica, que, en este último año, ha aportado humor a esta mente excesivamente analítica.

Por último, a Fernando, por ser un gran amigo y el mejor compañero de piso que uno pudiera imaginar; y a mis padres, María y Domingo, y mi hermano, Jose Antonio, por levantarme todas y cada una de las veces que he besado el suelo.

<div align="right">

Ricardo Blanco Aguilera

Santander, junio de 2020

</div>

Summary

The main step in urban wastewater treatment usually consists in a single aerobic activated sludge stage for organic matter removal. If the removal of nutrients (nitrogen and phosphorus) is also required, a more complex treatment process is needed, including anoxic and anaerobic stages. At this respect, conventional configurations for Biological Nutrient Removal (BNR) imply a significant increase in the volume needed and energy consumption compared to processes for only organic matter removal.

In this context, multi-environment reactors are an innovative alternative to simplify conventional BNR treatment trains since they are more compact and can adapt to existing quality requirements. Concretely, the AnoxAn reactor unifies the anaerobic and anoxic zones of the conventional BNR configurations in a single upflow reactor. Although its biological efficiency has been already demonstrated on a pilot scale, other physical characteristics significantly affect the performance of AnoxAn. Specifically, the multi-environmental zoning (hydraulic separation must be maintained between anaerobic and anoxic zones) and singular elements configuration (mixing devices and baffles) give rise to a complex hydrodynamic behaviour that interferes in the desired biological operation of the reactor.

Therefore, in this thesis, a comprehensive hydrodynamic assessment of AnoxAn is carried out, and the influence of the hydraulic behaviour on the biological efficiency of the process is evaluated. For that purpose, a Computational Fluid Dynamics (CFD)-based numerical tool is developed with the open source toolbox OpenFOAM®, and a hydrodynamic optimization methodology for multi-environment reactors is proposed. The results obtained in this work have contributed to the development of technological and operational improvements of AnoxAn.

Chapter 1 introduces the topic of this thesis and places it within the context of the current scientific research.

Chapter 2 presents the state of the art and the theoretical basis regarding the hydrodynamic analysis of multi-environment reactors for wastewater treatment. In resume, the literature shows that AnoxAn has promising environmental and energetic advantages, and its viability for BNR has been already demonstrated at pilot scale. However, there is a need for a deeper hydrodynamic analysis of AnoxAn in order to develop optimized and scalable configurations. Besides, the state of the art reveals that a correct hydrodynamic behaviour enhances an efficient biological performance in wastewater treatment reactors. On the other hand, CFD modelling represents an advanced tool for the qualitative and quantitative assessment of the hydrodynamic performance of wastewater treatment processes, being the level of detail of these numerical techniques a remarkable step forward compared to experimentation and compartment-based modelling. However, there is a lack of comprehensive hydrodynamic analysis and optimization CFD studies regarding multi-environment reactors. Besides, the optimization studies found in literature do not follow any standardized methodology.

Based on the findings and conclusions of the revision of the state of art, the scope and objectives of the thesis are presented in **Chapter 3**. The main objective of the research work is to comprehensively analyse and optimize the hydrodynamic behaviour of multi-environment bioreactors through the development of an open source three-dimensional numerical model based on CFD, validated and applied to the anaerobic-anoxic AnoxAn reactor.

The next four chapters (**Chapters 4-7**) are the main contribution of the thesis. In **Chapter 4**, the numerical CFD tool developed in this work is presented. The numerical tool includes several features that are not available in the original source code of OpenFOAM® such as (i) the tracer transport for turbulent flow, (ii) nitrate transport and denitrification biokinetics for turbulent flow and (iii) a porous media model. Although in the next chapters the CFD tool is applied to the specific case of AnoxAn, this new model can be used as a base to incorporate more physics in it, and also to be adapted to specific research interests within the water treatment field.

In **Chapter 5**, the numerical CFD tool developed in the previous chapter is applied to the hydrodynamic simulation, validation and analysis of the AnoxAn reactor. AnoxAn is an upflow reactor divided into anaerobic, anoxic and clarifications zones (from bottom to top). Mixing devices in the reactor consist on an impeller for the anoxic zone and a recirculation pump for the anaerobic. Besides, a baffle is located between the anoxic and clarification zones for the relaxation of the flow, and a deflector is placed between the anaerobic and anoxic zones to enhance the hydraulic separation between both environments. To characterise the liquid phase flow pattern and to validate the numerical results, experimental Residence Time Distribution (RTD) tracer tests performed in clean water are used.

Numerical results show the agreement between the experimental and the CFD tracer curves, validating the model for the overall mass transport behaviour of the reactor in clean water. Compared to previous research performed with experimentation and compartment-based models, CFD simulations provide a deeper understanding of the hydrodynamic performance of AnoxAn. Summarising, dead volumes are found mainly in the corner opposite the exit in the clarification zone, and near the deflector between the anaerobic and anoxic zones. Regarding short-circuiting, channelling paths are located near the walls, being the transport through them a 30% higher than in the central part of the reactor. Despite the existence of these non-ideal flow patterns, the analysis of the uniformity index (UI) shows that complete mixing is reached in the anoxic and clarification zones. Regarding the analysis of the influence of the reactor elements on the hydrodynamic of AnoxAn, the study evidences that the baffle located between the anoxic and clarification zones has no influence on the fluid-dynamics of the reactor. Conversely, the deflector has appeared to be essential to maintain the hydraulic separation between anaerobic and anoxic zones since the increase of tracer concentration in the anaerobic zone is around 84% when it is not used.

Once the hydrodynamic behaviour of the AnoxAn original prototype has been comprehensively analysed, the next step is to carry out the optimization of the reactor. However, as concluded after the revision of the state of knowledge, optimization examples found in literature do not follow any specific methodology.

In this regard, in **Chapter 6**, a standardized hydrodynamic optimization methodology for multi-environment reactors is developed combining CFD and dimensional analysis. Then, the applicability of the methodology is tested in AnoxAn.

In this methodology, a set of dimensionless hydraulic indexes (which describe features such as short-circuiting, dead volumes and mixing performance) are combined in a single expression, defined as the Global Hydraulic Efficiency (GHE) parameter. Additionally, a hydraulic separation index (HS) is proposed in order to assess the hydraulic separation between zones with different environmental conditions that is needed in multi-environment reactors. Based on dimensional analysis, all the aforementioned dimensionless indexes are expressed as a function of dimensionless geometric indexes, giving rise to mathematical formulations that relate hydraulic and geometric variables. Finally, relating the mathematical expressions for HS and GHE, and depending on the hydraulic separation degree desired in the analysed multi-environment reactor, the optimum configuration can be obtained.

Once developed, the hydrodynamic optimization methodology is applied to AnoxAn. At this aim, nine different reactor configurations are tested maintaining the original volume but varying the slenderness and the location of the impeller. Based on the CFD model validated in the previous chapter, numerical RTD tests are performed in each configuration. Simulated results show that hydraulic separation between anoxic and anaerobic zones is more efficient in high slenderness configurations and when the impeller is located in upper positions in the anoxic zone (farther from the deflector). Additionally, as observed in the previous chapter, main channelling is observed near the walls for all configurations tested. Short-circuiting phenomena is higher in low slenderness configurations and when the impeller is located closer to the deflector. Regarding dead volumes, they are also bigger in low slenderness configurations, where the effective volume is around 70% of the total volume of the reactor. Conversely, mixing efficiency is higher in low slenderness configurations. All in all, since it shows the highest GHE and the most efficient hydraulic separation, the optimum hydrodynamic AnoxAn configuration corresponds to the one with the highest slenderness and the impeller located to more distance from the anaerobic-anoxic deflector.

After the optimization study of the AnoxAn reactor, the influence of the hydrodynamic behaviour on the biological efficiency of the process is assessed in **Chapter 7**. At this aim, the denitrification model introduced in the developed CFD tool is applied to two different configurations of the reactor, i.e. one characterized by high slenderness and another with low slenderness. In both cases the impeller is located at the same distance from the deflector. Additionally, two different biomass concentrations (1 000 mg/L and 2 500 mg/L) are tested.

Results of this study confirm the correlation between the hydrodynamic performance and the biological efficiency reported in literature for other wastewater treatment processes. In the specific case of AnoxAn, the configuration with the highest GHE (high slenderness), reports smaller outlet nitrate concentration (three times smaller) than the one with lowest GHE (low slenderness). As also observed in the optimization study, high slenderness configurations are more resilient than low slenderness ones, since the more favourable hydraulic separation

between the anoxic and anaerobic zones in the high slenderness configuration gives rise to negligible nitrate concentration in the anaerobic zone.

Finally, **Chapter 8** presents the general conclusions and recommendations for future research of this doctoral thesis.

Summarizing, this research work has evidenced that higher slenderness AnoxAn configurations are preferred since they present a higher hydrodynamic, and therefore, biological efficiency. In addition, for the same theoretical treatment capacity (i. e., the same volume), high slenderness configurations present a smaller surface requirement compared to the configurations with lower slenderness. However, the configurations with higher slenderness give rise to reactors with less usual shapes and less studied in literature, since the implementation of several units of these configurations would cause larger length/width ratios. This aspect could be a disadvantage when proposing the layout of a new reactor implementation. In particular, it could be a handicap when reusing reactors in cases of retrofitting or upgrading existing treatment plants. Depending on the land availability or constructive limitations and requirements, slenderness (and consequently hydraulic separation) of the reactor could be reduced depending on the design influent nitrogen loads.

Resumen

El proceso principal en tratamiento de aguas residuales consiste, generalmente, en una etapa aerobia basada en un reactor de fangos activos para la eliminación de materia orgánica. Si además de ello se requiere la eliminación de nutrientes (nitrógeno y fósforo), es necesario un proceso más complejo que incluya también etapas anóxicas y anaerobias. Asimismo, comparadas con los procesos de solo eliminación de materia orgánica, las configuraciones convencionales de Eliminación Biológica de Nutrientes (EBN) suponen un incremento significativo de volumen necesario y consumo energético.

En este contexto, los reactores multi-ambiente representan una alternativa innovadora para simplificar los trenes de tratamiento convencionales de EBN, ya que son más compactos y pueden adaptarse a los requerimientos de calidad existentes. En concreto, el reactor AnoxAn es capaz de integrar las zonas anaerobia y anóxica del proceso convencional de EBN en un único reactor de flujo ascendente. A pesar de que su eficiencia biológica ya ha sido contrastada a escala piloto, otras características físicas afectan de manera significativa a la operación de AnoxAn. Específicamente, su zonificación multi-ambiental (debe asegurarse la separación hidráulica entre las zonas anaerobia y anóxica) y la configuración de elementos singulares (dispositivos de mezcla y bafles), dan lugar a un comportamiento hidrodinámico complejo que interfiere en el funcionamiento óptimo del reactor.

Es por ello que, en la presente tesis doctoral, se realiza un análisis exhaustivo de la hidrodinámica de AnoxAn, así como un estudio la influencia de la misma en la eficiencia biológica del proceso. Para ello, se desarrolla una herramienta numérica basada en Dinámica de Fluidos Computacional (CFD) con el software de código abierto OpenFOAM®, y se propone una metodología para la optimización hidrodinámica de reactores multi-ambiente. Los resultados obtenidos en este trabajo han contribuido al desarrollo tecnológico y operacional de AnoxAn.

El **Capítulo 1** introduce la temática de esta tesis y la enmarca dentro del contexto de la investigación científica actual.

El **Capítulo 2** presenta el estado del arte y las bases teóricas del análisis hidrodinámico de reactores multi-ambiente para tratamiento de aguas residuales. En resumen, la revisión de la bibliografía muestra que AnoxAn es un reactor con ventajas ambientales y energéticas prometedoras, y que su viabilidad para la EBN ya ha sido demostrada a escala piloto. Sin embargo, con el objetivo de desarrollar configuraciones optimizadas y escalables, se observa la necesidad de realizar un análisis hidrodinámico más completo de AnoxAn. Además, el estado del arte revela que un funcionamiento hidrodinámico adecuado en reactores de tratamiento de aguas favorece, de la misma manera, su eficiencia biológica. Por otro lado, la modelización CFD se presenta como una herramienta avanzada para la evaluación tanto cualitativa como cuantitativa de la hidrodinámica de procesos de tratamiento de aguas, suponiendo su nivel de detalle un avance significativo con respecto a la experimentación y a la modelización basada en compartimentos. Sin embargo, se observa una falta de estudios de análisis y optimización hidrodinámicos para biorreactores multi-ambiente, y, además, todos los estudios de

optimización hidrodinámica que han sido revisados no cuentan con una metodología estandarizada para ello.

En base a lo concluido en la revisión del estado del arte, en el **Capítulo 3**, se definen el alcance y los objetivos de la tesis doctoral. El objetivo principal de este trabajo de investigación es analizar y optimizar el comportamiento hidrodinámico de biorreactores multi-ambiente mediante el desarrollo de un modelo numérico tridimensional, de código abierto y basado en CFD, validado y aplicado al reactor anaerobio-anóxico AnoxAn.

Los siguientes cuatro capítulos (**Capítulos 4-7**) forman la contribución principal de la tesis doctoral. En el **Capítulo 4**, se presenta la herramienta numérica CFD desarrollada en este trabajo. La herramienta numérica desarrollada incluye varias aplicaciones de las que no dispone el código original de OpenFOAM®, tales como (i) el transporte de trazador para flujo turbulento, (ii) el transporte de nitratos y cinética de desnitrificación para flujo turbulento y (iii) un modelo de medio poroso. A pesar de que en los siguientes capítulos la herramienta CFD se aplica al caso específico de AnoxAn, este nuevo modelo puede servir como base para incorporar nuevas físicas en él, así como ser adaptado para diferentes intereses investigadores dentro del campo del tratamiento de aguas.

En el **Capítulo 5**, la herramienta numérica CFD desarrollada es aplicada a la simulación, validación y análisis hidrodinámicos de AnoxAn. AnoxAn es un reactor de flujo ascendente, y dividido (de abajo a arriba) en zonas anaerobia, anóxica y de clarificación. Los dispositivos de mezcla en el reactor consisten en un agitador para la zona anóxica y una bomba de recirculación para la anaerobia. Además, entre las zonas anóxica y de clarificación hay un bafle para la tranquilización del flujo, y entre las zonas anaerobia y anóxica, un deflector para favorecer la separación hidráulica entre ambos ambientes. Con el objetivo de caracterizar el comportamiento del flujo en el reactor, así como para validar los resultados numéricos, se emplean ensayos de trazadores (RTD) realizados en agua limpia.

Los resultados numéricos muestran la capacidad del modelo CFD para reproducir las curvas RTD experimentales, validando así el modelo con respecto al transporte global de masa del reactor en agua limpia. Si se comparan con investigaciones previas sobre AnoxAn realizadas tanto con experimentación como con modelos de compartimentos, las simulaciones CFD dan lugar a un conocimiento más detallado del comportamiento hidrodinámico del reactor. A este respecto, las zonas muertas se localizan principalmente en la esquina opuesta a la salida del flujo en la zona de clarificación, y también en torno al deflector que separa las zonas anaerobia y anóxica. En cuanto a los flujos preferenciales, éstos se forman cerca de las paredes del reactor, siendo el transporte de masa a través de ellas un 30% mayor que en la parte central del mismo. A pesar de existir todas estas variaciones respecto al flujo ideal, el análisis del índice de uniformidad (UI) muestra que se consigue la mezcla completa tanto en la zona anóxica como en la de clarificación. Con respecto al análisis de la influencia de los elementos singulares del reactor en la hidrodinámica, este estudio evidencia que el bafle situado entre las zonas anaerobia y de clarificación no tiene repercusión alguna en la hidráulica de AnoxAn. Por el contrario, el deflector resulta ser esencial para mantener la separación hidráulica entre las zonas anaerobia

y anóxica, siendo el incremento de concentración de trazador en la zona anaerobia en torno a un 84% mayor cuando no se dispone de él.

Una vez realizado un análisis exhaustivo del comportamiento hidrodinámico del prototipo original de AnoxAn, el siguiente paso es proceder a su optimización. Sin embargo, tal y como se concluyó en la revisión del estado del arte, los ejemplos de optimización estudiados no se basan en ninguna metodología específica.

Por ello, en el **Capítulo 6**, se desarrolla una metodología estandarizada para la optimización hidrodinámica de reactores multi-ambiente combinando CFD y análisis dimensional, y, a continuación, se comprueba su aplicabilidad para el caso específico de AnoxAn.

En esta nueva metodología de optimización, se combinan una serie de índices hidráulicos (los cuales describen diferentes fenómenos como flujos preferenciales, zonas muertas o capacidad de mezcla) en una única expresión, definida como el parámetro de Eficiencia Hidráulica Global (GHE). Además, se propone el índice de separación hidráulica (HS) para evaluar la separación hidráulica necesaria entre las diferentes zonas ambientales existentes en los reactores multi-ambiente. Empleando el análisis dimensional, todos estos índices hidráulicos pueden expresarse como función de índices geométricos adimensionales, dando lugar a expresiones matemáticas que relacionan las variables geométricas de los reactores con variables hidráulicas. Por último, relacionando las expresiones para HS y GHE, y en función del grado de separación hidráulica deseado en el reactor multi-ambiente analizado, la configuración óptima puede ser calculada.

Una vez desarrollada, la metodología de optimización hidrodinámica se aplica a AnoxAn. A este respecto, se ensayan numéricamente nueve configuraciones diferentes del reactor, manteniendo el volumen original del mismo, pero variando su esbeltez y la posición del agitador. Empleando el modelo CFD validado en el anterior capítulo, se realizan ensayos numéricos RTD en cada una de las configuraciones propuestas. Los resultados de las simulaciones muestran que la separación hidráulica entre las zonas anaerobia y anóxica es más eficiente en las configuraciones más esbeltas y en aquellas donde el agitador está situado más cerca de la zona de clarificación (a más distancia del deflector). Además, tal y como se observó en el anterior capítulo, para todas las configuraciones, los principales flujos preferenciales se forman en torno a las paredes de AnoxAn. Este fenómeno es más significativo en las configuraciones con menor esbeltez y en aquellas donde el agitador está situado más cerca del deflector. En cuanto a los volúmenes muertos o zonas estancas, éstas también resultan ser mayores en las configuraciones menos esbeltas, donde el volumen efectivo de los reactores llega a ser el 70% del volumen total de AnoxAn. Por el contrario, la capacidad de mezcla es mayor en las configuraciones con menor esbeltez. Por último, dado que muestra el valor más alto para el índice GHE y la separación hidráulica más eficiente, la configuración hidrodinámicamente óptima en AnoxAn corresponde a aquella con mayor esbeltez y en la que el agitador está situado a más distancia del deflector anaerobio-anóxico.

Después del estudio de optimización de AnoxAn, en el **Capítulo 7**, se procede a evaluar la influencia de la hidrodinámica en el comportamiento biológico del proceso. A este respecto, se aplica el modelo de desnitrificación introducido en la herramienta numérica CFD a dos configuraciones de AnoxAn con comportamiento hidráulico opuesto, una de ellas con esbeltez alta y otra con esbeltez baja. En ambos casos, el agitador está situado a la misma distancia del deflector. Además, las simulaciones de realizan para dos concentraciones de biomasa diferentes (1 000 mg/L y 2 500 mg/L).

Los resultados del estudio confirman la correlación entre la hidrodinámica y la eficiencia biológica, la cual también se observó en la revisión bibliográfica para otros procesos de tratamiento de aguas residuales. En el caso concreto de AnoxAn, la configuración con mayor índice GHE (la de mayor esbeltez), muestra una concentración menor de nitrato en el efluente (tres veces menor) que aquella con menor índice GHE (y menor esbeltez). Tal y como también se concluyó en el estudio de optimización, las configuraciones más esbeltas son más resilientes que aquellas menos esbeltas, ya que, en las primeras, se observa una mayor separación hidráulica entre las zonas anaerobia y anóxica, dando lugar a una menor concentración de nitratos en el ambiente anaerobio.

Por último, el **Capítulo 8** presenta las conclusiones generales de la presente tesis doctoral, así como recomendaciones para la investigación futura.

A modo de resumen, este trabajo de investigación ha evidenciado que las configuraciones de AnoxAn con mayor esbeltez son preferibles a aquellas menos esbeltas, ya que muestran mayor eficiencia hidrodinámica, y, por tanto, biológica. Además, para una misma capacidad teórica de tratamiento (mismo volumen), las configuraciones con mayor esbeltez presentan una necesidad menor de superficie en planta. Sin embargo, estas configuraciones dan lugar a reactores con una geometría inusual y menos estudiada en la bibliografía, ya que la implementación de varias unidades implicaría mayores ratios largo/ancho. Este aspecto podría suponer una desventaja a la hora de diseñar o proyectar la implementación de nuevos reactores, constituyendo un hándicap cuando se deseen reutilizar reactores existentes en aquellos casos en los que se necesite la ampliación de plantas de tratamiento. Dependiendo de la disponibilidad de terreno, y/o de las limitaciones y requerimientos constructivos, la esbeltez (y por lo tanto la separación hidráulica) del reactor puede ser reducida en función de la carga de nitrógeno afluente de diseño.

Laburpena

Hondakin-uren arazketa prozesua, orokorrean, materia organikoa kentzeko lohi aktibatuko erreaktoretan oinarritzen den fase aerobio batean datza. Horretaz gain, mantenugaiak (nitrogenoa eta fosforoa) kentzea beharrezkoa bada, fase aerobioaz aparte, etapa anoxiko eta anaerobioekin osatutako prozesu konplexuago bat diseinatzen da. Izan ere, soilik materia organikoa kentzen duten prozesuekin alderatuta, mantenugaiak biologikoki kentzeko (BNR) ohiko konfigurazioek bolumen eta kontsumo energetiko handiagoa behar dute.

Egoera honetan, multi-ingurugiro erreaktoreek alternatiba berritzailea suposatzen dute ohiko BNR tratamendu sistemak sinplifikatzeko. Izan ere, erreaktore hauek oso trinkoak dira eta kalitate-araudiari egokitzeko gaitasuna dute. Adibidez, AnoxAn erreaktoreak, ohiko BNR sistema baten fase anaerobio eta anoxikoak erreaktore bakar batean elkartzen ditu. Bere eraginkortasun biologikoa laborategi-eskalan frogatu den arren, beste ezaugarri fisiko batzuk AnoxAn-en funtzionamenduan eragin handia dutela ikusi da. Zehazki, multi-ingurugiroaren zonifikazioak (bereizketa hidraulikoa mantendu behar da eremu anaerobio eta anoxikoaren artean) eta elementu berezien konfigurazioak (nahasketarako gailuak eta bafleak) errektorearen funtzionamendu optimoa zailtzen duen hidrodinamika konplexua sortzen dute.

Horregatik, doktoretza tesi honetan, AnoxAn-en hidrodinamikaren analisi sakona egin, eta erreaktorearen hidraulikak prozesuaren eraginkortasun biologikoan duen influentzia aztertu da. Horretarako, Fluidoen Dinamika Konputazionalean (CFD) oinarritutako tresna numeriko bat garatu da kodigo-irekiko OpenFOAM® softwarearekin. Bestalde, multi-ingurugiro erreaktoreen optimizazio hidrodinamikorako metodologia berri bat proposatu da. Lan honen emaitzek AnoxAn-en garapen teknologikoa ahalbidetu dute.

1. Kapituluak tesiaren gaia aurkeztu eta gaur egungo testuinguru zientifikoan kokatzen du.

2. Kapituluak multi-ingurugiro erreaktoreen analisi eta optimizazio hidrodinamikorako bibliografia eta oinarri teorikoak aurkezten ditu hondakin-uren arazketaren testuinguruan. Laburbilduz, bibliografiaren berrikusteak AnoxAn abantaila ekologiko eta energetiko nabarmenak dituen erreaktorea dela eta BNR-rako duen bideragarritasuna laborategi-eskalan frogatu dela erakusten du. Hala ere, eskala industrialean aplikatu eta optimizatutako konfigurazioak garatzeko helburuarekin, AnoxAn-en analisi hidrodinamiko sakonago bat egiteko beharra dagoela ondorioztatu da. Izan ere, bibliografian aztertutako zenbait adibideetan, hondakin-uren arazketa prozesuen funtzionamendu hidrodinamiko egoki batek prozesu horien efizientzia biologikoa bermatzen duela erreparatu da. Beste alde batetik, CFD-ereduak uren tratamendu prozesuen hidrodinamika modu kuantitatibo zein kualitatiboan aztertzeko tresna aurreratu bat bezala aurkezten dira. Izan ere, CFD-arekin lortu daitekeen zehaztasun maila, esperimentazio edota kaxa-ereduena baino askoz handiagoa da. Hala ere, bibliografiari erreparatuz, multi-ingurugiro erreaktoreen analisi eta optimizazio hidrodinamikoa lantzen dituzten ikerketa lanen gabezia dagoela ondorioztatu da. Gainera, optimizazio hidrodinamikorako lan guzti hauek ez dira metodologia estandarizatu edo zehatz batean oinarritzen.

Hala, **3. Kapituluan**, doktoretza tesiaren helburuak ezartzen dira. Ikerketa honen helburu nagusia multi-ingurugiro bio-erreaktoreen hidrodinamika aztertu eta optimizatzea da hiru-dimentsioetako, kodigo-irekiko eta CFD-an oinarritutako eredu numeriko batekin, AnoxAn erreaktore anaerobio-anoxikoan baliozkotu eta aplikatuta.

Hurrengo lau kapituluek (**4-7 Kapituluak**) doktoretza tesiaren ekarpen nagusia osatzen dute. **4. Kapituluan**, lan honetan garatutako CFD-tresna numerikoa aurkezten da. Tresna numeriko honek OpenFOAM®-en jatorrizko kodigoan ez dauden zenbait aplikazio ditu, hala nola (i) trazatzailearen garraiorako ekuazioak jario turbulentuan, (ii) nitratoen garraiorako ekuazioak eta desnitrifikazio zinetikak jario turbulentuan eta (iii) eremu porotsu baten eredu matematikoa. Nahiz eta lan honetan garatutako CFD-tresna AnoxAn-en kasu espezifikora aplikatu, eredu numeriko berri hau berorretan fisika berriak gehitzeko eta beste kasu edota adibide batzuetara moldatzeko erabili daiteke.

5. Kapituluan, garatutako CFD-tresna numerikoa AnoxAn-en simulazio, baliozkotze eta analisi hidrodinamikorako erabiltzen da. AnoxAn, (behetik gorako norabidean) inguru anaerobio, anoxiko eta klarifikaziorako eremuetan banatutako goranzko jarioa duen erreaktorea da. Nahasketarako, helize formako irabiagailu bat (eremu anoxikoan) eta ber-zirkulazio ponpa bat (eremu anaerobioan) erabiltzen dira. Horretaz aparte, inguru anoxiko eta klarifikazio eremuaren artean jarioaren abiadura murrizten duen bafle bat kokatuta dago, eta inguru anaerobio eta anoxikoaren artean, bereizketa hidraulikoa bermatzeko deflektore bat. Erreaktorearen jarioa definitzeko eta emaitza numerikoak baliozkotzeko, ur garbian egindako trazatzaileen esperimentuak (RTD) erabiltzen dira.

Emaitza numerikoek CFD-ereduak laborategiko RTD kurbak errepikatzeko duen gaitasuna erakusten dute, erreaktorearen masa-garraio globala ur garbian baliozkotuz. Orain arte egindako kaxa-eredu eta laborategi-esperimentuekin alderatuta, CFD-simulazio hauek erreaktorearen hidrodinamikaren inguruko ezagutza sakonagoa ahalbidetzen dute. Hala, bolumen-iragazgaitzak jarioaren irteeraren kontrako izkinan (klarifikazio eremuan) eta deflektore anaerobio-anoxikoaren inguruan kokatzen dira. Lehentasunezko-kanalak, aldiz, erreaktorearen paretetan sortzen dira. Izan ere, masa-garraioa %30 baino handiagoa da AnoxAn-en periferia edo kanpoaldean bere erdigunean baino. Uniformetasun indizearekin (UI) egindako azterketaren arabera, jario-ideala saihesten dituzten fenomeno hidrodinamikoak dauden arren, nahaste-osoa lortzen da inguru anoxiko zein klarifikazio eremuan. AnoxAn-en elementu berezien analisiari dagokionez, CFD-emaitzek inguru anoxiko eta klarifikazio eremuaren artean kokatuta dagoen bafleak influentzia hidrodinamikorik ez duela adierazten dute. Beste alde batetik, deflektorea eremu anoxiko eta anaerobioen arteko bereizketa hidraulikoa bermatzeko ezinbestekoa dela ondorioztatzen da. Izan ere, elementu hau erabiltzen ez bada, trazatzailearen kontzentrazioa %84 inguru igotzen da eremu anaerobioan.

AnoxAn-en analisi hidrodinamiko sakonaren ostean, jatorrizko prototipoa optimizatzea da hurrengo pausua. Hala ere, lehen azpimarratu den bezala, optimizazio hidrodinamikorako metodologia estandarizatua jarraitzen dituzten ikerketarik ez da aurkitu bibliografian.

Horregatik, **6. Kapituluan**, multi-ingurugiro erreaktoreen optimizazio hidrodinamikorako metodologia estandarizatu bat garatzen da, ostera, metodologia honen bideragarritasuna AnoxAn-en kasu konkretuan frogatzeko.

Optimizazio metodologia berri honetan, zenbait indize hidrauliko (lehentasunezko-kanalak, bolumen-iragazgaitzak edo nahasketa gaitasuna deskribatzen dituztenak) parametro bakar batean konbinatzen dira, Efizientzia Hidrauliko Globala (GHE) lez izendatua. Horretaz gain, bereizketa hidraulikorako indizea (HS) proposatzen da multi-ingurugiro erreaktoreetan eremu desberdinen arteko beharrezkoa den bereizketa hidraulikoa aztertzeko. Analisi dimentsionalaren bitartez, indize hidrauliko guzti horiek indize geometriko adimentsionalen funtzio gisa definitu daitezke. Azkenik, HS eta GHE definitzen dituzten formula matematikoak erlazionatuz, aztertutako errektorearen konfigurazio optimoa kalkula daiteke beharrezko bereizketa hidraulikoaren arabera.

Behin garatuta, optimizazio hidrodinamikorako metodologia AnoxAn-en aplikatzen da. Horretarako, erreaktorearen bederatzi konfigurazio desberdin frogatu egiten dira aurreko kapituluan baliozkotutako CFD-ereduarekin. Erreaktorearen konfigurazio berriek jatorrizko prototipoaren bolumen berdina mantendu, baina lerdentasuna eta irabiagailuaren altuera aldatzen dituzte. Simulazioen emaitzen arabera, bereizketa hidraulikoa handiagoa da lerdentasun handiagoa duten prototipoetan eta irabiagailua deflektoretik urrunago kokatuta duten konfigurazioetan. Gainera, aurreko kapituluan ondorioztatu zen bezala, lehentasunezko-kanalak erreaktorearen paretetan ere sortzen direla erreparatzen da. Fenomeno hau lerdentasun txikiagoa eta irabiagailua deflektoretik gertuago dituzten konfigurazioetan areagotzen da. Bolumen-iragazgaitzei dagokienez, azken hauek handiagoak dira lerdentasun txikiagoa eta irabiagailua deflektoretik gertuago dituzten konfigurazioetan. Kasu hauetan, bolumen-efektiboa egiazko-bolumenaren %70a izatera heldu daiteke. Aitzitik, nahasketa gaitasuna handiagoa da lerdentasun txikiagoa duten prototipoetan. Azkenik, hidrodinamikari dagokionez, lerdentasun handiena eta irabiagailua deflektoretik urrutiago duen konfigurazioa da optimoa, GHE indizean baliorik altuena eta bereizketa hidraulikorik eraginkorrena erakusten baititu.

7. Kapituluan, hidrodinamikak AnoxAn-en efizientzia biologikoan duen eragina aztertzen da. Horretarako, CFD-tresna numerikoko desnitrifikazio eredua aurkako jokaera hidrodinamikoa duten bi konfiguraziootara aplikatzen da, hots, lerdentasun handia eta txikia duten bi prototipoetan. Irabiagailua deflektoretik distantzia berdinera kokatuta dago kasu bietan, eta simulazioak bi biomasa kontzentrazio desberdinetarako egiten dira (1 000 mg/L eta 2 500 mg/L).

Simulazioen emaitzek bibliografian erreparatutako hidrodinamika eta efizientzia biologikoaren arteko erlazioa berretsi egiten dute. AnoxAn-en kasu zehatzean, GHE indize altuagoa duen erreaktoreak (lerdentasun handiagokoa), efluentean nitrato kontzentrazio baxuagoa erakusten du (hiru aldiz txikiagoa). Aurreko kapituluan ikusi bezala, lerdentasun handiagoko konfigurazioak bereizketa hidrauliko handiagoa du, nitrato kontzentrazio txikiagoa neurtzen baita ingurune anaerobioan.

Bukatzeko, **8. Kapituluak** doktoretza tesi honen ondorio nagusiak aurkezten ditu etorkizuneko ikerketarako gomendioekin batera.

Laburbilduz, ikerketa lan honek, lerdentasun handiagoa duten AnoxAn-en konfigurazioek eraginkortasun hidrodinamiko eta biologiko handiagoa dutela erakusten du. Gainera, arazketa ahalmen berdinerako, hots, bolumen berdinerako, lerdentasun handiagoa duten konfigurazioek azalera txikiagoa behar dute. Haatik, konfigurazio hauek ezohiko geometria duten erreaktoreak eratzen dituzte. Izan ere, prototipo horien zenbait unitateen inplementazioak, luzera/zabalera ratio handiagoak behar izatea suposatzen du. Azkeneko hau, desabantaila nabaria bihurtu daiteke erreaktore berriak diseinatu eta proiektatzerako orduan, batez ere handitzeko beharra duten hondakin-uren araztegietan erreaktoreak berrerabili nahi badira. Lursailaren edo eraikuntzarako mugen arabera, erreaktorearen lerdentasuna (eta ondorioz bereizketa hidraulikoa) murriztu daiteke diseinuko nitrogeno kargaren arabera.

Scientific and academic activity and contribution

International journal publications

Blanco-Aguilera, R., Lara, J.L., Barajas, G., Tejero. I., Díez-Montero, R. (2020). CFD simulation of a novel anaerobic-anoxic reactor for biological nutrient removal: Model construction, validation and hydrodynamic analysis based on OpenFOAM®. Chem. Eng. Sci., 215. https://doi.org/10.1016/j.ces.2019.115390

Blanco-Aguilera, R., Lara, J.L., Barajas, G., Tejero. I., Díez-Montero, R. (2020). Hydrodynamic optimization of multi-environment reactors for biological nutrient removal: A methodology combining computational fluid dynamics and dimensionless indexes. Chem. Eng. Sci., 224. https://doi.org/10.1016/j.ces.2020.115766

Contributions to international congresses

Blanco-Aguilera, R., Lara, J.L., Barajas, G., Tejero. I., Díez-Montero, R. (2019). Development of a CFD based model and hydrodynamic analysis of an innovative anaerobic-anoxic reactor for nutrient removal. 14th OpenFOAM® Workshop. Duisburg (Germany), July 2019.

Blanco-Aguilera, R., Lara, J.L., Barajas, G., Tejero. I., Díez-Montero, R. (2019). Application of Computational Fluid Dynamics to the hydrodynamic evaluation of a novel multi-environment reactor for nutrient removal. 10th IWA Symposium on Modelling and Integrated Assessment, Watermatex. Copenhagen (Denmark), September 2019.

International research stays

09/2018 - 10/2018. North Carolina State University, Department of Civil, Construction and Environmental Engineering (Raleigh, NC, USA). Host researcher: Dr. Prof. Joel Ducoste.

Funding and research grants

02/2017 - 09/2017. Full scholarship from the Pre-doctoral Researcher Training Program of the University of Cantabria (PRE03, CVE-2016-11670, Programa de Personal Investigador en Formación Predoctoral de la Universidad de Cantabria). Competitive call.

10/2017 - End. Full scholarship from the University Professor Training Program of the Spanish Ministry of Education, Culture and Sport (FPU16-05036, Programa de Formación del Profesorado Universitario del Ministerio de Educación, Cultura y Deporte). Competitive call.

Teaching assistance and training

A total of 156.5 hours (15.65 ECTS) as Teaching Assistant in the Department of Water and Environmental Sciences and Technologies of the University of Cantabria divided in four academic years as follows:

- 2016 - 2017. 19 hours (1.9 ECTS) of teaching assistance in the BSc in Civil Engineering (School of Civil Engineering, University of Cantabria). Taught subjects: Sanitary Engineering, Water Supply and Wastewater Systems.

- 2017 - 2018. 57.5 hours (5.75 ECTS) of teaching assistance in the BSc in Civil Engineering, BSc in Mining Resources Engineering and MSc in Environmental Engineering (School of Civil Engineering and Polytechnical School of Mining and Energy Engineering, University of Cantabria). Taught subjects: Sanitary Engineering, Environmental Technology in Mining, Treatment Systems Modelling.

- 2018 - 2019. 47.5 hours (4.75 ECTS) of teaching assistance in the BSc in Civil Engineering and MSc in Environmental Engineering (School of Civil Engineering, University of Cantabria). Taught subjects: Sanitary Engineering, Water Supply and Wastewater Systems, Treatment Systems Modelling.

- 2019 - 2020. 32.5 hours (3.25 ECTS) of teaching assistance in the BSc in Civil Engineering (School of Civil Engineering, University of Cantabria). Taught subjects: Sanitary Engineering, Water Supply and Wastewater Systems.

Contents

Chapter 6. Hydrodynamic optimization of multi-environment reactors for biological nutrient removal: A methodology combining computational fluid dynamics and dimensionless indexes 105

List of Figures

List of Tables

Chapter 1

Introduction: Background and motivation

1.1. <u>General context and starting point</u>

Mankind is immersed in a global crisis. The maintenance of the current social model is based on the need of permanent economic growth and, in the same way, the latter can only be fed by means of an unlimited consumption of materials and energy. However, the physical environment and the material resources impose natural borders that cannot be exceeded.

Nevertheless, industrial societies have been built ignoring all these physical limits, continuously expanding and colonizing every corner of the planet Earth, and nowadays, many of them are beginning to be overtaken. Main consequences are resumed below:

- **Depletion of fossil resources.** All the available information indicates that non-renewable energy sources, which currently provides almost 90% of the global energy demand, are reaching their peak point (BP, 2019). The peak point of a non-renewable material is defined as the moment when the extraction capacity of the substance starts to decrease. According to the World Energy Outlook report of the International Energy Agency (IEA), the peak of conventional oil was reached in 2006 (IEA, 2010). The expected peak points for different non-renewable energy resources are shown in Fig. 1.1:
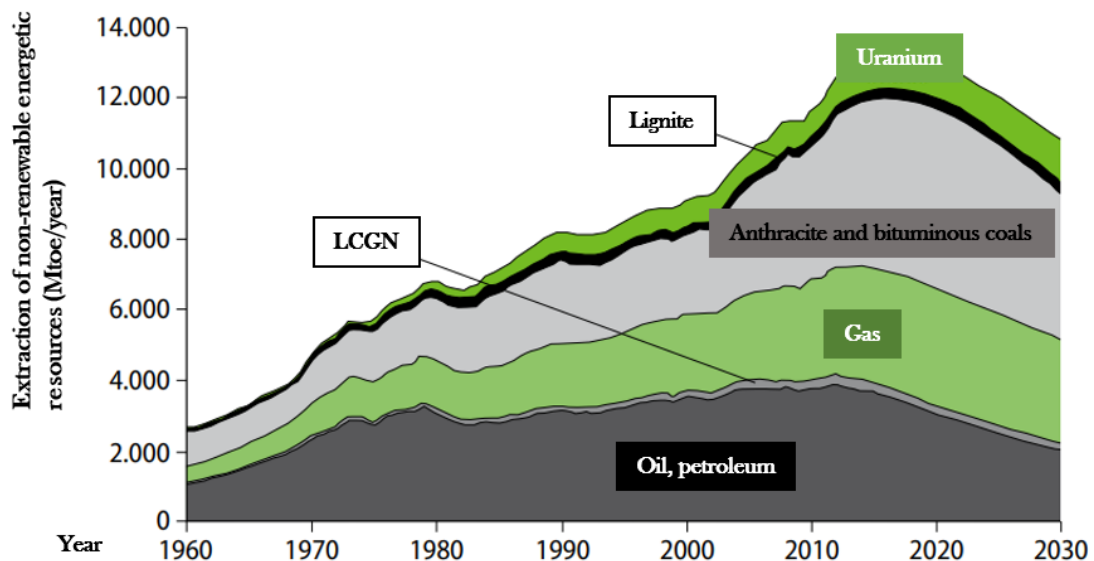
Figure 1.1. Expected extraction of non-renewable energetic resources (adapted from Zittel et al., 2013)

Additionally, the renewable energies (including biomass) are not enough to fulfil the energy consumption levels of the present. In fact, with the available technology, predictions state that only half of the total current energy demand could be provided by renewable sources (Ecologistas en Acción, 2019).

- **Climate change.** The latest report of the Intergovernmental Panel on Climate Change (IPCC), the expert committee of United Nations (UN), urged for drastic changes in the social, economic and productive model in order to mitigate the worst consequences

of the climate change (IPCC, 2019). Some of these consequences are the increase of the frequency and the intensity of extreme events (droughts, fires, hurricanes and floods), the acidification of water bodies, the decrease of glaciers or the elevation of the sea level, among many others. All these events have dramatic consequences on the agriculture, cattle raising or fishing.

- **Loss of biodiversity.** The Intergovernmental Science-Policy Platform on Biodiversity and Ecosystem Services (IPBES), warned in its latest report that the current level of destruction of biodiversity and ecosystems is threatening the future of the humanity as much as the climate change (IPBES, 2019). In fact, according to the IPBES report, 1 000 000 species are threatened with extinction due to the pressure made by extensive agriculture, fishing or climate change, and transformative changes are needed to restore and protect the nature.

- **Depletion of materials, soil and water.** In the same way as non-renewable energy sources, many non-energetic materials and minerals are about to reach their peak point. This is caused by the excessive and growing demand and consumption, which are much higher than their availability (Valero et al., 2014). For example, lithium, which is a strategic mineral for the production of car-batteries, is expected to reach its peak extraction point somewhen between 2015 (Zittel et al., 2013) and 2040 (Valeroet al., 2014). Additionally, 70% of the soil free of ice is overexploited for the extraction of resources, agriculture or silviculture (IPCC, 2019). According to the Food and Agriculture Organization of United Nations (FAO), approximately 25% of all land is highly degraded, while about 44% is moderately degraded (FAO, 2011). Fig 1.2 shows the status in global land degradation.
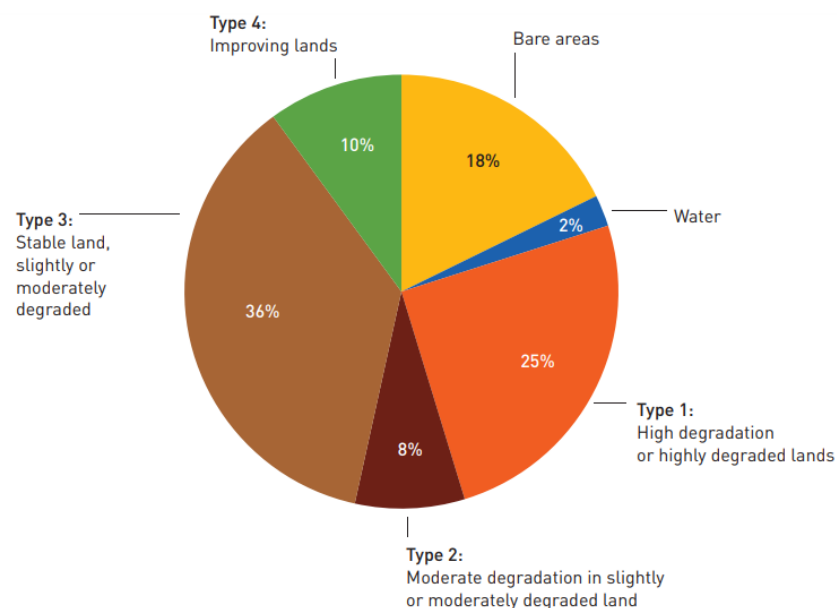
Figure 1.2. Status in global land degradation (FAO, 2011)

Regarding the water, according to FAO (2018), in the 20th century, the overexploitation of this resource without restriction has grown two times faster than the world's population. Nowadays, the demographic pressure, economic development, urbanization, pollution and the deficient management are giving rise to an excessive pressure to the water bodies.

As a resume, the global crisis can be conceived as a polyhedron with lots of edges. Besides, the relation between these edges is permeable and extremely interdependent. In consequence, every new solution or technology developed from now must be sustainable, respectful with the environment, energetically efficient and low resources demanding. Wastewater treatment sector cannot be an exception.

1.2. <u>Wastewater Treatment</u>

1.2.1. Current situation

Most human activities that use water produce wastewater in the process. The use of water is continuously growing and consequently, so does the amount of wastewater production and its associated pollution.

While 70% of municipal and industrial wastewater generated in high-income countries is treated, in middle-income and lower middle-income countries, the treatment ratio is reduced to 38% and 28%, respectively. In low-income countries, only 8% of the wastewater generated is treated before discharge or reuse (UNESCO, 2017). In fact, 2 400 million of people do not have access to an adequate and safe sanitation system, and 892 million are forced to relieve themselves open air (FAO, 2018). Additionally, 60% of people worldwide and only 38% in least developed countries have a basic handwashing facility, leaving approximately 3 billion people without basic handwashing facilities at home (UN, 2019). Overall, it is estimated that 80% of the produced wastewater is discharged to the environment without any treatment (UNESCO, 2017). The distribution of global water consumption and wastewater production is shown in Fig. 1.3.
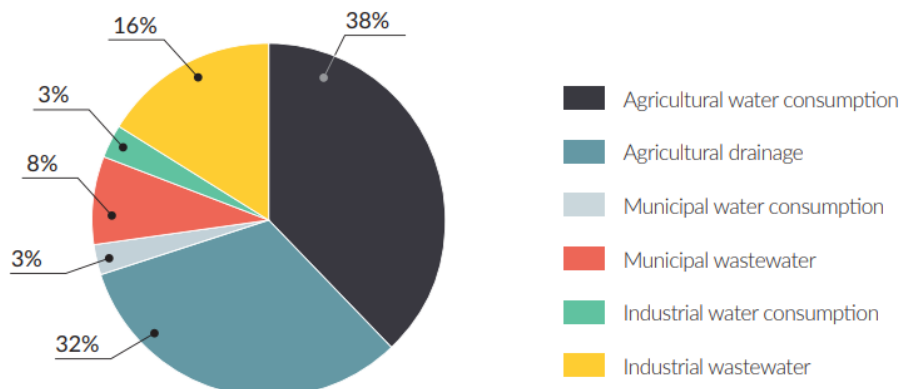
Figure 1.3. Global water consumption and wastewater production (UNESCO, 2017)

The direct discharge of wastewater into the environment causes pollution in surface water, soil and groundwater. Impacts of untreated or not properly treated wastewater can be classified into three different groups: (i) human health effects, (ii) economic effects and (iii) environmental effects.

- **Human health effects.** According to the World Health Organization (WHO), in 2012, 842 000 people died in middle- and low-income countries due to contaminated drinking water, inadequate handwashing facilities or inappropriate sanitation system (WHO, 2014). Additionally, many diseases such as cholera, dengue fever, dracunculiasis or lymphatic filariasis can be got by humans due to an inadequate sanitation (Aagaard Hansen et al., 2010).

- **Economic effects.** According to the United Nations Environment Programme (UNEP), contaminated water directly affects to industrial production, fisheries, aquaculture and tourism (UNEP, 2015). If environmental damages are taken as external costs, a proper wastewater management would generate potential benefits (UNESCO, 2017).

- **Environmental effects.** The discharge of untreated or not properly treated wastewater into the water bodies has a direct effect on water quality. For example, Corcoran et al. (2010) reported that around 245 000 km^2 of marine ecosystems are affected due to the discharge of untreated wastewater, creating de-oxygenated dead zones. Additionally, industrial and agricultural productive activities produce nutrient-rich wastewaters (nitrogen and phosphorus). The discharge of high loads of nutrients causes eutrophication in receiving water bodies, leading to potentially toxic algal blooms and decline of biodiversity.

All in all, an efficient wastewater treatment is essential to avoid human, economic and environmental affections. Additionally, as mentioned in section 1.1, these wastewater treatments need to be designed with sustainable criteria in order to not contribute to the depletion of energy resources and materials, the overexploitation of soil, the loss of biodiversity or to the climate change.

1.2.2. Multi-environment reactors: An innovative solution for Biological Nutrient Removal from wastewater

Wastewater treatment processes are carried out in Wastewater Treatment Plants (WWTP), in which the main stage is a secondary treatment for organic matter removal. Usually, the secondary treatment is based on the activated sludge process, which is a biological aerobic process including an aeration system that consists on electromechanical devices or air-bubble injection. In those cases in which, in addition to organic matter, nutrient removal is also required, an enhanced treatment train must be included in the activated sludge process.

Concretely, nutrient removal from wastewater before it is discharged into the environment represents one of the main concerns in the water treatment field. Current regulations establish strict water quality objectives as the number of areas being declared as sensitive to eutrophication has notably increased (European Union, 1991; European Union, 2000). In consequence, many existing WWTP are forced to upgrade or retrofit their configuration for nitrogen and phosphorus removal. However, conventional processes for Biological Nutrient Removal (BNR) require complex treatment systems. First, the aerobic reactor must have the enough volume to carry out the oxidation of the nitrogen (nitrification) and, additionally, it needs to be coupled with non-aerated reactors or compartments (i.e. anaerobic and anoxic). The latter gives rise to a significant increase in the volume needed for the wastewater treatment process if compared to a process only aiming at organic matter removal. However, the required space is not available on site in many cases. It must also be highlighted the high energetic demand of the nitrification process, that along with the necessity of recirculation pumping between the different reactors or compartments, generates a notable increase in the total energy consumption of the process.

One recent approach to simplify the complexity of conventional BNR treatment trains is the implementation of suspended growth multi-environment reactors, which combine different environmental conditions (aerobic, anoxic and/or anaerobic) in a single reactor. These reactors can provide high compactness and efficiency adaptable to the existing land, energy and water quality constraints. For instance, the BioCAST reactor unifies the aerobic and anoxic conditions for carbon and nitrogen removal (Yerushalmi et al., 2010); the upflow multi-layer bioreactor (UMBR) combines anoxic and anaerobic zones (with the anoxic at the bottom) for BNR (Kwon et al., 2005); and AnoxAn unifies the anaerobic and anoxic zones (with the anaerobic at the bottom) in a continuous upflow sludge blanket reactor (Tejero et al., 2010).

Concretely, AnoxAn (conceived and developed by the Group of Environmental Engineering (GIA) of the University of Cantabria) has already been studied at pilot scale, and results demonstrated the viability of the biological process (Díez-Montero et al., 2016). In fact, the reactor achieves a significant reduction of the occupied surface and a decrease of 55% of the energy consumption for mixing and agitation compared to conventional activated sludge rectors (Díez-Montero, 2015). However, hydrodynamics appeared to critically affect the stability and operation of the process. On one hand, hydraulic separation between anaerobic and anoxic zones must be maintained in order to guarantee the viability of the BNR process. At this aim, the reactor has independent mixing systems in each compartment and deflectors to enhance the hydraulic separation between both environments. These elements generate preferential paths and dead zones, reducing the global performance of AnoxAn. In fact, a non-desired hydraulic operation can give rise to an inadequate biological efficiency (Climent et al., 2018; Arnaldos et al., 2018; Wei et al., 2019). In order to optimize the reactor configuration and propose other reactor configurations applicable on a large scale, Diez-Montero (2015) pointed out the need for a deeper and more complete hydrodynamic analysis.

1.3. <u>Computational Fluid Dynamics</u>

The general equations in fluid mechanics (Navier-Stokes equations) do not admit analytical solutions. For this reason, the research in this area has commonly been carried out by means of experimental work. However, experimental techniques give rise to an excessive spatial and time cost, which can be overcome by means of computational modelling and numerical simulations.

One possible hydrodynamic modelling approach is the development of the widely used compartment-based models such as the tank-in-series and the dispersion model (Levenspiel, 1999). However, the black-box nature of this kind of models does not provide any information regarding spatial flow or concentration distribution (Plascencia-Jatomea et al., 2015; Qi et al., 2013). Moreover, in general, they are only useful for specific operational conditions, not allowing to test the effect of changing any geometrical parameter of the studied reactor.

With the evolution of computation since the half of the past century, numerical techniques in engineering have experienced a great development, being fluid mechanics one of the disciplines with more repercussion (Fernández, 2012). Computational Fluid Dynamics (CFD), consists in the use of computers and numerical techniques to solve problems related with the fluid flow and, in addition, other associated physical phenomena such as heat transfer or chemical reactions. In fact, compared to the compartment-based models, CFD allows a deeper hydrodynamic analysis including both quantitative and qualitative evaluation of dead zones, velocity profiles and flow patterns, mixing performance or short-circuiting. Unlike other industries where CFD is completely established (aeronautical industry, automotive industry, etc.), in the wastewater treatment field, CFD is now rapidly growing and being applied to the resolution of complex problems (Samstag et al., 2016; Wicklein et al., 2015). However, to our knowledge, there are only few studies based on CFD for evaluation and optimization of the hydrodynamics of multi-environment reactors (Calder et al., 2013), evidencing that further research is needed at this respect.

Finally, a remark regarding the existing CFD software and their usability must be done. Most CFD studies are carried out with commercial models developed by companies. These models include a fee for licenses and are usually closed source, not allowing the user to access to the source code to add custom features. On the other hand, there are open source models, whose main advantage is the possibility to share, modify and study de source code, allowing to develop custom solutions to very particular casuistry. In the field of CFD, OpenFOAM® (Jasak et al., 1996; Weller et al., 1998) is a free, universal, advanced, robust and open source toolbox, which is being used in a wide variety of industries and it is in continuous development by the research community. To our knowledge, there are very few works that use OpenFOAM® in the wastewater treatment field since its source code does not include some key physics or processes of the area (e.g., tracer transport or biokinetics). All in all, OpenFOAM® is a free and open source CFD tool with promising capabilities that promotes the free and universal access to science.

1.4. <u>Conclusions</u>

Concluding, this thesis aims to contribute to the research community in three different but interdependent aspects:

- Deepening in the research of AnoxAn, a novel anaerobic-anoxic multi-environment reactor for BNR. Concretely, this work is focused on the analysis and understanding of the complex hydrodynamic behaviour of this reactor, which is proposed to be comprehensively studied and optimized by means of CFD numerical techniques. At the same time, this study aims to help to cover the lack of research in literature regarding hydrodynamics of multi-environment reactors.

- Contributing to the development of a free and open source numerical tool in the field of wastewater treatment, adding custom features to the source code and sharing it to the research community. Concretely, an open source CFD tool built in OpenFOAM® for the anaerobic-anoxic reactor AnoxAn.

- From a more global perspective, the objective of this work is to contribute to the improvement of the environmental and energetic efficiency of wastewater treatment processes. Concretely, AnoxAn aims to reduce the energetic demand and the occupied surface and volume of conventional BNR treatment trains. At the same time, this technology contributes to the fulfilment of the European Regulation regarding the protection of continental-, coastal- and ground-waters.

This document is structured as follows. This introductory chapter (**Chapter 1**) serves to motivate and justify the topics studied in the thesis. In **Chapter 2**, a review of the literature is carried out and in **Chapter 3,** the scope and objectives of this work are presented based on the gaps found in the state of knowledge. The next four chapters form the main contribution of the thesis, and they present (i) the development and implementation of the numerical CFD tool based in OpenFOAM® (**Chapter 4**), (ii) the validation of the model and the hydrodynamic analysis of AnoxAn (**Chapter 5**), (iii) the development of a hydrodynamic optimization methodology for multi-environment reactors and its application to AnoxAn (**Chapter 6**), and (iv) the evaluation of the effect of the hydrodynamic behaviour on the biological efficiency of AnoxAn (**Chapter 7**). Finally, main conclusions and recommendations of this work are highlighted in **Chapter 8**.

Chapter 2

State of the art and theoretical basis

This chapter aims to serve as a guide for the current state of knowledge and theoretical basis of the different topics that converge in this work. First, fundamentals of Biological Nutrient Removal (BNR) and innovative multi-environment reactor configurations existing in the literature are described. Next, the two main approaches for wastewater treatment process modelling (biokinetic modelling and hydrodynamic modelling) are presented. Then, the theoretical fundamentals of the numerical modelling technique used in the present work, i.e. Computational Fluid Dynamics (CFD), are explained and some representative examples of CFD applied to water and wastewater treatment modelling are highlighted. Finally, main conclusions are summarised and the principal gaps found in the literature are reported.

2.1. Biological Nutrient Removal

2.1.1. Biological Nitrogen Removal

Biological nitrogen removal processes are based on the total or partial oxidation of ammonium (NH_4-N) to nitrite (NO_2-N) or nitrate (NO_3-N) and subsequent reduction to nitrogen gas (N_2). The process which is most widely extended in wastewater treatment facilities consists of complete nitrification (oxidation of NH_4-N to NO_3-N) and denitrification (reduction of NO_3-N to N_2). Concretely, nitrification is performed by aerobic autotrophic ammonium oxidizing bacteria (AOB), which carry out the oxidation of ammonium to nitrite (Eq. 2.1), and aerobic autotrophic nitrite oxidizing bacteria (NOB), which convert nitrite to nitrate (Eq. 2.2).

$$NH_4^+ + 1.5O_2 \rightarrow NO_2^- + 2H^+ + H_2O \tag{2.1}$$

$$NO_2^- + 2O_2 \rightarrow NO_3^- + 2H^+ + H_2O \tag{2.2}$$

In order to achieve the objective of total nitrogen removal by both NH_4-N oxidation and NO_3-N reduction to nitrogen gas, an anoxic zone or reactor should be added to the process in order to carry out the biological denitrification (Eq. 2.3). Denitrification is performed by heterotrophic bacteria in the absence of oxygen. At this respect, nitrate require an electron donor. The latter can be supplied in the form of influent wastewater Biochemical Oxygen Demand (BOD), by endogenous respiration, or using an external carbon source such as methanol.

$$10NO_3^- + C_{10}H_{19}O_3N \rightarrow 5N_2 + 10CO_2 + 3H_2O + NH_3 + 10OH^- \tag{2.3}$$
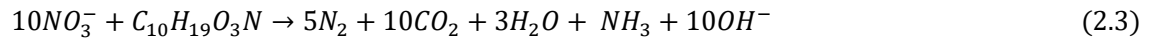
In single-sludge suspended growth treatment trains, three different nitrogen removal processes can be distinguished according to the location of the anoxic reactor relative to the nitrification stage: pre-anoxic process, post-anoxic process or a combination of both.

Regarding the pre-anoxic biological nitrogen removal process (see Fig. 2.1), the anoxic reactor receives the nitrate rich recycle from a subsequent aerobic reactor. Therefore, denitrifying bacteria in the anoxic zone can consume influent BOD and transform the nitrate to nitrogen gas.

This configuration is one of the most common ones (Water Environmental Federation, 2011) and the main advantages of using a pre-anoxic zone upstream of a nitrification zone are described below (Tchobanoglous et al., 2014):

- The relative ease to retrofit existing plants.

- The benefits of the anoxic selector operation for control of filamentous sludge.

- The production of alkalinity before the nitrification step.

- The energy savings due to the use of nitrate for oxidation of the influent BOD.
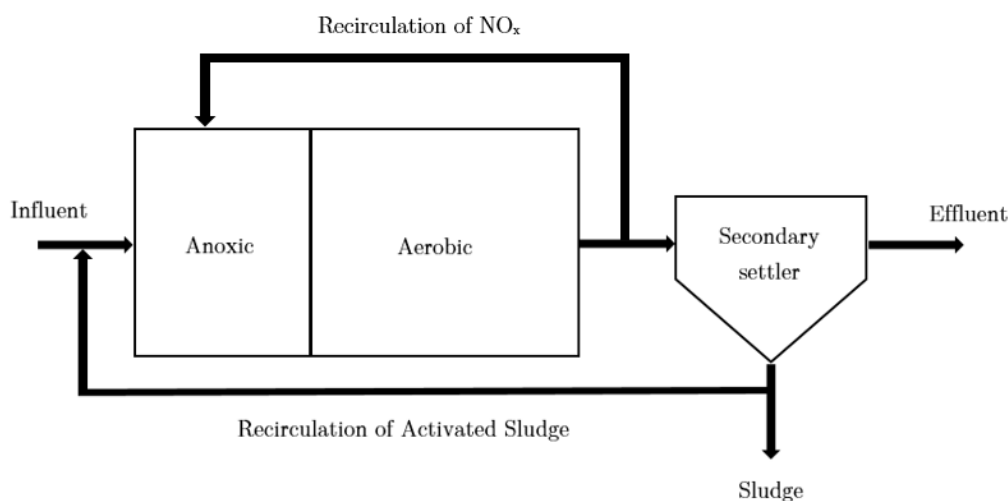
Figure 2.1. Pre-anoxic biological nitrogen removal process flow-chart

2.1.2. Biological Phosphorus Removal

Enhanced Biological Phosphorus Removal (EBPR) is based on the selection and growth of specialized accumulating organisms able to store polyphosphate in excess of their biological needs. The group of heterotrophic bacteria with this ability that take part in the EBPR process are known as Phosphate Accumulating Organisms (PAOs).

In Wastewater Treatment Plants (WWTP) performing the EBPR process, there is an anaerobic zone or reactor prior to the anoxic and aerobic stages. In this anaerobic zone, the activated sludge mixed liquor contacts with the influent wastewater or any other feed stream containing Volatile Fatty Acids (VFA). Unlike other ordinary heterotrophic organisms, PAOs are able to assimilate and transform simple carbon compounds in this stage, such as acetate and propionate, without the presence of an external electron acceptor, and accumulate them as intracellular carbohydrate storage products. During the anaerobic stage, PAO generate energy from internally stored polyphosphate, therefore they release significant amounts of phosphate. In the subsequent aerobic stage, PAO oxidize the carbohydrate storage products and grow

accumulating polyphosphate in excess of their biological needs, in order to store energy which will be used if the biomass is exposed to anaerobic conditions again. In addition, some PAO have the ability to use NO_3 instead of oxygen to grow and accumulate polyphosphate, performing what is called denitrifying phosphate uptake.

Different EBPR process configurations have been developed and applied at many WWTPs. The design selection depends on the wastewater treatment process and equipment, the wastewater characteristics and the treatment needs. If complete nutrient removal is required, i.e. nitrogen and phosphorus removal, combination of anaerobic, anoxic and aerobic environments is needed in the process. In that sense, the A^2O (anaerobic-anoxic-aerobic) and UCT processes (University of Capetown) are two of the most used design for BNR from urban wastewater (Tchobanoglous et al., 2014).

In the A^2O process (Fig. 2.2), the settled biomass is recycled to the anaerobic zone or reactor, which also receives the influent water. Anaerobic conditions (no oxygen nor nitrate) in this first stage in the presence of the influent wastewater organic matter, promote the growth of PAOs. However, although nitrate is almost removed by the anoxic-aerobic double stage, the returned activated sludge (RAS) still contains nitrate that is recycled to the anaerobic stage. If the influent wastewater has a high enough organic matter content (i.e. BOD/P ratio higher than 30/1, and BOD/N higher than 3-3.5) the Chemical Oxygen Demand (COD) concentration of the influent wastewater is enough for both nitrate removal and sufficient PAO growth. If the BOD/P ratio is lower, PAO growth is disabled as the heterotrophic denitrifying bacteria consume the COD needed for that purpose. In consequence, no phosphorus removal can be achieved under these conditions.
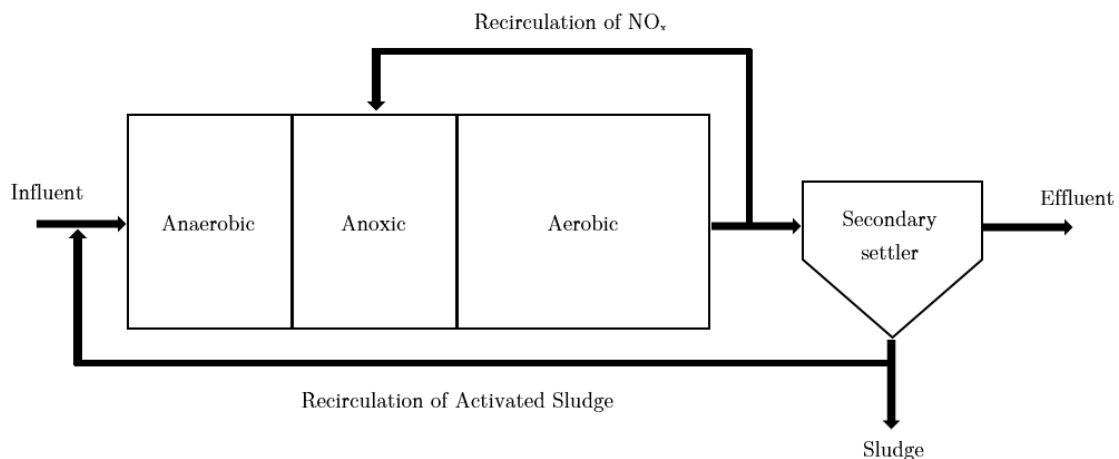
Figure 2.2. A^2O process flow-chart

The UCT process (Fig. 2.3), originally developed by the University of Cape Town (South Africa), was designed to minimize the recycle of nitrate to the anaerobic zone. Unlike the A^2O process, the UCT system has three recycle streams instead of two. First, the anoxic zone receives the recycle from the secondary clarifier (instead of the anaerobic zone). Additionally, a recycle from the anoxic zone is directed to the anaerobic zone with the aim recycling biomass

to the anaerobic stage but not introducing nitrate in this stage. Therefore, more influent COD is available for the PAOs in the anaerobic zone, improving the EBPR efficiency, and allowing EBPR in those cases with lower content organic matter in the influent wastewater (i.e. ratio BOD/P and BOD/N).
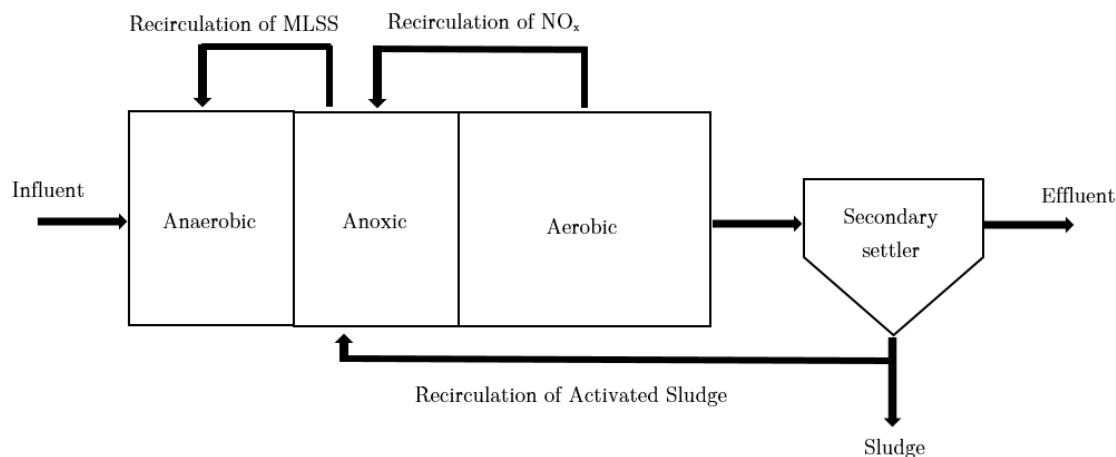
Figure 2.3. UCT process flow-chart

2.2. Multi-environment reactors for Biological Nutrient Removal

As introduced in Chapter 1, conventional BNR configurations in WWTP require a complex treatment system and entail several environmental impacts that are highlighted below:

- First, the aerobic reactor should be large enough to carry out ammonium oxidation (nitrification) and must be coupled with non-aerated compartments (anaerobic and anoxic). Therefore, a large volume is needed compared to organic matter removal processes (about 3 times the volume required for only organic matter removal). This issue becomes crucial in cases where land availability is limited and in cases of existing WWTPs design for organic matter removal that need to be upgraded to BNR.

- In addition, the high energy demand of the nitrification process, together with the need for recirculation pumping between the different compartments or reactors and the mixing of the non-aerated ones, result in a significant increase in energy consumption. In fact, the difference in the energy consumption between conventional activated sludge processes (only organic matter removal) and advanced ones (with nutrient removal) can be up to 50% (Panepinto et al., 2016) for WWTPs above 100 000 m³/d.

In this context, multi-environmental biological reactors with high compactness and efficiency have been developed to reduce the energy consumption and land use of conventional BNR treatment trains (Kwon et al., 2005; Yerushalmi et al., 2011; Tejero et al., 2010;

Ahn et al., 2003; Song et al., 2009) while fulfilling current quality regulations (European Union, 1991; European Union, 2000). The main features of these novel configurations are highlighted below.

Upflow multi-layer bioreactor

The upflow multilayer biological reactor (UMBR) (Kwon et al., 2005) is a plug-flow reactor that unifies the anaerobic and anoxic conditions in a single tank.

Rotating distributors located at the bottom of the reactor introduce the raw wastewater in the treatment unit. At the same time, these distributors also receive a nitrate-rich stream recycled from the subsequent aerobic reactor. As the flow generates an anoxic environment, the anoxic zone is located at the bottom of the reactor and nitrate is consumed in this zone. The anaerobic zone is located above the anoxic one, where the nitrate has been depleted. The UMBR was tested at pilot scale coupled with an aerobic biofilm reactor treating municipal wastewater (Fig 2.4). In these experiments, a total nitrogen removal efficiency of 75% was achieved. On the other hand, phosphorus removal was only performed by means of settling and absorption in the UMBR. Therefore, EPBR was not considered in the process as phosphate removal appeared to be minimum. In fact, COD consumption was mainly carried out in the anoxic zone, giving rise to insufficient substrate concentration for phosphate release in the anaerobic zone.
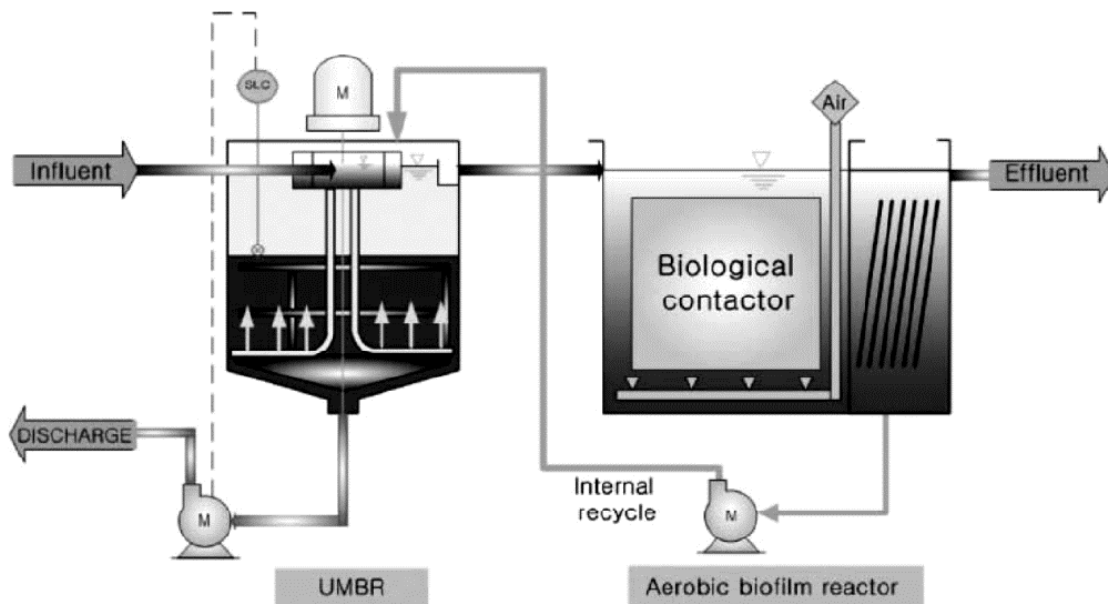
Figure 2.4. UMBR process scheme (Kwon et al. 2005)

BioCAST

BioCAST (Yerushalmi et al., 2010) is a multi-environment wastewater treatment technology designed and developed for high rate and simultaneous removal of organic carbonaceous compounds and nutrients.

It consists in two sequenced reactors (see Fig. 2.5):

- The first one comprises aerobic and anoxic zones for biological treatment together with a clarification section for liquid-solid separation. The aerobic zone consists in a combination of suspended and fixed biomass in order to increase solid retention in the process. Separation between different environments is achieved through deflectors and different sized apertures in them.

- The second reactor is formed by an anaerobic zone, another clarification zone for liquid-solid separation and a filtration unit prior to the secondary settler.

The influent gets into the reactor through the upper part of the aerobic zone, and the aeration is introduced by means of diffusers, enhancing nitrification. Denitrification process occurs in the anoxic zone located at the bottom of the reactor. Then, the mixed liquor goes into the second reactor, where the VFA needed for phosphorus removal are generated through sludge digestion (anaerobic zone). Additionally, solid liquid-separation (clarification and filtration zones) is also achieved in the second reactor. Recirculation from the anaerobic zone in the second reactor to the aerobic zone in the first one returns a mixed liquor full of PAO-s needed for phosphorus removal.

Experimentation results showed up to 98.9 and 98.3% of removal efficiency for carbon and nitrogen, respectively. Phosphorus removal efficiency was noted to be lower than 50% during the first part of the experimentation, but it reached a 94.1% of efficiency when C/N ratio was below 15 (Yerushalmi et al., 2011).
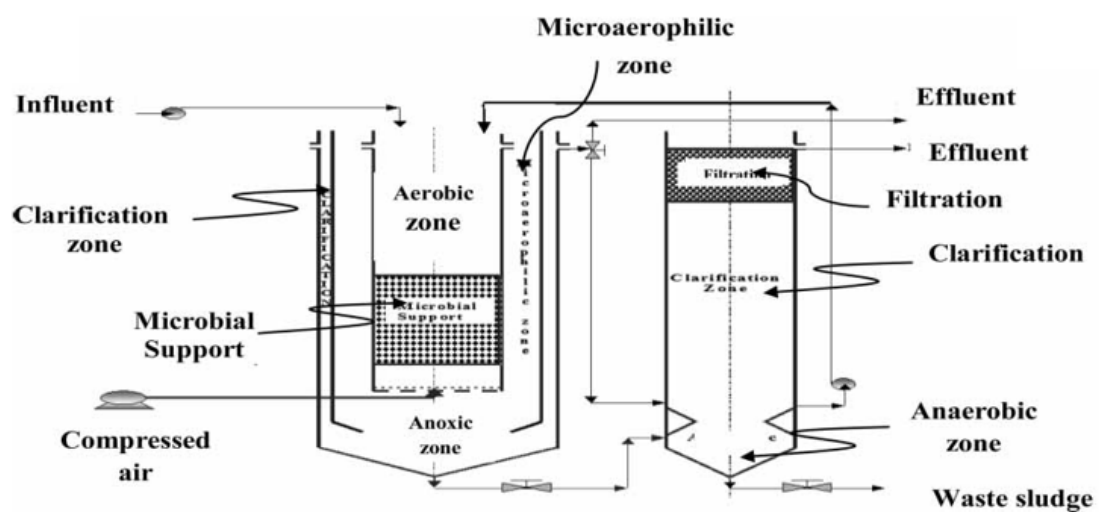
Figure 2.5. BioCAST process scheme (Yerushalmi et al. 2011)

Sequencing anoxic-anaerobic reactor

The sequencing anoxic-anaerobic reactor (SAAR) (Fig. 2.6) was conceived and studied by Ahn et al. and Song et al. at laboratory (Ahn et al., 2003; Song et al., 2009) and at pilot scale (Song et al., 2010). It consisted in a single reactor with alternate anaerobic and anoxic conditions which receives the influent wastewater, and it was coupled with an aerobic membrane bioreactor (MBR) to complete the nutrient removal process.

Both anoxic and anaerobic conditions were set in the same reactor through sequential operation by means of intermittent recirculation of the nitrate-rich stream from the MBR. In consequence, there was no need for building two separate tanks achieving a considerable spatial saving. Regarding the biological performance of the process, a 93% of phosphorus removal efficiency at lab scale was achieved. However, nitrogen removal efficiency was below 60%, which is lower than conventional BNR configurations.
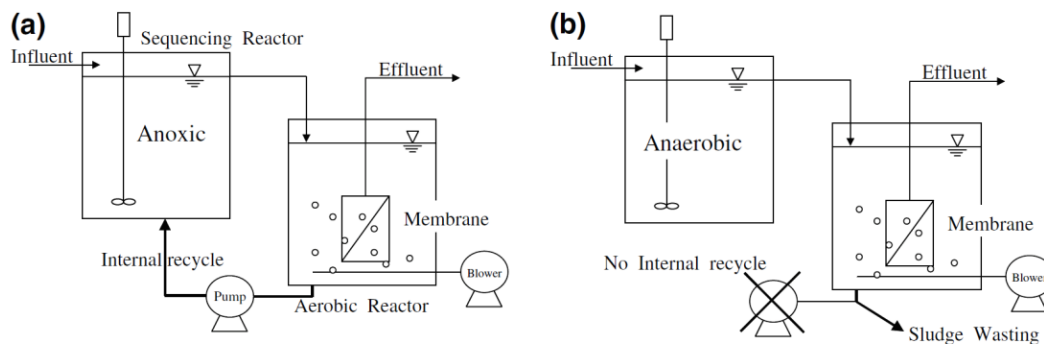
Figure 2.6. Operation of the sequencing anoxic/anaerobic membrane bioreactor process: (a) anoxic stage and (b) anaerobic stage (Song et al. 2009)

AnoxAn

AnoxAn (Tejero et al., 2010) is a continuous upflow reactor that reunites the main features of previously analysed multi-environment processes: a single reactor coupling different multi-environment conditions (anaerobic-anoxic), upflow sludge blanket operation and encouragement of denitrifying phosphate uptake. AnoxAn is divided into three different zones (see Fig. 2.7):

- An anaerobic zone at the bottom receiving the raw wastewater.

- An anoxic zone above receiving a nitrate-rich stream from a subsequent aerobic reactor for the nitrification and phosphate uptake.

- A clarification zone at the top of the reactor aiming to avoid the escape of large amounts of biomass.

It has to be highlighted that hydraulic separation between anoxic and anaerobic zones must be maintained in order to encourage the optimum biological performance of the system. In that

sense, a deflector is used between both zones in order to avoid the nitrate contamination in the anaerobic volume. Independent mixing devices such as mixers, impellers and recirculation pumps are also used in order to maintain the biomass in suspension and avoiding the settling process.
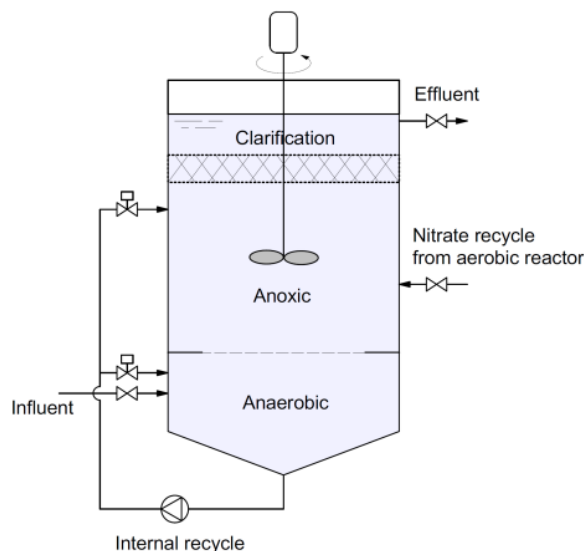
Figure 2.7. AnoxAn reactor scheme (Díez-Montero, 2015)

Regarding biological performance, AnoxAn was coupled with a subsequent aerobic reactor, and a removal efficiency of 75% and 89% was achieved for total nitrogen and total phosphorus respectively under no limiting organic availability in influent wastewater (C/N > 10) for both PAO and conventional denitrifying heterotroph bacteria (Díez-Montero et al., 2016). Although the results demonstrated the feasibility of the reactor concept, it was observed that some physical characteristics of AnoxAn significantly affect its performance, being hydrodynamics clearly relevant. In order to optimise the reactor configuration and propose other reactor configurations applicable on a large scale, Díez-Montero (2015) pointed out the need for a deeper and more complete hydrodynamic analysis.

2.3. Wastewater Treatment Process modelling

Modelling in engineering aims to represent with mathematical expressions what is observed experimentally, in order to support in process design, optimization, prediction of the performance and evaluation and comparison of alternatives. Every model relies on assumptions, so it must not be forgotten that they are just an approximation of the reality. Therefore, it is important to define the model goal and to have a deep understanding of their nature (including its simplifying assumptions and limitations) in order to be able to interpret and use the results correctly.

Models can be divided into empirical and mechanistic or structured. Empirical models are experience-based and relate directly measured variables. Besides, they are usually defined in

correlations or in graphical format. On the other hand, mechanistic or structured models are based on mathematical expressions and describe the behaviour of a variable (or series of variables) with a physical understanding of the underlying phenomena and mechanisms.

In wastewater treatment process modelling, the use of mechanistic models has allowed engineers, scientists and researchers to develop new processes, optimize existing ones and assess in the operation of ongoing WWTPs (Water Environmental Federation, 2011). Generally, two key aspects need to be modelled in the study of wastewater bioreactors: On one hand, the biological reactions or biokinetics occurring in the process, and on the other hand, reactor hydrodynamics. In the next sub-sections, these two aspects of a wastewater modelling process are described.

2.3.1. Biokinetic modelling

Biokinetic modelling aims to reproduce the biological and chemical reactions occurring in the studied wastewater treatment unit. At this respect, the Activated Sludge Models (ASM) proposed by the International Water Association (IWA) (Henze et al., 2000) are the most widely used ones among the suspended growth processes (Water Environmental Federation, 2014), and they include and simulate carbon, nitrogen and phosphorus removal. In the next paragraphs, the main features of the ASM models are summarised. For further information, the reader is referred to Henze et al. (2000).

Activated Sludge Model No.1

The Activated Sludge Model No.1 (ASM1) was the first activated sludge model released among all ASM models, and is also the most widely used one (Roeleveld et al., 2002). Based on Monod kinetics, ASM1 incorporates key processes in wastewater modelling such as carbon oxidation, nitrification and denitrification. The total influent COD is divided into four different fractions named soluble, particulate, biodegradable and un-biodegradable. Using a total of thirteen variables, eight different processes are described in the ASM1: Aerobic heterotrophic growth, anoxic heterotrophic growth, heterotrophic decay, aerobic autotrophic growth, autotrophic decay, ammonification of soluble organic nitrogen, hydrolysis of particulate organic matter and hydrolysis of nitrogen. In addition, the model has five stoichiometric parameters and fourteen kinetic parameters. Although default values proposed by Henze et al. (2000) can be assumed, these parameters are usually adjusted to achieve the calibration and validation of the constructed model.

Activated Sludge Model No.2 and No.2d

Using the ASM1 as a base model, Activated Sludge Model No.2 (ASM2) was developed to include EPBR to the already existing biological processes in ASM1. In that sense, ASM2 includes the accumulation of organic matter by PAOs in anaerobic conditions, and the growth of PAO-s and accumulation of polyphosphate in aerobic conditions. However, ASM2 neglects the PAO anoxic metabolism and denitrifying phosphate removal. To overcome this deficiency,

ASM2d was later developed and the denitrifying metabolism of PAO-s was included in the model.

Activated Sludge Model No.3

The Activated Sludge Model No.3 (ASM3) is also based on ASM1, and although it does not include the biological phosphorus removal, different approaches for carbon oxidation and nitrogen removal are added. The main difference with the ASM1 model is that ASM3 considers the bacterial growth metabolism based on the internal storage of carbon. In addition, in ASM3 bacterial decay is represented by an endogenous respiration approach. Finally, differently to ASM1, in ASM3 biomass decay does not produce substrate.

As a resume, Table 2.1 shows the main features of the presented ASM models:

Table 2.1. Summary of IWA activated sludge models (adapted from Water Environmental Federation, 2014)

Process / Model	ASM1	ASM2	ASM2d	ASM3
Particulate hydrolysis	X	X	X	X
Fermentation		X	X	
Carbon storage		X*	X*	X
Carbon oxidation	X	X	X	X
Nitrification	X	X	X	X
Denitrification	X	X	X	X
Biological phosphorus removal		X	X	
Denitrifying phosphorus removal			X	

* Only for biological phosphorus removal process

The ASM models are useful to evaluate the biological performance of wastewater processes, and they have been widely and successfully used for simulation of bioreactors in many studies. However, one of the main limitations of the ASM models is that they assume complete mixing in the analysed reactors. In fact, while conventional dimensioning of BNR processes suppose ideal complete mixing flow in reactors (DWA, 2000; Water Environment Federation, 2011), neglecting the hydrodynamic phenomena that interfere in ideal flow conditions, several studies have shown that a correct hydrodynamic behaviour enhances a desirable biological efficiency in bioreactors (Castrillo et al., 2019; Angeloudis et al., 2014; Climent et al., 2018; Arnaldos et al., 2018; Wei et al., 2019; Water Environment Federation, 2011). Hence, hydrodynamics must also be deeply studied to achieve an optimum bioreactor design.

2.3.2. Hydrodynamic modelling

General equations of fluid mechanics, i.e. Navier-Stokes equations, do not admit general analytical solutions. Therefore, the study of the hydrodynamics has been usually carried out from different perspectives such as experimental tests, dimensional analysis or simplified mathematical analysis. Concretely, hydrodynamic modelling has been traditionally based on empirical or semi-empirical models. These approaches can be reliable for well-known unit operations, but have appeared not to be adequate for the design of new processes (Andersson et al., 2012). Additionally, experimental tests at full-scale are expensive, time-consuming and space demanding. In addition, conventional techniques for hydrodynamic analysis are limited to relatively simple reactors or flow patterns, while the results are difficult to interpret in those cases of complex geometries or configurations. Since the second half of the past century, the evolution of the computational has led to a new tool has been added to the field: the computational analysis of flows, commonly known as Computational Fluid Dynamics (CFD).

All in all, hydrodynamic modelling in the wastewater treatment field is mainly carried out by means of compartment-based mathematical models and CFD techniques. A review of both approaches is presented below.

2.3.2.1. Compartment-based models

The compartment-based modelling or systemic modelling approach has been widely used to reproduce the hydrodynamic behaviour of wastewater treatment tanks or reactors. Within this approach, the non-ideal flow of a water treatment system is represented by means of combinations of ideal flow reactors such as Continuous Stirred Tank Reactors (CSTR) and Plug Flow Reactors (PFR). Additionally, dead volumes (DV) can also be considered within the models.

Further, CSTR and PFR have been expanded to the Tank in Series (TIS) model or Axial Dispersion Model (ADM). On one hand, ADM is used to represent the heterogeneity of the residence time of a fluid caused by the molecular diffusion, the velocity profile or the turbulence along with other phenomena, and it is usually defined as a PFR with diffusive behaviour in the axial direction. At this respect, ADM is limited to describe longitudinal motion flows with small deviations from the ideal plug-flow. Therefore, its application to complex water treatment systems with important recirculation flows or elements that interfere in the ideal flow patterns is limited and uncertain (Levenspiel, 1999). On the other hand, TIS models consist in the combination of several CSTR reactors with the same volume, and they are more common in water treatment units modelling. In fact, TIS is a simple but effective approach where any kind of kinetics can be used, and can be easily extended to different configurations with multiple compartments and recycle systems.

A complete reactor can be modelled by means of a combination of CSTR (completely mixed reactors) and PFR. Each compartment is aimed to reproduce a specific hydraulic behaviour of a particular section of the complete reactor. Moreover, inner or outer recirculation can be added

within different compartments, along with possible dead volumes. These models are usually constructed with the aim of reproducing the outlet response of Residence Time Distribution (RTD) experimental tests (Levenspiel, 1999). Thus, the complex hydrodynamic behaviour of water treatment units is aimed to be reproduced only knowing information about the inlet and the outlet of the system, giving rise to a black box nature.

A wide variety of compartment-based models applied to wastewater treatment units can be found in literature. Some examples are highlighted below:

Pons et al. (1993) performed a dynamic simulation of a municipal WWTP consisting of a primary settler, a conventional activated sludge reactor and a secondary settler. Additionally, a recycle flow was added. Each unit of the plant was divided up into several compartments: both settlers were divided up into two plug-flow zones (one for the liquid zone and another one for the sludge zone) and the aerated reactor was modelled by a series of n units (following Roche, 1989). Finally, these units were connected and the ASM1 (Henze et al., 2000) with only organic matter removal was applied. Although close agreement between modelled and experimental results was reached, the authors stated that due to the high number of kinetic parameters involved in the model, further research was needed.

Cheng et al. (1999) built a model for the Parada WWTP (Portugal) with the objective of evaluating the feasibility of upgrading it to BNR. The biological reactor was divided up into two different CSTR (matching with the aerobic and anoxic stages, respectively) and the clarifier was modelled as a single CSTR. ASM1 (Henze et al., 2000) biokinetic model was implemented, and reactors and compartments were linked. Results showed a good correlation between simulated and experimental results after using the stoichiometric and kinetic values proposed by the authors.

Ayesa et al. (2006) developed a full-scale compartment model for the Galindo WWTP in Bilbao (Spain) with the goal of monitoring and optimizing the nitrogen removal based on ASM1 (Henze et al., 2000). Using a compartment-based modelling approach, the authors successfully validated the model and were able to propose various control strategies to achieve a desirable nitrogen removal operation for the plant.

Díez-Montero et al. (2015) modelled the anaerobic-anoxic AnoxAn reactor with the aim of evaluating the hydraulic separation between both environments. To reproduce the complex hydrodynamic behaviour of this reactor, a combination of compartment-based models was needed. Concretely, the anaerobic zone was modelled as a combination of three CSTR in series. On the other hand, the anoxic zone was modelled as a single CSTR and the clarification zone as ADM in order to simulate a PFR behaviour caused by a baffle between both zones. Finally, a denitrification kinetic was added to the model. Results were successfully validated by means of experimental pulse tracer tests and hydraulic separation of the AnoxAn prototype was demonstrated.

Plascencia-Jatomea et al. (2015) modelled a novel Membrane Aerated Biofilm Reactor (MABR) by means of three different systemic approaches: ADM, TIS and the Mixing Cell Model (MCM). The models were compared against RTD tests for four different inflow rates and results showed that the MCM better reproduced the hydrodynamic behaviour of the reactor.

Rehman (2016) developed complex compartment models for two case studies: the Eindhoven WWTP (Netherlands) and La Bisbal d'Empordà WWTP (Spain). The research work proposed a novel compartmentalisation methodology divided into three different steps: (i) longitudinal compartmentalisation of reactors based on dividing the studied unit into different sections in the longitudinal direction, (ii) vertical compartmentalisation of reactors based on dividing the previously selected longitudinal compartments into additional sections in the vertical cross-section and, finally, (iii) convective flux calculations between the compartments created in the previous steps. The hydraulic compartment model was coupled with ASM1 (Henze et al., 2000) biological model. Results showed that although the development of the model needs a hard calculation process, they are very robust and suppose a step further from conventional TIS models.

Although the feasibility of compartment models to simulate the overall hydrodynamic behaviour and biological operation of water treatment units have been demonstrated, some important limitations of this approach must be pointed out. First, compartment-based models are developed for a certain geometric configuration and operation parameters (reactor dimensions, mixing devices operation, deflectors) and therefore, they are not suitable to evaluate the influence of these design constraints on the reactor operation. If any of these constraints is changed, the model needs to be reconstructed. In addition to this, in compartment-based models is not possible to carry out a detailed hydrodynamic analysis (local flow patterns inside compartments are absolutely unknown) and models assume ideal flow reactors (completely mixed and plug flow), neglecting the presence of local dead volumes or short circuiting. Besides, a tendency of over-calibration of kinetic parameters has been observed to correct errors that can be possibly generated by the inability to reproduce rigorously reactor hydrodynamics (Rehman, 2016). In conclusion, all these limitations give rise to the need for a more advanced tool for hydrodynamic modelling.

2.3.2.2. Computational Fluid Dynamics

Unlike other approaches, CFD is able to solve the Navier-Stokes equations with numerical techniques. This fact allows to perform comprehensive analysis of flows, also adding to the fluid mechanics additional physical features such as transport of chemical species, chemical reactions, combustion or solids transport among many others. In this sense, CFD is being successfully applied from the pure research to a wide variety of industries and applications, e.g. automobile industry, aerospace and aeronautical engineering, naval industry, chemical engineering, electric engineering, nuclear industry, renewable energies, power generation or biomedical applications.

CFD can be defined as a combination of three different disciplines (Fig. 2.8) such as fluid mechanics (comprehensive study of fluid flows), mathematics (description of all physics involved through equations and solving procedures) and computer science (the need for high-level computing resources to solve the constitutive equations).
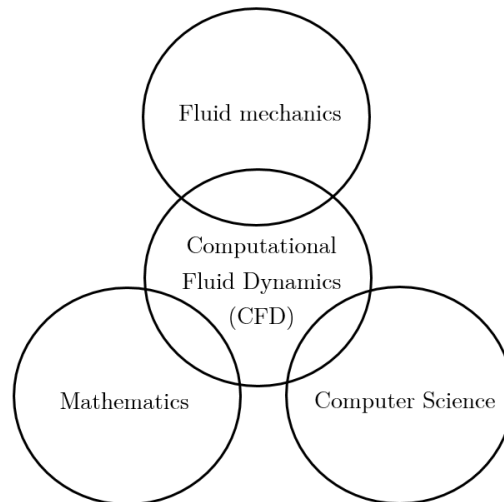
Figure 2.8. Different disciplines involved in CFD (adapted from Tu et al. 2013)

Schematically, the modelling process of every CFD approach can be divided into three different stages: pre-process, solving process and post-process.

Pre-process

In this stage the model is set up for the numerical solving process. Therefore, the physical problem must be defined within this stage. Main sub-stages are listed below:

- Definition of the geometry (computational domain) for the modelling process.

- Discretization of the defined geometry in a finite number of control volumes or cells (two-dimensional cells in 2D problems and three-dimensional cells in 3D problems). This step is known as the meshing process of the computational domain. Meshing is a key factor in every CFD simulation as a non-adequate grid give rise to inaccurate results. In that sense, some features as the independence of the solution from the grid size or geometrical quality ratios must be checked.

- Application, in every cell, of the general transport equation (Eq. 2.4) for mass, momentum, energy, etc. The general transport equation is formed by four different terms: the time term or rate of accumulation, the transport by convection, the transport by diffusion and the source terms.

$$\frac{\partial}{\partial t}\int_V \rho\emptyset\,dV + \oint_A \rho\emptyset\vec{v}\,d\vec{A} = \oint_A \Gamma\nabla\emptyset\,d\vec{A} + \int_V S_\emptyset\,dV \qquad (2.4)$$

| Rate of accumulation | Transport by convection | Transport by diffusion | Source terms |

Being ρ the density of the fluid, $\emptyset$ the transported variable, $\vec{v}$ the velocity of the fluid and $S_\emptyset$ the source term. V is the volume of the cell and A the area of the cell-face. Depending on the physical phenomena aimed to model, the transport equation to be solved varies.

- Definition of all physical properties for the fluids, e.g. density, viscosity or transport constants such as the Schmidt number.

- The last step of the pre-process stage is to set the boundary and initial conditions that define the physical problem: Inlet, outlet, walls and symmetry boundaries are the most common boundary conditions.

Solving process

The solver can be defined as the nuclear part of the modelling process. Within this stage, equations are solved and results for the fluid-dynamic field are obtained. In resume, the solving process follows the next two steps:

- Discretization and linearization (in time and space) of general transport equations in each discretized cell in order to obtain an algebraic system of equations.

- Numerical resolution of the algebraic system of equations by means of an iterative algorithm.

Post-process

In this last stage, the numerical results obtained from the solver are analysed. The first step is to evaluate the quality of the solution, i.e. the independence from the mesh size and physical coherence of results. Then, results (velocity fields, pressure, species transport, temperature, etc.) can be plotted and conclusions are obtained.

CFD also entails some disadvantages that must be highlighted. First, although CFD techniques significantly reduce the time and space consumption derived from the experimentation, very powerful computers such as clusters are needed for parallel computation. At the same time, qualified staff is required to carry out the modelling process. Additionally, a simplification of the physical phenomena can give rise to imprecise results. Finally, all the models available in

the state of the art have limitations to reproduce the real physical phenomena, and assumptions or simplifications must be taken into account.

All in all, CFD techniques have become a very important tool within the Computed Aided Engineering (CAE) and are widely used by the industry and the academy. Compared to the compartment-based modelling approach, CFD allows to perform deeper and more comprehensive hydrodynamic analysis as Navier-Stokes equations can be solved and essential information regarding flow fields can be obtained, being the level of detail of this approach almost unlimited. Besides, CFD simulation is also very adequate to study physical problems that are very difficult to reproduce experimentally such as hypersonic velocities, very high or low temperatures or dangerous systems (accidents, limit design of equipment). In this work, CFD tools are used to simulate hydrodynamic and biological phenomena in multi-environment bioreactors. The theoretical basis of these technique is presented in the next section.

2.4. Computational Fluid Dynamics: Theoretical basis

2.4.1. Spatial discretization of the equations

Several numerical approaches can be used to perform the spatial discretization of the transport equations, being the Finite Difference Method (FDM), Finite Element Method (FEM) and Finite Volume Method (FVM) the most common ones. Additionally, if the problem to solve is transient, time discretization of these equations is also needed. In this section, a stationary problem is assumed in order to point out the numerical characteristics of the spatial discretization.

Finite Difference Method

The Finite Difference Method is the simplest spatial discretization method and is based in approximating the partial differential equations derivatives to their expression in truncated Taylor series. Having a one-dimensional equation in partial derivatives for the transported variable $\emptyset$ and defined by Eq. 2.5:

$$\frac{d\emptyset}{dx} + \emptyset = 0 \; ; 0 \leq x \leq 1 \; ; \; \emptyset(0) = 1 \tag{2.5}$$

The equation is discretized following the one-dimensional domain shown in Fig. 2.9 (as an example with five nodes). The mesh has five nodes equally spaced, being Δx the distance between two consecutive nodes. As the Eq. 2.5 is valid for any point in the spatial domain, it can be expressed as in Eq. 2.6:

$$\left(\frac{d\emptyset}{dx}\right)_i + \emptyset_i = 0 \tag{2.6}$$

Being the subscript i the value in the node x_i.
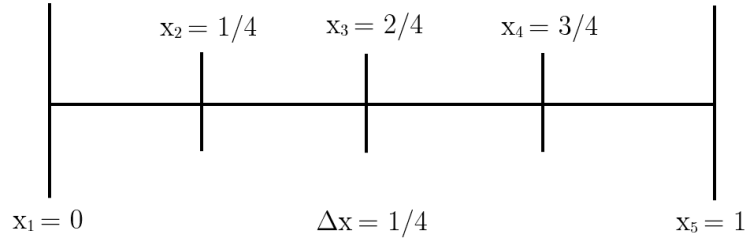
Figure 2.9. Five nodes discretization (adapted from Fernández, 2012)

To obtain the derivative in function of $\emptyset$ in every mesh point, a Taylor series is developed for backward differences (Eq. 2.7):

$$\emptyset_{i-1} = \emptyset_i - \Delta x \left(\frac{d\emptyset}{dx}\right)_i + \frac{\Delta x^2}{2}\left(\frac{d^2\emptyset}{dx^2}\right)_i - \frac{\Delta x^3}{3!}\left(\frac{d^3\emptyset}{dx^3}\right)_i + \ldots \tag{2.7}$$

Neglecting the high order terms of the Eq. 2.7, Eq. 2.8 is deduced:

$$\left(\frac{d\emptyset}{dx}\right)_i = \frac{\emptyset_i - \emptyset_{i-1}}{\Delta x} + O(\Delta x) \tag{2.8}$$

Where $O(\Delta x)$ represents the error for neglecting the high order terms of the equation. Finally, combining Eqs. 2.6 and 2.8, the following discrete equation is obtained, which is free of derivatives (Eq. 2.9):

$$\frac{\emptyset_i - \emptyset_{i-1}}{\Delta x} + \emptyset_i = 0 \tag{2.9}$$

In consequence, an algebraic equation defined in a single node of the spatial domain is deduced. To calculate the approximate solution of the $\emptyset$ variable, a differential equation similar to Eq. 2.9 needs to be defined in each node setting an algebraic system of equations.

Finite Element Method

The Finite Element Method is based on a functional representation of the numerical solution. Instead of obtaining a discrete representation of the solution in every node of the spatial domain, the variables are solved as a lineal combination of various continuous base functions, named v_i, as expressed in Eq. 2.10:

$$\emptyset = \sum_{i=1}^{N} \emptyset_i v_i \tag{2.10}$$

In this case, an exact solution is not calculated. A residual is obtained in the process, and the objective of the method is to minimize it by means of different functions. The base functions are defined as polynomic interpolations restricted to adjacent elements (usually triangles or

quadrilateral elements in two dimensions). Interpolations can be lineal, quadratic or high order approximations. In fluid mechanic applications, at least quadratic interpolations are recommended in order to approximate the second order derivatives with enough accuracy.

Finite Volume Method

The Finite Volume Method divides the spatial domain of the physical problem in a finite number of not superimposed cells. In the unidimensional example shown in Fig. 2.10, P is the analysed cell and E-W the cells located at the right (east) and left (west), respectively. In these cells, the conservation of the $\emptyset$ discrete variable is applied. Taking the Eq. 2.5 and integrating it through the P control volume (see Fig. 2.10) Eq. 2.11 is deduced:

$$\int_w^e \left(\frac{d\emptyset}{dx}\right) dx + \int_w^e \emptyset \, dx = 0 \qquad (2.11)$$
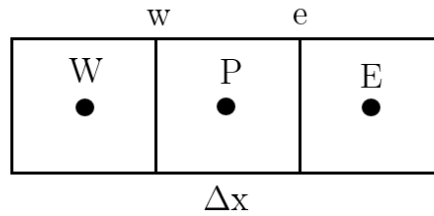
Figure 2.10. One-dimensional discretization by means of finite volumes (adapted from Fernández, 2012)

Finally, the Eq. 2.12 can be obtained from Eq. 2.11:

$$a_P \, \emptyset_P = a_E \, \emptyset_E + a_W \, \emptyset_W + b \qquad (2.12)$$

Being a_P, a_E, a_W the coefficients for the variables in each node. Similar equations can be obtained for each cell in the physical domain, giving rise to a new algebraic system of equations.

The FVM guarantees the conservation of the variable in each cell, i.e. the inlet flows and the outlet flows are equal. This property is fulfilled independently from the size of the cells. However, conservation and precision are not the same. In fact, the calculated solution for the transported variable can be conservative and imprecise at the same time if the mesh is too coarse. Main commercial software in the field use the FVM to numerically solve the governing equations for fluid mechanics.

2.4.2. Time discretization of the equations

In addition to spatial discretization of governing equations, if the physical problem is non-stationary, time discretization is needed. Generally, it can be stated that fluxes and source terms can be interpolated depending on the instant that are being evaluated by means of a f factor that vary between 0 and 1 following Eq. 2.13:

$$\int_{\Delta t} \vec{J} \cdot \vec{A} \, dt = \left(f J^n + (1-f) J^{n-1}\right) A \, \Delta t \tag{2.13}$$

Being $\vec{J} \cdot \vec{A}$ the flux in a face of the cell.

Explicit schemes

If $f = 0$, the numerical scheme is set to explicit since fluxes and source terms are evaluated using values from the beginning of the interval, i.e. values from the previous time step. This implies the following considerations:

- Explicit schemes are stable under specific numerical conditions (conditionally stable) and inherently contain an important limitation with respect to the maximum admissible time step of the CFD model (Δt_{max}).

- The maximum admissible time step is usually very small, especially in very convective flows, where Δt_{max} is set to $\Delta t_{max} < Co \, (\Delta x / c)$, being Co the Courant number, Δx the mesh size and c a velocity in the order of the velocity of the sound.

- In explicit schemes it is possible to evaluate the value of the transported variable in every cell and every time-step based on the values of the previous time-step. Therefore, is not necessary to solve any equation-system or to perform a matrix inversion, being the computational cost of these schemes small.

- On the other hand, due to the demanding stability criteria, a high number of iterations (high computational cost) are needed in explicit schemes.

Implicit schemes

If $f = 1$, the numerical scheme is set to implicit as fluxes and source terms are evaluated in the same instant when transported variables are calculated, i.e. in the current time step. In consequence:

- As the flux in each cell is evaluated in function of the values of adjacent cells, implicit schemes are more complex to solve. Those values could not be available depending on the sequence on which the spatial domain is being evaluated.

- Implicit schemes are usually unconditionally stable and a very large time step can be used.

- However, due to the non-linear behaviour of the Navier-Stokes equations, there are some restrictions regarding the maximum admissible time step of implicit schemes. Concretely, restrictions related to the physics of the problem and to the transient nature can overcome the mathematical restriction. In any case, the maximum time step of implicit schemes is always bigger than in the explicit ones.

- Additionally, the computational cost in implicit schemes is bigger as inversion of matrixes is needed in each time step.

A useful criterion to decide which kind of numerical scheme use for time discretization, is to calculate the value of the maximum time step, Δt_{max}, for mathematical and physical restrictions. If the maximum mathematical time step and the maximum physical time step are similar, then an explicit scheme is desirable. On the other hand, if the maximum physical time step is bigger than the maximum mathematical time step, an implicit scheme can be used for time discretization.

2.4.3. Meshing

As already mentioned, the generation of the mesh is one of the most important steps of a CFD model simulation. Every mesh created with the FVM discretizes the physical domain in a finite number of cells, constituting the fundamental unit of the grid. Every cell is associated to a centroid, and is bounded by a limited number of faces, which at the same time are defined by nodes (see Fig. 2.11).
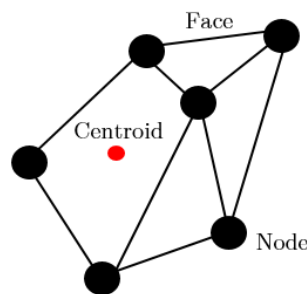
Figure 2.11. Scheme for a centroid, face and node of a computational cell

The connectivity type between cells of the computational grid defines the meshes in two categories: structured and non-structured. In the first ones (Fig. 2.12a), the group of cells is built based on a topological pattern that is reproduced in all directions of space. In non-structured meshes (Fig. 2.12b), the shape of the cells does not follow any preferential direction.
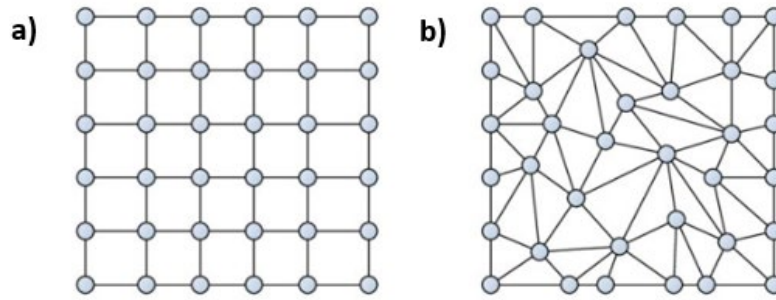
Figure 2.12. Examples of (a) a structured mesh and (b) a non-structured mesh (Aissa, 2017)

The development of non-structured meshes has been a consequence of the need of developing complex geometries in which it is not easy to adequate parallelepiped blocks to orthogonal meshes. Additionally, the use of this kind of computational grids leads to a significant time saving in the construction of models. On the other hand, in non-structured meshes, precision is reduced.

In any case, independently from the kind of mesh of the CFD model, it is essential to satisfy a set of requirements to obtain an adequate discretization (Fernández, 2012):

- The mesh must be generated according to the type of flow of the physical problem.

- A higher resolution (smaller cells) is needed in those zones where significant flow gradients are expected to appear.

- The mesh must be distributed in the most possible regular way across the computational domain.

- The resolution in the zones where the boundary layer is established must be in consonance with the turbulence and wall models applied.

- Singular elements such as very deformed and angular cells must be avoided.

- The total size of the mesh (number of elements) must be in concordance with the characteristics and capabilities of the computational-equipment where the CFD model is going to be solved.

One of the critical tasks in every CFD simulation is the loss of precision related to the use of non-structured meshes. In fact, although using high order numerical schemes (second- or higher-order spatial accuracy), if they are applied to meshes with high progressivity gaps (abrupt cell-size change), the schemes become automatically to first order ones. The first order numerical schemes give rise to significant errors. In fact, they are not recommended for transient problems and usually become a stationary problem very diffusive.

In addition to the mesh continuity, there are other factors related to the individual cells' distortion or their variation with respect to the ideal Cartesian cell that also imply loss of precision in CFD simulations. In this sense, parameters such as the aspect ratio ($\Delta x/\Delta y$) or the skewness factor (size of the angle between adjacent faces of a cell) are usually checked after any grid generation. Although it is not easy to quantify the effect of these parameters on the reliability of a numerical model, it must be taken into account that very distorted cells (high aspect ratio and high skewness factor) usually have a negative effect on the precision of the solution, and in consequence, on the convergence of any CFD model.

In resume, to obtain an adequate mesh quality, the following geometrical recommendations must be followed:

- The variation on the cells' size between the different zones of the computational domain must be progressive. Any abrupt change on the cells' size can reduce the local precision to zero order.

- The size variation of the mesh must be continuous in all directions.

- It is essential to eliminate, or at least minimize, the cells' distortion, avoiding wedge-shape or concave elements. If angles between cells' faces are too small (smaller than 20-30 degrees), there will be a significant loss on the reliability of the results.

All these recommendations are especially important in zones with significant flow gradients where high variations of the transported variables are expected.

2.4.4. Turbulence modelling

Introduction

Turbulence is an irregular and chaotic state of the movement of a fluid, created from irregularities in the initial or boundary conditions of a flow. These instabilities are amplified and also fed back in a cyclic way creating turbulent vortexes (eddies).

Turbulence is a characteristic of flows, not of fluids. Its appearance demands the existence of a fluid in movement, in which the convection phenomena (inertial) associated to velocity are various orders higher than the diffusive effects (dissipative) related to viscosity of the fluid. This relation is known as the Reynolds number (Re), and it sets the approximate border between laminar and turbulent flow. Non-turbulent flow can be found in many fluid transport applications, as well as in wastewater treatment systems in which calm conditions are desired, for example for the sedimentation of suspended solids in settling tanks. However, turbulent flow is usually desirable in bioreactors or compartments in which a good and intense mixing is required, as in wastewater treatment reactors where the contaminants of the water should come into contact with biological mass or chemicals.

The main characteristics of the turbulent nature of a flow are described next:

- <u>Randomness:</u> Also defined as irregularity, it emerges with the creation of fluctuations of fluid dynamic variables (velocity, pressure, temperature, concentration) with very different size and time scales. These instantaneous non-stationary variations are also developed in stationary flows (time averaged). The latter gives rise to the idea that statistical properties of flows are invariants. For this reason, statistical methods are used for the study and prediction of turbulence.

- <u>Vorticity:</u> The vorticity is essential to define a flow as turbulent. Every turbulent flow is rotational and with high vorticity levels that vary in time and space.

- <u>Diffusivity:</u> Also defined as mixing, turbulent phenomena intensify the mass, moment and energy transport as a result of the fluctuations at different scales. Particularly, fluctuations at macroscopic scales produce similar mixing effects to the pure molecular ones (only diffusive). Additionally, mixing lengths are similar to convective effects.

- <u>Three-dimensionality:</u> Smallest turbulence scales have an isotropic behaviour, and are consequently three-dimensional. Conversely, bigger turbulence scales, can also show two-dimensional or plane behaviour.

- <u>Dissipation:</u> Turbulent flows are always dissipative. By definition, they need to dissipate energy in the smallest scales. This energy and vorticity are obtained from the main flow and is redistributed to increasingly smaller scales by means of deformation processes. Once the turbulent flow is developed, the turbulence tends to be maintained by means of a continuum energy supply.

In resume, turbulence is a very complex phenomenon, formed by scales that can vary from the characteristic flow-length (a diameter or a characteristic length of the physical problem) to very small dissipative scales. Although being small scales, these are far from molecular length ones, and equations of fluid mechanics for the continuum can still be applied.

Numerical approximations to turbulence

The numerical solution for turbulent flows can be obtained through different approaches and with different levels of approximation. Depending on the size of scales aimed to solve in the simulation, i.e. the amount of turbulent kinetic energy transported in the constitutive equations, the detail of description of the flow should be higher or smaller.

Three main different approaches can be distinguished: Direct Numerical Simulations (DNS), Large Eddy Simulation (LES) and Reynolds Averaged Navier-Stokes (RANS).

- **Direct Numerical Simulations (DNS).** With the aim of solving every turbulent scale (Navier-Stokes equations for turbulent flow are solved directly), an extremely fine mesh must be used in this approach. In addition to this, the time step must guarantee the

description of the smallest turbulent scales. Approximately, the number of cells for a DNS simulation should be on the order of the Reynolds number to the power of 9/4. For that reason, DNS simulations cannot be used in a systematic way for industrial CFD problems, but they are very useful for pure academic research of turbulence.

- **Large Eddy Simulation (LES).** This modelling approach represents an intermediate technique between DNS and RANS. In this case, meshes are coarser than in DNS and allow to solve biggest turbulent scales (those which transport between 50 and 80% of all the turbulent kinetic energy). Conversely, smallest turbulence scales are modelled since they are nearly isotropic, homogeneous and universal, and less influenced by boundary conditions than the macroscale. Mathematically, LES techniques use a spatial averaging of transport equations by means of a filter defined as Δ. This works as a border between macroscales to be solved and microscales to be modelled. Although quite fine meshes are used in LES, being coarser than in DNS allows to solve industrial flows with high Re numbers.

- **Reynolds Averaged Navier-Stokes (RANS).** The RANS simulation is the most used method to introduce the modelling of turbulence. In this case, all scales are modelled by means of different turbulence models. In RANS simulations, an operator is used to find the statistical behaviour of the different flow variables. In order to separate the average value from the fluctuant one, this operator introduces a time averaging to the transported variables. It is important to note that the average flow is referred to the part with no turbulent fluctuations, which value does not strictly need to be stationary. As an effect of the fluctuations in the average behaviour of transported variables, an additional term, named as Reynolds stress, appears in the modelling process. In the last decades various turbulence models have been developed to replace those unknown Reynolds stresses with other mathematical relations to avoid to introduce more unknown variables to the problem.

  In spite of the assumed simplifications, RANS simulations are commonly used for engineering applications since they are able to explain and successfully reproduce the most part of the turbulent flows, even the most complex ones. However, the greatest drawback of RANS modelling is the need for modelling every scale of turbulence. As explained before, while microscale phenomena are highly isotropic and universal, macroscale turbulence is influenced by boundary conditions and characteristic dimension of the flow. Therefore, it is tough to find a single turbulence model able to reproduce and simulate the different phenomena at micro and macro scales at the same time. For that reason, different turbulence models have been developed for RANS simulations, aiming to describe different type of flows.

Turbulence models for RANS equations

k-epsilon model ($k - \varepsilon$)

The simplest method to simulate the turbulence is based in two equations. In that way, the independent resolution of turbulent velocities and length scales is enabled. Among the family of models with two equations, the k-epsilon (Launder and Spalding, 1972) is the most used one for industrial CFD and engineering applications as it is robust, economic and reasonably precise for a wide variety of turbulent flows.

Due to its massive popularity during the last decades, variations to the standard formulations have been developed, e.g. RNG k-epsilon (Yakhot et al., 1992) and Realizable k-epsilon (Shih et al., 1995).

The standard k-epsilon model is a semi-empirical model based on two equations that model the transport equation for the turbulent kinetic energy, k, and its dissipation rate, ε. The transport equation for the turbulent kinetic energy is obtained by means of its exact equation, and the dissipation rate is deduced from physical reasoning and analogies with k. Therefore, the turbulent dissipation rate determines the scale of the turbulence, and the turbulent kinetic energy is the variable that fixes the energy of turbulence.

Model closure equations for the standard k-epsilon model are expressed next (Eqs 2.14-2.15):

$$\frac{\partial(\rho k)}{\partial t} + \frac{\partial}{\partial x_i}(\rho k v_i) = \frac{\partial}{\partial x_j}\left[\left(\mu_l + \frac{\mu_t}{\sigma_k}\right)\frac{\partial k}{\partial x_j}\right] + G - \rho\varepsilon \tag{2.14}$$

$$\frac{\partial(\rho \varepsilon)}{\partial t} + \frac{\partial}{\partial x_i}(\rho \varepsilon v_i) = \frac{\partial}{\partial x_j}\left[\left(\mu_l + \frac{\mu_t}{\sigma_\varepsilon}\right)\frac{\partial \varepsilon}{\partial x_j}\right] + C_{1\varepsilon}\frac{\varepsilon}{k}G - C_{2\varepsilon}\rho\frac{\varepsilon^2}{k} \tag{2.15}$$

in which k is the turbulent kinetic energy, ε is the turbulent kinetic energy dissipation rate, G is the production rate of turbulent kinetic energy, σ_k, σ_ε, $C_{1\varepsilon}$ and $C_{2\varepsilon}$ are the k-ε model standard constants, and μ_t is the turbulent viscosity defined by Eq. 2.16:

$$\mu_t = \rho C_\mu \frac{k^2}{\varepsilon} \tag{2.16}$$

Numerical values for the constants are:

$$C_\mu = 0.09 \quad C_{1\varepsilon}=1.44 \quad C_{2\varepsilon}=1.92 \quad \sigma_k=1.0 \quad \sigma_\varepsilon = 1.3$$

k-omega model ($k - \omega$)

The k-omega model was originally developed by Wilcox (1988), and adds some modifications to the fundamentals of k-epsilon turbulence models in order to make them more appropriate for flows with small Re numbers. The transport equation for k is maintained with a similar formulation and a new one is added for the specific dissipation rate, named ω and defined as the relation between ε and k.

It has been demonstrated that the k-omega model is adequate for transient flow problems, even under the influence of high-pressure gradients. Additionally, a complementary model was developed by Menter (1994) and named k-omega SST, which is recommended for transition zones between the boundary layer (where standard k-omega is adequate) and the free surface (zone without turbulence, successfully modelled by k-epsilon models).

The closure equations for this model are defined below (Eq. 2.17-2.18):

$$\frac{\partial(\rho k)}{\partial t} + \frac{\partial}{\partial x_i}(\rho k v_i) = \frac{\partial}{\partial x_j}\left[\left(\mu_l + \frac{\mu_t}{\sigma_k}\right)\frac{\partial k}{\partial x_j}\right] + G - \rho \beta^* f_{\beta^*} k\omega \tag{2.17}$$

$$\frac{\partial(\rho \omega)}{\partial t} + \frac{\partial}{\partial x_i}(\rho \omega v_i) = \frac{\partial}{\partial x_j}\left[\left(\mu_l + \frac{\mu_t}{\sigma_\varepsilon}\right)\frac{\partial \omega}{\partial x_j}\right] + \alpha \frac{\omega}{k} G - \rho \beta f_\beta \omega^2 \tag{2.18}$$

in which k is the turbulent kinetic energy, ω is the specific turbulent kinetic energy dissipation rate, G is the production rate of turbulent kinetic energy, α, β, $C_{1\varepsilon}$ and β^* are the k-omega model standard constants , f_{β^*} and f_β are functions related to those constants and μ_t is the turbulent viscosity defined by Eq. 2.19:

$$\mu_t = \alpha^* \rho \frac{k}{\omega} \tag{2.19}$$

Being α^* is a mathematical function for correction. It is based on the Re number and is responsible for eliminating the turbulent viscosity when Re is very low.

2.4.5. Boundary conditions

To define a CFD simulation it is necessary to set the initial and boundary conditions of the problem. Additionally, it is important to develop numerical algorithms to preserve the physical sense and the mathematical influence of the governing equations. In CFD problems, initial conditions are mandatory as they set the starting point of any problem. Their implementation is automatic with the initialization of all the variables in every point of the computational domain. On the other hand, boundary conditions are spatial conditions and their study is more demanding. Next, some features of the most common boundary conditions in CFD simulations are introduced.

Inlet boundary condition is usually set in most CFD codes by the definition of the average velocity perpendicular to the inflow surface. Sometimes, a velocity distribution along that surface is defined, and if the average flow is unknown, a value for pressure can be set at the inlet boundary patch. Additionally, scalars as temperature or transported species are set as temperature and mass fractions in the inflow boundary.

Regarding **outlet boundaries**, in order to guarantee the stability of the simulation, they must be located far from geometrical perturbations and preferably where the flow is totally developed or at least stable. In addition, outlet boundary conditions are set perpendicular to the direction of the flow, forcing the gradients of the variable being null in that direction. In general, the pressure outlet boundary condition is defined as the default boundary for outflow physics,

setting its numerical value to zero. Velocity outlet boundary is rarely used in CFD simulations, as it hinders the mass conservation, destabilizing the convergence.

A no-slip boundary condition is usually defined as **wall boundary condition** in a physical problem, which sets the relative velocity between the wall and the fluid to zero.

Symmetry boundaries are set in a contour if there is no flow through it or if scalar transport is not allowed across the surface. To implement this boundary condition in the code, perpendicular velocities to the symmetry surface must be set to zero. **Slip** boundaries are also used when a flux across a surface is not expected but the velocity is not equal to zero, e.g. the free surface in a tank (avoiding, for instance, a two-phase water-air simulation).

2.5. <u>Computational Fluid Dynamics in Water Treatment applications</u>

The use of CFD in wastewater treatment processes is rapidly growing and is being applied in the resolution of complex problems (Samstag et al., 2016; Wicklein et al., 2015). Next, some interesting examples with respect to the topic of this thesis are highlighted.

Regarding the hydrodynamic behaviour, combination of RTD and CFD for reactor analysis and optimization has been previously applied for different treatment units. Brannock et al. (2010a-b) developed a CFD model for two full scale membrane bioreactors (MBR) and validated the hydrodynamics with experimental RTD tests. Besides, short-circuiting and dead zones were analysed and optimization of reactors was carried out in this study. Climent et al. (2018) used RTD tests to validate the hydrodynamic behaviour of a secondary treatment process consisting on a two-stage unit formed by an aerobic and a double anoxic reactor. ASM1 was added to the overall model and geometrical optimization of the original configuration was successfully carried out. Plascencia-Jatomea et al. (2015) developed a CFD model for a novel MABR and validated the hydrodynamics with experimental RTD tests. Velocity profiles inside the reactor were then analysed and results showed that in the central part of the MABR the mass transport was much higher than in the outer part. Terashima et al. (2009) studied the mixing performance of an anaerobic digester and used RTD tests to validate the hydrodynamic performance of the analysed reactor.

Hydrodynamics in stirred reactors has also been modelled and analysed for several configurations. Besides, different approaches can be undertaken for a correct representation of impellers with CFD techniques. Bridgeman (2012) used the Multi Reference Frame (MRF) method to simulate the rotation of two impellers in a lab-scale anaerobic digester and to evaluate its mixing performance. Bai et al. (2008) also used the same approach to simulate the effect of a three-stage agitation system on a 110 m^3 industrial-scale reactor with plunging jet inlet. The main goal of this study was to evaluate the flow patterns by means of RTD tests. In addition to MRF approach, the momentum source approach is a classical simplification that allows a significant computational resource saving and has been widely and successfully used in the wastewater field. In this context, Brannock (2003) used this approach to simulate the

effect of the location and direction of three stirrers on the biological and hydrodynamic performance of a mixed anoxic wastewater treatment vessel. Climent et al. (2018) also varied the position and direction of two impellers located in the anoxic zone of a two-stage anoxic-aerobic activated sludge process in order to optimize the hydrodynamic and biological performance of the treatment unit. In a subsequent work, Climent et al. (2019) performed a comprehensive analysis of a full-scale oxidation ditch and applied again the momentum source approach to reproduce the influence of the stirrer on the treatment process. Rehman (2016) modelled an oxidation ditch located in La Bisbal d'Emporda (Spain) and also used the momentum source approach to simulate the hydrodynamic influence of the stirrers.

Regarding the hydraulic optimization of water treatment systems, the hydrodynamic performance is commonly assessed through hydraulic indexes (Demirel et al. 2018). The optimization process usually consists in the evaluation of the hydraulic performance through dimensionless indexes for different geometrical configurations. These dimensionless indexes evaluate several hydrodynamic features such as short-circuiting, mixing efficiency or dead volumes, based on the analysis of the RTD or the results of model simulations. Examples of hydrodynamic optimization of water treatment systems using CFD simulations and hydraulic indexes can be found in literature for different water treatment units. Demirel et al. (2016, 2018) and Angeloudis et al. (2014) used CFD to test different geometries of disinfection contact tanks and assessed their hydrodynamic behaviour by means of short-circuiting and mixing hydraulic indexes. Gualteri et al (2009) tested the influence of the location of geometry of different baffles inside a water storage tank with CFD and evaluated the level of channelling and mixing degrees by means of hydraulic benchmarking parameters. Chang et al. (2016) and Rengers et al. (2016) evaluated the hydraulic efficiency of constructed wetlands by means of a hydraulic efficiency index (Persson et al., 1999) and also using additional indexes for the assessment of dead volumes, short-circuiting and mixing, all of them obtained through CFD simulations. Additionally, Latratch et al. (2018) carried out the optimization of a Multi-Soil-Layering (MSL) technology following an analogue procedure. The previously mentioned research performed by Climent et al. (2018) also used CFD and hydraulic indexes to evaluate the stagnant volumes of the new configurations for an anoxic-aerobic reactor sequence. Yan et al. (2015, 2016) evaluated the influence of the horizontal geometry and baffles on the shear stress caused by cross flow on membrane of an MBR. However, the optimization procedure applied in each case is different and hydraulic indexes are used separately without any standardization. A systemic methodology capable to join multiple features could aid in the hydrodynamic evaluation and optimization of multi-environment bioreactors, guaranteeing the best possible biological performance.

In addition, a lack of hydrodynamic optimization studies regarding multi-environment reactors has been noticed in the literature. Their complex hydraulic behaviour generates non-ideal flows that reduces the hydrodynamic performance, and in consequence, the biological efficiency. To our knowledge, there are only few studies based on CFD for evaluation and optimization of the hydrodynamics of multi-environment reactors. In this sense, Calder et al. (2013) changed a baffle geometry to assess the hydraulic behaviour of the aerobic-anoxic BioCAST reactor based on velocity fields, but did not use a systematized methodology of hydraulic indexes.

Finally, it must be pointed out that, to our knowledge, all the studies aforementioned are carried out with commercial codes. In this sense, the development of an open source model would give the possibility to share, modify and study the source code and adapt it to different problems within the field.

2.6. Final remarks and conclusions

In this section, a summary of the main ideas reported in the state of art is carried out along with some conclusions.

Many existing WWTP need to modify their configurations for nitrogen and phosphorus removal in order to fulfil current water quality regulations (European Union, 1991; European Union, 2000). However, conventional BNR processes entail complex treatment trains that give rise to a high energy consumption and derive in a larger volume (aerobic, anoxic and anaerobic tanks) that in many cases is not available on site.

To overcome this limitations, multi-environmental biological reactors represent an innovative alternative to simplify conventional BNR as they aim to combine different environmental conditions (aerobic, anoxic and/or anaerobic) in a single reactor (Kwon et al., 2005; Yerushalmi et al., 2011; Tejero et al., 2010; Ahn et al., 2003; Song et al., 2009). This approach generates innovative solutions with high compactness and efficiency. Concretely, AnoxAn (Tejero et al., 2010) is of especial interest as it is able to join the main features of the other configurations studied in the state of art (is a multi-environment reactor (anaerobic-anoxic) with upflow sludge blanket operation and encouragement of denitrifying phosphate uptake). Although the biological feasibility of this reactor has been proven at pilot scale (Díez-Montero et al., 2016), the need for a deeper hydrodynamic analysis was pointed out in order to develop optimized and scalable configurations.

Bioreactors can be studied by means of experimentation and/or modelling. In fact, modelling is usually coupled with experimental analysis in order to support in any process design and optimization. There can be distinguished two main modelling approaches for wastewater treatment units: (i) biokinetic modelling (biological and chemical reactions of processes) and (ii) hydrodynamic modelling (behaviour of the fluid flow inside the treatment units). While biokinetic modelling has been widely used for wastewater process conception and design, hydrodynamic analysis has been less applied within the field. In fact, conventional dimensioning of BNR processes suppose ideal complete mixing flow in reactors (DWA, 2000; Water Environment Federation, 2011), neglecting the hydrodynamic phenomena that interfere in ideal flow conditions. However, several studies have shown that a correct hydrodynamic behaviour enhances a desirable biological efficiency in bioreactors for water treatment (Castrillo et al., 2019; Angeloudis et al., 2014; Climent et al., 2018; Arnaldos et al., 2018; Wei et al., 2019; Water Environment Federation, 2011). Hence, as previously highlighted for AnoxAn, hydrodynamics must also be deeply studied to achieve an optimum bioreactor design.

Hydrodynamic modelling has been usually carried out by means of compartment-based models based on combination of CSTR and PRF reactors (Levenspiel, 1999). Although feasibility of compartment-based models to simulate the overall hydrodynamic behaviour and biological operation of water treatment units have been demonstrated (Pons et al., 1993; Cheng et al., 1999; Ayesa et al., 2006; Díez-Montero et al., 2015; Plascencia-Jatomea et al., 2015; Rehman, 2016), some important limitations of this approach have been pointed out such as (i) the difficulty to adapt to geometrical and operational variations and (ii) the impossibility to perform a detailed hydrodynamic analysis (flow patterns inside compartments are unknown).

In this context, CFD represents an advanced tool to perform numerical simulation of fluid flows and has been already used in a wide variety of industries. Within this approach, constitutive equations for fluid mechanics are solved and comprehensive and almost unlimited analysis of flows can be carried out. Further, additional physics can be combined with hydrodynamic such as combustion or chemical reactions. Due to the advantages of this modelling approach, CFD has already been applied to many wastewater treatment processes (Samstag et al., 2016; Wicklein et al., 2015). However, a lack of hydrodynamic and optimization studies regarding multi-environment reactors has been noticed (Calder et al. 2013).

Additionally, regarding the hydrodynamic optimization of water treatment processes, many examples have been reported in literature for a wide variety of applications (Demirel et al., 2016, 2018; Angeloudis et al., 2014; Gualteri, 2009; Chang et al., 2016; Rangers et al., 2016; Latratch et al., 2018; Climent et al., 2018; Yan et al., 2015, 2016). Nevertheless, the optimization procedures applied in each case are different and hydraulic indexes are used separately without any standardization.

All the aforementioned studies were carried out with commercial codes. In this sense, the development of an open source model would give the possibility to share, modify and study the source code and adapt it to different problems within the field.

In conclusion, the revision of the state of knowledge shows that although **AnoxAn** has appeared to be **a promising and efficient multi-environment technology** within the BNR field, previous research has evidenced the **need for deepening into the analysis of its complex hydrodynamic behaviour**. For that purpose, **CFD** represents an **advanced modelling tool** that is able to perform an exhaustive hydrodynamic assessment of water treatment processes, which cannot be achieved with experimental or compartment-based models. In addition, examples in the literature show that an **optimum hydrodynamic performance of bioreactors is essential** to guarantee a desired biological efficiency. However, optimization studies found in literature do not use any specific methodology. At this aim, a **standardized hydrodynamic optimization methodology** for multi-environment bioreactors would be **useful to assist in the design** and assessment of new and novel configurations. Finally, a detailed hydrodynamic analysis of AnoxAn would also help to **cover the lack of CFD** studies in literature **regarding multi-environment reactors**.

Chapter 3

Scope and objectives

Based on the findings and conclusions of the state of art, the initial assumptions of this research are the following:

(i)   The **AnoxAn reactor has promising environmental and energetic advantages**, and its viability for Biological Nutrient Removal (BNR) has been already demonstrated at pilot scale.

(ii)   The **numerical techniques based on Computational Fluid Dynamics (CFD)** are an essential tool for the hydrodynamic analysis, optimization and application at industrial scale of complex bioreactors.

(iii)   A **correct hydrodynamic behaviour** of wastewater treatment bioreactors enhances an **efficient biological performance**.

However, four significant gaps have been identified in the literature:

(i)   There is a need for a **deeper hydrodynamic analysis of the AnoxAn reactor** in order to develop optimized and scalable configurations.

(ii)   There is a lack of **comprehensive hydrodynamic and optimization CFD studies regarding multi-environment reactors.**

(iii)   The hydrodynamic optimization studies found in literature do not use a **standardized hydrodynamic optimization methodology.**

(iv)   Most of the **reviewed studies** were carried out with **commercial codes**, not allowing for sharing, modifying and studying the source code and adapting it to different problems within the field.

Having the aforementioned into account, the hypotheses of this thesis are:

H1) The availability of an open source numerical tool based on CFD would aid in the hydrodynamic evaluation and optimization of complex bioreactors such as multi-environment bioreactors for BNR from wastewater, and would serve as a base for different processes and future developments, being free and available for the research community.

H2) A comprehensive hydrodynamic analysis of the AnoxAn reactor based on CFD would lead to a better understanding of its complex hydrodynamic behaviour and would be relevant for the optimization and future design of large-scale reactor implementations.

H3) A standardized hydrodynamic optimization methodology combining the potentialities of CFD with dimensional analysis can be proposed for multi-environment bioreactors and would overcome the non-standardized nature of the hydrodynamic optimization procedures observed in literature.

H4) The influence of the hydrodynamic behaviour and optimization over the biological performance of a multi-environment reactor, including features such as removal efficiencies, spatial distribution of species and hydraulic separation, is significant and can be predicted and quantified using advanced models combining CFD and biokinetics.

3.1. <u>Objectives</u>

Based on the gaps found in the literature and the hypotheses of this work, the main research objectives of this thesis are presented below.

3.1.1. General objective

- To comprehensively analyse and optimize the hydrodynamic behaviour of multi-environment bioreactors through the development of an open source three-dimensional numerical model based on CFD, validated and applied to the anaerobic-anoxic AnoxAn reactor.

This general objective is specified in the following specific objectives.

3.1.2. Specific objective 1

Development of an open source numerical tool based on CFD for the hydrodynamic analysis of multi-environment reactors.

As reported in the revision of the state of art, to our knowledge, most of the CFD studies applied to water treatment are carried out with commercial codes. At this respect, the consecution of this first objective allows to develop an open source numerical tool based on CFD for the hydrodynamic analysis of multi-environment reactors. Although in the framework of this thesis the CFD tool is applied to the specific case of AnoxAn, this numerical model aims to serve as a base for different processes and future developments. For that purpose, the numerical CFD tool is built in the open source toolbox OpenFOAM®.

Regarding multi-environment bioreactors, the CFD tool needs to contain the following features and/or sub-models:

- o Hydrodynamic model for turbulent flow based on Reynolds Averaged Navier-Stokes (RANS) equations to simulate the fluid mechanics inside reactors.

- o Tracer transport model for turbulent flow with the aim of validating the reactors' hydrodynamics with experimental RTD tests.

- o Biological kinetics in order to assess the hydrodynamic effect on the biological performance of multi-environment reactors. In the specific case of AnoxAn, nitrate transport along with denitrification kinetics are needed.

o Porous media model. Baffle and deflectors are essential elements to maintain the hydraulic separation between different environments and usually, their 3D complex geometries give rise to computational domains with excessive elements. To overcome this issue, the equivalent head loss produced by these elements can be generated with a porous media model. Alternatively, a porous media can also be part of multi-environment reactors.

o Impeller model. The impeller or mixing devices play a key role in stirred reactors' hydrodynamics and their influence needs to be faithfully reproduced.

It must be pointed out that the original OpenFOAM® code does not include some of these features, and for that reason, these attributes need to be added to the toolbox. Finally, it is important to highlight that the numerical tool developed within the framework of this thesis does not consider the influence of the solid phase on the density of the fluid. Although this is not a completely realistic approach, this study aims to work as a base for future developments and research studies. Introducing the interaction of the biomass with the bulk liquid in the model is out of the scope of this research.

3.1.3. Specific objective 2

Model construction, validation and hydrodynamic analysis of the AnoxAn anaerobic-anoxic multi-environment reactor based on CFD.

Based on the CFD model constructed within the framework of the first specific objective, the consecution of this second objective allows to (i) develop and validate a CFD model of the novel anaerobic-anoxic AnoxAn reactor and (ii) deeply analyse its complex hydrodynamic behaviour. At this aim, key features of the reactor configuration that cannot be evaluated through conventional Residence Time Distribution (RTD) experimental procedures and compartment-based models are assessed, supposing a step forward compared to previous research about AnoxAn. These results are relevant for the optimization and future design of large-scale reactor implementations. In addition, modelling and simulation of reactor elements such as impellers or baffles provide a deeper hydrodynamic understanding that could be applied for the development and optimization of other multi-environmental reactors and conventional water treatment reactors.

- **Objective 2.1: Construction and simulation of a numerical model based on CFD for AnoxAn.**

  Generation of the geometry, meshing, implementation of the boundary conditions, setting the turbulence model, defining the transport physics and simulation of the complete model of the reactor.

- **Objective 2.2: Validation and hydrodynamic analysis of the CFD model.**

  Validation of the CFD model by means of tracer tests, and hydrodynamic analysis of the results. The main goal in this task is to go a step forward than the previous hydrodynamic research carried out with experimentation and compartment-based models in AnoxAn, i.e. location and quantification of flow patterns that interfere in the ideal-flow behaviour such as dead volumes and short-circuiting, along with the assessment of the influence of different elements such as deflectors and baffles in the hydrodynamic behaviour of AnoxAn.

3.1.4. Specific objective 3

Hydrodynamic optimization of multi-environment reactors for biological nutrient removal.

On one hand, the fulfilment of this objective allows to propose a standardized hydrodynamic optimization methodology for bioreactors combining the potentialities of CFD with dimensional analysis, capable to unify multiple hydraulic features with a benchmarking approach. On the other hand, this objective helps to cover the lack of CFD studies in literature regarding multi-environment reactors, extending and applying the proposed methodology to AnoxAn.

- **Objective 3.1: Development of a methodology for the hydrodynamic optimization of multi-environment reactors.**

  In order to overcome the non-standardized nature of the hydrodynamic optimization procedures reported in the state of knowledge, a hydrodynamic optimization methodology for multi-environment bioreactors combining CFD and dimensional analysis is developed within this objective. This methodology aims to integrate the evaluation of the different hydraulic features observed in the literature such as dead volumes, short-circuiting, mixing performance and hydraulic separation between environments in a standardized procedure.

- **Objective 3.2: Application of the hydrodynamic optimization methodology to AnoxAn.**

  In order to test the viability of the developed hydrodynamic optimization methodology, the latter is applied to the optimization of AnoxAn. For that, CFD models for different configurations and geometries of the reactor are built, simulated and evaluated. As a result, the optimized configuration of AnoxAn along with more insights regarding the hydrodynamic behaviour of the process (dead volumes, short-circuiting, mixing performance, hydraulic separation) are obtained.

3.1.5. Specific objective 4

Evaluation of the influence of the hydrodynamic behaviour in the biological performance of AnoxAn.

The fulfilment of this objective allows to assess the relation between the hydrodynamic performance and the biological efficiency in AnoxAn, which has been already observed for other water treatment processes in the revision of the literature. In other words, the goal is to evaluate and quantify how a configuration with better hydrodynamic operation ensures a more desirable biological performance (lower nitrate concentration at the outlet), along with the assessment of the influence of the flow field on the nitrate transport and its concentration distribution in the reactor. At this respect, the effect of the hydrodynamic phenomena observed within the framework of previous objectives (short-circuiting, mixing, hydraulic separation) must also be evaluated for the nitrate transport.

In short, this objective aims to: (i) assess the efficiency of nitrate removal, (ii) analyse the spatial distribution of nitrate in the reactor and (iii) evaluate the hydraulic separation between the anoxic and anaerobic zones including the influence of the denitrifying activity.

Chapter 4

Development of the numerical tool and implementation in OpenFOAM®

4.1. Introduction

In this chapter, the numerical setup of the Computational Fluid Dynamics (CFD)-based tool used in the thesis is presented. This CFD model is built in OpenFOAM® (**Open**-source **F**ield **O**peration and **M**anipulation), which is a free of charge and open source finite volume based toolbox. OpenFOAM® was originally created in the Imperial College (Jasak et al., 1996; Weller et al., 1998) with the aim of developing customized numerical solvers for CFD applications. It also includes additional features for model pre-processing such as meshing tools (blockMesh, snappyHexMesh), along with default applications or post-processing software as ParaView (see Fig. 4.1). The code is written in C++, is object oriented and is structured in a modular way.
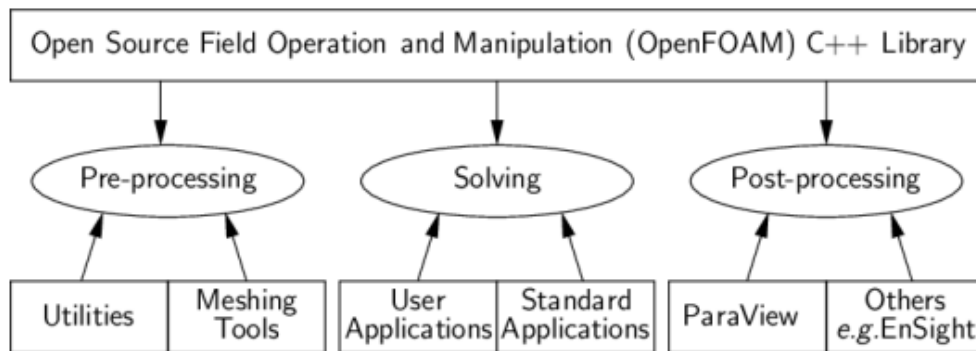
Figure 4.1. General overview of OpenFOAM® structure (www.openfoam.com)

Unlike most commercial CFD codes, OpenFOAM® is not a black box. This means that it allows users to control each stage of the modelling process by modifying the source code without any restriction. This fact enables to develop customized solvers for particular engineering problems, including governing equations, boundary conditions, incorporation of new physics and/or solving procedures.

At this respect, it must be highlighted that the original source code of OpenFOAM® is not prepared to deal with all the physics concerning this research. Concretely, it does not include some essential features for this study such as tracer transport for turbulent flow or denitrification kinetics. In the same way, existing algorithms need to be adapted to solve these new transport equations. For that reason, in order to fulfil all the objectives and the scope of this work, all the aforementioned attributes need to be added to the original source code of OpenFOAM®.

All in all, this chapter is structured as follows. First, the mathematical formulation for all the physical phenomena included in the model (hydrodynamics, tracer transport, bio-kinetics and singular elements) is defined. Subsequently, the different adapted algorithms used for solving the aforementioned constituent equations are described, and finally, the numerical implementation of the custom model in the code is presented.

4.2. <u>Description of the numerical tool</u>

The revision of the literature (Chapter 2) has shown that an optimum hydrodynamic behaviour enhances a correct biological performance of water treatment processes. For that reason, the main goal of this study is to comprehensively analyse and optimize the hydrodynamic behaviour of multi-environment bioreactors through the development of an open source three-dimensional numerical model based on CFD, validated and applied to the anaerobic-anoxic AnoxAn reactor (see Chapter 3). Having the aforementioned into account, the model built in this research solves the three-dimensional Reynolds Averaged Navier-Stokes (RANS) equations for turbulent flow in a single phase (water) by means of the Finite Volume Method (FVM). Concretely, the numerical tool developed consists in two different solvers (see Table 4.1):

- **stationaryDesnitriEqn**. Used for stationary simulations and constructed based on the simpleFOAM application from OpenFOAM®.

- **transientDesnitriEqn**. Used for transient simulations and constructed based on the pimpleFOAM application from OpenFOAM®.

Both solvers add to the original source code of OpenFOAM® the tracer transport for turbulent flow, the nitrate transport and denitrification biokinetics for turbulent flow, and a porous media model. Additionally, the solvers also incorporate different default models existing in OpenFOAM® such as the hydrodynamic model, the turbulence model and the applications to simulate the effect of the impeller. All mathematical formulation is presented in section 4.3. Moreover, default algorithms of the solvers are also adapted to solve all the added features, and are described in section 4.4.

Table 4.1. Summary of main features of the custom numerical tool

Custom solver	Original OpenFOAM® solver	Existing features in OpenFOAM®	Added features
stationaryDesnitriEqn	simpleFOAM	Hydrodynamic model	Tracer transport
		Turbulence model	Nitrate transport
		Impeller model	Porous media
transientDesnitriEqn	pimpleFOAM	Hydrodynamic model	Tracer transport
		Turbulence model	Nitrate transport
		Impeller model	Porous media

It must be highlighted that this numerical tool does not take into account the influence and effect of the biomass on the density of the fluid. Concretely, in all the simulations performed within the frame of this work, the density of the fluid does not change in time and space. Although this is not a realistic approach, as a first step, it will help to assess the relation between the complex hydrodynamic behaviour of multi-environment reactors and the biological efficiency of processes. Introducing the interaction of the biomass with the bulk liquid in the model is out of the scope and main objectives of this research.

4.3. <u>Governing equations and models</u>

4.3.1. Hydrodynamic model

Hydrodynamics of AnoxAn are simulated solving Navier-Stokes equations for turbulent and incompressible flow.

Numerical resolution of turbulent flows can be achieved through different approaches with several approximation degrees. As introduced in the state of the art (Chapter 2), RANS simulation is the most widely used approach in engineering due to its relative simplicity and lower computational cost. In RANS simulation, all turbulent scales are simulated by modelling, introducing a time averaging to the variables in order to separate their ensemble value and the fluctuant one.

RANS equations include continuity (Eq. 4.1) and momentum conservation (Eq. 4.2) equations, linking the pressure and the velocity.

$$\frac{\partial v_i}{\partial x_i} = 0 \tag{4.1}$$

$$\frac{\partial v_i}{\partial t} + v_j \frac{\partial v_i}{\partial x_j} = -\frac{1}{\rho}\frac{\partial P}{\partial x_i} + (\mu_l + \mu_t)\frac{\partial}{\partial x_j}\left(\frac{\partial v_i}{\partial x_j} + \frac{\partial v_j}{\partial x_i}\right) + g_i + f_{baffle} \tag{4.2}$$

where v_i is the ensemble velocity vector, ρ is the fluid density, μ_l is the fluid dynamic viscosity, μ_t is the eddy viscosity, P is the pressure, g_i is the gravitational acceleration and f_{baffle} the resistant force (F_{baffle}) produced by the baffle per unit of volume normalised by density.

In addition, model closure equations are needed for the turbulent stress tensor: In this work standard k-ε model (Launder and Spalding, 1972) is used (Eqs. 4.3-4.4):

$$\frac{\partial(\rho k)}{\partial t} + \frac{\partial}{\partial x_i}(\rho k v_i) = \frac{\partial}{\partial x_j}\left[\left(\mu_l + \frac{\mu_t}{\sigma_k}\right)\frac{\partial k}{\partial x_j}\right] + G - \rho\varepsilon \tag{4.3}$$

$$\frac{\partial(\rho\varepsilon)}{\partial t} + \frac{\partial}{\partial x_i}(\rho\varepsilon v_i) = \frac{\partial}{\partial x_j}\left[\left(\mu_l + \frac{\mu_t}{\sigma_\varepsilon}\right)\frac{\partial\varepsilon}{\partial x_j}\right] + C_{1\varepsilon}\frac{\varepsilon}{k}G - C_{2\varepsilon}\rho\frac{\varepsilon^2}{k} \tag{4.4}$$

in which k is the turbulent kinetic energy, ε is the turbulent kinetic energy dissipation rate, G is the production rate of turbulent kinetic energy, σ_k, σ_ε, $C_{1\varepsilon}$ and $C_{2\varepsilon}$ are the k-ε model standard constants, and μ_t is the turbulent viscosity defined by Eq. 4.5:

$$\mu_t = \rho C_\mu \frac{k^2}{\varepsilon} \tag{4.5}$$

Numerical values for the constants are:

$$C_\mu = 0.09 \quad C_{1\varepsilon}=1.44 \quad C_{2\varepsilon}=1.92 \quad \sigma_k=1.0 \quad \sigma_\varepsilon = 1.3$$

4.3.2. Tracer transport model

For tracer test simulation, the resolution of a transport equation without chemical reaction is modelled in the software. The tracer is assumed to behave as a passive scalar with no effect in local hydrodynamics.
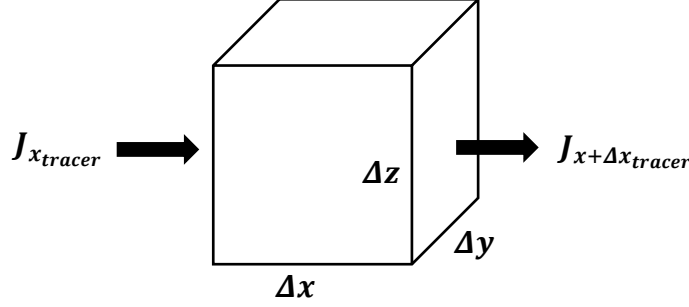
Figure 4.2. Tracer mass balance in the control volume

Supposing the tracer concentration variable, m_k, a control volume (CV) of $\Delta x, \Delta y, \Delta z$ dimensions is defined as shown in Fig. 4.2. $J_{x_{tracer}}$ represents the net flux of the transported variable across the x axis in the CV. In this case m_k is transported, and the flux is expressed as $J_{x_{tracer}} = \left(\rho u m_k - \Gamma \frac{dm_k}{dx} \right)_x$. The flux is then defined for the three axes. Applying the mass conservation principle, the time variation of the tracer inside the CV is described in Eq. 4.6:

$$\begin{bmatrix} Tracer\ increase\ in\ CV \\ respect\ to\ time \end{bmatrix} = \begin{bmatrix} Tracer\ net\ flow \\ in\ the\ CV \end{bmatrix} + \begin{bmatrix} Tracer\ net\ generation \\ in\ the\ CV\ respect\ to\ time \end{bmatrix} \qquad (4.6)$$

Each term of Eq. 4.6 is mathematically rewritten in Eq. 4.7:

$$\frac{(\rho m_k)_{t+\Delta t} - (\rho m_k)_t}{\Delta t} = \frac{\left(\rho u m_k - \Gamma \frac{dm_k}{dx} \right)_x - \left(\rho u C_{NO_3} - \Gamma \frac{dm_k}{dx} \right)_{x+\Delta x}}{\Delta x}$$

$$+ \frac{\left(\rho v m_k - \Gamma \frac{dm_k}{dy} \right)_y - \left(\rho v C_{NO_3} - \Gamma \frac{dm_k}{dy} \right)_{y+\Delta y}}{\Delta y}$$

$$+ \frac{\left(\rho w m_k - \Gamma \frac{dm_k}{dz} \right)_z - \left(\rho w C_{NO_3} - \Gamma \frac{dm_k}{dz} \right)_{z+\Delta z}}{\Delta z}$$

$$(4.7)$$

Being ρ is the density of the fluid, m_k the tracer concentration, and Γ a transport coefficient that represents the diffusion of the variable. No source term is added to the equation as no chemical reaction is occurring for the tracer in the CV.

Taking the limits when $\Delta x, \Delta y, \Delta z, \Delta t \rightarrow 0$, the differential form of the equation is obtained (Eq. 4.8):

$$\frac{\partial(\rho m_k)}{dt} = -\frac{\partial\left(\rho u m_k - \Gamma\frac{dm_k}{dx}\right)}{\partial x} - \frac{\partial\left(\rho v m_k - \Gamma\frac{dm_k}{dy}\right)}{\partial y} - \frac{\partial\left(\rho w m_k - \Gamma\frac{m_k}{dz}\right)}{\partial z} \tag{4.8}$$

Separating convective and diffusive terms of the equation and rewriting in vector form, general transport equation is obtained for tracer transport (Eq. 4.9):

$$\boxed{\frac{\partial(\rho m_k)}{dt} + \nabla \cdot (\rho \vec{v} m_k) - \nabla \cdot (\Gamma \nabla m_k) = 0} \tag{4.9}$$

The final expression is obtained by means of averaging the general transport equation for turbulent flow (Eq. 4.10):

$$\boxed{\frac{\partial(\rho m_k)}{\partial t} + \frac{\partial}{\partial x_i}(\rho v_i m_k) - \frac{\partial}{\partial x_j}\left[\left(\rho D_k + \frac{\mu_t}{S_{ct}}\right) \cdot \frac{\partial m_k}{\partial x_j}\right] = 0} \tag{4.10}$$

Being D_k the self-diffusion coefficient of the tracer. In order to only reproduce the convective transport, this value must be very low, at least 10^{-10} m^2/s (Fernández, 2012). In this work D_k is set to 10^{-20} m^2/s to ensure to convective behaviour. The $\frac{\mu_t}{S_{ct}}$ term represents the turbulent diffusion, in which Schmidt number appears ($Sc_t = \frac{\mu_t}{\rho \cdot D_t}$), being μ_t the turbulent viscosity and D_t the turbulent diffusivity.

The resolution method for tracer transport uses the concept of fluid mixture. First, continuity, momentum and energy equations are solved in the mixture field. Next, tracer transport is performed.

4.3.3. Biological model

In order to assess the hydrodynamic effect on the biological performance of multi-environment reactors for BNR, a saturation type (Monod equation) (Tchobanoglous et al., 2014) denitrification model is included in the code (Eqs. 4.11-4.12)

$$\frac{dC_{NO_3}}{dt} = -k_1 \cdot \frac{dC_{NO_3}}{K_{NO_3} + C_{NO_3}} \cdot X_H ; \tag{4.11}$$

$$\frac{dC_{NO_3}}{dt} = \left(-\frac{1 - Y_H}{2.86 \cdot Y_H} \cdot \mu_H \cdot \eta_{NO_3} \right) \cdot \frac{dC_{NO_3}}{K_{NO_3} + C_{NO_3}} \cdot X_H \tag{4.12}$$

Where C_{NO_3} is the nitrate concentration (mgN/L), k_1 is the denitrification rate (mgN/gVSS $\cdot$ day), K_{NO_3} is the half saturation constant for nitrate (mgN/L), X_H is the heterotrophic biomass concentration (mgVSS/L), Y_H is the heterotrophic yield coefficient (dimensionless), μ_H is the maximum growth rate on substrate (1/day) and η_{NO_3} is the reduction factor for denitrification (dimensionless).

Kinetics from equation 4.11-4.12 are taken from Henze et al. (2000), assuming substrate, nutrients and alkalinity to be present in non-limiting amounts. Besides, absence of oxygen is supposed. Default values for all variables are shown in Table 4.2:

Table 4.2. Default values for kinetic values of the biological model (T = 20ºC)

Symbol	Denomination	Value	Units
K_{NO_3}	Half saturation constant for nitrate	0.50	mgN/L
Y_H	Heterotrophic yield coefficient	0.67	[-]
μ_H	Maximum growth rate on substrate	6.00	1/day
η_{NO_3}	Reduction factor for denitrification	0.80	[-]

Similarly to tracer transport, general transport equation for nitrate is obtained by means of applying the mass conservation to a CV. The nitrate is also assumed to behave as a passive scalar with no effect in local hydrodynamics. Supposing that the nitrate concentration variable, named C_{NO_3}, a CV of $\Delta x, \Delta y, \Delta z$ dimensions is defined as shown in Fig. 4.3. $J_{x_{NO_3}}$ represents the net flux of the transported variable across the x axis in the CV. In this case C_{NO_3} is transported, and the flux is expressed as $J_{x_{NO_3}} = \left(\rho u C_{NO_3} - \Gamma \frac{dC_{NO_3}}{dx} \right)_x$. The flux is then defined for the three axes. Its time variation is expressed in the Eq. 4.13.
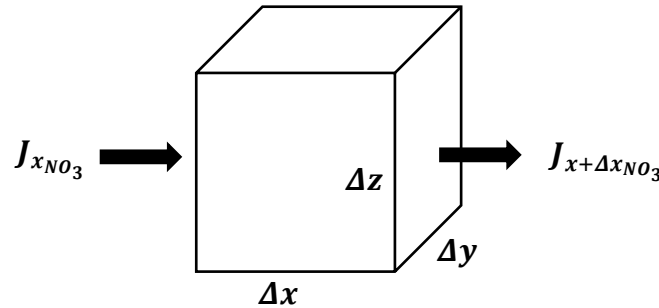
Figure 4.3. Nitrate mass balance in the control volume

$$\begin{bmatrix} Nitrate\ increase\ in\ CV \\ respect\ to\ time \end{bmatrix} = \begin{bmatrix} Nitrate\ net\ flow \\ in\ the\ CV \end{bmatrix} + \begin{bmatrix} Nitrate\ net\ consumption \\ in\ the\ CV\ respect\ to\ time \end{bmatrix} \quad (4.13)$$

Each term of the Eq. 4.13 is mathematically rewritten in Eq. 4.14:

$$\frac{(\rho C_{NO_3})_{t+\Delta t} - (\rho C_{NO_3})_t}{\Delta t} = \frac{\left(\rho u C_{NO_3} - \Gamma \frac{dC_{NO_3}}{dx}\right)_x - \left(\rho u C_{NO_3} - \Gamma \frac{dC_{NO_3}}{dx}\right)_{x+\Delta x}}{\Delta x}$$

$$+ \frac{\left(\rho v C_{NO_3} - \Gamma \frac{dC_{NO_3}}{dy}\right)_y - \left(\rho v C_{NO_3} - \Gamma \frac{dC_{NO_3}}{dy}\right)_{y+\Delta y}}{\Delta y}$$

$$+ \frac{\left(\rho w C_{NO_3} - \Gamma \frac{dC_{NO_3}}{dz}\right)_z - \left(\rho w C_{NO_3} - \Gamma \frac{dC_{NO_3}}{dz}\right)_{z+\Delta z}}{\Delta z} + S$$

$$(4.14)$$

Being ρ the density of the fluid, C_{NO_3} the nitrate concentration, and Γ a transport coefficient representing the diffusion of the variable. In this case, the source term is the biological kinetic expressed in Eq. 4.12.

Taking the limits when $\Delta x, \Delta y, \Delta z, \Delta t \rightarrow 0$, the differential form of the equation is obtained (Eq. 4.15):

$$\frac{\partial(\rho C_{NO_3})}{dt} = -\frac{\partial\left(\rho u C_{NO_3} - \Gamma \frac{dC_{NO_3}}{dx}\right)}{\partial x} - \frac{\partial\left(\rho v C_{NO_3} - \Gamma \frac{dC_{NO_3}}{dy}\right)}{\partial y} - \frac{\partial\left(\rho w C_{NO_3} - \Gamma \frac{dC_{NO_3}}{dz}\right)}{\partial z} + S$$

$$(4.15)$$

Separating convective and diffusive terms of the equation and rewriting in vector form (Eq. 4.16):

$$\frac{\partial(\rho C_{NO_3})}{dt} + \nabla(\rho \vec{v} C_{NO_3}) - \nabla(\Gamma \nabla C_{NO_3}) - \left(\frac{dC_{NO_3}}{dt}\right) = 0 \ ;$$

$$\boxed{\frac{\partial(\rho C_{NO_3})}{dt} + \nabla(\rho \vec{v} C_{NO_3}) - \nabla(\Gamma \nabla C_{NO_3}) - \left(-\frac{1-Y_H}{2.86 \cdot Y_H}\mu_H\,\eta_{NO_3}\right)\frac{dC_{NO_3}}{K_{NO_3} + C_{NO_3}}X_H = 0} \quad (4.16)$$

Averaging the nitrate transport equation for turbulent flow (Eq. 4.17):

$$\boxed{\begin{aligned}\frac{\partial(\rho C_{NO_3})}{\partial t} + \frac{\partial}{\partial x_i}(\rho v_i C_{NO_3}) - \frac{\partial}{\partial x_j}\left[\left(\rho D_{kn} + \frac{\mu_{tn}}{S_{ctn}}\right)\cdot\frac{\partial C_{NO_3}}{\partial x_j}\right] \\ - \left(-\frac{1-Y_H}{2.86 \cdot Y_H}\mu_H\,\eta_{NO_3}\right)\frac{dC_{NO_3}}{K_{NO_3} + C_{NO_3}}X_H = 0\end{aligned}} \quad (4.17)$$

Being ρ the density of the fluid, C_{NO_3} the nitrate concentration and v_i the ensemble velocity vector. The turbulent diffusion of nitrate is expressed in $\frac{\mu_{tn}}{S_{ctn}}$, in which Schmidt number of the nitrate appears ($Sc_{tn} = \frac{\mu_{tn}}{\rho \cdot D_{tn}}$), being μ_{tn} turbulent viscosity and D_{tn} turbulent diffusivity. D_{kn} is the self-diffusion coefficient of the nitrate, and as stated for the tracer, in this study is set to $10^{-20}\,\mathrm{m^2/s}$ to reproduce a convective transport (Fernández, 2012).

4.3.4. Porous media model

Multi-environment reactors usually have baffles or elements with complex configurations to slow the velocity of the flow and to maintain the desired environmental conditions. In the specific case of AnoxAn, the baffle between the anoxic and clarification zones consists of a plastic frame with a 3D complex geometry (see Chapter 5). The realistic definition of the geometry of these elements introduces a complexity in the computational mesh that results in a significant increase in the number of elements of the computational mesh, with the consequent increase in the computational cost. To avoid this increase, these baffles are proposed to be modelled as a porous media that simulates a pressure drop in the velocity field as a momentum sump. It is modelled by means of a Darcy type flow model defined in Eq. 4.18:

$$f_{baffle} = k \cdot |\vec{U}|; \; \forall \, Baffle \; region \tag{4.18}$$

Being k the friction coefficient. To calculate Reynolds number inside the baffle, the expression from Burcharth et al. (1995) and Losada et al. (2016) needs to be followed.

4.3.5. Impeller model

The impeller plays a key role in the hydrodynamics of the reactor because it is the main source of inner momentum supply. Since the purpose of this work is not to define in detail the hydrodynamic patterns produced around by impeller blades, and because the rotation speed of the impeller in AnoxAn creates very significant turbulent flow patterns, a simplified modelling of the impeller has been performed. To do this, the flat disk hypothesis has been used (Jasak et al., 2019; Seb, 2017), where the momentum induced by the impeller to the fluid is introduced into the model from a compound velocity field at an axial, radial and tangential velocity (i.e.: v_a, v_r and v_t), which are defined according to the rotation speed and the relative position of the different nodes that define the disk with respect to its centre (see Fig. 4.4). Those velocities are used as boundary conditions at the flat disk surface. The momentum source approach has been successfully used and validated in other studies about wastewater treatment reactors (Brannock, 2003; Climent et al., 2018; Climent et al., 2019; Rehman, 2016).

The simulation of the impeller through this approach has the advantage that it has a lower computational cost but allows an adequate flow characterization in the reactor.
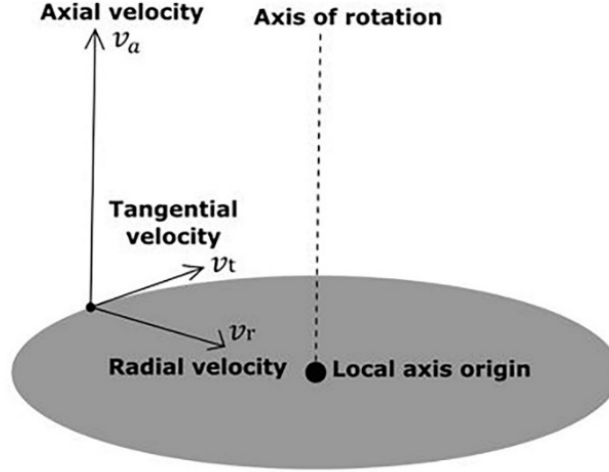
Figure 4.4. Schematic scheme of the impellers flat disk approach

Velocity boundary condition is set for three impeller velocities (Eqs. 4.19-4.21) as:

$$\vec{v_a} = U_{0,a} \cdot \vec{a} \tag{4.19}$$

$$\vec{v_r} = U_{0,r} \cdot \vec{r} \tag{4.20}$$

$$\vec{v_t} = U_{0,t} \cdot \vec{t} = \left(\omega_{0,t} \cdot R \right) \cdot \vec{t} \tag{4.21}$$

being $\vec{a}$ the vector normal to the impeller, $\vec{r}$ the radial vector and $\vec{t}$ tangential vector respectively. $U_{0,i}$ represent the module of three characteristic velocities, $\omega_{0,t}$ the angular velocity and R is the radial distance to each node in the impeller flat disk to the impeller centre in meters. More realistic approaches have been also tested in the presented work, i.e. Arbitrary Rotating Mesh (AMI) and Overset mesh approaches. In these cases, the real geometry of the impeller is defined, and by means of a rotating mesh algorithm, the movement of the impeller is simulated. Although satisfactory results have been achieved, these approaches led to an excessive computational cost. For more insights about these tests, the reader is referred to Annex A.

4.4. Solving procedure

In this section, the algorithms used for the resolution of the numerical model are presented.

4.4.1. SIMPLE algorithm

SIMPLE algorithm was originally developed by Patankar and Spalding (1972). It is a method based on the reformulation of the pressure and is commonly used for incompressible flows. The main idea of this algorithm is to define a discretized equation for the pressure starting from the equation of continuity. Additionally, SIMPLE algorithm uses the momentum equations to relate velocity fields defined at cell faces with cell centroids.

In OpenFOAM® (see Fig. 4.5), SIMPLE based solvers are used for steady state simulations as the time derivation term of the transport equation is omitted in the code. The absence of a natural limiter term as Δt, gives rise to the need for under-relaxing the equations in order to avoid numerical divergence.

In brief, SIMPLE algorithm consists on the following steps:

I)   Estimate a tentative field for the pressure, p^*.

II)   Solve the momentum equations with p^*, obtaining the approximate velocity fields $\vec{v}^*$.

III)   Calculate the mass fluxes F^* and solve the pressure correction equation to obtain the corrected pressure field, p'.

IV)   Calculate the correction term for the velocity $(\vec{v}')$, and then obtain the corrected velocity fields, $\vec{v}$.

V)   Solve the rest of equations (turbulence, scalar transport, biological kinetics) using the corrected velocity field.

VI)   If the solution reached has not converged, the procedure goes back to step II starting with the corrected pressure field of the previous iteration. If solution has converged, the algorithm stops.

Therefore, SIMPLE algorithm approximates to convergence by means of intermediate fields that satisfy continuity. The calculation of the rest of transported variables ø is performed after the velocity field correction in step V to ensure that convective fluxes for ø satisfy the continuity in each iteration.

4.4.2. PISO algorithm

PISO algorithm (Issa, 1986) is a procedure for the calculation of pressure and velocity fields that implies one predictor and two corrector steps (see Fig. 4.6). For that reason, it is considered an evolution of the SIMPLE algorithm with an additional corrector stage.

In OpenFOAM®, PISO based solvers are used for unsteady simulations and time derivation term of the transport equation is not omitted in the code. In this sense, the stabilization criterium is based on the Courant number (Eq. 4.22):

$$Co = \frac{U \cdot \Delta t}{\Delta x} \leq 1 \tag{4.22}$$

Being U the local cell velocity, Δt the time step and Δx the distance between cells (in OpenFOAM® it is defined as the volume of a computational cell). This condition defines the time step as the one that allows the propagation of the variables a maximum of the length of a single cell in the computational domain. If a variable is transported more than one cell within the maximum time step, numerical information is lost and solution diverges.

In brief, PISO algorithm consists on the following steps:

I) Estimate a tentative field for the pressure, p^*.

II) Solve the momentum equation with p^*, obtaining the approximate velocity fields, $\vec{v}^*$.

III) Calculate the mass fluxes F^* and solve pressure correction equation to obtain the corrected pressure field, p'.

IV) Calculate the corrected velocity fields $\vec{v}^{**}$ with a second correction stage.

V) Calculate the source term of the second equation for pressure correction using $\vec{v}^{**}$ and $\vec{v}^*$ and solve the equation to obtain the p' correction (p'').

VI) Correct the pressure and velocity fields. For the pressure the sum of all corrections is used: $p^{***} = p^* + p' + p''$.

VII) Solve the rest of equations (turbulence, scalar transport, biological kinetics) using the corrected velocity field.

VIII) Out of OpenFOAM® environments, if PISO is used for steady state simulations, when solution reached has not converged, the procedure goes back to step II starting with the corrected pressure field of the previous iteration. If solution has converged, the algorithm stops. In transient simulations, the algorithm goes forward the next time step after the double corrector loop.

It must be highlighted that using double corrector stage for the pressure demands more storage space to save velocity fields, corrected and without correction.

4.4.3. PIMPLE algorithm

PIMPLE (see Fig. 4.7) is the combination between SIMPLE and PISO algorithms and is one of the most used procedures to solve transient problems (Holzmann, 2019). PIMPLE algorithm operates as a SIMPLE algorithm for every time step, where outer correctors work as iterations to ensure that explicit parts of the equations are converged. Once a converged solution is obtained within the time step, the algorithm moves on to the next one to start a new iteration cycle until the end time of the simulation is reached. Therefore, better stability is obtained from PIMPLE over PISO, and for that reason, PIMPLE is used with large time steps where the maximum Courant number may consistently be above 1.
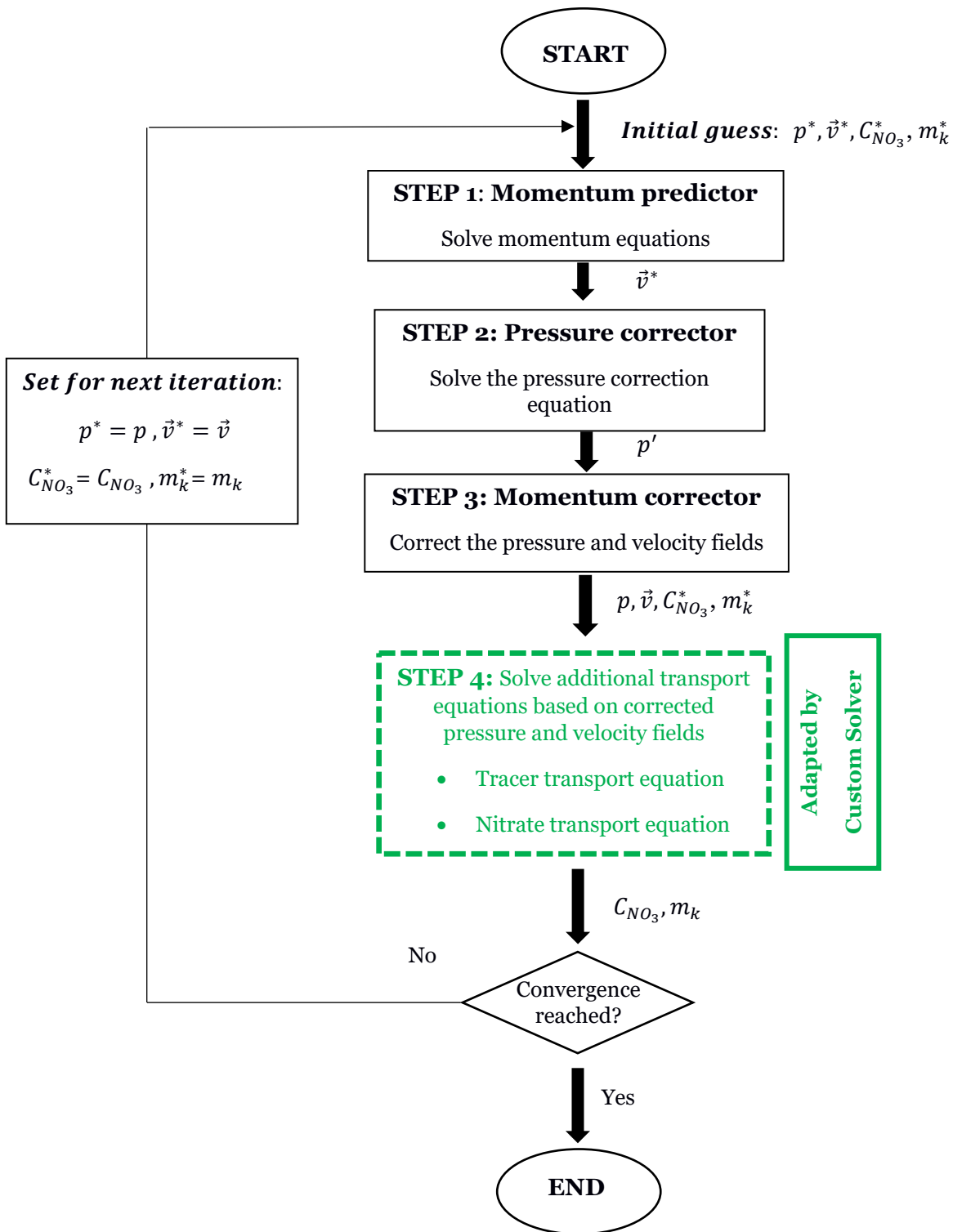
Figure 4.5. Flow chart for adapted SIMPLE algorithm

START

Initial guess: $p^*, \vec{v}^*, C_{NO_3}^*, m_k^*$

STEP 1-3 from SIMPLE algorithm

- Solve momentum equations

- Solve the first pressure correction equation

- Correct pressure and velocity fields

$p^{**}, \vec{v}^{**}, p'$

STEP 4: Second pressure corrector

Solve the second pressure correction equation

p''

STEP 5: Second momentum corrector

Correct the pressure and velocity fields

$p^{***}, \vec{v}^{***}$

Set:

$p = p^{***}, \vec{v} = \vec{v}^{***}$

$p, \vec{v}, C_{NO_3}^*, m_k^*$

STEP 6: Solve additional transport equations based on corrected pressure and velocity fields

- Tracer transport equation

- Nitrate transport equation

Adapted by Custom Solver

C_{NO_3}, m_k

Go for next time step:

$t_{n+1} = t_n + \Delta t$

$Co = \dfrac{U \cdot \Delta t}{\Delta x} \leq 1$

No

Simulation time finished?

Yes

END

Figure 4.6. Flow chart for adapted PISO algorithm

65

START

Initial guess: $p^*, \vec{v}^*, C^*_{NO_3}, m^*_k$

STEP 1: **Momentum predictor**

Solve momentum equations

$\vec{v}^*$

STEP 2: Pressure corrector

Solve the pressure correction equation

p'

STEP 3: Momentum corrector

Correct the pressure and velocity fields

$p, \vec{v}, C^*_{NO_3}, m^*_k$

STEP 4: Solve additional transport equations based on corrected pressure and velocity fields

- Tracer transport equation
- Nitrate transport equation

Adapted by Custom Solver

C_{NO_3}, m_k

Outer correction:

$p^* = p, \vec{v}^* = \vec{v}$

$C^*_{NO_3} = C_{NO_3}, m^*_k = m_k$

Go for next time step:

$t_{n+1} = t_n + \Delta t$

$Co = \dfrac{U \cdot \Delta t}{\Delta x} \gg 1$

Convergence reached?

No

Yes

Simulation time finished?

No

Yes

END

Figure 4.7. Flow chart for adapted PIMPLE algorithm

4.5. <u>Numerical implementation in OpenFOAM®</u>

In this section, the implementation of the numerical tool is described. Concretely, special attention is paid to the custom added features (tracer and nitrate transport) to the original code from OpenFOAM®. The original model for the porous media and its implementation can be found at IHFOAM application (https://ihfoam.ihcantabria.com/). For deeper information about original source code, the reader is referred to www.openfoam.com.

In Fig. 4.8, the general structure and all the files that are part of the solvers are presented. Concretely, pEqn.H and UEqn.H are the pressure and velocity files defining the solving algorithm (SIMPLE or PIMPLE). New transport equations for tracer and nitrate need to be included in this loop. Additionally, in the createFields.H file, the biomass and the new transport variables (tracer and nitrate) are defined. Transport properties and constant parameters regarding the new transport equations are also defined in the createFields.H file. Numerical implementation of all these features is presented in the next pages.
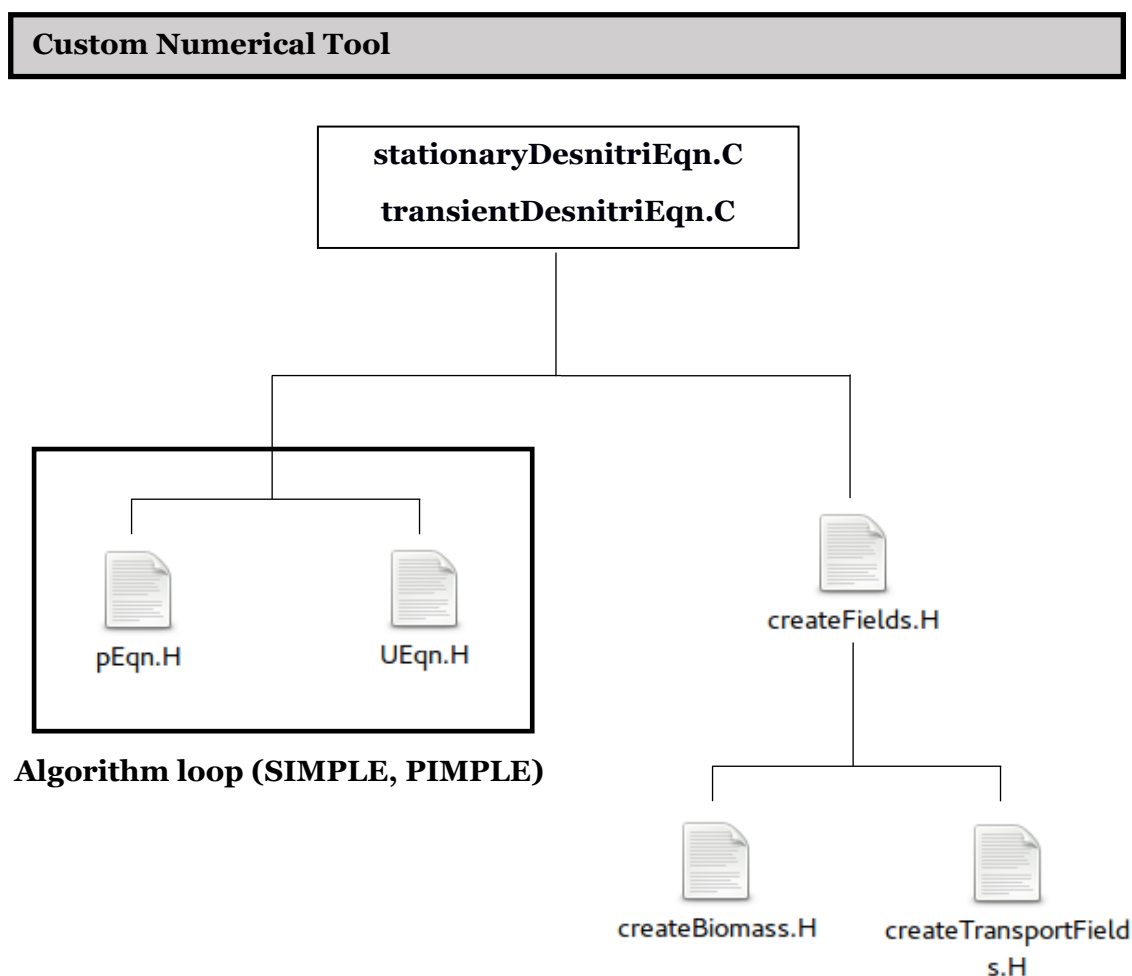
Figure 4.8. Structure of the Custom Numerical Tool

The main structure of the solver is contained in the main file of the numerical tool, i.e. **stationaryDesnitriEqn.C** or **transientDesnitriEqn.C** files. At the beginning of the code, all features of the solver are loaded:

---

stationaryDesnitriEqn.C | transientDesnitriEqn.C

```
#include "fvCFD.H"
#include "singlePhaseTransportModel.H"
#include "turbulentTransportModel.H"
#include "pimpleControl.H"
#include "simpleControl.H"
#include "fvOptions.H"

// * * * * * * * * * * * * * * * * * * * * * * * * * * * * * * *
* * * * * * //

int main(int argc, char *argv[])
{
    #include "postProcess.H"

    #include "setRootCase.H"
    #include "createTime.H"
    #include "createMesh.H"
    #include "createControl.H"
    #include "createTimeControls.H"
    #include "createFields.H"
    #include "createFvOptions.H"
    #include "initContinuityErrs.H"

    turbulence->validate();
```

The first lines of the code load general features to describe the physical problem (**fvCFD.H,** **singlePhaseTransportModel.H,** **turbulentTransportModel.H**, etc) and then, additional routines are also loaded in order to create time variables or to storage the mesh.

The transport equations for tracer and nitrate developed in sections 4.3.2 and 4.3.3 are coded after the momentum correction in the pressure field file, **pEqn.H**, introducing them into the loop of the SIMPLE and PIMPLE algorithms.

---

pEqn.H

```
 //IHC_dbg
    Info << " IH: Solving Pollutant Transport Eq..." << endl;
    fvScalarMatrix PollutantEqn
    (
        fvm::ddt(Pollutant)
      + fvm::div(phi, Pollutant)
      - fvm::laplacian((CoeffP + turbulence->nuEff()/Schmidt),
Pollutant)
    );

    PollutantEqn.solve();
    //------
```

```
//IHC_dbg
    Info << " IH: Solving Nitrate Transport Eq..." << endl;
    fvScalarMatrix NitrateEqn
    (
         fvm::ddt(Nitrate)
        + fvm::div(phi, Nitrate)
       - fvm::laplacian((CoeffPN + turbulence-
>nuEff()/SchmidtB), Nitrate)
        -(-K1*(Nitrate/(KNO+Nitrate))*biomass, Nitrate)
    );

    NitrateEqn.solve();
    //------
```

Then, all the variables concerning the added transport equations must be defined in the code. In the first lines of **createFields.H** file (remarked in red), additional files defining the transported variables (i.e. tracer and nitrate) and the biomass are loaded:

createFields.H

```
//IHC_dbg
#include "createTransportFields.H"
#include "createBiomass.H"
//----------

Info<< "Reading field U\n" << endl;
volVectorField U
(
    IOobject
    (
        "U",
        runTime.timeName(),
        mesh,
        IOobject::MUST_READ,
        IOobject::AUTO_WRITE
    ),
    mesh
);

#include "createPhi.H"
```

In the **createBiomass.H** file, a new dimensionless variable to represent the heterotrophic biomass inside the multi-environment reactor is created. As stated in section 4.2, the influence of the solid phase in the liquid phase is not taken into account in this study. In consequence, the nitrate transport is modelled as a scalar transport with biochemical denitrification kinetics and, consequently, the biomass can be defined as a dimensionless constant:

createBiomass.H

```
    Info<< "Reading field biomass\n" << endl;

    volScalarField biomass
    (
        IOobject
        (
            "biomass",
            runTime.timeName(),
            mesh,
            IOobject::READ_IF_PRESENT,
            IOobject::NO_WRITE
        ),
        mesh,
        dimensionedScalar( "biomass", dimless, 0.0 )
    );
```

In the same way, additional variables for tracer (named as Pollutant) and nitrate (named as Nitrate) are defined in **createTransportFields.H** file.

createTransportFields.H

```
Info<< "Reading field Pollutant\n" <<endl;
volScalarField Pollutant
(
    IOobject
    (
        "Pollutant",
        runTime.timeName(),
        mesh,
        IOobject::MUST_READ,
        IOobject::AUTO_WRITE
    ),
     mesh
);

Info<< "Reading field Nitrate\n" <<endl;
volScalarField Nitrate
(
    IOobject
    (
        "Nitrate",
        runTime.timeName(),
        mesh,
        IOobject::MUST_READ,
        IOobject::AUTO_WRITE
    ),
     mesh
);
```

Finally, just after the velocity field, default transport properties linked with the fluid and turbulence properties are loaded in the **createFields.H** file. Then, new transport properties related to the new transport variables (tracer and nitrate created in **createTransportFields.H**) are added. Concretely, self-diffusion coefficients and Schmidt number for the transport variables and biological constants for denitrification kinetics are coded. In the same way as the biomass, all coefficients concerning the nitrate biokinetics are defined in the solver as dimensionless parameters.

createFields.H

```
//IHC_dbg
Info<< "Reading transportProperties\n" << endl;

IOdictionary transportProperties
(
    IOobject
    (
        "transportProperties",
        runTime.constant(),
        mesh,
        IOobject::MUST_READ,
        IOobject::NO_WRITE
    )
);

dimensionedScalar CoeffP
(
    transportProperties.lookup("CoeffP")
);

dimensionedScalar CoeffPN
(
    transportProperties.lookup("CoeffPN")
);

dimensionedScalar Schmidt
(
    transportProperties.lookup("Schmidt")
);

dimensionedScalar SchmidtN
(
    transportProperties.lookup("SchmidtN")
);

dimensionedScalar K1
(
    transportProperties.lookup("K1")
);

dimensionedScalar KNO
(
    transportProperties.lookup("KNO")
);
```

4.6. <u>Conclusions</u>

In this chapter, an open source numerical tool based on CFD is developed in OpenFOAM®. The model is used in next chapters for the hydrodynamic simulation, analysis and optimization of the BNR AnoxAn reactor. Main conclusions are highlighted below:

- The numerical tool developed in this work incorporates several features that are not included in the original source code of OpenFOAM® such as tracer transport for turbulent flow, nitrate transport and denitrification biokinetics for turbulent flow and a porous media model.

- All sub-models are included in two custom solvers: stationaryDesnitriEqn for stationary simulations and transientDesnitriEqn for non-stationary simulations. Both solvers are adapted based on the original SIMPLE and PIMPLE algorithms to solve the added features.

- Although in the next chapters this numerical tool is applied to the simulation and optimization of AnoxAn, its free and open source nature makes it available for the research community to be adapted to different problems.

- The numerical model does not include the influence of the solid phase on the bulk liquid. Although this is not a complete realistic approach, this work aims to be the first step for future developments.

Chapter 5

CFD model construction, validation and hydrodynamic analysis of a novel anaerobic-anoxic reactor for biological nutrient removal

5.1. Introduction

For many years, the main objective of wastewater research has been to achieve the required efficiency of biological processes to meet regulations and preserve the ecological and healthy status of water bodies (rivers, lakes, reservoirs, oceans, etc.). Specifically, great efforts have been made to design and improve nutrient removal processes (i.e.: nitrogen (N) and phosphorus (P)) due to the increasing requirements of Wastewater Treatment Plants (WWTPs).

However, conventional biological nutrient removal (BNR) processes in WWTPs require a complex treatment system and entail several environmental impacts. First, the aerobic reactor should be large enough to carry out ammonia oxidation (nitrification) and must be coupled with non-aerated compartments (anaerobic and anoxic). Therefore, a large volume is needed compared to organic matter removal processes. This issue becomes crucial in cases where land availability is limited and in cases of existing wastewater treatment plants that need to be upgraded to BNR plants. In addition, the high energy demand of the nitrification process, together with the need for recirculation pumping between the different compartments or reactors and the mixing of the non-aerated ones, result in a significant increase in energy consumption.

In this context, multi-environmental biological reactors with high compaction and efficiency have been developed to reduce the energy consumption and land use of conventional BNR treatment trains (Kwon et al., 2005; Yerushalmi et al., 2011; Tejero et al., 2010; Tejero et al., 1991; Martin et al., 2012). Of special interest is the anaerobic-anoxic reactor AnoxAn, developed and patented by Tejero et al. (2010). AnoxAn is a continuous upward-flow sludge blanket reactor that unifies in a single reactor the anaerobic and anoxic zones necessary for the biological nutrient removal of conventional activated sludge from wastewater (Díez-Montero 2015; Díez-Montero et al., 2015; Díez-Montero et al., 2016). Due to its low energy consumption and minimal land use, the AnoxAn concept and technology can potentially be applied for the upgrade of a WWTP or in a new WWTP with limited space availability. In addition, primary settling tanks could be reused as anoxic-anaerobic reactors to develop innovative and compact treatment systems (Díez-Montero et al., 2019). Finally, the anaerobic-anoxic biological functioning of AnoxAn is intended to be coupled to an aerobic reactor (for residual organic matter removal, phosphate uptake and nitrification) and a secondary settling unit (or final filtration step), to complete the BNR treatment train (Díez-Montero, 2015).

The AnoxAn reactor consists of an anaerobic zone at the bottom (receiving the influent wastewater), before an anoxic zone above (receiving a nitrate-rich current from a subsequent aerobic reactor). In addition, a clarification zone is achieved in the upper part, avoiding the escape of large quantities of biomass. One of the main objectives of the reactor setup is to establish an anoxic-anaerobic hydraulic separation, i.e. to maintain an insignificant concentration of nitrates in the anaerobic zone, achieving at the same time adequate mixing conditions in both zones and maintaining the continuous flow of the effluent through it. For this purpose, the reactor has independent mixing systems in each zone: a recirculation pump provides the mixture in the anaerobic zone and a mixing impeller in the anoxic zone. In

addition, the deflectors and baffles improve hydraulic separation and retention of suspended solids within the reactor. Concretely, the upper baffle, BLAS® (Tejero et al., 1991) was originally conceived as a support media for biofilm, but in AnoxAn is used as a head loss generator reducing the velocity of the fluid flow. Specific elements with these characteristics and level of interference in the flow pattern increase the hydrodynamic complexity of the reactor, and could generate preferential flows and dead zones, reducing the overall performance of the system (Al-Sammarraee et al., 2009; Liu et al., 2018; Plascencia-Jatomea et al., 2015; Yan et al., 2015).

The viability of anoxic-anaerobic hydraulic separation of AnoxAn was tested in a 48.4 L prototype by means of Residence Time Distribution (RTD) analysis (Díez-Montero et al., 2015). A hydraulic model based on compartments was constructed and validated with experimental traceability tests. This model was a combination of complete mixed compartments and plug flow with axial dispersion compartments, implemented to describe the non-ideal flow of the reactor. The model predicted with high accuracy the experimental records (local measurements without spatial resolution). Then, it was applied to evaluate hydraulic anoxic-anaerobic separation. However, this type of modelling cannot provide complete information on hydrodynamics within the reactor. In a later work, the biological behaviour of the reactor in the treatment of municipal wastewater was studied (Díez-Montero et al., 2016). The results demonstrated the feasibility of the reactor concept. However, it was observed that some physical characteristics of AnoxAn significantly affect its performance, hydrodynamics being clearly relevant. In order to optimise the reactor configuration and propose other reactor configurations applicable on a large scale, Díez-Montero (2015) pointed out a deeper and more complete hydrodynamic analysis.

In fact, RTD experimental tests (Levenspiel, 1999), usually coupled to hydraulic models based on compartments such as the tank-in-series and the dispersion models, have been widely used for hydrodynamic analysis in wastewater treatment reactors. At this respect, mixing conditions (Hu et al., 2012; Olivet et al., 2005; Yerushalmi et al., 2013), flow type and characteristics (Behzadian et al., 2013; Gómez, 2010; Ji et al., 2012; Sarathai et al., 2010), dead volume (Hu et al., 2012; Ji et al., 2012; Sarathai et al., 2010), channeling (Gómez, 2010; Nemade et al., 2010; Zeng et al., 2005) and dispersal (Ji et al., 2012; Nemade et al., 2010; Yerushalmi et al., 2013; Zeng et al., 2005) were observed as the most important characteristics. However, experimental RTD analysis techniques require a lot of time and resources. In some cases, the complexity of experimental tests makes them impracticable in large-scale reactors (Fernández, 2012). In addition, experimental RTD models and compartment-based hydraulic models do not contain any information on spatial flow and concentration camp resolution (Plascencia-Jatomea et al., 2015; Qi et al., 2013).

The latter can be overcome by combining and developing advanced mathematical models and computational simulation. The application of numerical techniques to engineering has experienced great growth in recent decades, with Computational Fluid Dynamics (CFD) being one of the approaches with the greatest impact. The use of CFD in wastewater treatment processes is growing rapidly and is being applied in the resolution of complex problems

(Angeloudis et al., 2016; Brannock et al., 2010a-b; Liu et al., 2018; Klusener et al., 2007; Wicklein et al., 2016; Zhang et al., 2016).

Regarding hydrodynamic analysis, combination of RTD and CFD for reactor analysis and optimization has been previously applied for different reactors (Brannock et al., 2010a-b; Climent et al., 2018; Le Moullec et al., 2008; Pereira et al., 2011; Plascencia-Jatomea et al., 2015; Terashima et al., 2009). The present work follows the validation performed by many of them regarding the hydrodynamic field, which is only based on RTD tests (Brannock et al., 2010a-b; Plascencia-Jatomea et al., 2015; Terashima et al., 2009). Moreover, all the studies aforementioned were carried out with commercial codes, being the present research an open-source approach that completes the already existing ones.

Hydrodynamic in stirred reactors has also been modelled and analysed for several configurations (Bridgeman, 2012; Bai et al., 2008; Choi et al., 2004; Qi et al., 2013). Different approaches can be undertaken for a correct representation of the impeller: being MRF (Multi Reference Frame) approach (Bai et al., 2008; Bridgeman, 2012; Renade, 2002; Wu et al., 2009) or momentum source approach common ones. The latter is a classical simplification that allows a significant computational resource saving and has been widely and successfully used in wastewater field, all of them carried out with commercial codes (Brannock, 2003; Climent et al., 2018; Climent et al., 2019; Rehman, 2016).

Moreover, CFD modelling allows deeper hydrodynamic analysis including identification and location of dead zones, tracking of velocity profiles and flow patterns, mixing performance, and determination of the distribution of tracer concentration within the reactor (Climent et al., 2018; Dapelo et al., 2018; Michalopoulos et al., 2018; Plascencia-Jatomea et al., 2015; Terashima et al., 2009; Trad et al., 2015; Wei et al., 2019). In addition, this advanced knowledge will be essential for the operational optimization of reactors with complex hydrodynamic behaviour such as AnoxAn in terms of avoiding the presence of dead flow zones or preferred channelling in the design.

Finally, a calibrated and validated CFD model is more efficient than other approaches in terms of testing other forms or combination of different elements in a reasonable time.

Concretely, hydrodynamic evaluation is crucial in multi-environment reactors due to their specific shapes and combination of different elements, such as baffles and mixing devices, which interfere in the ideal hydraulic performance creating complex flow regimes (Kwon et al., 2005; Yerushalmi et al., 2011; Díez-Montero, 2015). However, to our knowledge, only few hydrodynamic studies have been performed based on CFD for multi-environment reactors and its elements influence (Calder et al., 2013). Finally, it has been widely proved that an optimum hydraulic operation ensures an adequate biological performance efficiency (Climent et al., 2018; Arnaldos et al., 2018; Wei et al., 2019), being hydrodynamic understanding and analysis a critical step for designing process.

The objective of this chapter is to develop a CFD model of the novel AnoxAn anaerobic-anoxic reactor and to analyse its hydrodynamic behaviour in order to identify the key features of the reactor configuration that cannot be achieved with conventional RTD experimental procedures.

These results are crucial for the optimization and future design of large-scale reactor implementations. In addition, modelling and simulation of reactor elements such as baffles and deflectors would provide a deeper hydrodynamic understanding that could be applied for the development and optimization of other multi-environmental reactors and conventional water treatment reactors. The model is built in the OpenFOAM® open source toolbox (Weller at al., 1998), and calibrated and validated with RTD experimental tests and simulations of previous models.

5.2.   Materials and methods

5.2.1. Description of experiments

5.2.1.1. Bench scale reactor setup

To evaluate the model's ability to reproduce the hydrodynamics of AnoxAn, a series of experiments were conducted on a prototype reactor built on a bench scale (Díez-Montero et al., 2015).
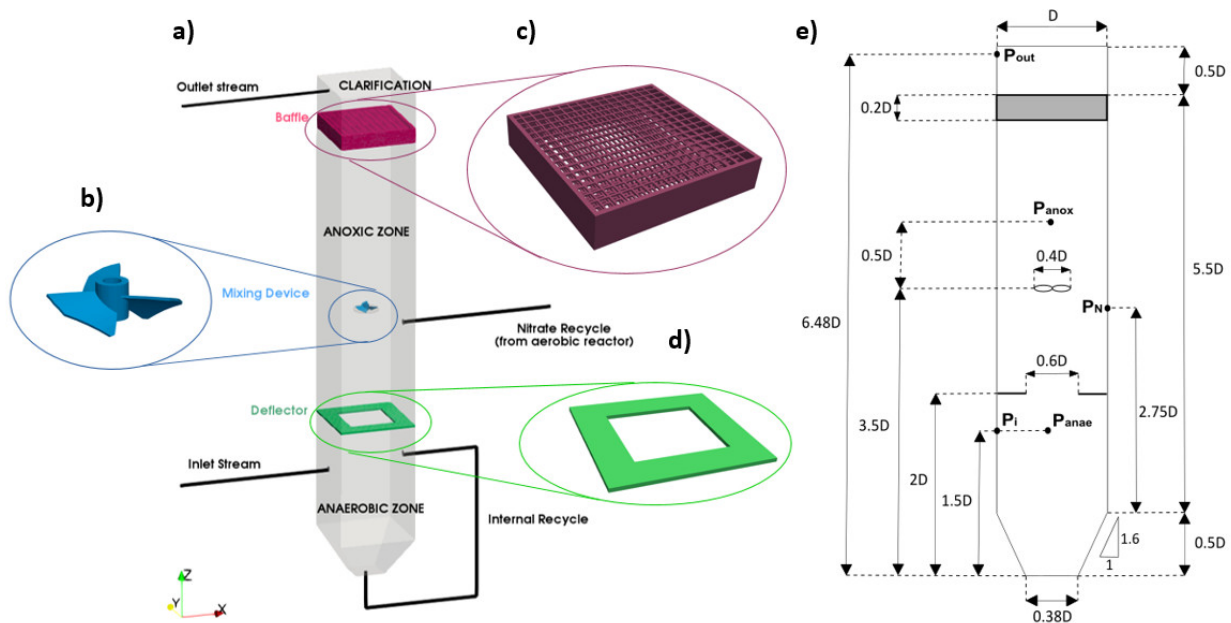
Figure 5.1. (a) 3D scheme of the bench scale AnoxAn reactor, (b) Impeller, (c) Baffle between anoxic and clarification zones, (d) Deflector between anaerobic and anoxic zones and (e) Detailed cross section geometry based on the square section side (D = 0.20 m)

AnoxAn prototype, see Fig. 5.1a, is a 48.4L upflow reactor made of polymethyl methacrylate (PMMA). The reactor is divided into three different zones: a clarification zone at the top (4.0 L; 8% of the total volume), an anoxic zone below (32.0 L, 66% of the total volume) and an anaerobic zone at the bottom (12.4 L; 26% of the total volume). Geometrically, it consists of

an internal square section of 0.20 x 0.20 m^2 and a height of 1.30 m. A cross section of the detailed reactor geometry based on the square section side (D = 0.20 m) is shown in Fig. 5.1e.

Mixing devices in the reactor consist in a Heidolph RZR- 2 000 impeller (100 rpm) (Fig. 5.1b) for the anoxic zone and a peristaltic pump Watson Marlow 313U for the continuous internal recycle of the anaerobic zone. Besides, a complex 3D geometry polyethylene (PE) baffle of 0.039 m height is placed (Fig. 5.1c) between the anoxic and clarification zones in order to improve suspended solids retention inside the reactor and reduce the up-flow velocity. Finally, a polyvinyl chloride (PVC) deflector of 4 cm width along the wall is introduced (Fig. 5.1d) to enhance the hydraulic separation between anoxic and anaerobic environments.

5.2.1.2. Experimental RTD conditions

Two experimental and a simulated tracer tests in clean water were performed in AnoxAn to characterise the liquid phase flow pattern. All details for the experiments are shown in Table 5.1 and Fig. 5.2. The AnoxAn reactor was designed for a hydraulic residence time (HRT) up to 5 h (depending on the organic load applied) and for all the experiments performed the inlet stream flow Q_{in} is 10.4 L/h, internal recycle rate (ratio between internal recycle stream flow and inlet stream flow, $R_{IR} = Q_{IR}/Q_{in}$) is 5.77 (-) and nitrate recycle rate (ratio between nitrate recycle stream flow and inlet stream flow, $R_{NR} = Q_{NR}/Q_{in}$) is 2.98 (-).
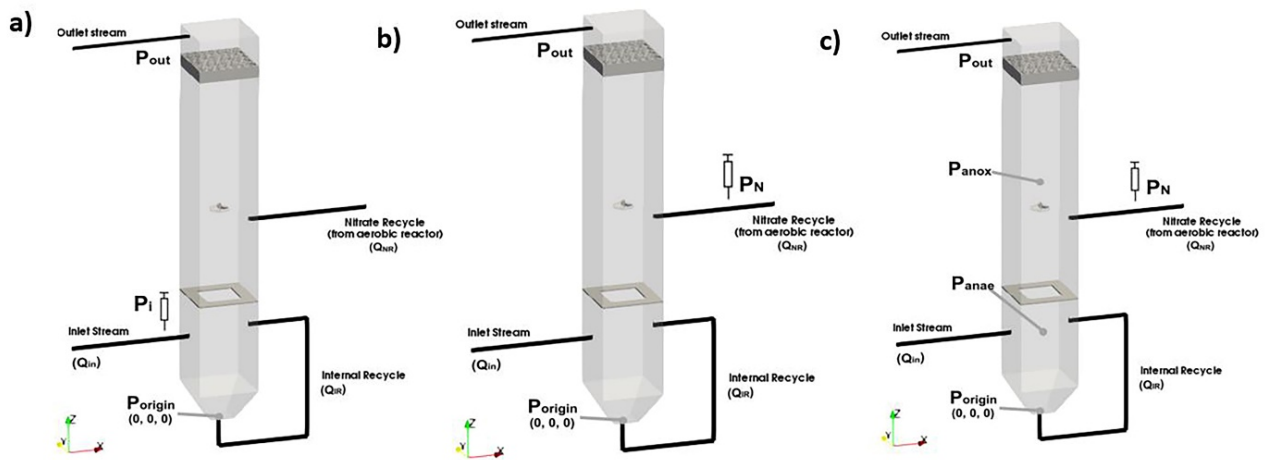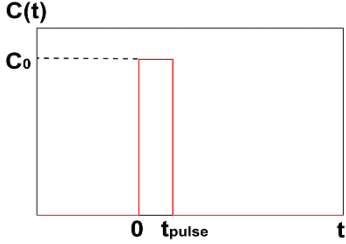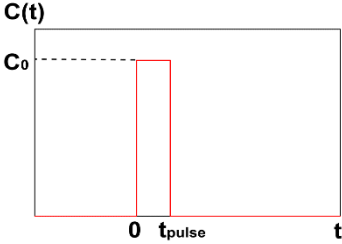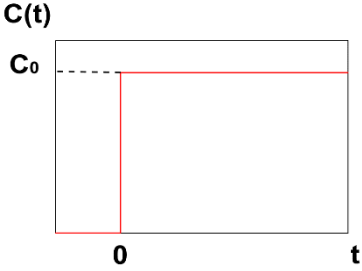
Figure 5.2. Schematic diagram of pulse tracer tests (a) RTD$_1$ (b) RTD$_2$ (c) RTD$_3$

Two pulse RTD tests were carried out for hydraulic characterization of AnoxAn: (i) RTD$_1$ injecting the tracer through the inlet stream (see RTD$_1$ in Table 5.1 and Fig. 5.2a) and (ii) RTD$_2$ injecting the tracer through the nitrate stream (see RTD$_2$ in Table 5.1 and Fig. 5.2b). For both pulse experiments, a concentrated solution of sodium chloride (NaCl, 350 g/L) was used as tracer. Moreover, in RTD$_1$, the volume injected was 58 mL and RTD$_2$ was 40 mL. Output concentration was estimated measuring the conductivity through a linear relationship between them (Tang et al., 2004; Martín-Dominguez et al., 2005) with a Hach CDC40103 probe connected to a HQ30d meter.

In addition to pulse experiments, and in order to better assess the hydraulic separation between the anoxic and anaerobic zones, a step RTD test (RTD$_3$) was simulated using the calibrated and validated hydraulic compartment-based model described in Díez-Montero et al. (2015) and presented in Annex B. In RTD$_3$, a constant concentrated solution of tracer (10 mg/L) is continuously injected in the nitrate recycle stream and tracer concentration is continuously measured in the outlet and in both anaerobic and anoxic zones (see RTD$_3$ in Table 5.1 and Fig. 5.2c).

Table 5.1. RTD tests conditions

RTD experiment	Type	Tracer injection location (m)	Tracer injection duration	Tracer concentration measurement (m)
RTD$_1$	Pulse. Experimental	Inlet stream P$_i$ (-0.1, 0, 0.30)	t_{pulse} = 3 s	Outlet P$_{out}$ (-0.1, 0, 1.295)
RTD$_2$	Pulse. Experimental.	Nitrate recycle stream P$_N$ (0.1, 0, 0.65)	t_{pulse} = 3 s	Outlet P$_{out}$ (-0.1, 0, 1.295)
RTD$_3$	Step. Simulated.	Nitrate recycle stream P$_N$ (0.1, 0, 0.65)	Continued injection	Anaerobic zone P$_{anae}$ (0, 0, 0.30) Anoxic zone P$_{anox}$ (0, 0, 0.80) Outlet P$_{out}$ (-0.1, 0, 1.295)

5.2.2. Numerical model setup

In this section, the computational setup of the CFD model is presented. The model is validated based on RTD experiments described in the previous section.

Based on the results from the numerical simulations, a comprehensive hydrodynamic analysis for the different zones of the reactor is performed. For that purpose, a transient flow analysis is needed. At this respect, unlike RTD analysis, transient CFD models provide high spatial flow and tracer concentration resolution, along with time history of the latter. Besides hydrodynamics, reactor elements are also modelled. At this aim, the local mixing effect of the impeller is reproduced by means a flat disk approach and the baffle situated between anoxic and clarification environments is simulated as a porous media. Both approaches led to a significant computational cost saving.

5.2.2.1. Computational Fluid Dynamics. Governing equations and models.

The numerical CFD tool used is constructed in OpenFOAM ® and has been already presented in Chapter 4.

Hydrodynamics are simulated solving Reynolds Averaged Navier-Stokes (RANS) equations for incompressible flow and turbulence is modelled by means of standard k-ε model (Launder and Spalding, 1972). Regarding tracer transport, physics are coded as a mass transport equation for turbulent flow without chemical reaction. The value of the Schmidt number used for the tracer transport is 0.8 as it provides good agreement with experimental results, being this parameter typically between 0.7 and 1 (Brannock, 2003; De Clercq, 2003).

Finally, the model also includes additional sub-models for different feature elements: an impeller sub-model reproduced by means of a flat disk approach (Jasak et al., 2019; Seb, 2017) and the complex 3D baffle (Tejero et al., 1991) simulated as a porous media. Concretely, Reynolds number of the fluid inside the baffle is between 40 and 75 (being the friction coefficient 500 000 kg/s following Mihovilovic, 2010) which is consistent with the range of applicability of Darcy's flow modelling and the porous media model proposed in Chapter 4. Regarding the impeller, the rotational speed is 100 rpm, the diameter is 0.08 m and the kinematic viscosity of the fluid is 10^{-6} m^2/s. Taking these into account, the Reynolds number yields 10 670, and in consequence, fully developed turbulent flow can be considered in that zone (see Couper at al., 2010).

5.2.2.2. Boundary conditions

Boundary conditions used are shown in Fig. 5.3. Inflow boundary conditions are set at inlet, nitrate recycle inlet and impellers disk face. When pulse RTD tests are simulated (Fig. 5.2a-b), a time dependent boundary condition is set (Eqs. 5.1-5.2) for the tracer in the inlet stream boundary:

$$C = C_0; 0 < t \leq t_{pulse} \tag{5.1}$$

$$C = 0; \, t > t_{pulse} \tag{5.2}$$

Being C the tracer concentration in function of time and C_0 the initial tracer concentration.

Fixed value boundary condition (Eq. 5.3) is set for the tracer in the inlet stream boundary (Fig. 5.2c) when step RTD test is simulated.

$$C = C_0; \forall t \tag{5.3}$$

Outflow boundary condition is set at outlet. Wall boundary conditions are applied to AnoxAn's outer case, the deflector and the backward of the impeller. A non-slip wall boundary condition is used at the walls. For the free surface, a slip boundary condition is implemented.
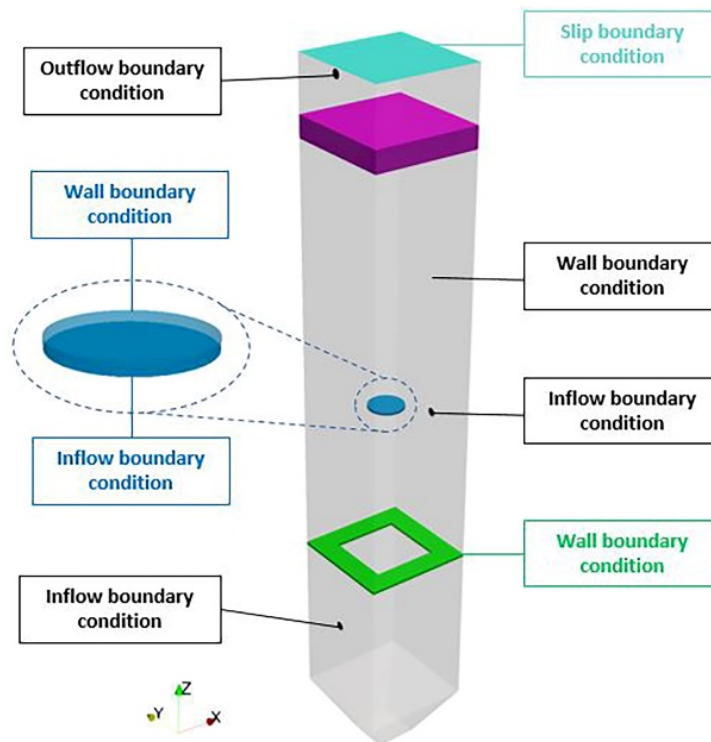
Figure 5.3. Boundary conditions scheme in the numerical model

5.2.2.3. Computational domain

Meshing is carried out by means of a hexahedral nonconforming mesh. First, a background uniform mesh is created, and then non-uniform refinement is performed at walls, deflector and impeller as it is shown in Fig. 5.4:
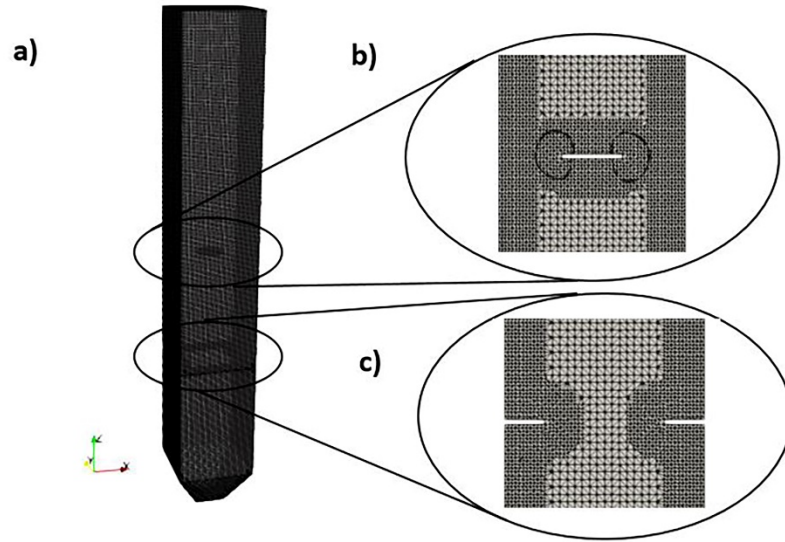
Figure 5.4. Computational grid (a) overall reactor (b) impeller zone refinement and (c) deflector zone refinement

In this study, three different grids are generated. Main characteristics for the different meshes are shown in Table 5.2. All grids contain approximately 95% of hexahedral cells and 5% of polyhedral cells.

Table 5.2. Mesh characteristics

Mesh Nº	Background uniform mesh cell size	Background uniform mesh cell number	Final refined mesh cell size	Final refined mesh cell number
Mesh Nº1	1.75 cm	128 000	0.28 cm	433 081
Mesh Nº2	1.50 cm	160 000	0.20 cm	720 633
Mesh Nº3	1.25 cm	192 000	0.15 cm	1 040 612

Mesh sensitivity analysis is performed in order to ensure mesh independency of the obtained results. In this sense, Grid Converged Index (GCI) is calculated for the different meshes according to Celik et al. (2008), a method based on Richardson Extrapolation. GCI is carried out for different XY sections across the AnoxAn reactor. The study shows that with the mesh nº2 of 720 633 elements, the cell size has no impact on simulation results. In fact, Table 5.3 shows the average-weighted velocity magnitudes for different z sections in the reactor and Table 5.4 shows that maximum GCI values for mesh Nº2 are around 5%, confirming the grid independency of the results for this mesh in the CFD model. Considering the above, mesh nº2 is used in the present work.

Table 5.3. Average-weighted velocity magnitude for different sections

Mesh Nº	Area-weighted velocity magnitude (m/s)			
	z = 0.3 m	z = 0.6 m	z = 1.0 m	z = 1.295 m
Mesh Nº1	$2.268 \cdot 10^{-4}$	0.0318	0.0022	0.0012
Mesh Nº2	$5.140 \cdot 10^{-4}$	0.0305	0.0030	$8.027 \cdot 10^{-4}$
Mesh Nº3	$4.934 \cdot 10^{-4}$	0.0302	0.0029	$7.947 \cdot 10^{-4}$

Table 5.4. Grid Convergence Index for different sections

GCI Nº	GCI			
	z = 0.3 m	z = 0.6 m	z = 1.0 m	z = 1.295 m
GCI^{21}_{coarse}	62.7%	10.9%	32.0%	51.2%
GCI^{32}_{coarse}	5.3%	5.1%	4.9%	1.1%

In addition, results of the RTD_2 tracer test simulations (see section 5.2.1.2) are shown in Fig. 5.5. Results show that the mesh nº2 provides a result close to the one obtained with the largest mesh decreasing the computational time in a factor of 5.
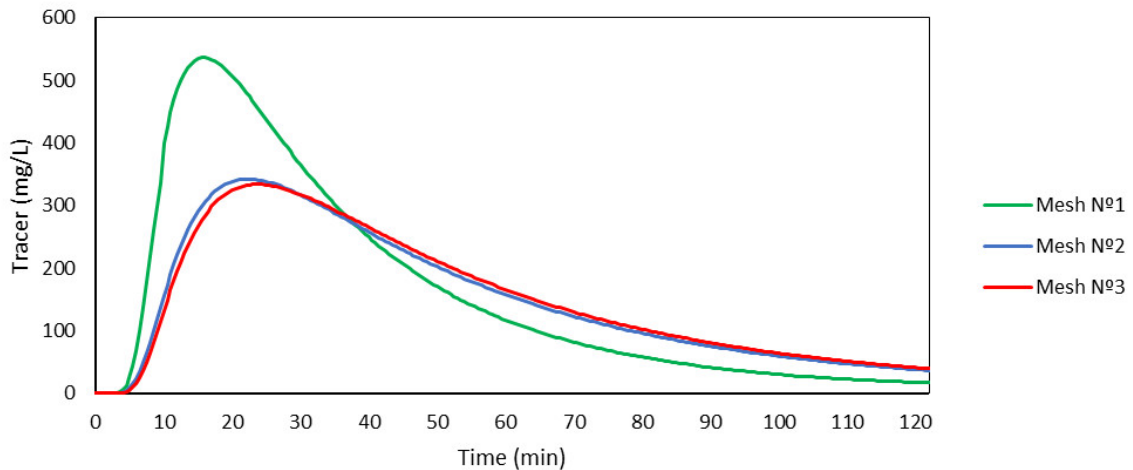
Figure 5.5. RTD_2 results for different meshes

5.2.2.4. Numerical modelling methodology

Numerical model flow chart is performed in two different stages. First, velocity field is solved (without tracer) forcing the model to reach a steady state solution. For that purpose, Semi-Implicit Method for Pressure Linked Equations (SIMPLE) algorithm was used for solving governing equations. A steady state solution is obtained when the relative error for the different variables within iterations is less than 10^{-4}. Once reached the steady state solution, hydrodynamic field is kept constant in time. Then, transient flow simulations are considered when injecting the tracer. Experimental tracer concentration is introduced, and PIMPLE

algorithm (combination of SIMPLE and Pressure Implicit with Splitting of Operators (PISO) algorithms) is used for solving the tracer transport under transient flow. Hypothesis that ρ of the fluid does not change in time is assumed. With transient results, calibration and validation are performed. Fig. 5.6 shows a flow chart explaining the numerical model solving procedure.
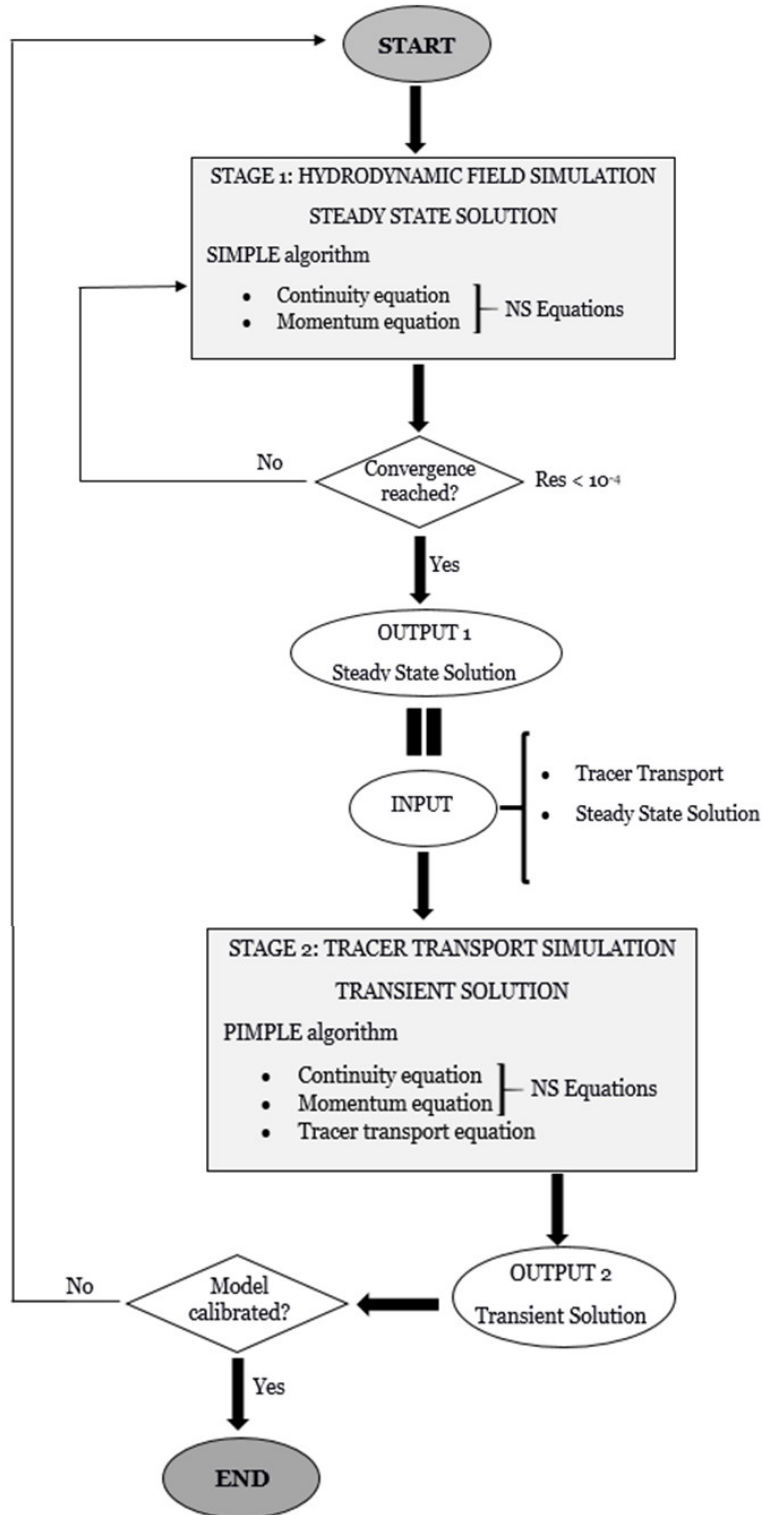
Figure 5.6. RTD$_2$ results for different meshes

5.2.3. Mixing assessment

Uniformity index (UI) is used for quantitative mixing assessment following Terashima et al. (2009) and Dapelo et al. (2018). Being V_i the volume of the i-th cell in the computational domain and χ_i the tracer concentration in the i-th cell in the same region, the total volume V (Eq. 5.4) and the average tracer concentration in the reactor $\bar{\chi}$ (Eq. 5.5) are described by the following expressions:

$$V = \sum_i V_i \tag{5.4}$$

$$\bar{\chi} = \frac{1}{V} \sum_i V_i \cdot \chi_i \tag{5.5}$$

Thus, *UI* (Eq. 5.6) is defined as:

$$UI = \frac{1}{2V\bar{\chi}} \cdot \sum_i |\chi_i - \bar{\chi}| \cdot V_i \tag{5.6}$$

As demonstrated in Terashima et al. (2009), *UI* is bounded between 0 and 1, meaning $UI = 0$ total homogeneity in tracer concentration in the complete domain and $UI = 1$ complete inhomogeneity for the analysed region.

5.3. <u>Results and discussion</u>

In this section, main results obtained are discussed. The model is validated based on tracer tests described in 5.2.1.2. Modelling parameters used by the model are shown in Table 5.5. and are kept constant in all numerical simulations of this chapter.

5.3.1. Model calibration and validation

AnoxAn reactor is modelled in 3D using the toolbox OpenFOAM®, a free and open-source CFD software. RANS equations for turbulent flow are solved for turbulent flow at Altamira supercomputer, which is part of the Spanish Supercomputing Network. It is equipped with Intel Sandybridge E5-2670 at 2.6 GHz CPU, with 158 compute nodes IBM dx360 with two Intel Sandybridge E5-2670 processors, each one with 8 cores operating at 2.6 GHz and a cache of 20 MB, 64 GB of RAM memory (i.e. 4 GB/core) and 500 GB local disk. The running time for each model simulated is between two and three weeks for a maximum of 220 minutes, using 8 cores per simulation.

Table 5.5. Model calibration parameters

Model	Calibration parameters
Tracer transport model	Self-diffusion coefficient. $D_k = 10^{-20}\,\mathrm{m^2/s}$
	Schmidt number. $Sc_t = 0.8$
Impeller model	Tangential velocity module. $V_t = 100$ rpm $= 10.5$ rad/s
	Radial velocity module. $V_r = 0$
	Axial velocity module. $V_a = 0$
Baffle model	Friction coefficient. $k = 500\ 000$ kg/s

The fit between the experimental and simulated results at different tracer inlet configurations are shown in Fig. 5.7. The experimental RTD results (circles) are compared with the CFD model (green lines) simulations.
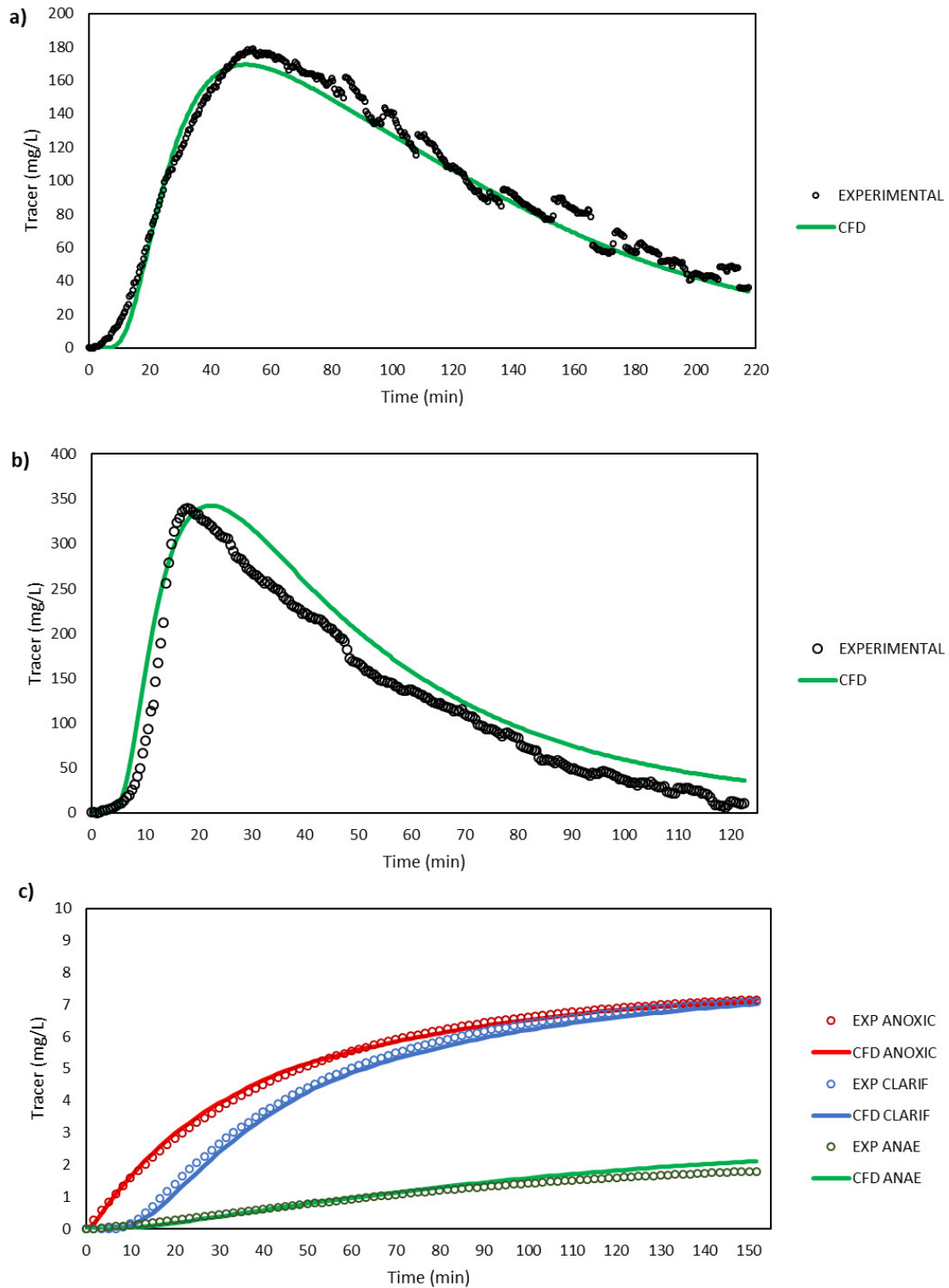
Figure 5.7. Comparison of experimental (black circles) and simulated CFD (coloured lines) RTD curves for the experimental setups: (a) Pulse RTD test with tracer injection in the anaerobic zone, (b) Pulse RTD test with tracer injection in the anoxic zone and (c) Step tracer test with tracer injection in the anoxic zone

Comparing the experimental RTD results (circles) to the CFD model simulations (green lines) it can be observed that the predictions of the model agree with the experimental measurements. This verifies that the Navier-Stokes solutions for the turbulent flow and diffusion-convection equations reliably represent tracer transport within AnoxAn. In addition, the coefficient of determination R^2 has been determined in order to quantify the fit between the simulated and experimental results (Díez-Montero et al., 2015; Fang et al., 2011; López et al., 2010; Makinia et al., 2006), obtaining high values in all the cases (Table 5.6).

Table 5.6. R^2 coefficient of determination for different CFD models

RTD Curve	R^2
RTD_1	0.98
RTD_2	0.96
RTD_3 – Anoxic curve	0.99
RTD_3 – Clarification curve	0.99
RTD_3 – Anaerobic curve	0.99

Moreover, experimental HRT in pulse tests and numerical HRT taken from CFD models are compared for further validation (Brannock et al., 2010a-b; Plascencia-Jatomea et al., 2015; Climent et al., 2018) and results are shown in Table 5.7. Both HRT have been calculated cutting the curve in the time corresponding to the last experimental measurement. The HRT numerical result is observed to have a difference of less than 7% in both cases. Therefore, modelling approaches followed for single elements, i.e. impeller and deflector, are considered satisfactory.

Besides, the difference between real (experimental) and theoretical HRT is also discussed. It is observed that real HRT is smaller than the theoretical value. This means that not the overall volume is being used in the mixing process, resulting in dead volumes (Eq. 5.7) or stagnant zones (Climent et al., 2018). It should be highlighted that cutting the curve in the time corresponding to the last experimental measurement, it could lead to slightly underestimated HRT, due to the tracer mass not taken into account in the tail of the curve. Therefore, the real dead volumes could be slightly lower than the calculated ones, as shown in Table 5.7.

$$V_d = \left(1 - \frac{HRT_{exp}}{HRT_{theo}} \right) \cdot 100\% \tag{5.7}$$

Table 5.7. HRT comparison for theoretical, experimental and CFD models

Experiment	HRT_{theo}	HRT_{exp}	HRT_{CFD}	Dead Volume
RTD_1	124 min	97 min	96 min	≤22%
RTD_2	50 min	44 min	47 min	≤12%

5.3.2. Hydrodynamic analysis based on RTD curves

Analyzing the experimental RTD measurements (Fig. 5.7, black circles), the following can be stated:

With respect to the pulse tracer tests (Fig. 5.7a and 5.7b), the non-ideal AnoxAn flow pattern is analysed. The time evolution of the RTD curve allows to confirm that they are between the Continuous Stirred Tank Reactor (CSTR) and a Plug Flow Reactor (PFR). This deviation in ideal flow patterns is a consequence of the presence of some preferential flow and channelling zones in the AnoxAn. In addition, in both RTD_1 and RTD_2 (Fig. 5.7a-b) experiments a remarkable tailing is observed. This is the result of the presence of stagnant or dead flow zones, where tracer transport is low, resulting in higher tracer concentration. The existence of stagnant zones means that the entire reactor volume is not being used efficiently, which may lead to a decrease in the actual HRT compared to the design value. However, the RTD curves do not provide information on the location and size of the channelling zones or dead volumes. This information can be crucial for the optimization of the AnoxAn design and its scalability. Thus, using a calibrated and validated CFD model, an additional hydrodynamic analysis can be performed. Detailed velocity fields and tracer concentration can be tracked in order to better understand the flow and mixing mechanisms within the reactor and identify dead flow zones.

Regarding step tracer test (Fig. 5.7c), a remarkable hydraulic separation between anoxic and anaerobic zones is confirmed. In fact, the tracer concentration reached in the anaerobic zone for the last measurement is 25% of the concentration observed in anoxic and clarification zones. In addition, a delay in the stabilization of the concentration in the clarification zone is observed compared to the anoxic one. According to compartment-based hydraulic models built (Díez-Montero et al., 2015), this delay is due to the influence of the baffle, which in theory, reduces the up-flow velocity. However, a further hydrodynamic analysis based in CFD techniques are needed to study that hypothesis.

5.3.3. Hydrodynamic analysis based on CFD simulations

Dead flow zones and short-circuiting can be studied based on velocity field analysis. In this sense, CFD model results regarding velocity vectors and/or streamlines have been previously used in water treatment studies (Arnaldos et al., 2018; Brannock et al., 2010a; Climent et al., 2018; Plascencia-Jatomea et al., 2015; Rehman, 2016). In this regard, the velocity magnitude (Fig. 5.8a, Fig. 5.8d and Fig. 5.8g), the vertical velocity component (Fig. 5.8b, Fig. 5.8e and Fig. 5.8h) and flow streamlines (Fig. 5.8c, Fig. 5.8f and Fig. 5.8i) for the most representative zones in AnoxAn are presented in Fig. 5.8.

A cross section XZ is represented together with horizontal cross sections XY at different levels to better visualise the magnitude and vertical component of the velocity fields. For the streamlines, a full 3D representation of the main flow patterns is presented.

Note that for velocity magnitudes, a logarithmic scale has been used for better visualization. For vertical velocities, negative downstream values are shown in blue and positive upstream values are shown in red. Different vertical velocity scales have been used for the flow lines in order to obtain more detailed information for each zone.
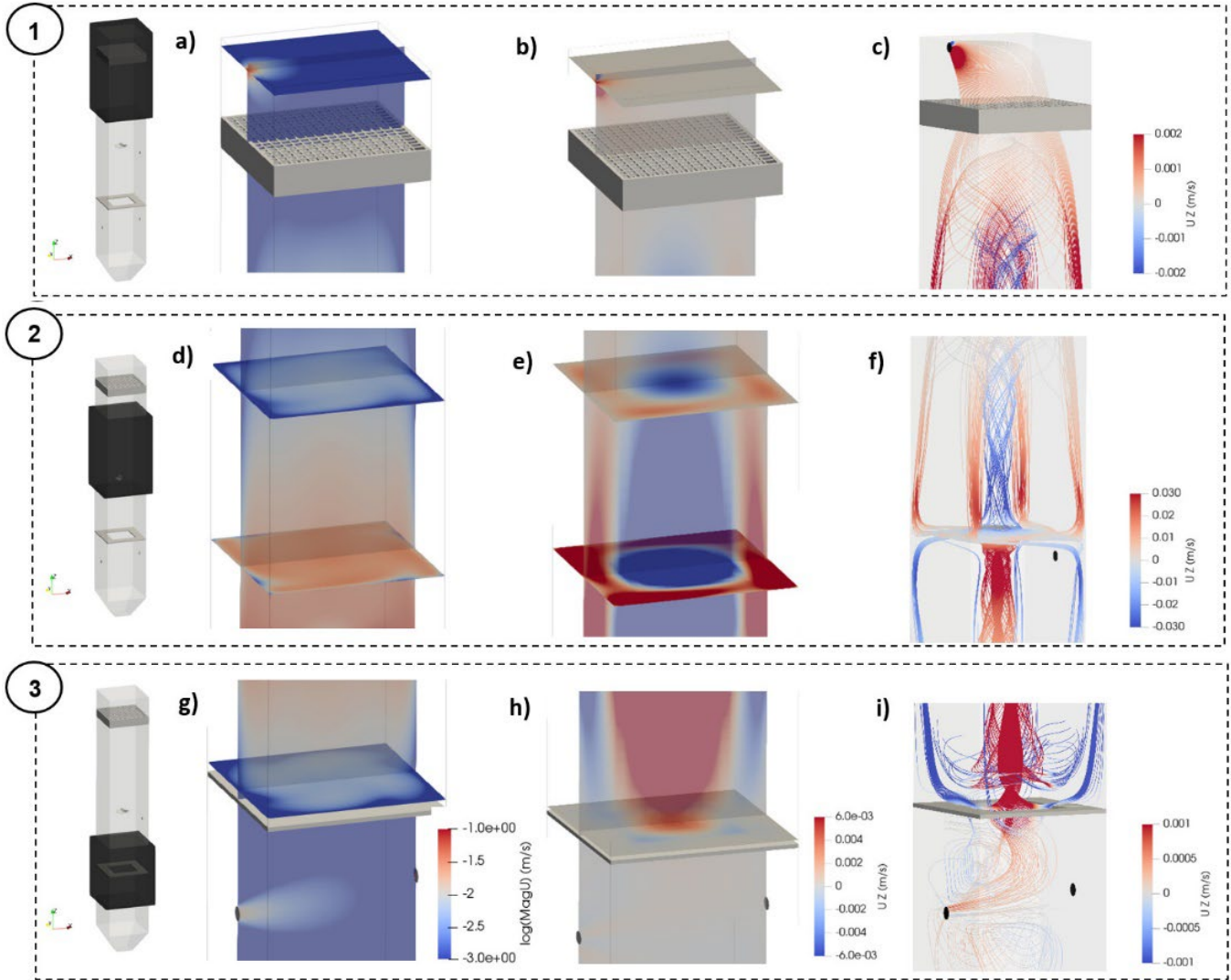
Figure 5.8. Velocity fields in AnoxAn: (a) velocity magnitude in anoxic-clarification transition zone, (b) vertical velocity in anoxic-clarification transition zone, (c) streamlines in anoxic-clarification zone, (d) velocity magnitude in the main anoxic zone, (e) vertical velocity in the main anoxic zone, (f) streamlines in the main anoxic zone, (g) velocity magnitude in anaerobic-anoxic transition zone, (h) vertical velocity in anaerobic-anoxic transition zone and (i) streamlines in anaerobic-anoxic transition zone.

5.3.3.1. Anoxic-clarification transition zone

Velocity fields for the upper anoxic and clarification zones which are separated by the baffle (in grey) are shown in Fig. 5.8a-c. The highest velocity profiles in that section are noted in the outlet. Similarly to other research (Arnaldos et al., 2018; Climent et al., 2018; Plascencia-Jatomea et al., 2015), those high velocities enhance a preferential flow channelling through it, creating a stagnant zone in the opposite corner of the outlet. In that zone, near zero velocities are observed. The aforementioned preferential path formation is represented in Fig. 5.8c, where it is observed that principal streamlines avoid outlets opposite corner. Besides, the baffle seems not to have influence in the hydrodynamic behaviour. This is attributed to the low velocity in this zone, caused by the limited influence of the impeller.

5.3.3.2. Main anoxic zone

Fig. 5.8d, Fig. 5.8e and Fig. 5.8f show the values of the magnitude of the velocity, the vertical velocity and the flow lines in the main anoxic zone. It can be observed that the velocity magnitude profile (Fig. 5.8d) in the different XY sections reproduces a flow pattern with high rotationality as a consequence of the action of the impeller. It is also observed that the highest values of the velocity module are found on the sides and in the central part of the reactor.

As for the vertical component of the velocity (Fig. 5.8e), preferential upward flow zones are observed near the reactor walls, with a flow channel on the outside of AnoxAn. This is also observed in Fig. 5.8f, where the flow lines describe an upward flow path formed through the walls. Consequently, most of the mass transport in the main anoxic zone occurs through the reactor walls. As a result, downward flow velocity profiles are found mainly in the central part of the reactor.

In addition, the limited influence of the impeller is shown in Fig. 5.8d-f. Both the magnitude of the velocity and the vertical value of the velocity decrease with the height of the reactor. This coincides with what was observed and discussed for the anoxic-clarification transition zone in Fig. 5.8a-c. Consequently, the zone of influence of the impeller barely reaches the baffle in the clarification zone, which implies a delay in the homogenization of the concentration of the anoxic and clarification zones, as observed for RTD_3 in Fig. 5.7c.

5.3.3.3. Anaerobic-anoxic transition zone

Finally, the magnitude of the velocity, vertical velocity and flow lines in the volume around the deflector between the anaerobic and anoxic zones are shown in Fig. 5.8g, Fig. 5.8h and Fig. 5.8i respectively. The deflector, with a width of 4 cm from the reactor walls, is represented in grey.

As in the main anoxic zone (Fig. 5.8d), the velocity magnitude profile (Fig. 5.8g) also reproduces the rotational flow patterns induced by the impeller. Due to the influence of the deflector, it is observed that the highest values of the velocity modulus are located in the inner part of the reactor while near the walls the velocity magnitude is lower.

For the vertical component of the velocity (Fig. 5.8h), and due to the influence of the deflector, the highest positive value is clearly concentrated in the central part of the reactor, forming preferential upward flow patterns in the inner part of the section. This generation of preferential flow patterns can also be observed at Plascencia-Jatomea et al. (2015). Once the influence of the impeller on the anoxic volume has been reached, an upward flow channel is formed through the walls as explained for the main anoxic zone in Fig. 5.8d-f.

As shown in Fig. 5.8h, there are no vertical velocities around the deflector, suggesting the presence of dead flow zones. The latter is represented in Fig. 5.8i, where the flow lines avoid the outer corners of the deflector, which improves the behaviour of the stagnant flow. In addition, downward flow can be observed near the internal walls of the deflector (Fig. 5.8h-i), in the anoxic zone. Although these observed velocity values are very small and not very significant in this case, depending on the geometry of the reactor they can contribute to creating a downward flow channel, causing unwanted mixtures or contamination from the anoxic zone to the anaerobic zone.
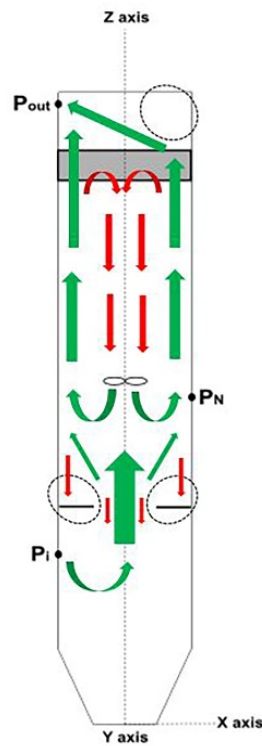
Figure 5.9. Hydrodynamic scheme of AnoxAn.

All the main phenomena previously explained in the hydrodynamic analysis are resumed in Fig. 5.9, where green arrows represent main up flow zones and the red ones down flow zones. Dashed line zones mean potential stagnant or dead flow volumes.

5.3.4. Tracer transport analysis based on CFD simulations

Tracer concentration evolution is analysed next, analysing pulse RTD_2 and step RTD_3 tests for the anoxic-clarification transition, main anoxic and anaerobic-anoxic transition zones. RTD analysis combined to CFD and velocity field analysis in order to evaluate dead volumes and chanelling have been already used in the water treatment field (Brannock et al., 2010a; Climent et al., 2018; Wei et al., 2019).

5.3.4.1. Anoxic-clarification transition zone

Fig. 5.10 shows the concentration range of the tracer for the different time steps in the RTD_2 pulse test. It is observed that the tracer slowly reaches the effluent outlet. It takes between 5 and 10 minutes to reach the clarification zone due to the limited influence of the impeller in the upper part of the anoxic zone. This is consistent with the results obtained in the hydrodynamic analysis of the fluid in the reactor.

In addition to this and as the simulation progresses, the presence of a preferential flow pattern towards the outlet is observed. A greater concentration of tracer is found around the outlet. This pattern is developed after 15 minutes of simulation, confirming the existence of a dead volume in the opposite corner of the outlet, as it was shown in Fig. 5.8a-c.
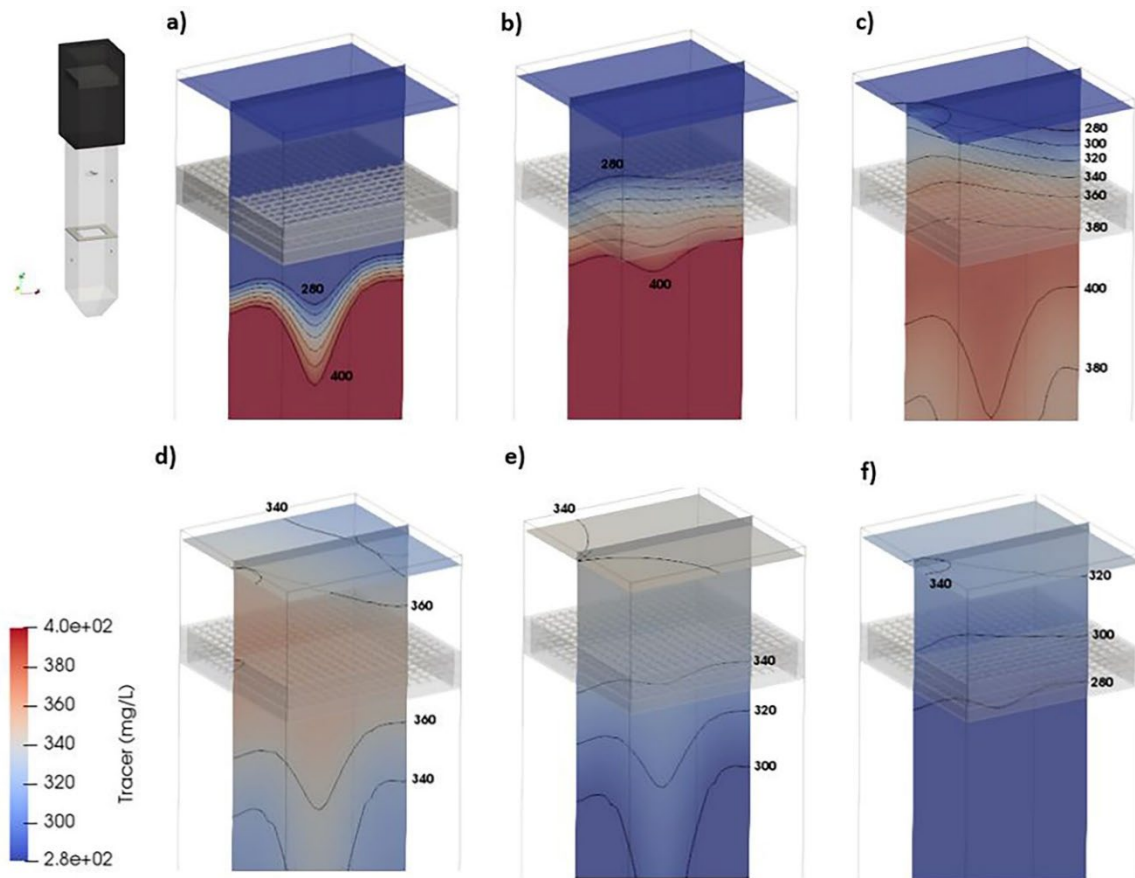
Figure 5.10. Tracer concentration field in anoxic-clarification transition zone for different time steps in RTD_2 (a) 5 min, (b) 10 min, (c) 15 min, (d) 20 min, (e) 25 min and (f) 30 min.

Fig. 5.11 shows the evolution of the concentration of the tracer for two different points at the exit and its opposite corner (P_1 and P_2). First, it is observed that the maximum concentration value of the tracer at the exit (P_1) is slightly higher than that of its opposite corner (P_2). The delay between the two peaks is 2.5 minutes (5% of the total RTD_2 HRT). Although P_1 is located further from the tracer injection point (P_N) than P_2, the tracer first arrives at the outlet due to the channelling zone observed in Fig. 5.8a-c and 5.10c-d and similar to Climent et al. (2018). The difference in tracer concentration at both points is less than 5% after 20.5 minutes of experiment (44% of total RTD_2 HRT). After 26 minutes of experiment, the concentration of the tracer in the opposite corner (P_2) is higher than in the output (P_1) for the first time, reaching a maximum of 5% higher at t = 66 minutes. This confirms that tracer dilution first happens through the preferential flow formed around the outlet (P_1), generating a zone of stagnant behaviour in its opposite corner (P_2) as shown in Fig. 5.8a-c and Fig. 5.10.
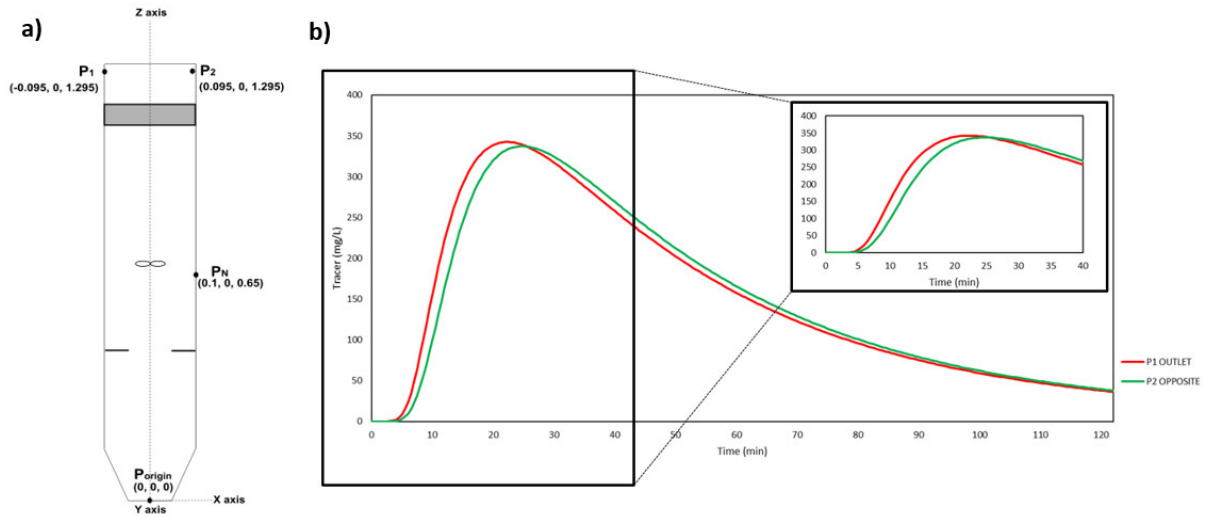
Figure 5.11. (a) Scheme of tracer concentration measurement points in anoxic-clarification transition zone (dimensions in meters) and (b) Tracer concentration evolution in the outlet (P_1) and its opposite corner (P_2) for RTD_2

5.3.4.2. Main anoxic zone
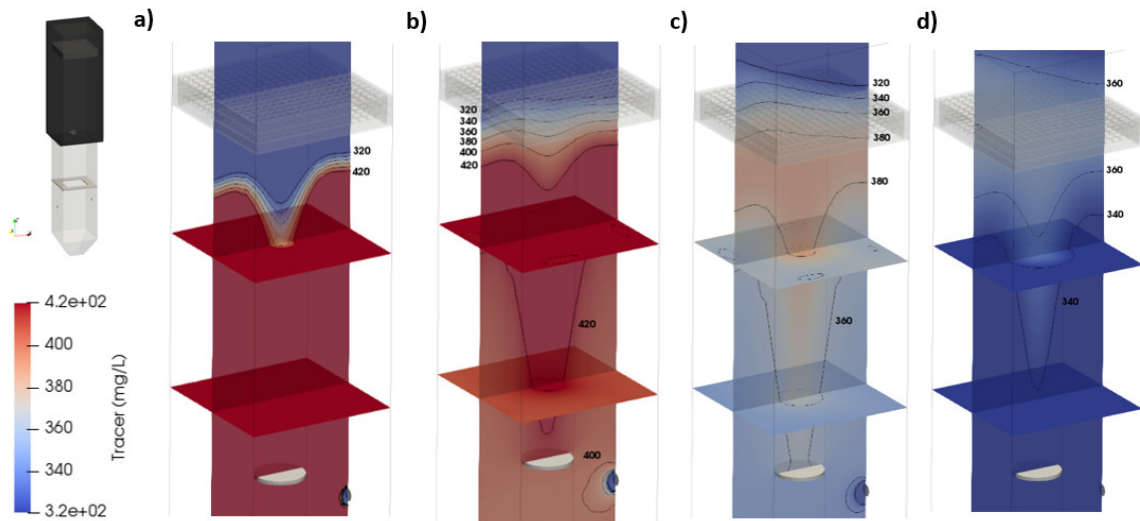
Figure 5.12. Tracer concentration field in main anoxic zone for different time steps in RTD$_2$ (a) 5 min, (b) 10 min, (c) 15 min and (d) 20 min.

Fig. 5.12 shows the tracer concentration fields for the different time steps in the RTD$_2$ pulse test. It is observed that, first of all, the main tracer transport exists in the zones with higher upper velocity, i.e. the preferential flow channels near the walls. The latter matches with the observed in velocity field analysis for Fig. 5.8d-f. As the simulation time progresses, it is observed that due to a higher vertical velocity, the tracer is firstly diluted in the mentioned outer part of AnoxAn, which is attributed to the action of the impeller. On the other hand, the tracer remains stagnant in the internal part of the system. This is attributed to a very low value of the previously observed flow velocities.
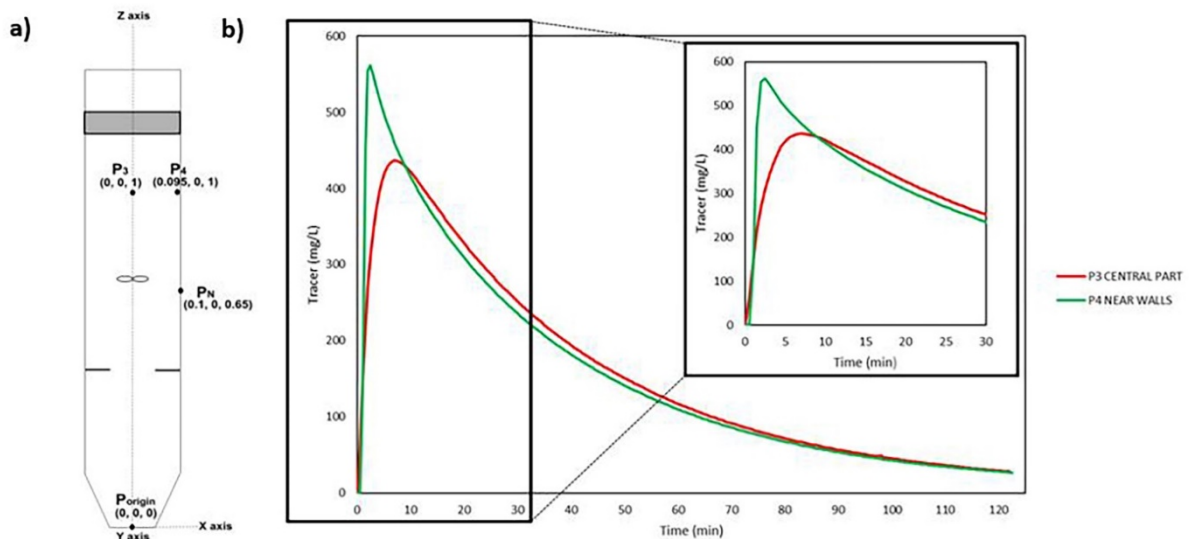
Figure 5.13. (a) Scheme of tracer concentration measurement points in main anoxic zone (dimensions in meters) and (b) Tracer concentration evolution in the central part (P$_3$) and near the walls of the reactor (P$_4$) for RTD$_2$.

Fig. 5.13 shows the evolution of the tracer concentration for the central points and near the wall (P_3 and P_4). Firstly, it is observed that the maximum tracer concentration value in P_4 is 30% higher than in the internal part of the reactor (P_3), with the delay in time between the two peaks being 5 minutes (10% of the total RTD_2 HRT). These differences in the value and time of the tracer concentration peaks reveal that the mass transport is greater through the walls (P_4) than in the central part of AnoxAn (P_3), confirming the channelling phenomena observed in Fig. 5.8d-f, Fig. 5.12 and also noticed for Climent et al. (2018). In addition, it is observed that a difference between the tracer concentration of both points is less than 5% after 7.5 minutes (16% of the total RTD_2 HRT). After 9 minutes, the concentration of the tracer in the central part (P_3) is higher than that of the walls (P_4), reaching a maximum of 10% higher in t = 58 minutes. This is due to the preferential flow that is formed through the walls. In consequence, dilution occurs first in the outer part of AnoxAn, while in the central part of the reactor a stagnant zone is formed, as also indicated in Fig. 5.8d-f and Fig. 5.12 of the analysis.

5.3.4.3. Anaerobic-anoxic transition zone
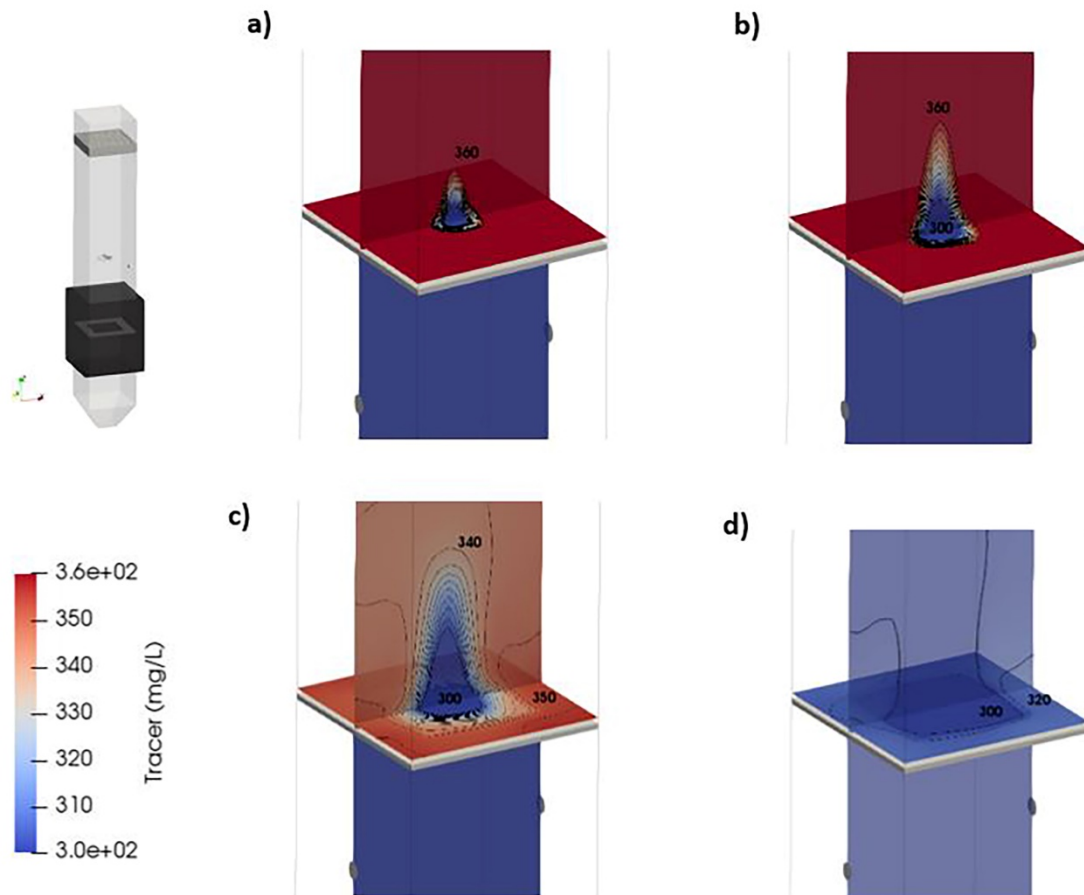
Figure 5.14. Tracer concentration field in anaerobic-anoxic transition zone for different time steps in RTD_2 (a) 5 min, (b) 10 min, (c) 15 min and (d) 20 min.

The concentration range of the tracer for different time steps in the RTD_2 simulated pulse test is shown in Fig. 5.14. Fig. 5.14c-d clearly shows the shape of the deflector in the concentration field. The lower concentration profiles are observed in the central part of the reactor, coinciding with the higher velocities of flow rise. In addition, a higher concentration of the tracer is observed in the zones where zero or low velocities are registered, especially in the zone above the deflector.

This confirms that dead volumes and stagnant areas are found in these sections with the highest concentration of tracers. Furthermore, it shows that the tracer does not reach the anaerobic zone due to the presence of the deflector, suggesting that this element is crucial to achieve the desired anoxic-anaerobic hydraulic separation as also observed for a different multi-environmental reactor in Calder et al. (2013). Finally, as the time of the experiment progresses, a complete dilution in the reactor is observed.
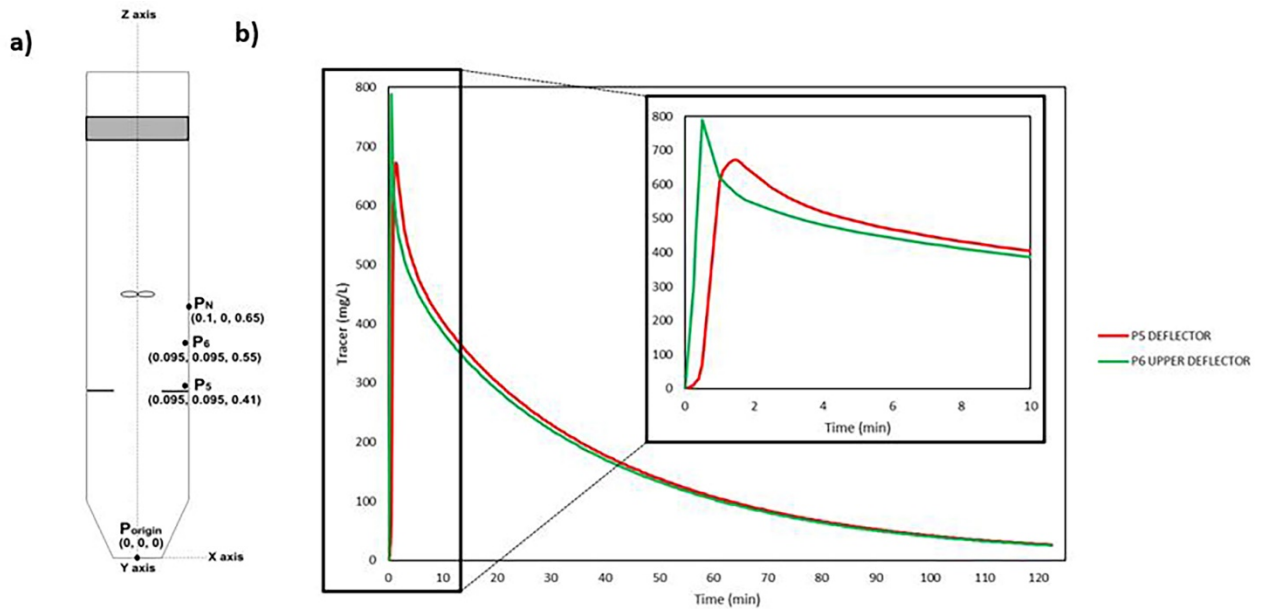
Figure 5.15. (a) Scheme of tracer concentration measurement points in anaerobic-anoxic transition zone (dimensions in meters) and (b) Tracer concentration evolution in the upper deflector zone (P_5) and in the deflector (P_6) for RTD_2.

Fig. 5.15 shows the evolution of the tracer concentration for two different points near the deflector (P_5 and P_6). First, it is observed that the maximum tracer concentration value at P_6 is 20% higher than near the deflector (P_5). However, almost from the beginning of the experiment, the tracer concentration remains at least 5% higher at P_5 than at P_6 until complete dilution. That confirms that a stagnant zone is formed under the influence of the deflector as shown in Fig. 5.8g-i and Fig. 5.14.

5.3.4.4. Overall reactor

Fig. 5.16 shows the evolution of the tracer concentration in AnoxAn for the simulated step RTD_3 test. First, it is clearly observed that contamination of the anaerobic zone is avoided. Thus, as concluded with the analysis of step tracer tests, the hydraulic separation between the anoxic and anaerobic zones is reaffirmed. The presence of the deflector between the two environments together with the velocity of the upward flow seems to be crucial to avoid contamination between them.

In addition, the formation of a zone with a high concentration of tracer in the anoxic zone that does not occupy the entire anoxic volume due to the limited influence of the impeller can be detected. In fact, the complete mixing of the tracer in the anoxic zone is not reached until the step test is after 40 minutes (Fig. 5.16b-c). The main anoxic volume mentioned above coincides with the main anoxic zone observed in the velocity field analysis (Fig. 5.8d-f) and with the compartment model in Díez-Montero et al. (2015). In the upper AnoxAn zone, which comprises the upper anoxic zone, the baffle and the clarification zone, the tracer moves slowly and progressively as also observed in the RTD_2 pulse tracer analysis (Fig. 5.10-5.11).
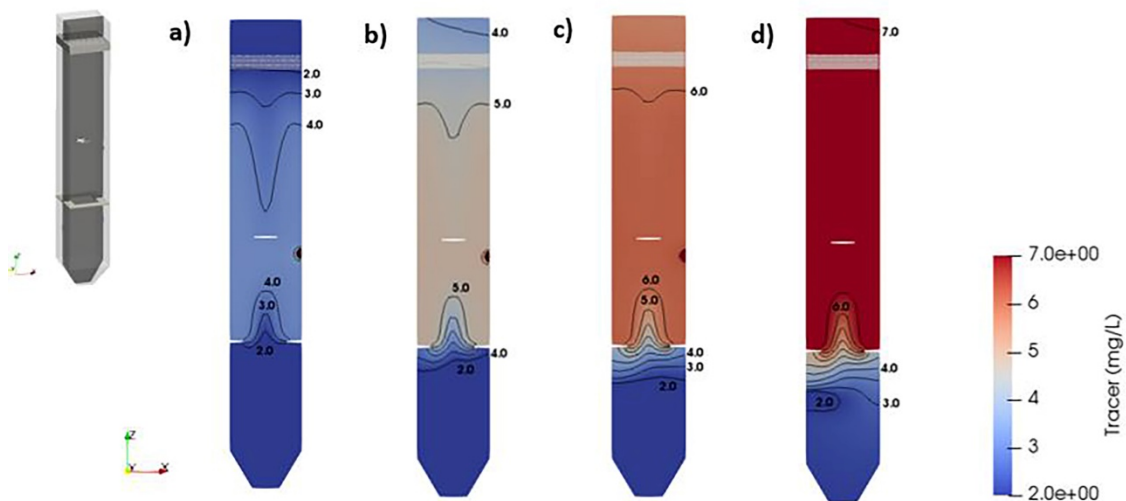
Figure 5.16. Tracer concentration field in AnoxAn for different time steps in RTD_3 (a) 20 min, (b) 40 min, (c) 80 min and (d) 150 min.

5.3.5. Homogenization time and uniformity index analysis

The evolution of the UI over step tracer – RTD_3 is shown in Fig. 5.17, for the overall reactor and the combination of the anoxic and clarification zones (Fig. 5.17a), and the three zones of the reactor independently (Fig. 5.17b). On the one hand, a clear and fast decrease of the UI is observed after starting the injection of the tracer in the anoxic and clarification zones, as well as in the combination of both them. This indicates that good mixing is achieved in both zones,

and also between them. On the other hand, only a slight decrease is observed in the UI for the overall reactor, confirming the hydraulic separation between the anoxic and anaerobic zones.

In addition, in order to quantify the degree of mixing, $t_{0.20}$, $t_{0.10}$ and $t_{0.02}$ have been calculated and are reported in Table 5.8. These values represent the times when the UI reaches 0.20, 0.10 and 0.02, and can be interpreted as the time to reach an 80%, 90% and 98% of mixing degree, respectively (Dapelo et al., 2018). Concretely, $t_{0.02}$ has been considered to represent the homogenization time or complete mixing time (Terashima et al., 2009). Finally, the ratio between $t_{0.20}$, $t_{0.10}$, $t_{0.02}$ and the HRT are also shown in Table 5.8.
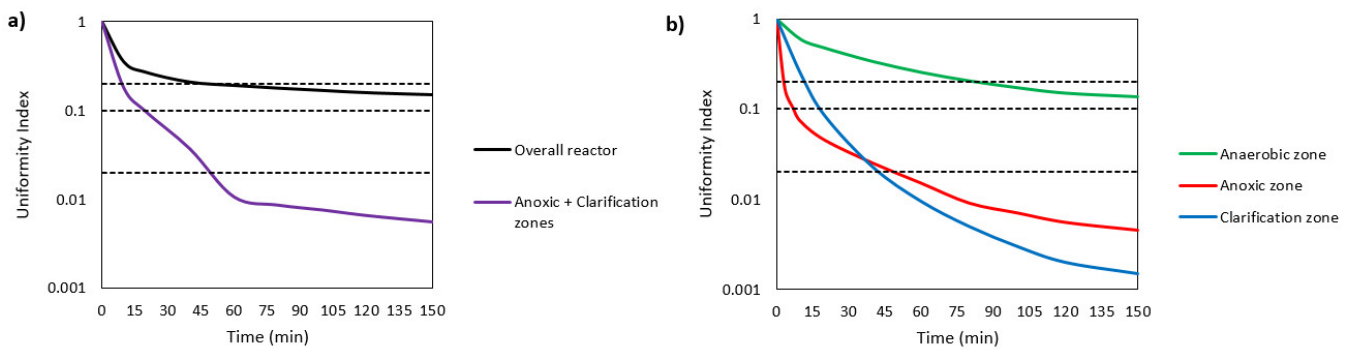
Figure 5.17. Evolution of the uniformity index (in logarithmic scale) over step tracer test – RTD$_3$: (a) Overall reactor and anoxic plus clarification zones and (b) Anaerobic, anoxic and clarification zones independently.

Table 5.8. Principal uniformity indexes at different zones of the reactor

	$t_{0.20}$ (min)	$t_{0.20}$/HRT	$t_{0.10}$ (min)	$t_{0.10}$/HRT	$t_{0.02}$ (min)	$t_{0.02}$/HRT
Overall reactor	45	0.96	-	-	-	-
Anoxic + Clarification zones	13	0.28	18	0.38	46	0.98
Anaerobic zone	82	1.74	-	-	-	-
Anoxic zone	4	0.09	7.5	0.16	50	1.06
Clarification zone	14	0.30	18	0.38	45	0.96

Complete mixing is never achieved in the overall reactor, being the UI over 0.15, while complete mixing between the anoxic and anaerobic zones is reached in 46 minutes, approximately one HRT after starting the injection of the tracer (Fig 5.17a).

Analysing the zones independently (Fig. 5.17b), it can be observed that the $t_{0.20}$ and $t_{0.10}$ are first reached in the anoxic zone. This is attributed to the fact that the tracer is injected in this zone and matches with the limited influence of the impeller in the clarification zone noted in sections 5.3.3 and 5.3.4. However, complete mixing degree is first achieved in the clarification zone, which could be explained due to its small volume and the significant short circuiting in the anoxic zone discussed in section 5.3.4. Anyway, those mixing limitations in the anoxic zone do not avoid achieving complete mixing, and their effect only delays the homogenization until approximately one HRT is completed after starting the injection of the tracer, as shown in Fig. 5.16 and Fig. 5.17b.

Regarding the anaerobic zone, complete mixing is not reached, and a UI of 0.20 is achieved after 82 minutes (1.74 times the HRT). This suggests that the degree of mixing in the anaerobic zone is limited, and could be explained by the intrusion of some tracer and the presence of dead zones around the deflector, as discussed previously in section 5.3.4.

5.3.6. Hydrodynamic analysis of reactor elements

This section analyses the influence of the clarification baffle and the anaerobic-anoxic deflector on flow hydrodynamics and mixing processes.

Comparison between RTD_2 pulse tracer test curves with and without the baffle between clarification and anoxic zones in shown in Fig 5.18. This baffle is intended for the retention of suspended solids inside the reactor, providing a quiet clarification zone with enhanced settling capability. It is expected that the baffle will be able to reduce the upward flow velocity, creating a tortuous path for the upward flow of suspended solids, and to provide an improved settling surface. However, according to the simulations performed in this work, no significant variation is observed between the two simulated RTD curves, with and without the baffle. This suggests that the effect of this element is negligible from a hydrodynamic point of view, which is attributed to the limited influence of the impeller already indicated in previous sections.

However, the baffle could be useful to improve the retention of suspended solids within the reactor, but such an assessment is beyond the scope of the present study. Further investigations should address the behaviour of suspended solids within the reactor and confirm this fact.
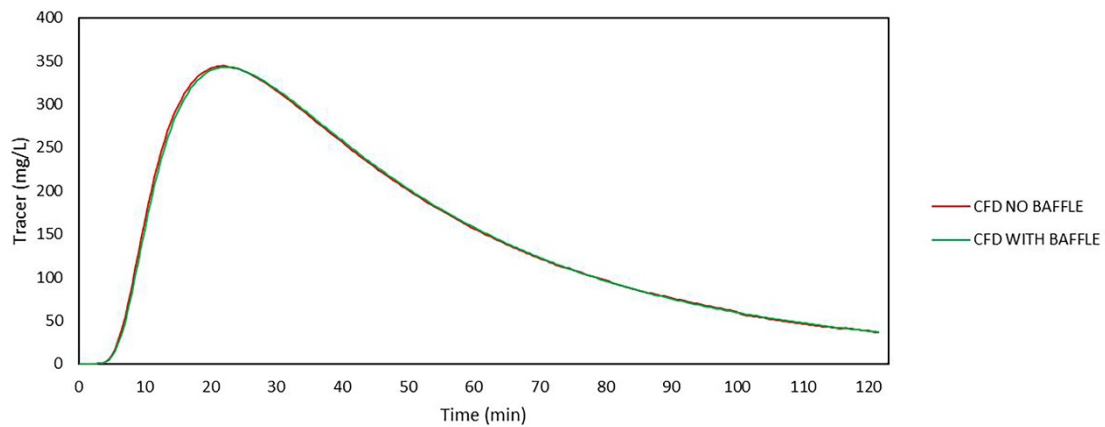
Figure 5.18. Comparison of RTD_2 curves for pulse tracer test with tracer injection in the nitrate recycle with baffle (green line) and without baffle (red line)

The comparison of velocity fields with and without the deflector between anaerobic and anoxic zones is shown in Fig. 5.19. It is observed that the velocity field changes considerably compared to that obtained with the presence of the deflector (Fig. 5.8g-h) in the anaerobic-anoxic transition section. The velocity of the upward flow is approximately 10 times lower without the deflector, due to the increase in the effective cross-section. In addition, due to the absence of the deflector, a downspout channel is observed near the corners of the section, which enhances

the mixture between anoxic and anaerobic environments. This demonstrates the need to use this element for a correct hydraulic separation between anaerobic and anoxic volumes. Finally, the upward flow channelling occurs mainly in the internal part of the section.
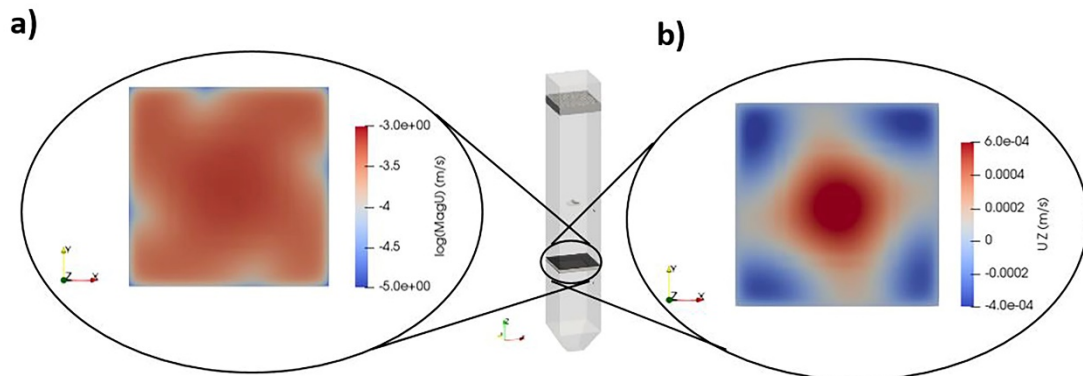
Figure 5.19. Velocity field without deflector in anaerobic-anoxic transition zone (a) velocity magnitude and (b) vertical velocity

Fig. 5.20 shows the evolution of the tracer concentration in the anaerobic, anoxic and clarification zones of the reactor for the RTD$_3$ step tests, with and without the deflector. The anoxic and clarification zones are hardly affected by the absence of the deflector. However, the concentration of the tracer in the anaerobic zone increases significantly compared to the one observed in the simulation with the deflector as it was predicted in Fig. 5.19. Concentration values in the anaerobic volume of almost double compared to those obtained with the deflector are observed. The increase is estimated at 84%. These results confirm that this specific element is essential for maintaining hydraulic separation between the two zones.
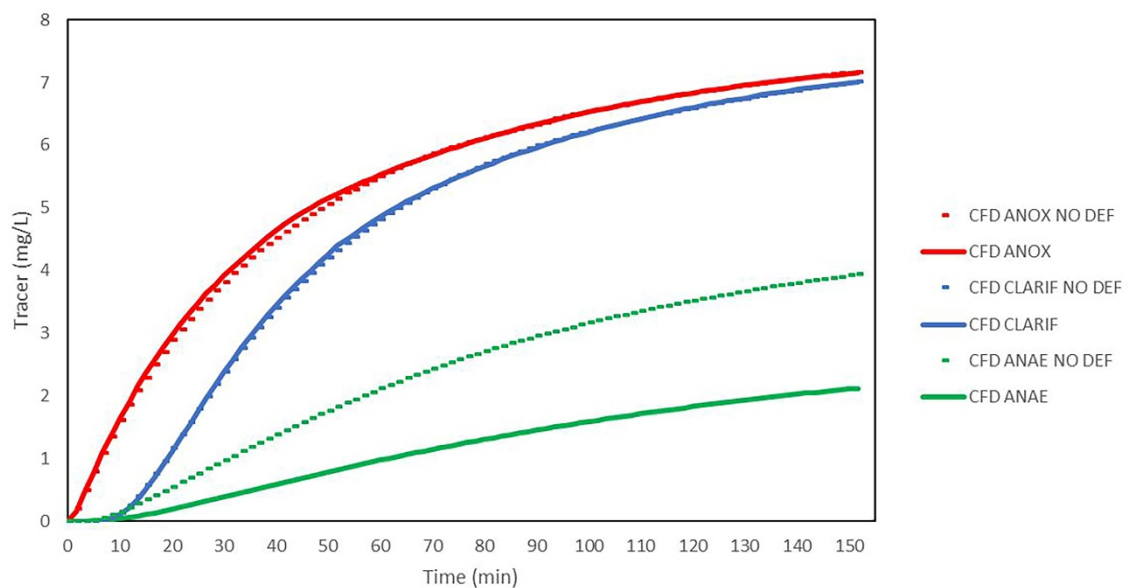
Figure 5.20. Comparison of RTD$_3$ curves for step tracer test with tracer injection in the anoxic zone with deflector (continuous lines) and without deflector (dashed lines).

5.4. <u>Conclusions</u>

In this study a hydrodynamic analysis of the novel anaerobic-anoxic AnoxAn reactor is performed. A numerical CFD model is constructed and validated for tracer transport using the open source OpenFOAM® toolbox. The conclusions of this work are summarised:

- The numerical model constructed in this work adequately reproduces the global mass transport behaviour of the simulated multi-environment reactor. Therefore, the validity of the numerical modelling approach is confirmed for reactor elements such as the impeller and the baffle.

- CFD simulations provide a deeper understanding of the hydraulic behaviour of the fluid within the reactor, compared to previous models based on compartments and RTD tests. This allows detecting not only the existence, but also the location and quantification of preferential flow channelling and dead volumes.

- The stagnant zones in the AnoxAn reactor are located mainly in the corner opposite the exit in the clarification zone, and near the deflector between the anaerobic and anoxic zones.

- The main preferential flow patterns are found on the outside of the anoxic zone, specifically near the walls, being transport through them a 30% higher than in the internal part of the anoxic zone. In addition, another channelling is observed in the clarification zone due to the influence of the flow outlet, and despite being farther from the tracer injection location, the tracer reaches the outlet 2.5 min before its opposite corner.

- The analysis of the uniformity index shows that, despite the existence of short-circuiting and dead zones, complete mixing is achieved in the anoxic and clarification zones. The homogenization time in anoxic and clarification zones was approximately one HRT after starting the injection of a pulse of tracer.

- Although the use of the baffle is assumed to be necessary to avoid excessive transport of solids to the clarification zone, it is observed that this has no influence on the hydrodynamics of the reactor. This is attributed to the limited influence of the the impeller, which generates very small upward flow velocities in the clarification zone.

- It has been observed that the deflector located between the anoxic and anaerobic zones is essential to maintain the required hydraulic separation, being the increase of tracer concentration in anaerobic zone around 84% when deflector is not used.

Chapter 6

Hydrodynamic optimization of multi-environment reactors for biological nutrient removal: A methodology combining computational fluid dynamics and dimensionless indexes

6.1. <u>Introduction</u>

Nutrient removal from wastewater before it is discharged to the environment represents one of the main concerns in the water treatment field. Current regulations establish strict water quality objectives as the number of areas being declared as sensitive to eutrophication has notably increased (European Union, 1991; European Union, 2000). In consequence, many existing Wastewater Treatment Plants (WWTP) are forced to upgrade or retrofit their configuration for nitrogen and phosphorus removal. Conventional processes for Biological Nutrient Removal (BNR) include anoxic and anaerobic environments or compartments, in addition to the aerobic one, which entail much more complex treatment trains compared to those for only organic matter removal (Water Environment Federation, 2011). This increase of complexity implies higher energy consumption and derives in a larger volume that in many cases is not available on site.

One recent approach to simplify the complexity of conventional BNR treatment trains is the implementation of suspended growth multi-environment reactors, which combine different environmental conditions (aerobic, anoxic and/or anaerobic) in a single reactor. These reactors can provide high compactness and efficiency adaptable to the existing land, energy and water quality constraints. For instance, the BioCAST reactor unifies the aerobic and anoxic conditions for carbon and nitrogen removal (Yerushalmi et al., 2010); the upflow multi-layer bioreactor (UMBR) combines anoxic and anaerobic zones (with the anoxic at the bottom) for BNR (Kwon et al., 2005); and AnoxAn unifies the anaerobic and anoxic zones (with the anaerobic at the bottom) in a continuous upflow sludge blanket reactor (Tejero et al., 2010). Although efficiency and feasibility of these multi-environment reactors have been mainly studied from a biological perspective (Yerushalmi et al., 2011; Kwon et al., 2005; Díez-Montero et al., 2016), fluid mechanics of the systems have appeared to significantly affect their performance (Yerushalmi et al., 2013; Díez-Montero et al., 2015). While conventional dimensioning of BNR processes suppose ideal complete mixing flow in reactors (DWA, 2000; Water Environment Federation, 2011) neglecting the hydrodynamic phenomena that interfere in ideal flow conditions, several studies have shown that a correct hydrodynamic behaviour enhances a desirable biological efficiency in bioreactors for water treatment (Castrillo et al., 2019; Angeloudis et al., 2014; Climent et al., 2018; Arnaldos et al., 2018; Wei et al., 2019; Water Environment Federation, 2011). In particular, the different environmental zones in multi-environment reactors usually imply the presence of baffles or deflectors, or different mixing devices in each zone, giving rise to complex hydrodynamic behaviour, which is not easy to characterize.

Hydrodynamic analysis is usually based on experimental work, which is highly resource and time demanding, and in many cases impracticable at large-scale (Fernández, 2012). In addition, for the optimization of reactors, physical and geometrical changes are required in order to evaluate the hydrodynamic performance of alternative configurations. The use of modelling, combined with experimentation, can overcome or reduce the aforementioned issues. One possible hydrodynamic modelling approach is the development of the widely used compartment-based models such as the tank-in-series and the dispersion model

(Levenspiel, 1999). However, the black-box nature of this kind of models does not provide any information regarding spatial flow or concentration distribution (Plascencia-Jatomea et al., 2015; Qi et al., 2013; Blanco-Aguilera et al., 2020a). Moreover, in general they are only useful for specific operational conditions, not allowing to test the effect of changing any geometrical parameter of the studied reactor. That is one of the reasons why numerical techniques based on Computational Fluid Dynamics (CFD) have grown up in the last decades and are being applied in a wide variety of problems within the wastewater field (Samstag et al., 2016; Wicklein et al., 2016). In fact, they allow a deeper hydrodynamic analysis including both quantitative and qualitative evaluation of dead zones, velocity profiles and flow patterns, mixing performance or short-circuiting.

Regarding the hydraulic optimization of water treatment systems, the hydrodynamic performance is commonly assessed through hydraulic indexes (Demirel et al., 2018). The optimization process usually consists in the evaluation of the hydraulic performance through dimensionless indexes for different geometrical configurations. These dimensionless indexes evaluate different hydrodynamic features such as short-circuiting, mixing efficiency or dead volumes based on the analysis of the Residence Time Distribution (RTD) or the results of model simulations. Examples of hydrodynamic optimization of water treatment systems using CFD simulations can be found in literature for contact tanks (Demirel et al., 2016; Dapelo et al. 2018; Angeloudis et al., 2014; Gualteri et al., 2009), constructed wetlands (Chang et al., 2016; Rengers et al., 2016; Persson et al., 1999), multi soil layering (MSL) technology (Latrach et al., 2018), anaerobic digesters (Wei et al., 2019; Dapelo et al., 2018; Terashima et al., 2009), conventional activated sludge systems for nitrogen removal (Climent et al., 2018) or membrane bioreactors (Yan et al., 2015, 2016). However, the optimization procedure applied in each case is different and hydraulic indexes are used separately without any standardization. A systemic methodology capable to join multiple features could aid in the hydrodynamic evaluation and optimization of multi-environment bioreactors, guaranteeing the best possible biological performance.

In addition, there is a lack of hydrodynamic optimization studies regarding multi-environment reactors. Their complex hydraulic behaviour generates non-ideal flows that reduces the hydrodynamic performance, and in consequence, the biological efficiency. To our knowledge, there are only few studies based on CFD for evaluation and optimization of the hydrodynamics of multi-environment reactors (Calder et al., 2013; Blanco-Aguilera et al., 2020a). Calder et al. (2013) changed a baffle geometry to assess the hydraulic behaviour of the aerobic-anoxic BioCAST reactor based on velocity fields, but did not use a systematized methodology of hydraulic indexes. Blanco-Aguilera et al. (2020a) (Chapter 5 of this document) performed a comprehensive analysis assessing the presence of dead zones, channelling and studying the mixing efficiency and hydrodynamic influence of some feature elements (deflector and baffles) in the anaerobic-anoxic AnoxAn reactor, but did not deepen into a holistic and systematic hydrodynamic optimization. At this respect, the need for comprehensive hydrodynamic analysis to carry out the geometric optimization and propose other reactor configurations applicable on a large scale has been pointed out (Díez-Montero et al., 2019; Blanco-Aguilera et al., 2020a).

All in all, the objective of this study is double: on one hand, to propose a standardized hydrodynamic optimization methodology for bioreactors combining the potentialities of CFD with dimensionless indexes, capable to unify multiple hydraulic features with a benchmarking approach. On the other hand, the goal is to cover the lack of CFD studies in literature regarding multi-environment reactors, extending and applying the proposed methodology to a case study.

The present chapter is structured as follows. After this introduction, a discussion of the existing hydraulic indexes is performed and new indexes and modifications of existing ones are proposed for multi-environment reactors. Then, based on the previous discussion, general expressions combining different hydraulic indexes are developed for the hydrodynamic optimization of multi-environment bioreactors. After that, the CFD model setup used for the hydrodynamic evaluation is presented. The latter has been built in the OpenFOAM® open source toolbox (Weller et al., 1998) and has been already developed, tested and validated in Blanco-Aguilera et al., 2020a (Chapters 4 and 5 of this document). Subsequently, the proposed methodology is applied to a case study, the optimization of the AnoxAn reactor. Finally, the conclusions of the study are highlighted.

6.2. <u>Materials and methods</u>

In sub-section 6.2.1, the theoretical basis and methodology for the hydrodynamic optimization of multi-environment reactors are presented. Different indexes used to characterize the hydraulic performance of water treatment systems are critically discussed first, new indexes are then developed, and the hydrodynamic optimization methodology is finally proposed. In sub-section 6.2.2, the case study is described and the numerical CFD model setup is presented.

6.2.1. Hydrodynamic optimization for multi-environment reactors

6.2.1.1. Dimensionless indexes of hydrodynamic performance

The hydraulic efficiency of a water treatment reactor is commonly assessed by means of several indexes that are mainly extracted from RTD functions (Demirel et al., 2018). These indexes help to evaluate the hydrodynamic performance of a water treatment unit quantifying key features such as mixing, short-circuiting or dead volumes. Plug flow conditions are usually pursued as they guarantee more rapid substrate uptake kinetics than in completely mixed conditions (Stensel, 1991; Jeyanayagam, 2007; Narayanan et al., 2006; Water Environment Federation, 2011).

Hydraulic separation

In multi-environment reactors, a hydraulic separation between different zones of the reactor is usually desired. The concept of hydraulic separation is interpreted as the ability of maintaining at least two zones under different environmental conditions inside a single reactor, such as aerobic-anaerobic, aerobic-anoxic, anaerobic-anoxic, or other combinations. These configurations imply a differentiation between the concentration of some compound or

characteristic involved in the biological process in the different zones, usually dissolved oxygen, nitrate, or redox potential (Díez-Montero et al., 2015). The hydraulic separation dimensionless index between two zones (HS) can be defined as the ratio between the concentrations of the desired compound in the two different environments (Eq. 6.1):

$$HS = \frac{C_{zone1}}{C_{zone2}} \hspace{6cm} (6.1)$$

Where C_{zone1} and C_{zone2} are the concentrations of the compound in two zones, being zone 2 the one with the highest expected concentration. Therefore, HS ranges between 0 and 1. HS close to zero indicates strong hydraulic separation, while HS close to 1 indicates inefficient hydraulic separation. HS can be measured under operational conditions, and in some multi-environment configurations by means of RTD analysis of pulse tracer experiments (Díez-Montero et al., 2015; Blanco-Aguilera et al., 2020a).

Dead Volumes

To determine the extent of the dead volumes inside a reactor, the effective volume ratio *e* can be used (Eq. 6.2). *e* is defined as the ratio between the measured Hydraulic Retention Time (HRT) and the theoretical HRT (Climent et al., 2018; Latrach et al., 2018; Chang et al., 2016):

$$e = \frac{HRT_{real}}{HRT_{theo}} = \frac{V_{effective}}{V_{total}} \hspace{5cm} (6.2)$$

Being $V_{effective}$ the effective or real volume and V_{total} the total or theoretical volume of the reactor. When the effective volume ratio, *e*, is equal to 1, the whole volume of the reactor is supposed to be used in the process (with no dead volumes), while for $e = 0$, the overall reactor would be a dead volume.

Short-circuiting

Short-circuiting or channelling is a convective hydrodynamic phenomenon that forces part of the fluid to leave the studied reactor earlier than the theoretical HRT by means of preferential paths. Short-circuiting must be minimized as it generates poor hydraulic and biological performances (Water Environment Federation, 2011). Among all different parameters used to characterise short-circuiting, t_{10} (defined as the time required for 10% of the injected tracer concentration to leave the reactor) has shown to be the one that better represents such phenomenon (Teixeira et al., 2008). In addition, t_{10} is the parameter used to report the hydraulic performance of contact tanks by the Environmental Protection Agency of the United States (USEPA, 1991; USEPA, 2003). In fact, many different studies have used it for short-circuiting quantification (Angeloudis et al., 2014; Demirel et al., 2016; Demirel et al., 2018; Gualteri, 2009; Rengers et al., 2016). This parameter is usually presented in its dimensionless form, θ_{10}, divided by the theoretical HRT. θ_{10} takes values between 0 and 1, being 0 high short-circuiting rate and 1 low short circuiting, representing the ideal plug flow condition. For ideal complete mixed flow conditions, the value for θ_{10} is approximately 0.1.

Mixing

Mixing in a rector refers to the turbulent diffusion that can cause spreading or retention of part of the fluid inside of it, generating stagnant and/or recirculation zones. Various indexes have been commonly used to evaluate the mixing performance of a water treatment system.
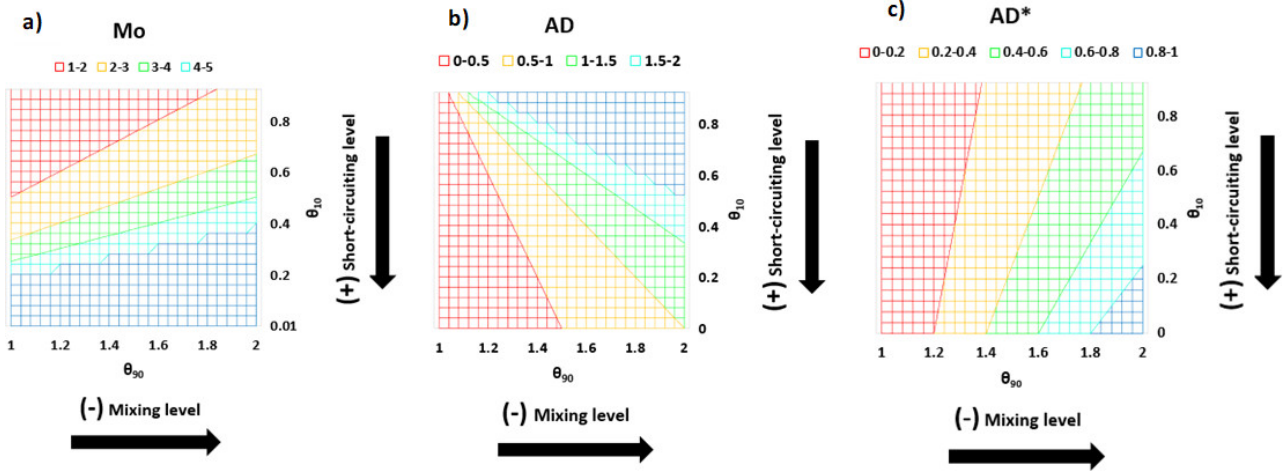
Figure 6.1. Values for mixing performance indexes: (a) Morril index, (b) AD index and (c) AD* index

First, Morrill index (Mo) was defined as the relation between θ_{90} and θ_{10} (θ_{90}/θ_{10}), where θ_{90} and θ_{10} are the dimensionless time required for 90% and 10% of the injected tracer concentration to leave the reactor, respectively. As θ_{10} ranges between 0 and 1, and θ_{90} usually between 1 and 2 (Demirel et al., 2018), Mo index is approximately bounded between 1 and 30. Although Mo has been widely used for mixing performance evaluation (in fact, Teixeira et al., 2008 concluded that it was the best index for this purpose), the influence of the short-circuiting parameter in the expression, i.e. θ_{10}, has led to interpretation problems as pointed out in Demirel et al. (2018). Concretely, when short-circuiting phenomena is remarkable, $\theta_{10} < \sim 0.5$, high values of Mo index are obtained although having low θ_{90} values (see Fig. 6.1a). In fact, for these cases, it can be observed how the ranges are quite parallel to θ_{10}, almost neglecting the influence of θ_{90} in Mo index. Hence, the short-circuiting phenomenon dominates Mo magnitude and in consequence, is impossible to reliably determine if high Mo values are due to an unsatisfying mixing performance or to high short-circuiting rate.

To overcome this problem in Mo interpretation, AD (Aral and Demirel) index was proposed by Demirel et al. (2016) for combined evaluation of short-circuiting and mixing characteristics of a tank. This index is defined by the following expression (Eq. 6.3):

$$AD = \frac{\theta_{90} - \theta_m}{\theta_m - \theta_{10}} = \frac{\theta_{90} - 1}{1 - \theta_{10}} \tag{6.3}$$

Being θ_m the mean residence dimensionless time. In this case, it is observed in the curve that both forming indexes, θ_{10} and θ_{90}, have a similar effect on AD values (see Fig. 6.1b). In consequence, there is a balance between θ_{10} and θ_{90}, and none of them dominates the AD index. However, according to the proposed expression, as mixing increases, θ_{90} decreases and gets closer to mean residence time, θ_m, and in consequence, AD tends to 0. At the same time, as

short-circuiting decreases, θ_{10} increases, and AD tends to infinite. The latter is an incongruous effect for the AD parameter: While a desirable hydraulic effect, i.e decrease of short-circuiting, increases AD value, another hydraulic desirable performance, i.e increase of mixing, decreases the AD value. Hence, the evaluation of AD parameter becomes again confusing.

Having all the aforementioned into account, a modification of the original AD expression is proposed in the present work in order to obtain the same effect for desirable hydraulic performance (increase of mixing and decrease of short-circuiting). The modification is renamed as AD*, and is defined by the Eq. 6.4:

$$AD^* = \frac{\theta_{90} - \theta_m}{\theta_m + \theta_{10}} = \frac{\theta_{90} - 1}{1 + \theta_{10}} \tag{6.4}$$

In this case, regarding the denominator, when short circuiting decreases, θ_{10} increases and AD* decreases. At the same time, when mixing increases, θ_{90} decreases and so does AD* (see Fig. 6.1c). In addition, AD* is bounded between 0 and 1 which is better understandable. Values of AD* close to 0 represent an excellent mixing performance, while values close to one are related to poor mixing. The contour lines for this parameter are nearly parallel to θ_{90} which demonstrates the reduced influence of θ_{10}, i.e. short-circuiting phenomena, in AD*, making this parameter more suitable for mixing evaluation.

However, in all discussed parameters, mixing performance is not evaluated independently as short-circuiting appears in all the expressions. For that reason, Uniformity Index (UI) is proposed to quantitatively evaluate the mixing capacity of a water treatment system. Unlike Mo, AD and AD*, calculation of UI can only be carried out based on a CFD model and simulations of tracer tests. In addition, different UI values can be obtained for different sections or zones of the analysed system. This index, defined by Eq. 6.7, has been used in previous research works for anaerobic digesters (Terashima et al., 2009; Dapelo et al., 2018) and multi-environment anaerobic-anoxic reactors (Blanco-Aguilera et al., 2020a).

Being V_i the volume of the i-th cell and χ_i the tracer concentration in the i-th cell in the computational domain, the total volume V and the average tracer concentration in the reactor $\bar{\chi}$ are defined by Eq. 6.5 and Eq. 6.6, respectively.

$$V = \sum_i V_i \tag{6.5}$$

$$\bar{\chi} = \frac{1}{V} \sum_i V_i \cdot \chi_i \tag{6.6}$$

Thus, *UI* (Eq. 6.7) is defined as:

$$UI = \frac{1}{2V\bar{\chi}} \cdot \sum_i |\chi_i - \bar{\chi}| \cdot V_i \tag{6.7}$$

UI is bounded between 0 and 1 (Terashima et al., 2009), meaning $UI = 0$ a total homogenous tracer concentration in the analysed domain, and $UI = 1$ total inhomogeneity. It must be highlighted that while the rest of mixing parameters discussed (Mo, AD, AD*) base their optimum value in ideal plug flow conditions, an optimum UI value can be obtained either in plug or completely mixed conditions as total tracer homogeneity ($UI = 0$) can be reached in both flow hypothesis. This fact can be explained because the mixing concept is different for both indexes: while for Mo, AD and AD* efficient mixing is related to the type of flow (plug flow conditions), for UI it is closely related to the existence of significant dead zones that could avoid or difficult the complete homogeneity of tracer-mass concentration in a reactor. Therefore, UI can be used as a complementary mixing index to the already existing ones.

Finally, hydrodynamic performance based on hydraulic dimensionless indexes can be considered as excellent, good, compromising, fair or poor depending on the numerical value they take. An overview of the discussed hydraulic parameters and assumed constraint values are shown in Table 6.1 and Table 6.2, respectively.

Table 6.1. Hydraulic indexes and references

Index	Hydraulic feature	Reference
HS	Hydraulic separation	Current work
e	Dead zones	Climent et al. (2018), Latrach et al. (2018), Chang et al. (2016)
θ_{10}	Short circuiting	Teixeira et al (2008), Angeloudis et al. (2014), Demirel et al. (2016, 2018), Gualteri et al. (2008), Wei et al. (2019), Rengers et al. (2016)
θ_{90}	Mixing	Gualteri et al. (2008), Angeloudis et al. (2014), Wei et al. (2019)
Mo	Mixing	Teixeira et al. (2008), Gualteri et al. (2008, 2009), Demirel et al. (2016, 2018), Angeloudis et al. (2014), Wei et al. (2019), Rengers et al. (2016)
AD	Mixing	Demirel et al. (2016, 2018)
AD*	Mixing	Current work
UI	Mixing	Terashima et al. (2009), Dapelo et al. (2018), Blanco-Aguilera et al. (2020a)

Table 6.2. Hydraulic indexes and constraint values

Index	Excellent	Good	Compromising	Fair	Poor
HS	HS = 0	-	-	-	HS = 1
e	1.0 > e > 0.90	0.90 > e > 0.75	0.75 > e > 0.50	0.50 > e > 0.25	0.25 > e
θ_{10}	1.0 > θ_{10} > 0.7	0.7 > θ_{10} > 0.5	0.5 > θ_{10} > 0.3	-	0.3 > θ_{10} > 0
θ_{90}	1.3 > θ_{90}	1.7 > θ_{90} > 1.3	2.8 > θ_{90} > 1.7	-	θ_{90} > 2.8
Mo	1.5 > Mo	2.5 > Mo > 1.5	3.5 > Mo > 2.5	5.0 > Mo > 3.5	Mo > 5.0
AD	AD > 3.5	3.5 > AD > 1.75	1.75 > AD > 0.50	0.50 > AD > 0.20	0.20 > AD
AD*	0.25 > AD	0.50 > AD* > 0.25	0.75 > AD* > 0.50	0.90 > AD* > 0.75	1 > AD* > 0.90
UI	0.02 > UI > 0	0.15 > UI > 0.02	0.30 > UI > 0.15	0.50 > UI > 0.30	UI > 0.50

6.2.1.2. Methodology for hydrodynamic optimization of multi-environment reactors

The methodology proposed in this study for hydrodynamic optimization of multi-environment reactors aims at determining the best geometric configuration which enhances the hydraulic separation and the hydraulic efficiency. Following dimensional analysis (Buckingham, 1914), the dimensionless hydraulic indexes presented in the previous section $\left(\Pi^{hyd}\right)$ can be expressed as a function of dimensionless geometric indexes $\left(\Pi^{geom}\right)$ (Zlokarnik, 2002). This type of relation is expressed in Eq. 6.8:

$$\Pi_i^{hyd} = f_k\left(\Pi_j^{geom}\right) \tag{6.8}$$

Analytical relations based on Eq. 6.8 are obtained for all hydraulic and dimensionless geometric indexes (see Eqs. 6.9-6.15):

$$HS = \frac{C_{zone1}}{C_{zone2}} = f_{HS}\left(\Pi_j^{geom}\right) \tag{6.9}$$

$$e = \frac{HRT_{real}}{HRT_{theo}} = f_e\left(\Pi_j^{geom}\right) \tag{6.10}$$

$$\theta_{10} = \frac{t_{10}}{HRT_{theo}} = f_{\theta_{10}}\left(\Pi_j^{geom}\right) \tag{6.11}$$

$$Mo = \frac{\theta_{90}}{\theta_{10}} = f_{Mo}\left(\Pi_j^{geom}\right) \tag{6.12}$$

$$AD = \frac{\theta_{90} - 1}{1 - \theta_{10}} = f_{AD}\left(\Pi_j^{geom}\right) \tag{6.13}$$

$$AD^* = \frac{\theta_{90} - 1}{1 + \theta_{10}} = f_{AD^*}\left(\Pi_j^{geom}\right) \tag{6.14}$$

$$UI = \frac{\theta_{90} - 1}{1 + \theta_{10}} = f_{UI}\left(\Pi_j^{geom}\right) \tag{6.15}$$

Dimensionless geometric indexes, Π_j^{geom}, are based on reactor's dimensions and ratios between dimensions, position of mixing devices or relations between singular elements as baffles or deflectors. They vary depending on the studied reactor or system and its particular operational features.

After obtaining the analytical relations between hydraulic and geometric indexes $\left(\Pi^{hyd}, \Pi^{geom}\right)$, the hydrodynamic optimum geometry for the studied reactor is calculated. In multi-environment reactors, hydraulic separation between different zones (HS) is proposed to be considered as the fundamental hydraulic index, as no biological efficiency is achieved if incompatible environments, e.g. aerobic and anaerobic, are completely mixed. In consequence, HS is compared separately against the rest of hydraulic indexes.

Concretely, with the aim of evaluating the hydrodynamic performance combining the rest of hydraulic indexes in a single expression, a Global Hydraulic Efficiency (GHE) parameter is proposed in the present work (Eq. 6.16):

$$GHE = \sum_{i=m}^{n} \alpha_i \cdot \Pi_i^{hyd} \tag{6.16}$$

Being α_i the relative weight for each hydraulic index in GHE with $\sum_{i=m}^{n} \alpha_i = 1$, and Π^{hyd} the set of dimensionless indexes used in the optimization. In order to obtain a value bounded between 0 and 1 (being 0 poor GHE and 1 excellent GHE), all hydraulic indexes concerning this parameter are fitted to this hierarchical range. As an example, if the effective volume ratio e is used for dead volume evaluation, θ_{10} for short-circuiting, and AD* and UI for mixing assessment, GHE would be calculated following Eq. 6.17:

$$GHE = \sum_{i=m}^{n} \alpha_i \cdot \Pi_i^{hyd} = \alpha_1 \cdot e + \alpha_2 \cdot \theta_{10} + \alpha_3 \cdot (1 - AD^*) + \alpha_4 \cdot (1 - UI) \tag{6.17}$$

Finally, depending on the hydraulic separation degree desired in the analysed multi-environment reactor, the optimum reactor configuration can be obtained relating HS and GHE following Eq. 6.18. Then, the geometry that matches with the best hydrodynamic performance can be calculated.

$$\frac{HS}{GHE} = \frac{f_{HS}\left(\Pi_j^{geom}\right)}{\sum_{i=m}^{n} \alpha_i \cdot \Pi_i^{hyd}} = \frac{f_{HS}\left(\Pi_j^{geom}\right)}{f_{GHE}\left(\Pi_j^{geom}\right)} = F(\Pi_j^{geom}) \tag{6.18}$$

6.2.2. Case study

The proposed methodology for hydrodynamic optimization based on dimensional analysis has been applied to the AnoxAn reactor, a novel multi-environment upflow sludge blanket reactor that unifies the anaerobic and anoxic zones of the biological nutrient removal treatment train (Tejero et al., 2010). The reactor setup aims at guaranteeing hydraulic separation between anoxic and anaerobic environments, i.e. to maintain negligible concentration of nitrate in the anaerobic zone, achieving at the same time adequate mixing conditions in both zones. In Chapters 4 and 5 of this document (Blanco-Aguilera et al., 2020a), a numerical CFD model based on OpenFOAM® was developed and validated for AnoxAn and a comprehensive hydrodynamic analysis of the reactor was performed.

In this section, the numerical experiments to obtain the hydraulic indexes via CFD are described. Then, the CFD model setup to carry out the numerical simulations is presented and finally, the methodology for hydrodynamic optimization discussed in 6.2.1.2 is adapted and applied to AnoxAn.

6.2.2.1. Description of numerical experiments

Reactor setup

A set of numerical tracer tests are performed in clean water to evaluate the influence of different geometric parameters in the hydrodynamic performance of AnoxAn. The numerical experiments are carried out in a representative slice of a prototype reactor (see Fig. 6.2), i.e. a US_i unity-section, being the complete reactor the sum of n representative slices $\sum_{i=1}^{n} US_i$ repeated in the y axis direction.
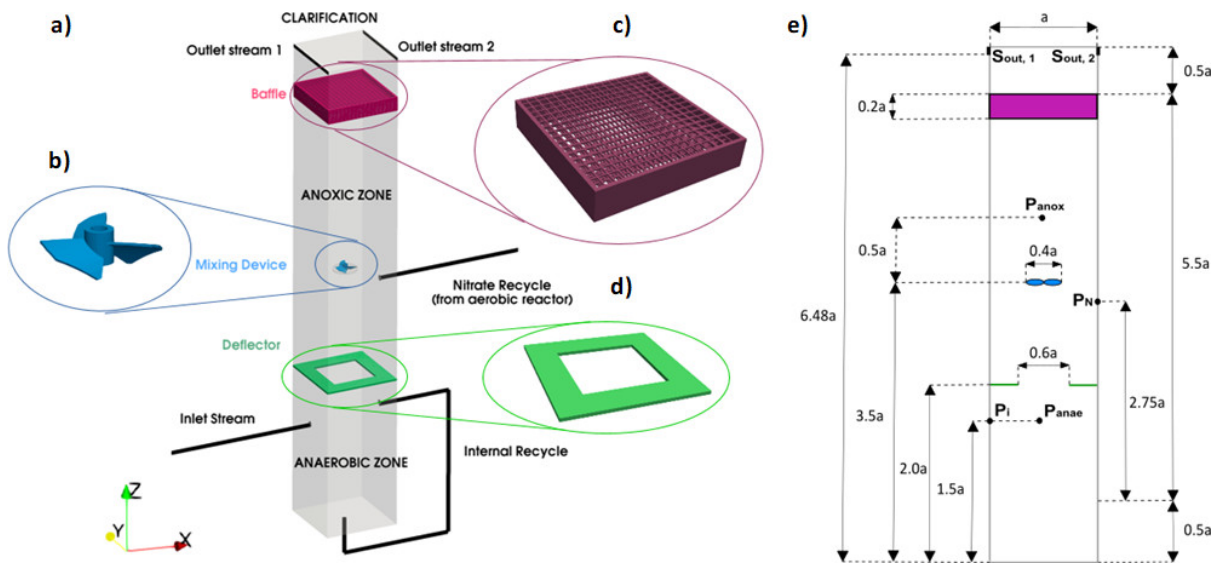
Figure 6.2. (a) 3D scheme of the bench scale AnoxAn reactor slice (US_i unity-section), (b) Impeller, (c) Baffle between anoxic and clarification zones, (d) Deflector between anaerobic and anoxic zones and (e) Detailed cross section geometry based on the square section side (a = 0.20 m)

The AnoxAn prototype slice has a total volume of 52.0 L and consists of an anaerobic zone at the bottom (16.0 L, 31% of the total volume), receiving the inlet stream; an anoxic zone above (32.0 L, 61% of the total volume), receiving the nitrate recycle from an aerobic reactor; and a clarification zone at the top (4.0 L, 8% of the total volume), designed to avoid the escape of large quantities of biomass. The outlet of the reactor are two open channels located in the y axis, and XZ is the symmetry plane of the depicted slice (see Fig 6.2a). In order to maintain the hydraulic separation between the anoxic and anaerobic zones, separate mixing devices are implemented in each zone. The stirrer located in the anoxic zone (Fig. 6.2b) works at 100 rpm. A deflector (4 cm width along the wall, 64% of void surface) situated between the anoxic and anaerobic environments minimizes the contamination between both zones (Fig. 6.2d). A baffle with a width of 0.039 m and a complex geometry is placed between clarification and anoxic volumes to reduce the escape of suspended solids (Fig. 6.2c).

A prototype of the reactor with an internal square section of 0.20 x 0.20 m^2 and a height of 1.30 m was built and used for the CFD model development and validation (Blanco-Aguilera et al., 2020a). A cross section of the detailed reactor geometry based on the square section side (a = 0.20 m) is shown in Fig. 6.2e.

Numerical RTD conditions

The AnoxAn reactor was designed for an HRT up to 5 h (depending on the organic load applied). For all the experiments, the inlet stream flow Q_{in} was 10.4 L/h, the internal recycle rate (ratio between internal recycle stream flow and inlet stream flow, $R_{IR} = Q_{IR}/Q_{in}$) was 5.77 (-), and the nitrate recycle rate (ratio between nitrate recycle stream flow and inlet stream flow, $R_{NR} = Q_{NR}/Q_{in}$) was 2.98 (-).

In order to evaluate the influence of the geometry of the reactor on the hydrodynamic behaviour of AnoxAn, a set of numerical RTD experiments are carried out for nine different geometric configurations (see Table 6.3). For the particular case of the AnoxAn reactor, the new configurations should be designed with the objective of implementing geometries easily reproducible on an industrial scale (Blanco-Aguilera et al. 2020a). For that purpose, the original cross-section of AnoxAn needs to be increased maintaining the same theoretical treatment capacity of the process (i.e. the same volume). Additionally, as also reported in Blanco-Aguilera et al. (2020a), the impeller is the main inner momentum supply of the reactor, and consequently, its influence on the mixing capacity and on the hydraulic separation between anoxic and anaerobic environments is significant. Therefore, evaluating the hydrodynamic effect of the impeller at different heights also appears to be determinant for the development of new AnoxAn configurations.

Having the aforementioned into account, new configurations are built based on the variation of the height of the impeller (H_{imp}) and the a side of the original square section (see Fig. 6.3) from the original prototype (Díez-Montero et al., 2015), which is represented by the configuration C2 in the present work. Concretely, the relative height of the impeller (H_{imp}/b) indicates the specific location of the impeller within the anoxic zone; and the relation of the cross-section sides (a/b) indicates the shape of the horizontal cross-section of the reactor (being a/b=1 the square section). It should be highlighted that the different shapes of the cross section give rise to different cross section areas (a/b ratios), and therefore different slenderness (λ), since the volume of the reactor is kept constant (maintaining the theoretical treatment capacity of the original configuration). In this study, the slenderness λ of the AnoxAn reactor is defined as a/h (the relation between the length of the main side, a, and the total height of the reactor, h). The void surface percentage of the deflector is also kept constant in all configurations.
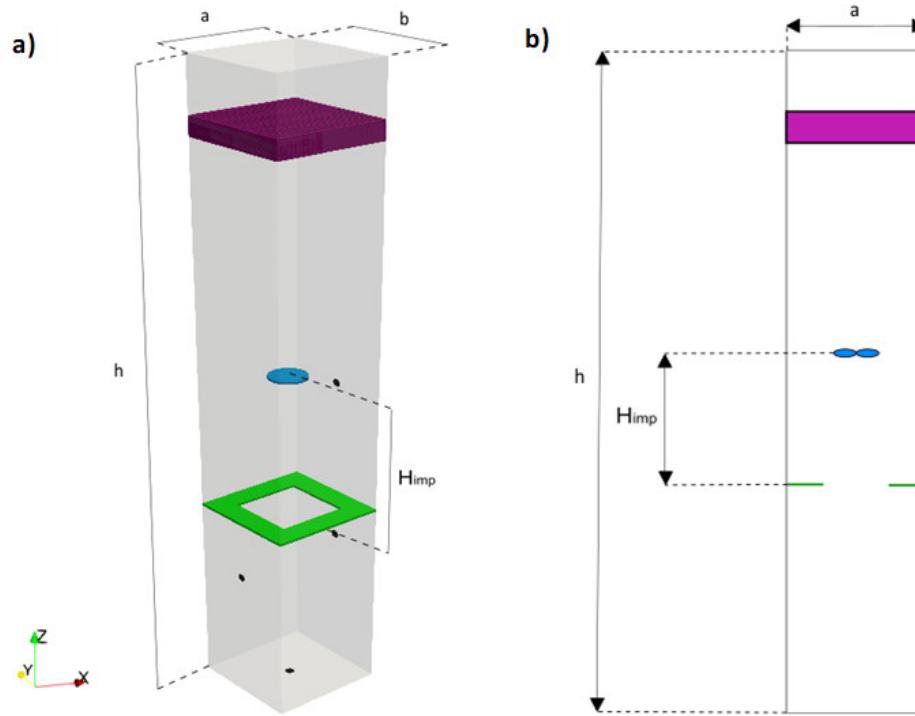
Figure 6.3. Numerical testing scheme of AnoxAn including XY cross section (a/b), height of the impeller (H_{imp}) and slenderness (λ): (a) 3D scheme and (b) XZ cross section
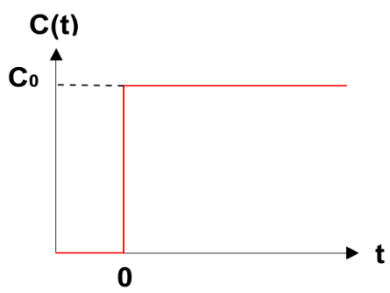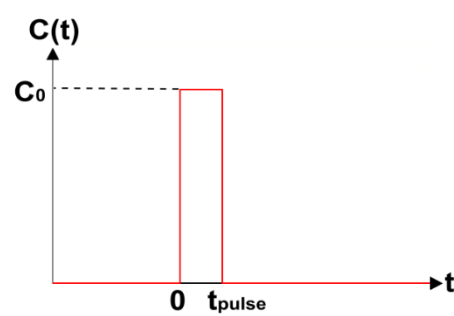
Table 6.3. Tested geometric configurations of AnoxAn

Configuration	a (m)	b (m)	a / b	h (m)	λ	H_{imp} (m)	H_{imp} / b
C1	0.20	0.20	1.00	1.30	1/6.5	0.20	1.00
C2*	0.20	0.20	1.00	1.30	1/6.5	0.30	1.50
C3	0.20	0.20	1.00	1.30	1/6.5	0.40	2.00
C4	0.25	0.20	1.25	1.04	1/4.2	0.20	1.00
C5	0.25	0.20	1.25	1.04	1/4.2	0.30	1.50
C6	0.25	0.20	1.25	1.04	1/4.2	0.40	2.00
C7	0.30	0.20	1.50	0.87	1/2.9	0.20	1.00
C8	0.30	0.20	1.50	0.87	1/2.9	0.30	1.50
C9	0.30	0.20	1.50	0.87	1/2.9	0.40	2.00

*Configuration C2 represents the original prototype

In order to evaluate and optimize the hydrodynamic performance of the configurations, pulse and step numerical tracer tests are conducted with all of them. Concretely, for the evaluation of the hydraulic separation (HS) and the mixing efficiency through UI, a step RTD test is performed (see Table 6.4), in which a solution of 10 mg/L of tracer is continuously injected in the nitrate recycle stream and the tracer concentration is measured in both the anaerobic and anoxic zones. For short-circuiting (θ_{10}), dead zones (e) and mixing performance analysis (Mo, AD, AD*), pulse RTD tests (see Table 6.4) are used. In these cases, a solution of 350 mg/L tracer is injected through the inlet stream and measured at the outlet.

Table 6.4. RTD tests conditions

RTD experiment	Type	Tracer injection location	Tracer injection duration	Tracer concentration measurement
Step RTD		Nitrate recycle stream P_N	Continued injection	Anaerobic zone P_{anae} Anoxic zone P_{anox} Outlet S_{out}
Pulse RTD		Inlet stream P_i	$t_{pulse} = 3$ s	Outlet S_{out}

6.2.2.2. Numerical model setup

In the following sub-section, a description of the numerical setup of the CFD model is given. First, a brief overview of the governing equations and sub-models is presented based on Chapter 4 of this document (Blanco-Aguilera et al., 2020a). Boundary conditions and computational domain for AnoxAn are then described. To conclude, a description of the numerical modelling methodology is provided.

Computational Fluid Dynamics. Governing equations and sub-models.

The model used in the current work (Blanco-Aguilera et al., 2020a) is an open source numerical application based on CFD and developed in OpenFOAM® toolbox. Hydrodynamics are simulated solving Reynolds Averaged Navier-Stokes (RANS) equations for turbulent and

incompressible flow and turbulence is modelled by means of standard k-ε model (Launder and Spalding, 1972). Regarding tracer transport, physics are coded as a mass transport equation for turbulent flow without chemical reaction. Finally, the model also includes additional sub-models for different feature elements: an impeller sub-model reproduced by means of a flat disk approach (Jasak et al., 2019; Seb, 2017) and a complex 3D baffle (Tejero et al., 1991) simulated as a porous media. The numerical methodology is based in two separate stages: First, by means of SIMPLE algorithm, continuity and momentum equations are solved (without tracer) reaching a steady state solution. Next, experimental tracer concentration introduced and tracer transport under transient flow is solved using PIMPLE algorithm. For extensive validation, the reader is referred to Chapter 5 (Blanco-Aguilera et al., 2020a).

Boundary conditions

Different boundary conditions are applied in the numerical model: inflow boundary conditions (inlet, nitrate recycle and impellers disk face), outflow boundary condition (outlet), non-slip wall boundary conditions (outer faces of the reactor at x axis, deflector, backward of the impeller), slip boundary conditions (free surface) and symmetry boundary condition (outer faces of the reactor at y axis, to simulate flow symmetry). All numerical boundary conditions are depicted in Fig. 6.4.
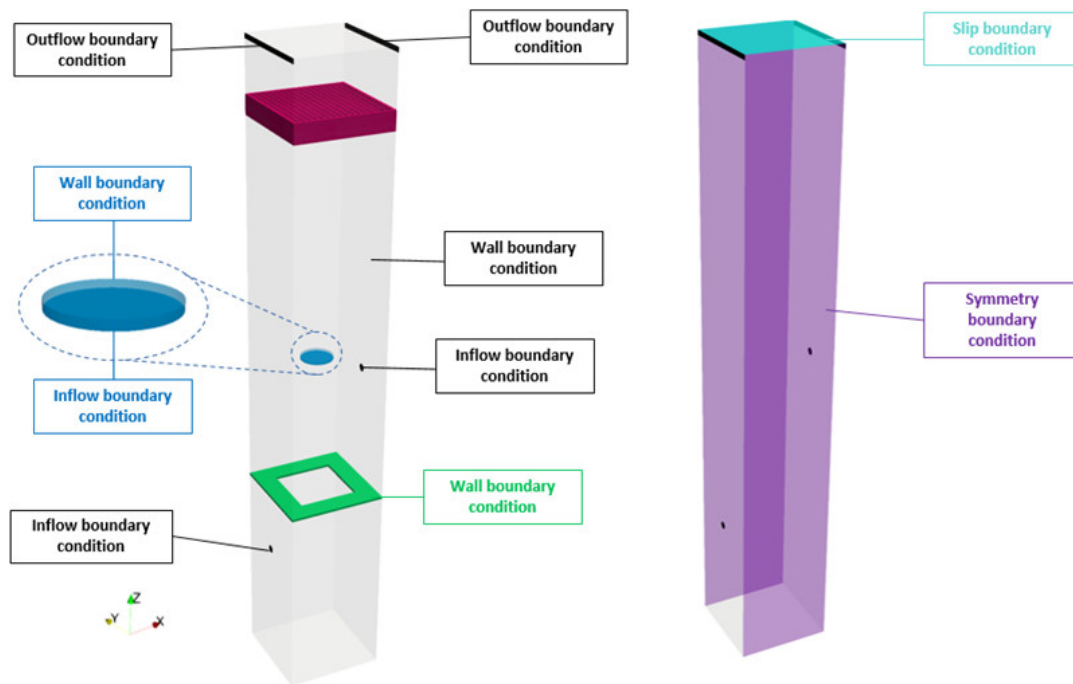
Figure 6.4. Boundary conditions used in the numerical model

When step RTD test is simulated, fixed value boundary condition (Eq. 6.19) is set for the tracer in the inlet stream boundary:

$$C = C_0; \forall t \tag{6.19}$$

Being C the tracer concentration in function of time and C_0 the initial tracer concentration.

When pulse RTD tests are simulated, a time dependent boundary condition is applied (Eqs. 6.20-6.21) for the tracer in the inlet stream boundary:

$$C = C_0; 0 < t \leq t_{pulse} \tag{6.20}$$

$$C = 0; \ t > t_{pulse} \tag{6.21}$$

Computational domain

Computational grids consist on hexahedral nonconforming meshes. First, a background uniform mesh is generated. Next, a refinement is carried out at singular zones in order to better reproduce the hydrodynamic effects near the walls similar to Chapter 5.

Three different grids are generated for each slenderness with different mesh cell sizes (see Tables 6.5-6.7).

Table 6.5. Mesh characteristics for 0.20x0.20x1.30 m³ prototypes (C1, C2, C3)

Mesh	Background uniform mesh cell size	Background uniform mesh cell number	Final refined mesh cell size	Final refined mesh cell number
M1a	1.75 cm	128 000	0.28 cm	433 081
M2a	1.50 cm	160 000	0.20 cm	720 633
M3a	1.25 cm	192 000	0.15 cm	1 040 612

Table 6.6 Mesh characteristics for 0.20x0.25x1.04 m³ prototypes (C4, C5, C6)

Mesh	Background uniform mesh cell size	Background uniform mesh cell number	Final refined mesh cell size	Final refined mesh cell number
M1b	1.75 cm	90 720	0.32-0.88 cm	494 005
M2b	1.50 cm	136 000	0.24-0.76 cm	705 417
M3b	1.20 cm	250 000	0.24-1.20 cm	1 169 667

Table 6.7. Mesh characteristics for 0.20x0.30x0.87 m³ prototypes (C7, C8, C9)

Mesh	Background uniform mesh cell size	Background uniform mesh cell number	Final refined mesh cell size	Final refined mesh cell number
M1c	1.50 cm	115 200	0.75 cm	688 240
M2c	1.33 cm	164 025	0.18-1.33 cm	888 941
M3c	1.20 cm	225 000	0.20-1.20 cm	1 147 478

With the aim of ensuring the mesh independence of the numerical results, a grid sensitivity analysis by means of Grid Convergence Index (GCI) is performed for each slenderness according to Celik et al. (2008) based on Richardson Extrapolation. GCI is carried out for different XY sections across different configurations of the AnoxAn reactor. Mesh sensitivity analysis is carried out in one configuration for each prototype geometry: C2 in 0.20x0.20x1.30 m³ prototype

(Tables 6.8-6.9), C5 in 0.20x0.25x1.04 m³ prototype (Tables 6.10-6.11), and C8 in 0.20x0.30x0.87 m³ prototype (Tables 6.12-6.13).

Table 6.8. Average-weighted velocity magnitude for different sections – 0.20x0.20x1.30 m³ prototypes (C1, C2, C3)

	Area-weighted velocity magnitude (m/s)		
Mesh	z = 0.30 m	z = 0.60 m	z = 1.00 m
M1a	$2.268 \cdot 10^{-4}$	0.0318	0.0022
M2a	$5.140 \cdot 10^{-4}$	0.0305	0.0030
M3a	$4.934 \cdot 10^{-4}$	0.0302	0.0029

Table 6.9. Grid Convergence Index for different sections – 0.20x0.20x1.30 m³ prototypes (C1, C2, C3)

	GCI		
GCI Nº	z = 0.30 m	z = 0.60 m	z = 1.00 m
GCI^{21}_{coarse}	62.7%	10.9%	32.0%
GCI^{32}_{coarse}	5.3%	5.1%	4.9%

Table 6.10. Average-weighted velocity magnitude for different sections – 0.20x0.25x1.04 m³ prototypes (C4, C5, C6)

	Area-weighted velocity magnitude (m/s)		
Mesh	z = 0.30 m	z = 0.70 m	z = 1.00 m
M1b	$9.190 \cdot 10^{-5}$	0.0161	$3.050 \cdot 10^{-4}$
M2b	$7.610 \cdot 10^{-5}$	0.0150	$2.550 \cdot 10^{-4}$
M3b	$7.062 \cdot 10^{-5}$	0.0145	$2.620 \cdot 10^{-4}$

Table 6.11. Grid Convergence Index for different sections – 0.20x0.25x1.04 m³ prototypes (C4, C5, C6)

	GCI		
GCI Nº	z = 0.30 m	z = 0.70 m	z = 1.00 m
GCI^{21}_{coarse}	5.9%	3.4%	1.1%
GCI^{32}_{coarse}	1.1%	1.0%	0.05%

Table 6.12. Average-weighted velocity magnitude for different sections – 0.20x0.30x0.87 m³ prototypes (C7, C8, C9)

	Area-weighted velocity magnitude (m/s)		
Mesh	z = 0.28 m	z = 0.40 m	z = 0.75 m
M1c	0.0014	0.0077	0.0023
M2c	0.0011	0.0072	0.0021
M3c	0.0010	0.0070	0.0020

Table 6.13. Grid Convergence Index for different sections – 0.20x0.30x0.87 m³ prototypes (C7, C8, C9)

GCI Nº	GCI		
	z = 0.28 m	z = 0.40 m	z = 0.75 m
GCI^{21}_{coarse}	15.9%	6.1%	10.5%
GCI^{32}_{coarse}	5.9%	2.9%	5.5%

Table 6.8, 6.10 and 6.12 show the average-weighted velocity magnitudes for different z sections in the reactor and Table 6.9, 6.11 and 6.13 show that maximum GCI values for M2 are around 5% in all cases, i.e. with intermediate size meshes the cell size has no impact on the obtained results. In consequence, mesh M2 has been used for each slenderness in the present study.

6.2.2.3. Methodology for hydrodynamic optimization applied to AnoxAn

Then, the hydrodynamic optimization methodology presented in section 6.2.1.2 is applied to AnoxAn. Hydraulic indexes discussed in section 6.2.1.1 are calculated based on representative dimensionless geometrical numbers. For AnoxAn optimization, as stated in section 6.2.2.1, two geometrical relations will be tested: the relative height of the impeller (H_{imp}/b) and the relation of the cross-section sides (a/b). The hydraulic separation between the anaerobic and anoxic zones should be guaranteed in AnoxAn, therefore the hydraulic separation index (HS) is represented by the quotient between the tracer concentration in the anaerobic and anoxic zones, $\frac{c_{anae}}{c_{anox}}$. All indexes used in this case study are shown in Table 6.14. For analytical development of the geometrical and hydraulic indexes via dimensional analysis (Buckingham, 1914), the reader is referred to Annex C.

Based on Eq. 6.8, general expression for relation between hydraulic and geometric indexes in AnoxAn is expressed in Eq. 6.22:

$$\Pi_i^{hyd} = f_k \left(\frac{H_{imp}}{b}, \frac{a}{b} \right) \tag{6.22}$$

Then, based on Eq. 6.17, GHE is calculated for AnoxAn. In order to give the same significance to each hydraulic feature (short-circuiting, dead volumes and mixing), they are weighted equally. Hence, GHE for AnoxAn is obtained following Eq 6.23:

$$GHE = \sum_{i=m}^{n} \alpha_i \cdot \Pi_i^{hyd} = \frac{1}{3} \cdot e + \frac{1}{3} \cdot \theta_{10} + \frac{1}{3} \cdot \left[\left(\frac{(1 - AD^*) + (1 - UI_{Anae}) + (1 - UI_{Anox})}{3} \right) \right] \tag{6.23}$$

Following Eq. 6.18, the analytical relation between HS and GHE in AnoxAn is expressed as follows (Eq. 6.24):

$$\frac{HS}{GHE} = \frac{f_{HS} \left(\frac{H_{imp}}{b}, \frac{a}{b} \right)}{f_{GHE} \left(\frac{H_{imp}}{b}, \frac{a}{b} \right)} = F(\frac{H_{imp}}{b}, \frac{a}{b}) \tag{6.24}$$

Table 6.14. Dimensionless numbers for AnoxAn

Geometrical dimensionless numbers	Hydraulic indexes
$\dfrac{H_{imp}}{b}$	$\dfrac{C_{anae}}{C_{anox}} = HS$
$\dfrac{a}{b}$	$\dfrac{HRT_{real}}{HRT_{theo}} = e$
	$\dfrac{t_{10}}{HRT_{theo}} = \theta_{10}$
	$\dfrac{\theta_{90}}{\theta_{10}} = Mo$
	$\dfrac{\theta_{90} - 1}{1 - \theta_{10}} = AD$
	$\dfrac{\theta_{90} - 1}{1 + \theta_{10}} = AD^*$
	UI

6.3. <u>Results and discussion</u>

The different AnoxAn configurations shown in Table 6.3 are modelled in 3D using the toolbox OpenFOAM®, a free and open-source CFD software. RANS equations for turbulent flow are solved at Altamira supercomputer, which is part of the Spanish Supercomputing Network. It is equipped with Intel Sandybridge E5-2670 at 2.6 GHz CPU, with 158 compute nodes IBM dx360 with two Intel Sandybridge E5-2670 processors, each one with 8 cores operating at 2.6 GHz and a cache of 20 MB, 64 GB of RAM memory (i.e. 4 GB/core) and 500 GB local disk. The running time for each model simulated is between three and four weeks for a maximum of 380 minutes, using 8 cores per simulation.

In this section, the qualitative and quantitative hydrodynamic assessment carried out by means of velocity fields, simulated RTD curves and hydraulic indexes, is presented.

6.3.1. Hydrodynamic analysis based on velocity fields

Prior to the quantitative analysis through hydraulic indexes, a qualitative hydrodynamic analysis is performed for all geometric configurations of AnoxAn, based on the CFD simulations. The aim of this analysis is to overcome analysis limitations of RTD curves and hydraulic indexes, not only quantifying but also locating and visualizing hydrodynamic deficiencies such as dead zones, flow patterns, or short-circuiting.

For that purpose, vertical velocity component above the impeller, and vertical velocity component through the deflector between anaerobic and anoxic zones are presented in Figures 6.5 and 6.6, respectively. In order to focus on the main short-circuiting paths and dead volumes generated in the anoxic zone of AnoxAn, only the zone above the impeller is depicted in Figure 6.5. Dashed lines show the limit with the deflector between the anaerobic and anoxic zones. Additionally, results are divided into three groups: for high slenderness configurations ($\lambda = 1/6.5$, Fig. 6.5a-c and Fig. 6.6a-c), intermediate slenderness configurations ($\lambda = 1/4.2$, Fig. 6.5d-f and Fig. 6.6d-f) and low slenderness configurations ($\lambda = 1/2.9$, Fig. 6.5g-i and Fig. 6.6g-i). Velocities represented in blue are downflow velocities.
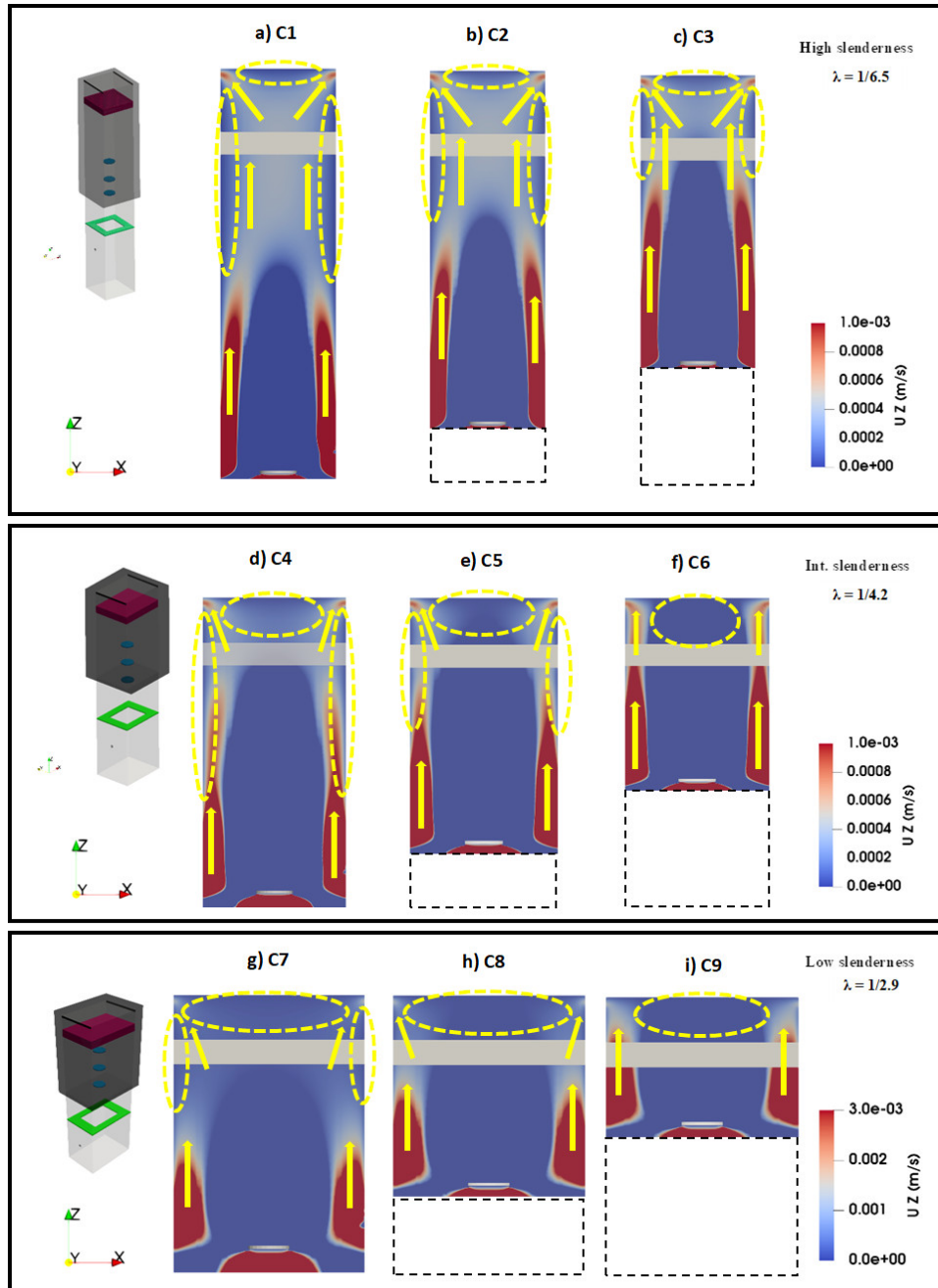
Figure 6.5. Vertical velocity component in XZ section above the impeller: (a) C1, (b) C2, (c) C3, (d) C4, (e) C5, (f) C6, (g) C7, (h) C8 and (i) C9
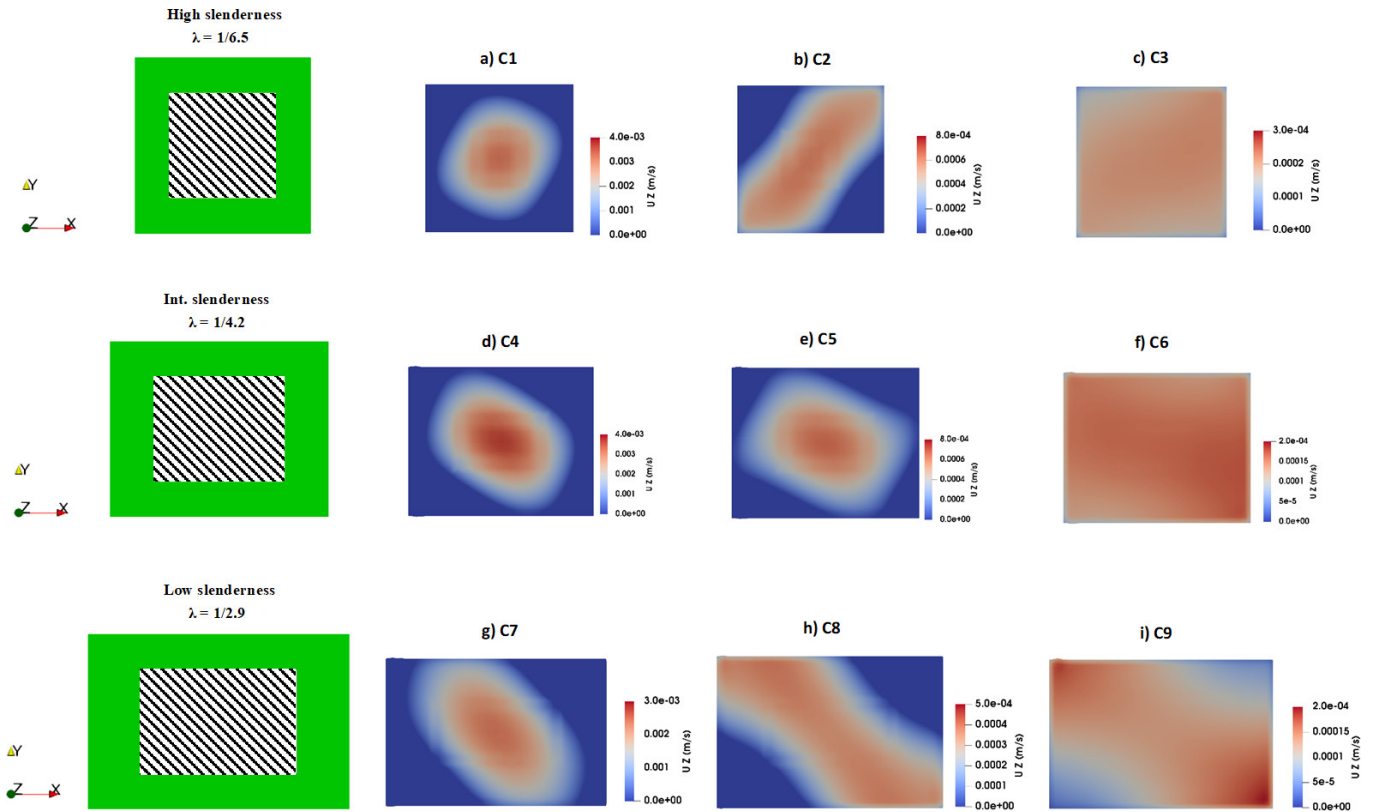
Figure 6.6. Vertical velocity component XY section through the deflector (striped area): (a) C1, (b) C2, (c) C3, (d) C4, (e) C5, (f) C6, (g) C7, (h) C8 and (i) C9

6.3.1.1. High slenderness ($\lambda = 1/6.5$)

In Fig. 6.5a-c it is noted that upward velocity is located in the outer part of the reactor, close to the walls. In consequence, main tracer transport takes place through these areas, forming preferential paths and short-circuiting. Moreover, additional preferential paths are formed under the influence of the outlet channels. As a result of this short-circuiting phenomena (represented with yellow arrows), dead volumes (represented with yellow dashed ovals) are generated close to the walls and in the upper central part of the clarification zone. However, although the size of the dead zones created in the central part of the clarification zone are similar for the three configurations, the ones formed through the walls vary depending on the location of the impeller. Concretely, when the impeller is located in higher positions, the size of stagnant volumes is remarkably reduced (see Fig. 6.5a-c), increasing the real HRT and the effective volume of the reactor.

Regarding the effect of the impeller height (H_{imp}) in the anaerobic zone, it is clearly observed the variation in the vertical velocity field for different configurations (Fig. 6.6a-c). In that sense, when the impeller is located close to the deflector (Fig. 6.6a) a larger downflow stream area is observed. Therefore, the influence of the impeller in the anaerobic zone is remarkable and a deficient hydraulic separation is expected. In fact, in Fig. 6.6c, in which the impeller is located farther from the deflector, almost homogeneous upward flow is noticed in the complete section, enhancing the hydraulic separation between both environments. Additionally, it is observed

that the upward flow is oriented along the diagonal of the reactor in the horizontal XY plane showing a maximum in the centre of the cross section. This is caused by the effect of the outlet patch located in the top of AnoxAn in the y axis, and the symmetry plane of the x axis.

6.3.1.2. Intermediate slenderness ($\lambda = 1/4.2$)

In intermediate slenderness configurations (Fig. 6.5d-f and Fig. 6.6d-f), the overall hydrodynamic behaviour is similar to the one observed in high slenderness (Fig. 6.5a-c and Fig. 6.6a-c). Concretely, preferential paths are located again close to the walls and under the influence of the outlet, and dead volumes are analogously formed. However, as the cross section is bigger compared to high slenderness configurations, the width and the total volume of stagnant and short-circuiting zones are also expected to be bigger, reducing the effective volume of the reactor.

Regarding the influence of H_{imp} on the hydraulic separation, higher downflow is again noted when the height of the impeller is small (Fig. 6.6d) increasing the mixing between anaerobic and anoxic environments. Comparing with high slenderness configurations (Fig. 6.6a-c), as the void cross-section of the deflector is larger and inflow is maintained for intermediate slenderness cases (Fig. 6.6d-f), more deficient hydraulic separation is expected for these configurations. In fact, larger downflow sections are observed in Fig. 6.6d-f. Further, the direction of the diagonal orientation of the upward flow is contrary to the observed for high slenderness configurations. Nevertheless, since the cross-section and outer boundary conditions are symmetric, the effect is analogue.

6.3.1.3. Low slenderness ($\lambda = 1/2.9$)

In Fig. 6.5g-i, vertical velocity component for lower slenderness configurations are shown. As happened for all the configurations and slenderness tested, preferential paths are located close to the walls of the reactor and towards the outlets. Dead zones in the central part of the clarification zone are bigger (as the cross-sectional a/b ratio is higher), which will decrease the real HRT and the effective volume.

Regarding the influence of H_{imp} on the hydraulic separation (see Fig. 6.6g-i), the void area of the deflector is bigger in low slenderness configurations. Hence, hydraulic separation is expected to decrease compared to high slenderness configurations. In addition, as different zones are more cube shaped, the mixing between both environments is enhanced. Finally, the diagonal orientation of the vertical velocity is analogue to what observed for intermediate slenderness, and caused by the effect of the outlet patch and symmetry planes.

Summarizing, in configurations where the impeller is located in higher position, the size of dead zones is reduced increasing the effective volume of the reactor. At the same time, as the impeller is located farther from the deflector, the influence to the anaerobic zone is negligible, increasing the hydraulic separation. Finally, stagnant zones are observed to be smaller in high slenderness configurations as the cross-section is also smaller.

6.3.2. Hydrodynamic analysis based on simulated RTD curves

Simulated CFD pulse RTD curves are shown in Fig 6.7. On the one hand, same coloured figures (Fig. 6.7a-c) show results for configurations with the same slenderness and cross-sectional ratio (λ, a/b) but different impeller height (H_{imp}). On the other hand, figures with curves with the same line type, i.e. continuous, dashed or dotted (Fig 6.7.d-f), show results for configurations with the same impeller height but different slenderness. Additionally, original AnoxAn prototype's experimental RTD is represented with black dots (Blanco-Aguilera et al. 2020a). As stated in section 6.2.2.1, C2 model represents the original AnoxAn prototype (Díez-Montero et al., 2015).

Channelling and dead zones observed in velocity fields (Fig. 6.5) generate a non-ideal flow behaviour that is depicted in all RTD curves (Fig. 6.7): remarkable tailing is noted in all curves, which confirm the existence of stagnant or dead volumes.

Regarding configurations with the same slenderness (Fig. 6.7a-c), it is noted that the height of the impeller significantly influences the hydrodynamic behaviour of the reactor. In configurations with the lowest H_{imp} (continuous lines), the peak concentration increases and the RTD curve tightens compared to higher H_{imp} configurations (dashed and dotted lines). In consequence, real HRT and other time dependent variables (θ_{10}, θ_{90}) are smaller for configurations with the impeller located closer to the deflector. In fact, when the impeller is located nearer from the inlet, the flow gets first under its influence. Therefore, as also observed in Figure 6.5, in these cases short-circuiting is enhanced and the effective volume of the reactor is reduced. Hence, higher locations of the impeller delay and displace the RTD curve in time, enhancing plug-flow conditions.

Regarding configurations with the same height of the impeller (Fig. 6.7d-f), it is noted that the a/b ratio and the slenderness of the reactor also affect to the RTD curve shape. Concretely, in configurations with high a/b ratios and small slenderness (green lines), the RTD curve of the reactor gets tighter compared to configurations with high slenderness (blue and red lines). As happened due to the variation of H_{imp}, when RTD curve tightens, time dependent variables (real HRT, θ_{10} and θ_{90}) become smaller. In this case, although the total volume of the reactor is maintained, the formation of preferential flows and short-circuiting is enhanced.

Finally, taking the original configuration as reference (Díez-Montero et al., 2015, Blanco-Aguilera et al., 2020a), it is observed that reducing the slenderness (increasing a/b ratio) diverts the hydrodynamic behaviour from optimum plug-flow conditions. Additionally, if it is desired or required to reduce the slenderness of the reactor, the only way to maintain a more preferable plug-flow behaviour is to increse the relative height of the impeller.
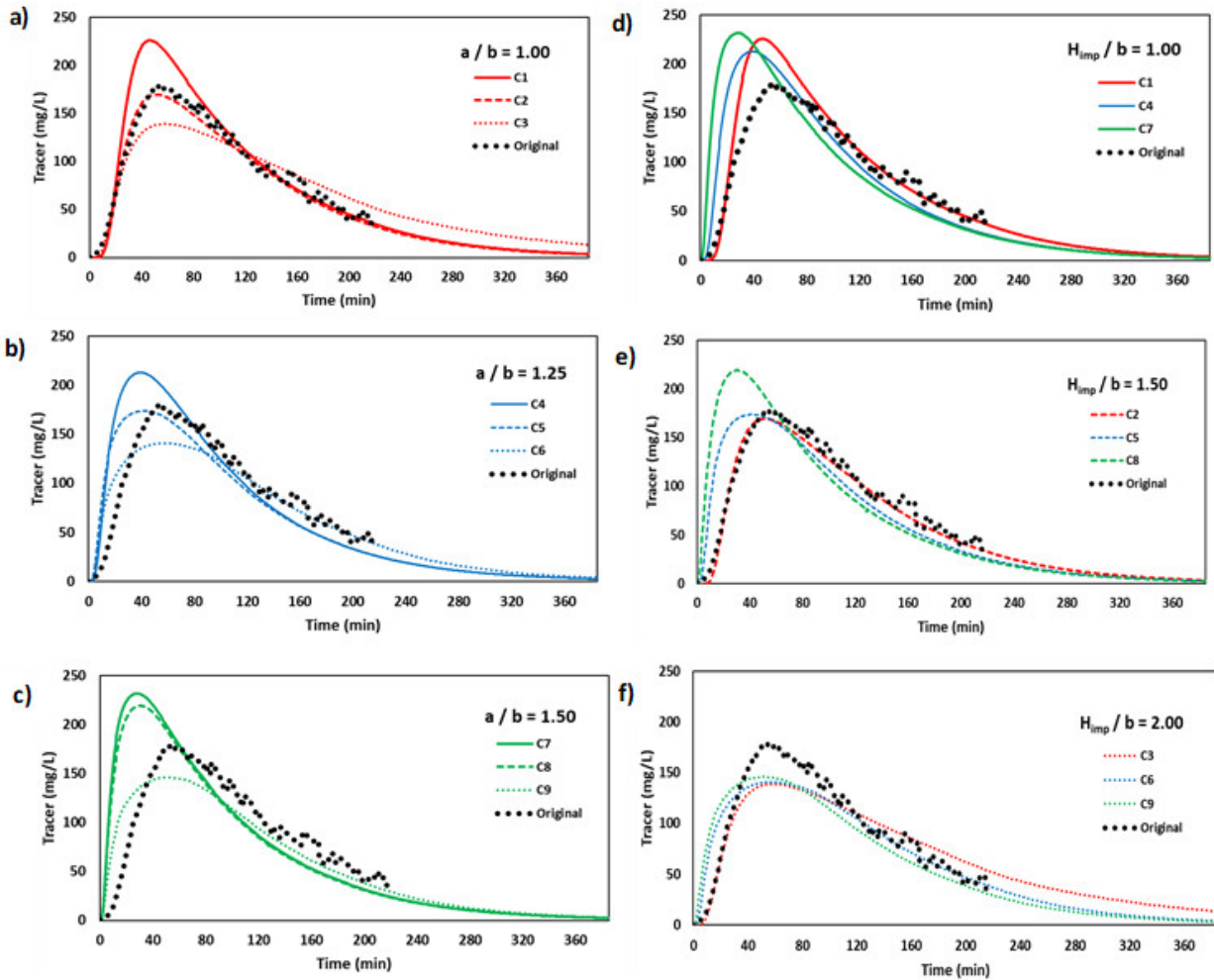
Figure 6.7. Comparison of simulated CFD pulse RTD curves for the different configurations:
Configurations with (a) a / b = 1.00, (b) a / b = 1.25, (c) a / b = 1.50, (d) H_{imp}/b = 1.00,
(e) H_{imp}/b = 1.50 and (f) H_{imp}/b = 2.00

6.3.3. Hydrodynamic analysis based on dimensionless numbers

6.3.3.1. Development of general analytical expressions

With the aim of quantifying the hydrodynamic performance of different configurations and obtaining general expressions for the hydraulic behaviour of the studied reactor, the hydraulic indexes are calculated for each simulated configuration and are listed in Table 6.15.

Following section 6.2.2.3, analytical relations between hydraulic and geometric indexes are obtained by means of regression adjusting second order polynomial curves to CFD results. Obtained expressions relating hydraulic and geometrical indexes along with statistical parameters to evaluate the goodness of fit are shown in Table 6.16. Values for Sum of Squared

Estimate of Errors (SSE) and Root Mean Square Error (RMSE) are near 0, and coefficient of determination R^2 and Adjusted R^2 near 1, which confirm a good fit of the expressions to predict the hydraulic indexes under the constraints applied (Draper et al., 1998). In fact, these expressions conform new dimensionless numbers relating time, length and/or concentration in AnoxAn, which can be used as the starting point for the scalability process of the reactor.

Table 6.16. Analytical expressions of hydrodynamic performance of AnoxAn

Index	Equation	SSE	R^2	Adjusted R^2	RMSE
HS	$1.18 - 0.24\dfrac{H_{imp}}{b} - 0.83\dfrac{a}{b} - 0.13\left(\dfrac{H_{imp}}{b}\right)^2 + 0.26\left(\dfrac{H_{imp}\cdot a}{b^2}\right) + 0.42\left(\dfrac{a}{b}\right)^2$	0.00164	0.996	0.989	0.01970
HE	$0.85 - 0.65\dfrac{H_{imp}}{b} - 0.023\dfrac{a}{b} + 0.29\left(\dfrac{H_{imp}}{b}\right)^2 - 0.019\left(\dfrac{H_{imp}\cdot a}{b^2}\right) - 0.12\left(\dfrac{a}{b}\right)^2$	0.00106	0.991	0.977	0.01882
e	$2.09 - 0.33\dfrac{H_{imp}}{b} - 1.51\dfrac{a}{b} + 0.26\left(\dfrac{H_{imp}}{b}\right)^2 - 0.21\left(\dfrac{H_{imp}\cdot a}{b^2}\right) + 0.57\left(\dfrac{a}{b}\right)^2$	0.00082	0.993	0.982	0.01654
Θ_{10}	$1.22 - 0.22\dfrac{H_{imp}}{b} - 1.16\dfrac{a}{b} + 0.08\left(\dfrac{H_{imp}}{b}\right)^2 + 0.028\left(\dfrac{H_{imp}\cdot a}{b^2}\right) + 0.344\left(\dfrac{a}{b}\right)^2$	0.00020	0.993	0.982	0.00819
Θ_{90}	$3.17 - 0.32\dfrac{H_{imp}}{b} - 1.93\dfrac{a}{b} + 0.40\left(\dfrac{H_{imp}}{b}\right)^2 - 0.47\left(\dfrac{H_{imp}\cdot a}{b^2}\right) + 0.84\left(\dfrac{a}{b}\right)^2$	0.00689	0.975	0.934	0.04793
Mo	$-11.45 + 9.06\dfrac{H_{imp}}{b} + 14.41\dfrac{a}{b} - 1.25\left(\dfrac{H_{imp}}{b}\right)^2 - 4.57\left(\dfrac{H_{imp}\cdot a}{b^2}\right) - 0.58\left(\dfrac{a}{b}\right)^2$	0.62910	0.961	0.897	0.45790
AD	$4.22 - 0.46\dfrac{H_{imp}}{b} - 4.50\dfrac{a}{b} + 0.64\left(\dfrac{H_{imp}}{b}\right)^2 - 0.82\left(\dfrac{H_{imp}\cdot a}{b^2}\right) + 1.87\left(\dfrac{a}{b}\right)^2$	0.01862	0.978	0.941	0.08779
AD*	$1.29 - 0.21\dfrac{H_{imp}}{b} - 0.94\dfrac{a}{b} + 0.28\left(\dfrac{H_{imp}}{b}\right)^2 - 0.34\left(\dfrac{H_{imp}\cdot a}{b^2}\right) + 0.45\left(\dfrac{a}{b}\right)^2$	0.00391	0.969	0.917	0.03610
UI$_{Anae}$	$0.065 + 0.004\dfrac{H_{imp}}{b} - 0.044\dfrac{a}{b} + 0.018\left(\dfrac{H_{imp}}{b}\right)^2 - 0.014\left(\dfrac{H_{imp}\cdot a}{b^2}\right) + 0.011\left(\dfrac{a}{b}\right)^2$	$3.2\cdot10^{-6}$	0.998	0.996	0.00126
UI$_{Anox}$	$0.018 - 0.016\dfrac{H_{imp}}{b} - 0.009\dfrac{a}{b} + 0.016\left(\dfrac{H_{imp}}{b}\right)^2 - 0.018\left(\dfrac{H_{imp}\cdot a}{b^2}\right) + 0.012\left(\dfrac{a}{b}\right)^2$	$6.5\cdot10^{-6}$	0.966	0.882	0.00180

Table 6.15. Simulated hydraulic indexes for AnoxAn configurations

Config	Geometry			Hydraulic Separatio	Dead Volumes			Short Circuiting			Mixing performance			
	a/b	$H_{imp}/$	λ	HS	HRT_{Theo}	HRT_{real}	e	Θ_{10}	Θ_{90}	Mo	AD	AD*	UI_{Anae}	UI_{Anox}
C1	1.00	1.00	1/6.5	0.635	124 min	108 min	0.867	0.284	1.69	5.95	0.969	0.540	0.040	0.003
C2	1.00	1.50	1/6.5	0.496	124 min	113 min	0.910	0.296	1.73	5.84	1.040	0.565	0.059	0.004
C3	1.00	2.00	1/6.5	0.275	124 min	138 min	1.114	0.326	2.11	6.47	1.656	0.840	0.084	0.017
C4	1.25	1.00	1/4.2	0.740	124 min	95 min	0.767	0.209	1.54	7.38	0.694	0.453	0.032	0.003
C5	1.25	1.50	1/4.2	0.625	124 min	98 min	0.794	0.199	1.62	8.16	0.786	0.525	0.047	0.003
C6	1.25	2.00	1/4.2	0.410	124 min	114 min	0.922	0.241	1.79	7.41	1.047	0.640	0.073	0.010
C7	1.50	1.00	1/2.9	0.880	124 min	88 min	0.713	0.153	1.50	9.84	0.600	0.441	0.024	0.003
C8	1.50	1.50	1/2.9	0.770	124 min	89 min	0.721	0.159	1.51	9.51	0.614	0.445	0.039	0.003
C9	1.50	2.00	1/2.9	0.650	124 min	106 min	0.855	0.209	1.69	8.07	0.877	0.573	0.050	0.009

6.3.3.2. Graphical representation and results discussion

Analytical expressions from Table 6.16 are graphically represented in Fig. 6.8 and results are discussed in following sub-sections. Additionally, based on the constraint values shown in Table 6.2, benchmarking of the hydraulic indexes for each AnoxAn configuration has been performed and it is shown in Table 6.17.
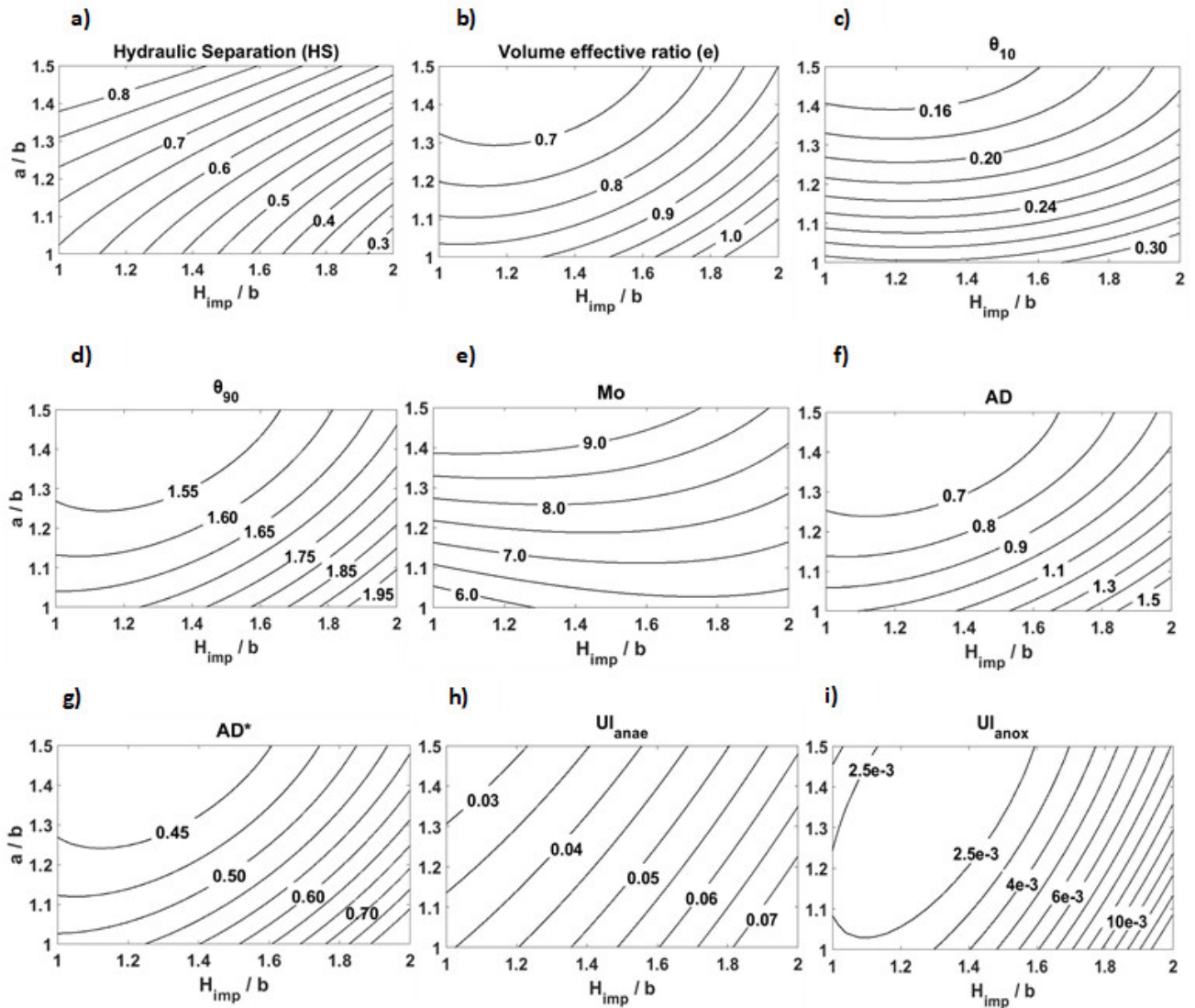
Figure 6.8. 2D contour-line plots for (a) Hydraulic separation (HS), (b) Volume effective ratio (e), (c) θ_{10}, (d) θ_{90}, (e) Morril index (Mo), (f) AD index, (g) AD* index, (h) Uniformity Index in anaerobic zone (UI_{anae}) and (i) Uniformity Index in the anoxic zone (UI_{anox})

Hydraulic separation

Fig. 6.8a shows the hydraulic separation index (HS) between anaerobic and anoxic zones. As explained in section 6.2.1.1, HS values near 1 represent null hydraulic separation, and values near 0 represent complete hydraulic separation between both environments.

As deduced in vertical velocity field analysis in Fig. 6.6, it is observed that the highest hydraulic separation is achieved for highest location of the impeller and slenderness values. Regarding the influence of the location of the impeller, the lower the H_{imp} (location nearer from the deflector) the higher becomes the mixing rate between anaerobic and anoxic zones. In consequence, in these cases, the hydraulic separation between both environments is more deficient. On the contrary, if H_{imp} is high, the impeller is placed farther from the deflector and the influence to the anaerobic zone is smaller, increasing the hydraulic separation in AnoxAn.

With respect to the influence of the slenderness on HS, the higher the slenderness is (lower a/b ratios) the higher is the hydraulic separation between anoxic and anaerobic zones. It can be explained due to the fact that for lower slenderness configurations, the different zones are more cube shaped and the mixing between environments is enhanced.

Dead volumes

In Fig. 6.8b, the spatial distribution of effective volume ratio *(e)* is represented. As observed in the velocity fields in the anoxic and clarification zones (Fig. 6.5), lowest effective volume ratios, i.e. bigger dead zone volumes, are observed for lower impeller heights and lower slenderness. For these configurations, it is estimated that the percentage of dead zones could reach 30% of the total volume of AnoxAn. On the other hand, excellent conditions can be achieved for a wide range of configurations tested ($1.0 > e > 0.90$, according to the constraint values and benchmarking shown in Table 6.2 and Table 6.17), where stagnant zones are almost null. In fact, as the cross-section that needs to be under the impeller's influence is smaller, higher slenderness are associated with smaller dead volumes.

Regarding configurations with the same slenderness, *e* increases with the height of the impeller, decreasing the volume of stagnant zones. According to values from Table 6.15, this effect is higher for high slenderness configurations, where, depending on the H_{imp}/b ratio, the variation of *e* can be up to 22.2%. For low slenderness configurations, the maximum variation in *e* depending on H_{imp}/b is around 16.6%. Finally, as the slope of the curve is higher for the a/b ratio than for the H_{imp}/b ratio, it can be concluded that in this reactor the slenderness has more influence on effective volume than the height of the impeller.

Short-circuiting

Fig. 6.8c shows the variation of the short-circuiting index, θ_{10}, depending on the geometrical characteristics of the reactor. According to the benchmarking values discussed in Table 6.2, regarding short-circuiting, not adequate hydrodynamic performance could be reached in

AnoxAn. In fact, it is observed that, for most configurations, the value for θ_{10} is under 0.3, defining the hydraulic performance of AnoxAn as poor. Just a small area around highest slenderness and H_{imp} ($\theta_{10} > 0.3$) improves short-circuiting performance to compromising (see Table 6.17). In fact, increasing θ_{10} value with the aim of reducing the short-circuiting phenomena would imply higher reactor slenderness.

Regarding configurations with the same slenderness, θ_{10} increases with the height of the impeller, decreasing the short-circuiting phenomena as discussed in section 6.3.2. According to values from Table 6.15, this effect is higher in low slenderness configurations, where the variation of θ_{10} can be up to 26.8% depending on the H_{imp}/b ratio. For high slenderness configurations, the maximum variation of θ_{10} depending on the height of the impeller is around 12.9%. Finally, it is observed that the slenderness has more influence on θ_{10} than the height of the impeller as the slope of the curve is higher for the a/b ratio than for the H_{imp}/b ratio.

Mixing

Mixing is evaluated by means of different parameters (Fig. 6.8d-i). First, spatial distribution for θ_{90} is discussed. Then, the deficiencies stated in section 6.2.1.1 for Mo and AD indexes are reported for the case study, and finally, discussion for AD* and UI parameters is carried out.

In Fig. 6.8d, the contour-line plot for θ_{90} is depicted. Although θ_{90} is not a hydraulic performance indicator itself, it is a key factor of several mixing evaluation parameters (Mo, AD, AD*) being important to analyse its behaviour. According to the benchmarking values shown in Table 6.2, there is a wide zone in the θ_{90} contour line that imply a good hydraulic performance ($1.7 > \theta_{90} > 1.3$). In these cases, smaller impeller relative heights and slenderness show values for θ_{90} closer to 1, representing a performance nearer from ideal plug flow conditions. However, this tendency goes against the one that has been observed for hydraulic separation, short-circuiting and dead zones: ranges that match with best hydraulic performance for HS, θ_{10} and e parameters (high slenderness and high impeller heights) show compromising or poor efficiency for θ_{90}, and in consequence, for mixing (see Table 6.17). Regarding configurations with the same slenderness, θ_{90} increases with the height of the impeller, decreasing the mixing performance. Following results from Table 6.15, this effect is higher in high slenderness configurations, where the variation of θ_{90} can be up to 19.9% depending on the H_{imp}/b ratio. For small slenderness configurations, the maximum variation is around 10.9%. Finally, similarly to the previous indexes, it is observed that the slenderness has more influence on θ_{90} than the height of the impeller as the slope of the curve is higher for the a/b ratio than for the H_{imp}/b ratio.

The Mo index spatial distribution for all the geometrical configurations is shown in Fig. 6.8e. The limitation of this index is clearly noted, according to what was discussed in section 6.2.1.1. Although the highest θ_{90} values were observed for high H_{imp}/b and low a/b ratios, the highest Mo values are related to the smallest impeller relative heights and slenderness. As already stated, this is because high short-circuiting rate (very small θ_{10} values) drastically influences Mo parameter. In consequence, short circuiting phenomena clearly interferes in the evaluation

of mixing performance through the Morrill index. In fact, according to the constraint values presented in Table 6.2, the higher the Mo index value is, the worse is the mixing efficiency in a water treatment system. For this particular case, due to the big influence of θ_{10}, highest Mo values (bad mixing performance) match with small θ_{90} values (good mixing performance) as shown in Table 6.17.

Contour-line plot for AD index is represented in Fig. 6.8f. As discussed in section 6.2.1.1, it is observed that the highest AD values (good mixing performance and low short-circuiting rate) match with high θ_{90} values (bad mixing performance), which is contradictory.

The resulting values for AD^* are shown in Fig. 6.8g for the range of geometric configurations considered. In this case, it is observed that the smallest AD^* values (desired mixing performance) are related to low H_{imp}/b and high a/b ratios, matching with smaller θ_{90} values (desired mixing performance). According to the constraint values of Table 6.2, there is a wide range of the geometric configurations that implies a compromising mixing performance of AnoxAn $(0.75 > AD^* > 0.50)$ and a remarkable range for good performance $(0.50 > AD^* > 0.25)$. Regarding configurations with the same slenderness, as observed for θ_{90}, AD^* value increases with the height of the impeller, decreasing the mixing performance of AnoxAn. This effect is higher in high slenderness configurations, where the variation of AD^* can be up to 35.7% depending on the H_{imp}/b ratio and, while for small slenderness configurations, the maximum variation is around 23.0%. As it happened for θ_{90}, the geometries that match with the best hydraulic performance for HS, θ_{10} and e parameters (high slenderness and high impeller relative heights) result in compromising or poor efficiency for AD^* (see Table 6.17). Finally, it is again observed that the slenderness has more influence on AD^* than the height of the impeller.

Values for UI in the anoxic and anaerobic zones of AnoxAn are depicted in Fig. 6.8h-i. Similarly to θ_{90} and AD^*, UI is higher for high H_{imp}/b ratios and high slenderness, implying a worse mixing performance for those configurations. The agreement between the behaviour of UI and AD^*, confirms the ability of the latter to evaluate mixing efficiency in contrast to AD and Mo indexes. According to the benchmarking values shown in Table 6.2, excellent mixing is achieved in the anoxic zone for all the configurations tested, while in the anaerobic environment the mixing efficiency is benchmarked as good in all the range (see Table 6.17). As it happens for θ_{90} and AD^*, the geometries that match with the best hydraulic performance for HS, θ_{10} and e parameters (high slenderness and high impeller relative heights) result in good efficiency for UI. Finally, it is observed that the height of the impeller has more influence on UI than the slenderness as the slope of the curve is higher for the H_{imp}/b ratio than for the a/b ratio.

It has also to be mentioned, that according to the constraint values of Table 6.2, for AD^* and θ_{90} excellent mixing performance is never achieved, while for UI-s the mixing performance is good or excellent for all configurations tested. This is attributed to the fact that AD^* or θ_{90} are based on RTD curves taking the plug flow behaviour as the most ideal, while UI is based on the quantitative measurement of tracer concentration in every cell of the computational domain of the analysed reactor.

Table 6.17. Benchmarking for hydraulic indexes in AnoxAn

Config.	Geometry			Hydraulic Separation	Dead Volumes	Short Circuiting		Mixing performance		
	a/b	H_{imp}/b	λ	HS	e	θ_{10}	θ_{90}	AD*	UI_{Anae}	UI_{Anox}
C1	1.00	1.00	1/6.5	0.635	Good	Poor	Good	Compromising	Good	Excellent
C2	1.00	1.50	1/6.5	0.496	Excellent	Compromising	Compromising	Compromising	Good	Excellent
C3	1.00	2.00	1/6.5	0.275	Excellent	Compromising	Compromising	Fair	Good	Excellent
C4	1.25	1.00	1/4.2	0.740	Good	Poor	Good	Good	Good	Excellent
C5	1.25	1.50	1/4.2	0.625	Good	Poor	Good	Compromising	Good	Excellent
C6	1.25	2.00	1/4.2	0.410	Excellent	Poor	Compromisng	Compromising	Good	Excellent
C7	1.50	1.00	1/2.9	0.880	Compromising	Poor	Good	Good	Good	Excellent
C8	1.50	1.50	1/2.9	0.770	Compromising	Poor	Good	Good	Good	Excellent
C9	1.50	2.00	1/2.9	0.650	Good	Poor	Good	Compromising	Good	Excellent

6.3.4. Global Hydraulic Efficiency

Finally, the Global Hydraulic Efficiency of AnoxAn is determined according to Eq. 6.23. Values for GHE index along with HS for all configurations are shown in Table 6.18:

Table 6.18. Global Hydraulic Efficiency for AnoxAn configurations

	Geometry			Hydraulic Separation	Global Hydraulic Efficiency
Configuration	a/b	H_{imp} / b	λ	HS	GHE
C1	1.00	1.00	1/6.5	0.635	0.628
C2	1.00	1.50	1/6.5	0.496	0.630
C3	1.00	2.00	1/6.5	0.275	0.665
C4	1.25	1.00	1/4.2	0.740	0.574
C5	1.25	1.50	1/4.2	0.625	0.578
C6	1.25	2.00	1/4.2	0.410	0.611
C7	1.50	1.00	1/2.9	0.880	0.547
C8	1.50	1.50	1/2.9	0.770	0.550
C9	1.50	2.00	1/2.9	0.650	0.583

Following the same procedure discussed in section 6.3.3.1, the analytical relation concerning GHE and the geometric characteristics is expressed in Eq. 6.25:

$$GHE = f_{GHE} = 1.18 - 0.14\frac{H_{imp}}{b} - 0.68\frac{a}{b} + 0.06\left(\frac{H_{imp}}{b}\right)^2 - 0.002\left(\frac{H_{imp} \cdot a}{b^2}\right) + 0.21\left(\frac{a}{b}\right)^2$$

(6.25)

General expresions relating HS, GHE and geometric characteristics are obtained according to Eq. 6.24 and presented in Fig. 6.9. Concretely, in Fig 6.9a GHE values (black circles) for the range of AnoxAn geometric configurations are plotted against HS and, in Fig 6.9b, contour lines for GHE (black) and HS (coloured) are depicted for the different AnoxAn geometries.
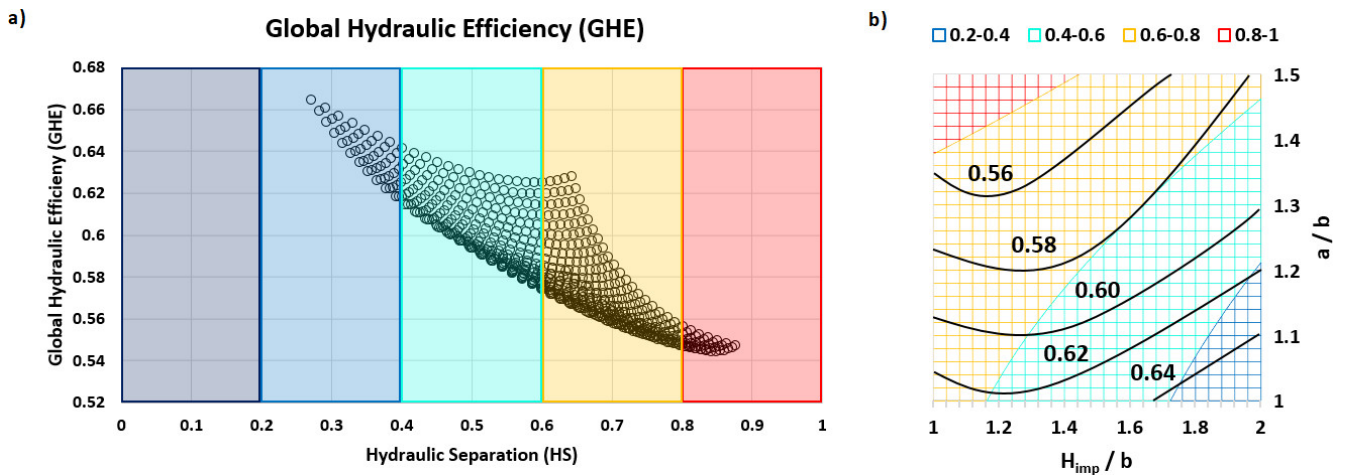
Figure 6.9. Global Hydraulic Efficiency in AnoxAn: (a) GHE-HS plot and (b) contour lines for GHE (black) and HS (coloured)

It is observed in Fig. 6.9a that the highest GHE is achieved for the lowest HS value, i.e. highest hydraulic separation between anoxic and anaerobic environments. According to the benchmarking results (shown in Table 6.18), such configuration corresponds to C3, i.e. the prototype with highest slenderness and relative heigh of the impeller (see also Fig. 6.9b). The original AnoxAn prototype configuration, i.e. C2, presents good GHE and HS, close to the most efficient prototype. Additionally, configuration C6, which is less slender but with a higher H_{imp}, has similar hydraulic characteristics.

Although HS has a wide range of variation (0.275-0.880), GHE varies in a smaller range (0.547-0.665). The latter is because the most efficient configurations regarding dead volumes and short-circuiting, have the worst mixing performance and viceversa.

6.3.5. Practical considerations

The analysis carried out in this work indicates that configurations of AnoxAn with the highest slenderness are more efficient, since they present a smaller surface requirement compared to the configurations with lower slenderness, for the same theoretical treatment capacity (i. e., the same volume). In addition, the configurations with higher slenderness give rise to reactors with less usual shapes and less studied in literature, since the implementation of several units of these configurations would cause larger length/width ratios. This aspect could be a disadvantage when proposing the layout of a new reactor implementation. In particular, it could be a handicap when reusing existing reactors in cases of retrofitting existing treatment plants. Normally, bioreactors with vertical axis mixers are constructed according to dimensioning guidelines such as the width/dept ratio between 2.5 and 5 (Hernández, 2015), and AnoxAn implementations with high slenderness can be difficult to fit in such reactor shapes.

Regarding the hydrodynamic behaviour, according to the results of this study, configurations with higher slenderness are preferred in multi-environment reactors, due to the higher GHE values. There is a maximum variation of 18% in the resulting GHE values between the different studied configurations, being the highest for C3 (GHE = 0.665) and the lowest C7 (GHE = 0.547). Therefore, in addition to the lower surface requirement, the configurations with higher slenderness achieve a higher hydraulic efficiency, potentially increasing the biological performance of the reactor.

All in all, the choice and selection of one of the configurations for the industrial scale implementation of the AnoxAn reactor should depend on the characteristics of each case, according to the constructive limitations and requirements. Higher slenderness is preferable, but the slenderness of the reactor could be reduced if, according to the design influent loads of pollutants (nitrogen), the required hydraulic separation and efficiency can be reduced.

6.4. Conclusions

In the present chapter, hydrodynamic optimization methodology for multi-environment bioreactors is proposed based on the systematization of hydraulic indexes in combination with CFD. Then, the proposed procedure is applied to AnoxAn, an anaerobic-anoxic reactor for biological nutrient removal. The main conclusions of this study are:

- Global Hydraulic Efficiency (GHE) parameter is proposed in this work as a new approach for global hydrodynamic performance assessment in multi-environment bioreactors. GHE joins several hydraulic indexes to establish an integrated and holistic benchmarking procedure.

- A new dimensionless index is proposed for the quantitative assessment of hydraulic separation in multi-environment reactors, named HS. Additionally, existing hydraulic indexes for mixing performance assessment, i.e. Mo and AD, have shown limitations to evaluate this feature. New indexes, i.e. AD* and UI, are proposed and have appeared to reliably evaluate the mixing efficiency.

- The hydraulic separation between anoxic and anaerobic zones environments in AnoxAn is more efficient in configurations with high slenderness and the impeller located in upper positions since with that setup, the influence of the impeller to the anaerobic zone is limited.

- For all AnoxAn geometric configurations tested, hydraulic performance for short-circuiting becomes poor or compromising, and no desirable performance can be reached regarding this hydraulic feature.

- Dead volumes are bigger in low slenderness configurations, where the effective volume is around 70-80% of the total volume of the reactor.

- While the mixing efficiency in all AnoxAn configurations is improvable regarding AD* index, excellent mixing is achieved with respect to UI. This is because the optimum value for AD* is based on ideal plug-flow conditions and, conversely, optimum value for UI is based on the tracer concentration homogeneity. Both mixing indexes have shown to be complementary.

- The optimum hydrodynamic AnoxAn configuration corresponds to the one with the highest slenderness and largest distance from the impeller to the anaerobic-anoxic deflector.

Chapter 7

Influence of the hydrodynamics in the biological performance of a novel anaerobic-anoxic reactor for biological nutrient removal

7.1. <u>Introduction</u>

The previous chapters of this thesis have strictly focused on the hydrodynamic analysis and optimization of multi-environment reactors and the anaerobic-anoxic reactor AnoxAn (Tejero et al., 2010; Díez-Montero et al., 2015). Concretely, in Chapter 5, Computational Fluid Dynamics (CFD) model validation and a comprehensive hydrodynamic analysis of the original prototype were carried out (Blanco-Aguilera et al., 2020a). Subsequently, in Chapter 6, hydrodynamic optimization of AnoxAn was performed by means of a new methodology that combines CFD and dimensional analysis (Blanco-Aguilera et al., 2020b). In the optimization process, nine different AnoxAn configurations were tested and main hydraulic features of multi-environment reactors such as hydraulic separation, short-circuiting, dead volumes and mixing were evaluated. In fact, as already highlighted in Chapter 6, several studies in the literature have demonstrated that an optimum hydrodynamic operation enhances a correct biological performance (Climent et al., 2018; Arnaldos et al., 2018; Wei et al., 2019; Castrillo et al., 2019), which is the main and ultimate goal of any water treatment process.

Having the aforementioned into account, the objective of this chapter is to evaluate the influence of the hydrodynamic optimization of multi-environment reactors, such as AnoxAn, in the biological performance. For that purpose, the biological behaviour of two of the different configurations of the AnoxAn reactor analysed in Chapter 6, are tested and compared in this study. The aim is to determine if the difference that exists in the hydrodynamic operation of both configurations is relevant regarding their biological behaviour. For that purpose, the complete numerical CFD tool developed in Chapter 4 is used in this study, including a nitrate transport equation with denitrification biokinetics, which has not been introduced in the simulations of previous chapters.

It must be reminded that the influence of the biomass on the density of the fluid is not taken into account in the model. Although this is not a realistic approach, as a first step, it will help to assess the relation between the hydrodynamic and the biologic efficiency of the reactor. The introduction of the physical interaction of the biomass and the bulk liquid in the model is out of the scope of this research.

All in all, the present chapter is structured as follows. After this introduction, AnoxAn configurations and the numerical experiment conditions used for the evaluation of the biological efficiency of the process are described. Then, the CFD model setup used to assess the biological performance is briefly presented. The model has been built in the OpenFOAM® open source toolbox (Weller et al., 1998). Subsequently, main results are presented and discussed and finally, the conclusions of the study are highlighted.

7.2. <u>Materials and methods</u>

7.2.1. Description of numerical experiments

7.2.1.1. Bench scale reactors setup

With the aim of assessing the influence of the hydrodynamics in the biological performance of AnoxAn, a series of numerical experiments are conducted in configurations C2 and C8. Geometrical characteristics and main hydrodynamic efficiency indexes of both configurations are shown in Table 7.1 and Fig. 7.1. For further information, the reader is referred to Chapter 6.

Table 7.1. Main characteristics for AnoxAn tested configurations

Configuration	a (m)	b (m)	a / b	h (m)	λ	H_{imp} (m)	H_{imp} / b	HS	GHE
C2*	0.20	0.20	1.00	1.30	1/6.5	0.30	1.50	0.496	0.630
C8	0.30	0.20	1.50	0.87	1/2.9	0.30	1.50	0.770	0.550

*Configuration C2 represents the original prototype

C2 is a high slenderness configuration and it has been chosen because (i) it corresponds to the original AnoxAn prototype, (ii) it has been used to validate the hydrodynamic behaviour of the process in Chapter 5, and (iii) it showed a desirable hydrodynamic behaviour and efficiency in Chapter 6. On the other hand, C8 represents the lowest slenderness configuration with the same height of the impeller as C2. This configuration showed a deficient hydrodynamic behaviour and efficiency in Chapter 6. In fact, the hydraulic separation and the overall hydrodynamic performance are more favourable for configuration C2 (lower HS index and higher GHE index) than for C8.
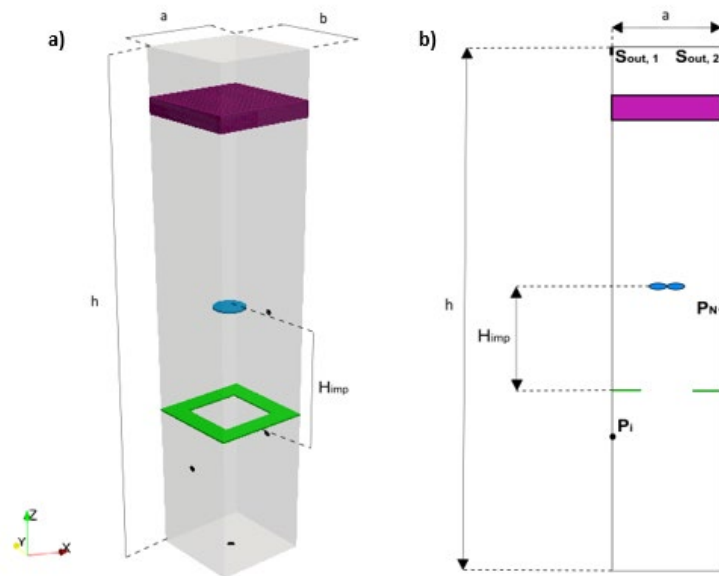
Figure 7.1. Numerical testing scheme of AnoxAn including XY cross section (a/b), height of the impeller (H_{imp}) and slenderness (λ): (a) 3D scheme and (b) XZ cross section

7.2.1.2. Numerical experiments setup

Two numerical experiments (NE1 and NE2) are performed in both AnoxAn configurations, including the denitrification phenomena in order to evaluate the biological performance of the reactor. The objectives of the experiments are (i) to assess the efficiency of nitrate removal, (ii) to analyse the spatial distribution of nitrate in the reactor, and (iii) to assess the hydraulic separation between the anoxic and anaerobic zones including the influence of the denitrifying activity. All details for the experiments are shown in Table 7.2. and Fig. 7.2. As introduced in previous chapters, for all the experiments the inlet stream flow Q_{in} is 10.4 L/h, the internal recycle rate (ratio between internal recycle stream flow and inlet stream flow, $R_{IR} = Q_{IR}/Q_{in}$) is 5.77 (-), and the nitrate recycle rate (ratio between nitrate recycle stream flow and inlet stream flow, $R_{NR} = Q_{NR}/Q_{in}$) is 2.98 (-).

The first numerical experiment, named NE1 (see Fig. 7.2a-b), consists in continuously injecting 20 mg/L of nitrate through the nitrate stream at P_N. As initial conditions, nitrate concentration in the whole reactor is set to 0 mg/L. Nitrate concentration is continuously monitored in the outlet (P_{out}) and in check points at different heights located in the centre of the reactor (P_c) and near the walls (P_w).

The second numerical experiment, named NE2 (see Fig. 7.2c-d), consists in setting a homogeneous nitrate concentration of 20 mg/L in the anoxic zone as an initial condition for the simulation, and injecting clean water through all the inlet patches. Nitrate concentration is then continuously monitored in the anaerobic zone (P_a).

All the experiments are performed assuming a constant active biomass concentration performing denitrification in the whole reactor. Although the experiments have been carried out for three different biomass concentrations (1 000 mg/L, 2 500 mg/L and 5 000 mg/L), only results for 1 000 mg/L and 2 500 mg/L are shown since for 5 000 mg/L, excessively rapid nitrate consumption has been achieved, making results unsuitable for discussion.

Table 7.2. Numerical experiments conditions

Numerical Experiment	N_0^{Anae} (mg/L)	N_0^{Anox} (mg/L)	Nitrate injection location	Nitrate injection concentration (mg/L)	Type	Nitrate concentration monitoring
NE1	0	0	P_N	20	Step	P_{out}, P_c, P_w
NE2	0	20	-	-	-	P_a
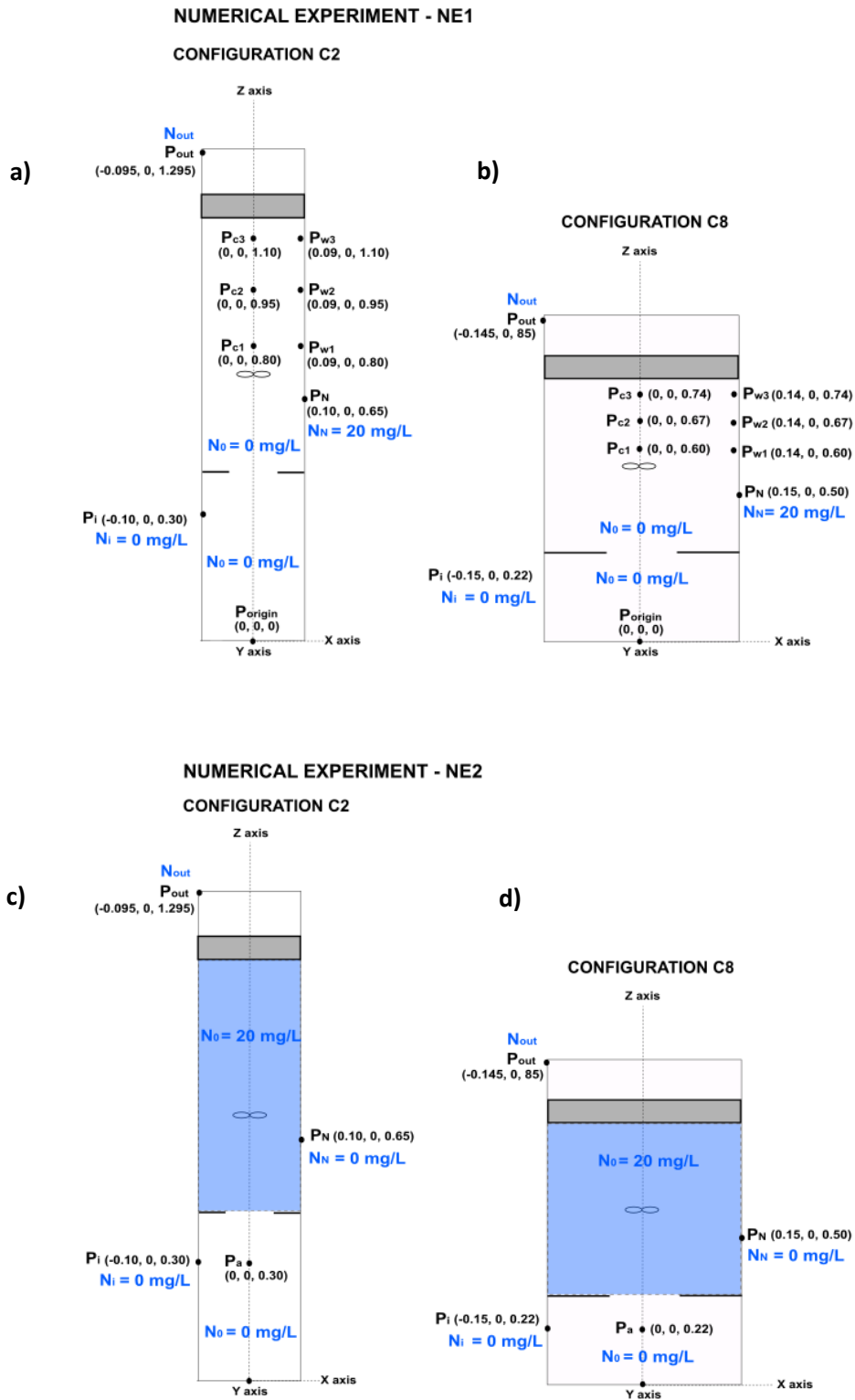
Figure 7.2. Schematic diagram of numerical experiments (a) NE1 for C2, (b) NE1 for C8, (c) NE2 for C2 and (d) NE2 for C8

7.2.2. Numerical model setup

The numerical model setup, i.e. physics, boundary conditions, computational domain and algorithms used in this study are analogue to what has been presented in previous chapters. For an extensive development of the numerical tool, the reader is referred to Chapter 4, and for hydrodynamic validation, to Chapter 5 (Blanco-Aguilera et al., 2020a).

In short, the model used in this study is an open source numerical application based on CFD and developed in OpenFOAM®. Reynolds Averaged Navier-Stokes (RANS) equations for turbulent and incompressible flow are used to simulate hydrodynamics, being the turbulence model the standard k-ε model developed by Launder and Spalding (1972). In addition, a flat disk approach is used for the impeller (Jasak et al., 2019; Seb, 2017) and the baffle between the anoxic and the clarification zone (Tejero et al., 1991) is simulated by means of a porous media.

Additionally, the nitrate transport equation incorporates the denitrification biokinetic presented in Chapter 4 as a source term. The complete transport equation for nitrate is presented in Eq. 7.1, which includes advection, diffusion, turbulent diffusion and denitrification.

$$
\frac{\partial(\rho C_{NO_3})}{\partial t} + \frac{\partial}{\partial x_i}\left(\rho v_i C_{NO_3}\right) - \frac{\partial}{\partial x_j}\left[\left(\rho D_{kn} + \frac{\mu_{tn}}{S_{ctn}}\right)\cdot\frac{\partial C_{NO_3}}{\partial x_j}\right]
$$
$$
- \left(-\frac{1-Y_H}{2.86\cdot Y_H}\mu_H\,\eta_{NO_3}\right)\frac{dC_{NO_3}}{K_{NO_3}+C_{NO_3}}X_H = 0 \tag{7.1}
$$

Being ρ the density of the fluid, C_{NO_3} the nitrate concentration and v_i the ensemble velocity vector. $\frac{\mu_{tn}}{S_{ctn}}$ term represents the turbulent diffusion of the nitrate, in which Schmidt number appears ($Sc_{tn} = \frac{\mu_{tn}}{\rho\cdot D_{tn}}$), being μ_{tn} turbulent viscosity and D_{tn} turbulent diffusivity. D_{kn} is the self-diffusion coefficient of nitrate in water. As discussed in Chapter 4, in this study D_{kn} is set to $10^{-20}\,\mathrm{m^2/s}$ to reproduce a convective transport for nitrate (Fernández, 2012).

The last term of the equation corresponds to the denitrification phenomena, in which X_H is the heterotrophic biomass concentration (mgVSS/L). Regarding the kinetic and stoichiometric parameters, K_{NO_3} is the half saturation constant for nitrate (mgN/L), Y_H is the heterotrophic yield coefficient (dimensionless), μ_H is the maximum growth rate on substrate (1/day) and η_{NO_3} is the reduction factor for denitrification (dimensionless). Values for all these parameters are taken from Henze et al. (2000) and are shown in Table 7.3.

Table 7.3. Default values for kinetic parameters of the biological model (T = 20ºC)

Symbol	Denomination	Value	Units
K_{NO_3}	Half saturation constant for nitrate	0.50	mgN/L
Y_H	Heterotrophic yield coefficient	0.67	[-]
μ_H	Maximum growth rate on substrate	6.00	1/day
η_{NO_3}	Reduction factor for denitrification	0.80	[-]

Regarding the transport properties, analogue values used for an inert non-reactive tracer (see Chapter 5) are set to the nitrate specie in order to strictly evaluate the kinetic influence (see Table 7.4).

Table 7.4. Transport properties for tracer and nitrate

Model	Parameters
Nitrate transport model	Self-diffusion coefficient for nitrate
	$D_{kn} = 10^{-20}\,\mathrm{m}^2/\mathrm{s}$
	Schmidt number for nitrate
	$Sc_{tn} = 0.8$

The numerical methodology is based in two separate stages: First, SIMPLE algorithm is used to solve the continuity and momentum equations (without nitrate) in order to reach a steady state solution for all hydrodynamic parameters. Next, nitrate initial conditions are introduced depending on the numerical experiment (see Table 7.2 and Fig 7.2), and nitrate transport equation is solved: (i) using SIMPLE algorithm to reach another steady state solution in NE1 and (ii) using PIMPLE algorithm for a transient flow simulation in NE2.

7.3. Results and discussion

7.3.1. Numerical Experiment - NE1

The experiment NE1 simulates a continuous injection of nitrate in the anoxic zone of AnoxAn through the nitrate recycle stream. This recycle stream would come from a subsequent nitrifying reactor. The aim of the experiment is to assess the efficiency of nitrate removal and to analyse the spatial distribution of nitrate in the reactor. Fig. 7.3 shows the stationary nitrate concentration at different monitoring points of AnoxAn for the two configurations tested (C2, C8) and two biomass concentrations (1 000 mg/L, 2 500 mg/L) in NE1. Results for a biomass concentration of 2 500 mg/L are shown in red and results for a biomass concentration of 1 000 mg/L are represented in green. In addition, results for C2 are depicted in filled bars and results for C8 in striped bars.

First of all, the biological performance results higher in configuration C2, achieving lower effluent nitrate concentrations than C8 for both biomass concentrations. A similar behaviour was reported in Arnaldos et al. (2018) and Climent et al. (2018) when lower outlet nitrate concentrations were observed in higher real Hydraulic Retention Time (HRT) configurations (i.e. C2 in this study) since there is more time available to degrade the substrate. Concretely, when the concentration of biomass in the reactor is 1 000 mg/L, the nitrate concentration at the outlet is three times lower for C2 compared to C8. On the other hand, when the concentration of biomass in the reactor is 2 500 mg/L, the nitrate concentration at the outlet in C2 is negligible. The latter suggests that the reactor is oversized and the volume could be decreased.

Next, it is clearly observed that the nitrate concentration is more homogeneous in configuration C8 compared to C2 since there is a smaller variation across all the monitoring points located at different heights and positions (centre and walls check points). This suggests that the lower slenderness configuration (C8) has a better mixing performance compared to the higher slender one (C2), behaving more similar to a complete mixed reactor. This result is consistent with what has been already observed in Chapter 6, where results for modified Aral-Demirel (AD*) and uniformity index (UI) indexes for tracer transport show that low slenderness configurations are more efficient regarding mixing. A similar behaviour was observed in Arnaldos et al. (2018), where in a study for an aerobic reactor, configurations with higher measured or real HRT-s (i.e. C2 in this study) showed worse mixing conditions and a greater pollutant concentration heterogeneity compared to configurations with lower measured HRT-s (i.e. C8 in this study).
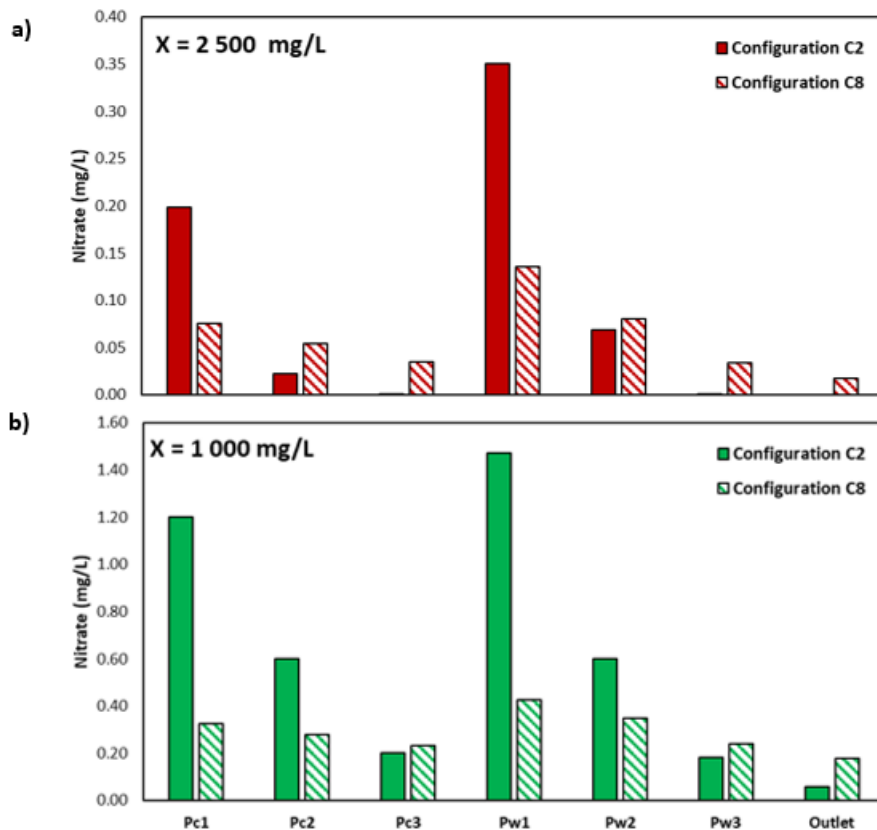
Figure 7.3. Nitrate concentration in the different monitoring points simulated by the experiment NE1: (a) tracer concentrations for the different measurement points in C2 (red filled bars) and C8 (red striped bars) with biomass of 2 500 mg/L and (b) tracer concentrations for the different measurement points in C2 (green filled bars) and C8 (green striped bars) with biomass of 1 000 mg/L

Table 7.5 shows the UI values for nitrate in the anoxic zone with different biomass concentrations in both configurations. Concretely, lower UI values (better mixing efficiency) are reported for C8 compared to C2 for both 2 500 mg/L and 1 000 mg/L biomass concentrations. As previously mentioned, these results are also consistent with what was observed for tracer transport and mixing efficiency in Chapter 6, where lower UI indexes (i.e. better mixing efficiency) were observed in low slenderness configurations. In addition, a

significant difference in the UI is observed between the same configurations but with different biomass concentration. Concretely, the nitrate concentration homogeneity is higher with smaller biomass concentration (see Table 7.5). In fact, a simulation without biomass has been already tested in Chapters 5 and 6 (pure tracer transport with no chemical reaction), and the UI value was under 0.01, achieving a complete mixing state. It suggests that the heterogeneity of nitrate concentration is amplified by the biological activity, what can be explained because with a higher biomass concentration, the influence of the denitrification term on the nitrate transport equation is more remarkable, making the heterogeneities between zones higher.

Table 7.5. UI values for nitrate in the anoxic zone for 1 000 mg/L and 2 500 mg/L biomass concentrations

Configuration	Biomass concentration (mg/L)	Nitrate UI anoxic zone
C2	1 000	0.23
C8	1 000	0.13
C2	2 500	0.36
C8	2 500	0.28

Regarding the nitrate transport close to the walls (P_w) and in the centre of the reactor (P_c), some remarks can be highlighted. First, for both biomass concentrations, it is observed that the nitrate concentration is higher at the walls than in the centre zone of the reactor. This is in agreement with the main conclusions of the hydrodynamic analysis presented in Chapters 5 and 6, where principal channelling and, in consequence, mass and tracer transport were observed close to the walls. With the incorporation of denitrification, this effect is more evident: in dead zones or lower velocity-zones (central part of the reactor) nitrate is depleted to lower values due to the limited exchange with the rest of the reactor. An analogue effect was observed in Arnaldos et al. (2018), where more biological activity was reported in dead zones and stagnant volumes of the aerobic reactor studied. In fact, it is noted that the difference on the nitrate concentration between the centre points and the walls is higher for biomass concentration of 2 500 mg/L than for 1 000 mg/L, since the influence of the denitrification term in the nitrate transport equation is higher for higher biomass concentration. This matches with what discussed regarding the mixing efficiency and UI indexes in the previous paragraph, and explains why with more biomass, the heterogeneity of nitrate concentration is higher.

Finally, a clear plug-flow behaviour is reported in both configurations: nitrate concentration decreases as moving forward through the reactor length. Climent et al. (2018) also modified the original configuration of an aerobic-anoxic conventional activated sludge process with the aim of achieving a similar denitrification behaviour through plug-flow. Comparing both configurations, a linear reduction is observed in C8 from P_{C1} and P_{W1} to P_{C3} and P_{W3}, respectively, while an exponential one is observed in C2. In fact, although nitrate concentration in the first monitoring points is higher in C2 (P_{c1}, P_{w1}) than in C8, the exponential reduction behaviour of the plug-flow in C2 gives rise to a lower concentration at the outlet. The latter is explained because in plug flows, the higher the concentration is, the more significant is the effect of the kinetic activity. This difference in the plug-flow behaviour between C2 and C8 was

already observed in Chapter 6 when the different residence time distribution (RTD) curves of tracer tests in both configurations were analysed.

7.3.2. Numerical Experiment - NE2

The experiment NE2 simulates the time-dependent evolution of nitrate concentration in the AnoxAn reactor starting from an initial condition with high concentration of nitrate in the anoxic zone. This condition could represent a specific situation such as the start-up of the reactor or an unusual temporary high concentration of nitrate. The aim of the experiment is to assess the hydraulic separation between the anoxic and anaerobic zones in the reactor including the influence of the denitrifying activity. In other words, the goal is to assess the extent of nitrate intrusion into the anaerobic zone, which should be avoided or reduced in order to keep anaerobic conditions in it. Fig. 7.4 shows the results of the simulations of NE2, where the nitrate concentration in the anaerobic zone for the different biomass concentrations and in both configurations are depicted. Results for a biomass concentration of 2 500 mg/L are shown in red and results for a biomass concentration of 1 000 mg/L are represented in green. In addition, results for C2 are depicted with continuous lines and results for C8 with dashed lines.
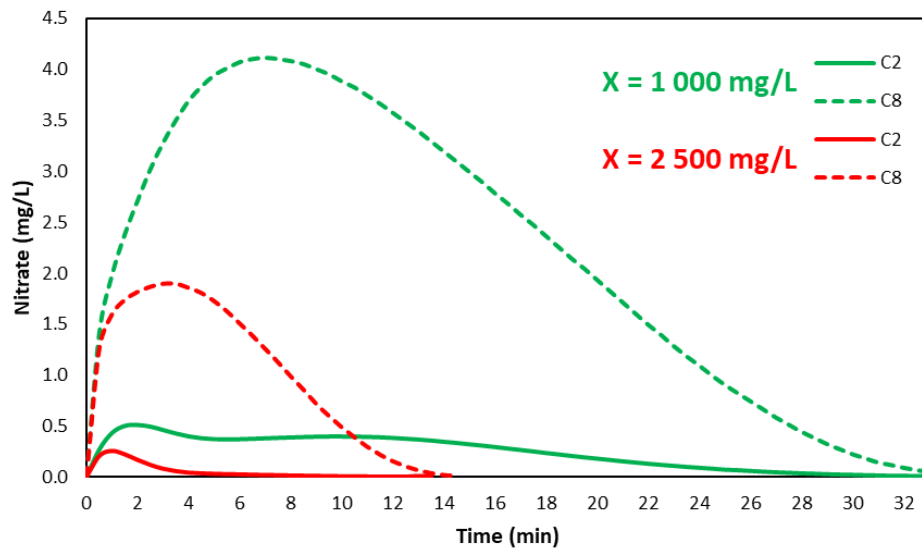
Figure 7.4. Evolution of nitrate concentration simulated by the experiment NE2: nitrate concentration in the anaerobic zone with biomass of 2 500 mg/L (red continuous line for C2 and red dashed line for C8) and nitrate concentration in the anaerobic zone with biomass of 1 000 mg/L (green continuous line for C2 and green dashed line for C8)

In the hydrodynamic evaluation performed in Chapter 6, tracer transport results showed that the hydraulic separation between the anaerobic and the anoxic zones was higher in high slenderness configurations than in lower ones. Concretely, for C2 the HS was 0.496, while for C8 it was 0.770 (see Table 7.1). The nitrate concentrations simulated by NE2 show an analogue behaviour for the hydraulic separation between both environments, including the influence of the denitrifying activity. For a biomass concentration of 2 500 mg/L, the maximum nitrate concentration in the anaerobic zone for C8 is 1.90 mg/L, which is seven times higher than the maximum nitrate concentration in the anaerobic zone for C2 (0.26 mg/L). On the other hand,

for a biomass concentration of 1 000 mg/L, the maximum nitrate concentration in the anaerobic zone for C8 reaches 4.11 mg/L, which is eight times higher than the maximum nitrate concentration in the anaerobic zone for C2 (0.51 mg/L). It can be concluded that the configuration with higher slenderness gives rise to almost negligible nitrate concentration in the anaerobic zone, even in a scenario of unusual high nitrate concentration in the anoxic zone. However, not negligible concentrations are observed in the anaerobic zone for the lower slenderness configuration. Thus, C2 is a much more resilient configuration than C8. This is due to the higher hydraulic separation between both zones, as indicated by the lower HS index.

7.4. <u>Conclusions</u>

In this chapter, the influence of the hydrodynamic behaviour on the biological efficiency of AnoxAn is studied. For that purpose, the biological performance of two configurations with different slenderness, i.e. C2 (which showed a desirable hydrodynamic performance) and C8 (which showed a deficient hydrodynamic performance), is compared by means of numerical experiments. The main conclusions of this study are:

- The relation between a desired hydrodynamic behaviour and biological efficiency is confirmed since the outlet nitrate concentration is significantly lower in C2 than in C8.

- Better mixing efficiency is obtained in low slenderness configurations, as observed for tracer transport during previous hydrodynamic evaluation and optimization. Additionally, denitrification amplifies the nitrate concentration heterogeneity observed without biological activity.

- A clear plug-flow behaviour is observed in both configurations and for the two biomass concentrations as nitrate concentration is reduced with the height. At the same time, C2 presents an exponential and more efficient nitrate consumption than C8, which is linear. This matches with the RTD curves of the hydraulic behaviour studied during hydrodynamic evaluation and optimization.

- High slenderness configurations are more resilient than low slenderness ones, since the more favourable hydraulic separation between the anoxic and anaerobic zones in the high slenderness configuration gives rise to negligible nitrate concentration in the anaerobic zone.

Chapter 8

Conclusions and recommendations

A Computational Fluid Dynamics (CFD)-based numerical tool for the hydrodynamic assessment and optimization of multi-environment bioreactors has been developed within the framework of this thesis. The numerical tool has been built based on the free and open source toolbox OpenFOAM®, and includes several features that are not available in the original source code. This new model can be used as a base to incorporate more physics in it, and also to be adapted to specific research interests within the water treatment field. Additionally, it is free and fully available for the research community.

The developed numerical tool has been applied to the hydrodynamic simulation, analysis and optimization of AnoxAn, a novel anaerobic-anoxic reactor for Biological Nutrient Removal (BNR) from wastewater. The results and findings of this research contribute to the development of technological and operational improvements of AnoxAn, which aims to reduce the land occupation and energy consumption of conventional BNR processes.

In each chapter of this thesis, the conclusions of each specific study have been presented. In this chapter, main ideas taken from the previous ones and general conclusions emerged from the results of the research are reported. The study has also allowed to identify several gaps, uncertainties and suggestions for future work that must be pointed out. Those, along with the conclusions, are presented in this final chapter, structured according to the specific objectives of the thesis.

Development of an open source numerical tool based on CFD for the hydrodynamic analysis of multi-environment reactors

- A CFD-based numerical tool is developed by selecting and combining specific features of OpenFOAM® aimed at describing the hydrodynamic behaviour of water treatment reactors. Several default features of the toolbox, such has the hydrodynamic model, the k-ε turbulence model and the flat disk approach for impellers, are included in the model.

- Various features that are not present in the original source code of OpenFOAM® but are essential to fulfil the objectives of the present study, are included in the numerical tool: (i) tracer transport model for turbulent flow, (ii) nitrate transport model and denitrification biokinetics for turbulent flow and (iii) a porous media model for the representation of baffles.

- All the previous elements are incorporated to the two solvers that are part of the numerical tool: (i) stationaryDesnitriEqn for stationary simulations, based on the simpleFOAM solver and (ii) transientDesnitriEqn for non-stationary simulations, based on the pimpleFOAM solver. Both are adapted to solve the new included features.

Model construction, validation and hydrodynamic analysis of the AnoxAn anaerobic-anoxic multi-environment reactor based on CFD

- The numerical tool is applied to the AnoxAn original prototype and the overall hydrodynamic behaviour is validated against Residence Time Distribution (RTD) experimental tests. The agreement between experimental and simulated results evidence that the numerical model reliably represents the mass transport within AnoxAn, and also confirms the applicability of the flat disk approach for the impeller and the porous media for the baffle.

- The CFD analysis of the hydrodynamic behaviour of the AnoxAn original prototype supposes a remarkable step forward with respect to the previous work carried out with compartment-based models. At this respect, the non-ideal flow generated in AnoxAn is not only observed through RTD curves, but also concretely defined with the location and quantification of short-circuiting and dead zones. Moreover, CFD analysis allows to evaluate the mixing level in the different compartments and the overall reactor through the uniformity index (UI), which is not calculable with RTD curves. Finally, the influence of the deflector (located between anoxic and anaerobic zone) and the baffle (located between anoxic and clarification zones) on the hydrodynamic behaviour of AnoxAn is also evaluated with the CFD model. Such detailed evaluation cannot be carried out with the previous compartment-based models since they are only useful for the original operational conditions, not allowing to test the effect of changing the geometry or elements.

The research needs identified in this study can be summarized as:

- The use of the flat disk for representing the impeller is a simplified approach that does not simulate in detail the hydrodynamic patterns around the stirrer. More realistic approaches have been tested too, i.e. the Arbitrary Mesh Interface (AMI) and Overset mesh, and satisfactory validation results have been achieved for the first time-steps. Nevertheless, they give rise to an excessive computational cost. Further research should be done in this regard in order to make these approaches computationally affordable for long-time experiments.

- The hydrodynamics of AnoxAn cannot be defined as fully validated since the velocity fields have not been checked in this study. In this sense, a validation campaign through Particle Image Velocimetry (PIV) or similar techniques should be performed in the future.

Hydrodynamic optimization of multi-environment reactors for biological nutrient removal

- A new hydrodynamic optimization methodology for multi-environment reactors is proposed combining CFD and dimensional analysis. At this aim, different existing dimensionless hydraulic indexes along with new ones developed in this study are joined into a single Global Hydraulic Efficiency (GHE) parameter. This new index includes several hydrodynamic features such as short-circuiting, dead volumes and mixing efficiency, establishing an integrated and holistic benchmarking procedure. This optimization approach implies a significant progress regarding the hydrodynamic optimization examples found in the literature, in which although different hydraulic indexes have been applied in several studies, those are used without any standardization. The proposed methodology can be used and adapted for the optimization of other multi-environment bioreactors and processes.

- New hydraulic indexes are developed and defined within the framework of this study. Concretely, (i) the HS index is used to evaluate the hydraulic separation between different environmental zones and (ii) the AD* index is used to evaluate the mixing performance. The AD* is developed based on the existing AD parameter, which, along with the widely used Morrill index (Mo), both show limitations to evaluate the mixing efficiency. Finally, the uniformity index (UI) is also proposed to evaluate this feature in a complementary way.

- Results for GHE index in AnoxAn report that the most efficient configurations regarding the hydrodynamic behaviour are those with (i) highest slenderness and (ii) the impeller located farther from the deflector between the anaerobic and anoxic zones. Additionally, these configurations ensure a higher hydraulic separation.

- As a result of the optimization study, a set of mathematical equations that relate the studied hydraulic indexes (HS, e, Mo, AD, AD*, UI) to the cross section and the location of the impeller are developed. These expressions are applicable at prototype scale and under the imposed geometric constraints. In fact, a high goodness of fit has been achieved between the predicted values by the equations and the obtained results with CFD simulations. These mathematical equations can be used as a starting point for the design of AnoxAn reactors at industrial scale.

The research needs identified in this study can be summarized as:

- Only two geometric parameters, i.e. the height of the impeller and the slenderness of the reactor have been tested in the optimization study. Additional CFD simulations should be performed varying other geometric characteristics such as the angle and direction of the impeller and/or the geometry of the deflector in order to assess the influence of different parameters in the overall hydrodynamic performance.

- The mathematical equations relating the hydraulic indexes to the geometrical characteristics of the AnoxAn reactor can be used as a starting point for the design of AnoxAn configurations at industrial scale. However, as the scalability procedure is not direct, further research is needed regarding the validation and application of the developed expressions at a larger scale.

Evaluation of the influence of the hydrodynamic behaviour in the biological performance of AnoxAn

- With the aim of assessing the influence of the hydrodynamic behaviour in the biological performance of AnoxAn, a denitrification model is introduced in the CFD tool and is applied to two different configurations of the reactor, i.e. one high slenderness and another low slenderness configuration. In both cases the impeller is located at the same distance from the deflector. Additionally, two different biomass concentrations (1 000 mg/L and 2 500 mg/L) have been tested. Obtained results evidence the correlation between the hydrodynamic and the biological efficiency.

- The configuration with the highest slenderness reports a higher GHE and smaller outlet nitrate concentration (three times smaller) than the one with lowest slenderness, resulting in a better biological performance and efficiency. Additionally, as observed for tracer concentration in the hydrodynamic optimization study, the low slenderness configuration shows a better mixing efficiency (less nitrate concentration heterogeneity) compared to the high slenderness one. Besides, the effect of the denitrification kinetics gives rise to more concentration heterogeneity compared to the observed without biological activity.

- The analysis of the fluid flow and the velocity fields shows that short-circuiting zones are located near the walls, enhancing the mass transport through these paths. Consequently, compared to the central part of the reactor, greater tracer (hydrodynamic) and nitrate transport (biological) is observed along these channelling zones. As also observed in the hydrodynamic optimization study, a higher hydraulic separation is confirmed in the high slenderness configuration, leading to negligible nitrate concentration in the anaerobic zone. The latter makes high slenderness configurations more resilient than low slenderness ones.

The research needs identified in this study can be summarized as:

- Is important to highlight that the developed model does not include the effect of the solid phase (biomass) on the density of the liquid phase. Thus, neither the hydrodynamic behaviour nor the biological efficiency simulations are completely realistic, but they help to characterize and understand the operation of AnoxAn. In the same way as it has been observed that the denitrification kinetic increases the

heterogeneities in the concentration fields, a higher solid phase concentration (and consequently less nitrate concentration) is expected in stagnant volumes, and less biomass (and more nitrate concentration) in short-circuiting zones. In any case, the next step of the research should take the numerical tool presented in this thesis as a base and introduce the interaction of the solid phase in the code. Additionally, next developing stages should include more complex biological models, extending the current one to the ASM1 and considering the incorporation of phosphorus removal to assess the complete BNR process (ASM2d). All the modelling process should come along with a deeper validation experimental campaign.

Summarising, this research work has evidenced that higher slenderness configurations of AnoxAn are preferred to lower slenderness ones since they present a higher hydrodynamic, and therefore, biological efficiency. In addition, high slenderness configurations present a smaller surface requirement compared to the configurations with lower slenderness, for the same theoretical treatment capacity (i. e., the same volume). However, the configurations with higher slenderness give rise to reactors with less usual shapes and less studied in literature, since the implementation of several units of these configurations would cause larger length/width ratios. This aspect could be a disadvantage when proposing the layout of a new reactor implementation. In particular, it could be a handicap when reusing existing reactors in cases of retrofitting existing treatment plants. Depending on the land availability or constructive limitations and requirements, slenderness (and consequently hydraulic separation) of the reactor could be reduced depending on the design influent nitrogen loads.

Conclusiones y recomendaciones

En la presente tesis doctoral se ha desarrollado una herramienta numérica basada en Dinámica de Fluidos Computacional (CFD) para la evaluación y optimización hidrodinámicas de biorreactores multi-ambiente. Dicha herramienta numérica ha sido construida con el software gratuito y de código abierto OpenFOAM®, e incluye, además, varias aplicaciones que no están disponibles en su código fuente. Este nuevo modelo numérico puede servir como base para incorporar nuevas físicas en él, así como ser adaptado para diferentes intereses investigadores dentro del campo del tratamiento de aguas. Además, es una herramienta gratuita y está totalmente disponible para la comunidad científica.

La herramienta numérica desarrollada se ha aplicado a la simulación, análisis y optimización hidrodinámicas de AnoxAn, un reactor anaerobio-anóxico para Eliminación Biológica de Nutrientes (EBN) de las aguas residuales. Los resultados de esta investigación han contribuido al desarrollo tecnológico y operacional de AnoxAn, el cual pretende reducir la ocupación de espacio y consumo energético de los procesos convencionales de EBN.

Las conclusiones para cada estudio específico se han presentado ya en su capítulo correspondiente dentro de esta tesis. En este texto, se detallan las ideas principales obtenidas del resto de capítulos, así como las conclusiones generales que han emergido durante la investigación. Este trabajo ha generado también ciertas incertidumbres, así como propuestas y sugerencias para la investigación futura que deben ser subrayadas. Todas ellas, junto con las conclusiones, se presentan a continuación estructuradas acorde a cada uno de los objetivos específicos de la tesis doctoral.

Desarrollo de una herramienta numérica basada en CFD para el análisis hidrodinámico de reactores multi-ambiente

- Se ha desarrollado una herramienta numérica basada en CFD seleccionando y combinando características específicas del software OpenFOAM® con el objetivo de reproducir el comportamiento hidrodinámico de reactores multi-ambiente. En esta herramienta numérica se han incluido varias aplicaciones preexistentes en el código original de OpenFOAM®, tales como el modelo hidrodinámico, el modelo de turbulencia k-ε, y el modelo de disco plano para los agitadores.

- En la herramienta numérica CFD se han incluido también varias aplicaciones que no están disponibles en el código fuente de OpenFOAM®, pero que se han identificado como cruciales para poder cumplir los objetivos de la investigación: (i) modelo transporte de trazador para flujo turbulento, (ii) modelo de transporte de nitratos y cinética de desnitrificación para flujo turbulento y (iii) modelo de medio poroso para la simulación de bafles.

- Todos los elementos previos han sido incorporados a los dos solvers que forman la herramienta numérica: (i) stationaryDesnitriEqn para simulaciones estacionarias, basado en el solver simpleFOAM y (ii) transientDesnitriEqn para simulaciones no estacionarias, basado en pimpleFOAM. Ambos solvers han sido adaptados para poder resolver las nuevas ecuaciones introducidas en el modelo.

Construcción, validación y análisis hidrodinámicos mediante modelo CFD del reactor anaerobio-anóxico multi-ambiente AnoxAn

- La herramienta numérica desarrollada se aplica al prototipo original de AnoxAn, y se valida el comportamiento hidrodinámico con ensayos de trazadores (RTD). Las simulaciones evidencian que el modelo numérico es capaz de predecir los resultados experimentales, representando de manera fidedigna el transporte de masa global en AnoxAn. Además, confirman la aplicabilidad del modelo del disco plano para simular el agitador, así como la del medio poroso para el bafle.

- El análisis de la hidrodinámica del prototipo original de AnoxAn mediante técnicas CFD supone un avance significativo con respecto al trabajo previo realizado en dicho reactor con modelos de compartimentos. A este respecto, el flujo no ideal generado en AnoxAn, no solo ha podido observarse a través de curvas RTD, sino que también se ha definido mediante la localización espacial y cuantificación de flujos preferenciales y zonas estancas. Además, el análisis CFD permite evaluar la capacidad de mezcla en las diferentes zonas del reactor mediante el índice de uniformidad (UI), el cual no puede calcularse a través de curvas RTD. Por último, mediante el modelo CFD, también han podido evaluarse tanto la influencia del deflector (situado entre las zonas anaerobia y anóxica) como la del bafle (situado entre las zonas anóxica y de clarificación) en la hidrodinámica de AnoxAn. Este estudio no puede realizarse con los modelos de compartimentos desarrollados en investigaciones precedentes, ya que éstos solo son útiles para las condiciones originales de operación, no dando opción a evaluar el efecto de modificar la geometría o la disposición de los elementos operacionales.

A continuación, se concretan las necesidades de investigación futuras identificadas en este estudio:

- El uso del modelo del disco plano para simular el agitador es una simplificación que, por sí misma, no es capaz de simular en detalle el campo hidrodinámico alrededor del dispositivo de mezcla. Se han llevado a cabo aproximaciones más realistas tales como la Interfaz de Malla Arbitraria (AMI) y Overset, obteniendo resultados de validación satisfactorios para los primeros intervalos de simulación. Sin embargo, estas aproximaciones dan lugar a un excesivo coste computacional, evidenciando que debe profundizarse en la investigación a este respecto, con el objetivo de hacer que estas aproximaciones sean computacionalmente rentables para experimentos de larga duración.

- La hidrodinámica de AnoxAn no puede ser definida como totalmente validada ya que, en el presente estudio, los campos de velocidad no han sido comprobados. A este respecto, en el futuro, debe realizarse una campaña de validación basada en Velocimetría de Imágenes de Partículas (PIV) o técnicas similares.

Optimización hidrodinámica de reactores multi-ambiente para eliminación biológica de nutrientes

- Se ha propuesto una nueva metodología para la optimización hidrodinámica de reactores multi-ambiente combinando CFD y análisis dimensional. A este respecto, se desarrolla un nuevo parámetro denominado índice de Eficiencia Hidráulica Global (GHE), el cual aúna varios índices hidráulicos adimensionales existentes en el estado del arte, así como nuevos índices desarrollados en la presente tesis. El índice GHE evalúa características hidráulicas como los flujos preferenciales, zonas muertas o capacidad de mezcla, estableciendo un procedimiento integrado y holístico de evaluación hidrodinámica. Esta metodología supone adelanto significativo con respecto a los ejemplos de optimización hidrodinámica de reactores revisados en la bibliografía, en los cuales, a pesar de haber aplicado diferentes índices hidráulicos, éstos han sido empleados sin ningún tipo de estandarización. La metodología propuesta en esta tesis puede ser utilizada y adaptada para la optimización hidrodinámica de otros biorreactores y procesos multi-ambiente.

- En el marco de esta metodología se han desarrollado nuevos índices hidráulicos adimensionales. En concreto, se proponen (i) el índice HS para evaluar la separación hidráulica entre diferentes zonas ambientales y (ii) el índice AD* para evaluar la capacidad de mezcla. Éste último índice se ha desarrollado en base al índice AD ya existente; pero que, junto con el comúnmente empleado índice de Morrill (Mo), ambos han mostrado limitaciones para evaluar la eficiencia de mezcla. Por último, también se ha propuesto el índice de uniformidad (UI) para evaluar esta misma característica de una manera complementaria.

- Los valores para GHE en AnoxAn muestran que las configuraciones hidrodinámicamente más eficientes son aquellas (i) con mayor esbeltez y (ii) en las que el agitador situado a más distancia del deflector situado entre las zonas anaerobia y anóxica. Además, estás configuraciones aseguran una mayor separación hidráulica.

- Como resultado del estudio de optimización, se han desarrollado una serie de ecuaciones que relacionan los índices hidráulicos estudiados (HS, e, Mo, AD, AD*, UI) con la sección transversal del reactor y la altura del agitador. Estas expresiones son aplicables a escala de prototipo y bajo las condiciones geométricas estudiadas. De hecho, se ha obtenido una alta bondad de ajuste entre los valores predichos por dichas ecuaciones y los resultados obtenidos mediante simulación CFD. Estas expresiones matemáticas pueden emplearse como punto de partida para el diseño de AnoxAn a escala industrial.

A continuación, se concretan las necesidades de investigación futuras identificadas en este estudio:

- Tan solo se han analizado dos parámetros geométricos (la esbeltez del prototipo y la altura del agitador) en el estudio de optimización. Con el objetivo de evaluar la influencia de diferentes parámetros en el comportamiento hidrodinámico global del sistema, deben realizarse simulaciones CFD variando otras características geométricas tales como el ángulo y dirección del agitador y/o la geometría del deflector.

- Las ecuaciones matemáticas que relacionan los índices hidráulicos con las características geométricas de AnoxAn pueden emplearse como punto de partida para el diseño de nuevas configuraciones a escala industrial. Sin embargo, debe profundizarse en la investigación acerca de la validación y aplicabilidad de las expresiones desarrolladas en una escala mayor, ya que el propio proceso de escalado no es directo.

Evaluación de la influencia del comportamiento hidrodinámico en la eficiencia biológica de AnoxAn

- Se ha empleado el modelo de desnitrificación introducido en la herramienta numérica CFD con el objetivo de evaluar la influencia del comportamiento hidrodinámico en la eficiencia biológica de AnoxAn. Dicho modelo se aplica a dos configuraciones diferentes del reactor, una con esbeltez alta y otra con esbeltez baja, y, además, se han realizado simulaciones para dos concentraciones de biomasa diferentes (1 000 mg/L y 2 500 mg/L). Los resultados obtenidos evidencian la correlación entre la hidrodinámica y la eficiencia biológica observada en la revisión del estado del arte.

- La configuración con mayor esbeltez muestra un mayor valor de GHE y menor concentración de nitrato en el efluente (tres veces menor que la configuración con menor esbeltez), dando lugar a un comportamiento biológico más deseado. Por otra parte, tal y como se ha observado para la concentración de trazador en el estudio de optimización hidrodinámica, la configuración con menor esbeltez muestra una mejor eficiencia de mezcla (menor heterogeneidad de concentración de nitrato). Además, comparado con lo observado sin actividad biológica, el efecto de la cinética de desnitrificación da lugar a una mayor heterogeneidad de concentración en el reactor.

- El análisis del flujo y de los campos de velocidades muestran que los flujos preferenciales están situados cerca de las paredes del reactor, facilitando el transporte de masa a través de ellas. Como consecuencia, comparado con la parte central del reactor, se observa un mayor transporte de trazador (hidrodinámico) y de nitrato (biológico) en estas zonas. Tal y como también se observó en el estudio de optimización, se reporta una mayor separación hidráulica en la configuración más esbelta, dando lugar a una concentración despreciable de nitratos en la zona anaerobia. Esto último hace que las configuraciones con mayor esbeltez sean más resilientes.

A continuación, se concretan las necesidades de investigación futuras identificadas en este estudio:

- Es importante subrayar que el modelo desarrollado no incluye el efecto de la fase sólida (biomasa) en la densidad de la fase líquida. Por lo tanto, ni el comportamiento hidrodinámico, ni la eficiencia biológica simuladas son completamente realistas, pero ayudan a caracterizar, entender y profundizar en el funcionamiento de AnoxAn. Del mismo modo que se ha observado que la cinética de desnitrificación incrementa las heterogeneidades en los campos de concentración, se espera una mayor concentración de fase sólida (y por lo tanto menor concentración de nitrato) en las zonas muertas, y menos biomasa (y mayor concentración de nitrato) en las zonas de flujo preferencial. En cualquier caso, en el siguiente paso de la presente investigación, se debería tomar la herramienta numérica desarrollada en esta tesis como base para introducir la influencia de la biomasa en el código. Además, las siguientes fases de desarrollo deberían incluir modelos biológicos más complejos, ampliando el utilizado al ASM1 y considerando la incorporación de eliminación de fósforo para evaluar el proceso completo de EBN (ASM2d). Todo este nuevo proceso de modelización deberá incluir nuevas campañas experimentales de validación.

En resumen, este trabajo de investigación ha evidenciado que las configuraciones de AnoxAn con mayor esbeltez son preferibles a aquellas menos esbeltas, ya que muestran una mayor eficiencia hidrodinámica, y, por tanto, biológica. Además, para una misma capacidad de tratamiento teórica (mismo volumen), las configuraciones con una mayor esbeltez presentan una necesidad menor de superficie en planta. Sin embargo, estas configuraciones dan lugar a reactores con una geometría inusual y menos estudiada en la bibliografía, ya que la implementación de varias unidades implicaría mayores ratios largo/ancho. Este aspecto podría suponer una desventaja a la hora de diseñar o proyectar la implementación de nuevos reactores, constituyendo un hándicap cuando se deseen reutilizar reactores existentes en aquellos casos en los que la ampliación de plantas de tratamiento es necesaria. Dependiendo de la disponibilidad de terreno, o de las limitaciones y requerimientos constructivos, la esbeltez (y por lo tanto la separación hidráulica) del reactor puede ser reducida en función de la carga de nitrógeno afluente de diseño.

Chapter 9

References

Aagaard-Hansen, J., Chaignat, C. L. (2010). Neglected tropical diseases: Equity and social determinants. Geneva, Switzerland, World Health Organization. https://bit.ly/3d9LBMm

Al-Samarraee, M., Chan, A. (2009). Large-eddy simulation of particle sedimentation in a longitudinal sedimentation basin of water treatment plant. Part 2: The effects of baffles. Chem. Eng. J. 152, 315-321. https://doi.org/10.1016/j.cej.2009.01.052

Andersson, B., Andersson, R., Hakansson, L., Mortensen, M., Sudiyo, R., Van Wachem, B. (2012). Computational Fluid Dynamics for Engineers. Cambridge University Press, ISBN 978 1-107-01895-2.

Angeloudis, A., Stoesser, T., Falconer, R.A. (2014). Predicting the disinfection efficiency range in chlorine contact tanks through a CFD based approach. Water Res. 60, 118-129. https://doi.org/10.1016/j.watres.2014.04.037

Ahn, K.H., Song, K.G., Cho, E., Cho, J., Yun, H., Lee, S., Kim, J. (2003). Enhanced biological phosphorus and nitrogen removal using a sequencing anoxic/anaerobic membrane bioreactor (SAM) process. Desalination 157(1-3), 345-352. https://doi.org/10.1016/S0011-9164(03)00415-6

Aissa, M.H. (2017). GPU-accelerated CFD simulations for turbomachinery design optimization. Ph.D Diss, TU Delft, Netherlands.

Arnaldos, M., Rehman, U., Naessens, W., Amerlick, Y., Nopens, I. (2018). Understanding the effects of bulk mixing on the determination of the affinity index: Consequences for process operation and design. Water Sci. Technol. 77(3), 576-588. https://doi.org/10.2166/wst.2017.550

Ayesa, E., De La Sota, A., Grau, P., Sagarna, J.M., Salterain, A., Suescun, J. (2006). Supervisory control strategies for the new WWTP of Galindo-Bilbao: The long run from the conceptual design to the full-scale experimental validation. Water. Sci. Technol. 53, 193-201. https://doi.org/10.2166/wst.2006.124

Bai, H., Stephenson, A., Jimenez, J., Jewell, D., Gillis, P. (2008). Modeling flow and residence time distribution in an industrial-scale reactor with a plunging jet inlet and optional agitation. Chem. Eng. Res. Des. Vol 86, pp 1462-1476. https://doi.org/10.1016/j.cherd.2008.08.012

Behzadian, F., Yerushalmi, L., Alimahmoodi, M., Mulligan, C.N. (2012). Hydrodynamic characteristics and overall volumetric oxygen transfer coefficient of a new multi-environment bioreactor. Bioprocess Biosyst. Eng. 36, 1043–1052. https://doi.org/10.1007/s00449-012-0857-3

Blanco-Aguilera, R., Lara, J.L., Barajas, G., Tejero. I., Díez-Montero, R. (2020a). CFD simulation of a novel anaerobic-anoxic reactor for biological nutrient removal: Model construction, validation and hydrodynamic analysis based on OpenFOAM®. Chem. Eng. Sci., 215. https://doi.org/10.1016/j.ces.2019.115390

Blanco-Aguilera, R., Lara, J.L., Barajas, G., Tejero. I., Díez-Montero, R. (2020b). Hydrodynamic optimization of multi-environment reactors for biological nutrient removal: A methodology combining computational fluid dynamics and dimensionless indexes. Chem. Eng. Sci., 224. https://doi.org/10.1016/j.ces.2020.115766

BP Statistical Review of World Energy, 68th edition. (2019). https://on.bp.com/392pap6

Brannock, M. (2003). Computational Fluid Dynamics Tools for the design of Mixed Anoxic Wastewater Treatment Vessels. Ph.D Diss, University of Queensland, Australia.

Brannock, M., Wang, Y., Leslie, G. (2010a). Mixing characterisation of full-scale membrane bioreactors: CFD modelling with experimental validation. Water Res., Vol. 44, pp 3181-3191. https://doi.org/10.1016/j.watres.2010.02.029

Brannock, M., Leslie, G., Wang, Y., Buetehorn, S. (2010b). Optimising mixing and nutrient removal in membrane bioreactors: CFD modelling and experimental validation. Desalination 250 (2), 815-818. https://doi.org/10.1016/j.desal.2008.11.048

Bridgeman, J. (2012). Computational Fluid Dynamics modelling of sewage sludge mixing in anaerobic digester. Adv. Eng. Software, Vol 44, pp 54-62. https://doi.org/10.1016/j.advengsoft.2011.05.037

Buckingham, E. (1914). On physically similar systems; Illustrations of the use of dimensional equations. Physical Review 4, 345-376. https://doi.org/10.1103/PhysRev.4.345

Burcharth, H., Andersen, O. (1995). On the one-dimensional steady and unsteady porous flow equations. Coastal Eng., 24(3–4), 233–257. https://doi.org/10.1016/0378-3839(94)00025-S

Calder, R.S.D., Yerushalmi, L., Li, S.S. (2013). Computational Fluid Dynamics model of BioCAST multienvironment air-lift bioreactor. J. Environ. Eng. 139, 849-863. https://doi.org/10.1061/(ASCE)EE.1943-7870.0000678

Castrillo, M., Díez-Montero, R., Esteban-Garcia, A.L., Tejero, I. (2019). Mass transfer enhancement and improved nitrification in MABR through specific membrane configuration. Water Res. 152, 1-11. https://doi.org/10.1016/j.watres.2019.01.001

Celik, I.B., Ghia, U., Roache, P.J., Freitas, C.J., Coleman, H., Raad, P.E. (2008). Procedure for estimation and reporting of uncertainty due to discretization in CFD applications. J. Fluids Eng., Vol 130(7), 078001 1-4- https://doi.org/10.1115/1.2960953

Chang, T.J., Chang, Y.S., Lee, W.T., Shih, S.S. (2016). Flow uniformity and hydraulic efficiency improvement of deep-water constructed wetlands. Ecol. Eng. 92, 28-36. http://dx.doi.org/10.1016/j.ecoleng.2016.03.028

Cheng, C., Ribarova, I. (1999). Activated sludge system modelling and simulations for improving the effluent water quality. Water. Sci. Technol. 39, 93-98. https://doi.org/10.1016/S0273-1223(99)00190-0

Choi, B., Wan, B., Philyaw, S., Dhanasekharan, K., Ring, T. (2004). Residence Time Distributions in a Stirrer Tank: Comparison of CFD Predictions with Experiment. Ind. Eng. Chem. Res., Vol 43, pp 6548-6556. https://doi.org/10.1021/ie0308240

Climent, J., Basiero, L., Martínez-Cuenca, R., Berlanga, J.G., Julián-López, B., Chiva, S. (2018). Biological reactor retrofitting using CFD-ASM modelling. Chem. Eng. J. 348, 1-14. https://doi.org/10.1016/j.cej.2018.04.058

Climent, J., Martinez-Cuenca, R., Carratalá, P., González-Ortega, M.J., Abellán, M., Monrós, G., Chiva, S. (2019). A comprehensive hydrodynamic analysis of a full-scale oxidation ditch using Population Balance Modelling in CFD simulation. Chem. Eng. J., Vol 374, pp 760-775. https://doi.org/10.1016/j.cej.2019.05.195

Corcoran, E., Nellemann, C., Baker, E., Bos, R., Osborn, D., Savelli, H. (2010). Sick Water? The Central Role of Wastewater Management in Sustainable Development. United Nations Environment Programme. https://www.grida.no/publications/218

Couper, J.R., Pennwy, W.R., Fair, J.R., Wallas, S.M. (2010). Chemical Process Equipment – Selection and Design (Revised 2nd Edition). Burlington MA, ISBN 978-0-12-372506-6.

Dapelo, D., Bridgeman, J. (2018). Assessment of mixing quality in full-scale, biogas-mixed anaerobic digestion using CFD. Bioresour. Technol., Vol 265, pp 480-489. https://doi.org/10.1016/j.biortech.2018.06.036

De Clercq, B. (2003). Fluid Dynamics of Settling Tanks: Development of experiments and rheological, settling and scraper submodels. Ph.D Diss, Universiteit Gent, Belgium.

Demirel, E., Aral, M.M. (2016). Unified analysis of multi-chamber contact tanks and mixing efficiency evaluation based on vorticity fields. Part II: Transport analysis. Water, 8(11), 537. https://doi.org/10.3390/w8110537

Demirel, E., Aral, M.M. (2018). Performance of efficiency indexes for contact tanks. J. Environ. Eng. 144(9). https://doi.org/10.1061/(ASCE)EE.1943-7870.0001431

Díez-Montero, R. (2015) AnoxAn: a novel anaerobic-anoxic reactor for biological nutrient removal from istewater. Ph.D. Diss, University of Cantabria, Santander.

Díez-Montero, R., De Florio, L., González-Viar, M., Volcke, E.I.P., Tejero, I. (2015). Feasibility of hydraulic separation in a novel anaerobic-anoxic upflow reactor for biological nuetrient removal. Bioprocess Biosyst. Eng. 38, 93-103. https://doi.org/10.1007/s00449-014-1247-9

Díez-Montero, R., De Florio, L., González-Viar, M., Herrero, M., Tejero, I. (2016). Performance evaluation of a novel anaerobic–anoxic sludge blanket reactor for biological nutrient removal treating municipal wastewater. Bioresour. Technol. 209, 195-204. https://doi.org/10.1016/j.biortech.2016.02.084

Díez-Montero, R., Castrillo, M., Casao, M., Tejero, I. (2019). Model-based evaluation of a trickling filter facility upgrade to biological nutrient removal. Sci. Total. Environ. 661, 187-195. https://doi.org/10.1016/j.scitotenv.2019.01.136

Draper, N.R., Smith, H. (1998). Applied Regression Analysis. Wiley Series in Probability and Statistics. ISBN 9780471170822.

DWA, (2000). Standard ATV-DVWK-A 131E: Dimensioning of Single-Stage Activated Sludge Plants. DWA German Association for Water, Wastewater and Waste, Hennef, Germany. ISBN 978-3-935669-96-2.

Ecologistas en Acción. (2019). Caminar sobre el abismo de los límites. Políticas ante la crisis ecológica, social y económica (Walk over the abyss of limits. Policies for the ecological, social and economic crisis). Ecologistas en Acción y La Transicionera, ISBN 978-84-947850-0-9 (in Spanish).

European Union. (1991). Council Directive 91/271/EEC of 21 May 1991 concerning urban wastewater treatment. Official Journal L 135, 30/05/1991, 0040-0052.

European Union. (2000). Directive 2000/60/EC of the European Parliament and of the Council of 23 October 2000 establishing a framework for Community action in the field of water policy. Official Journal L 327, 22/12/2000, 0001-0073.

Fang, F., Bing-Jie, N., Wen-Wei, L., Guo-Ping, S., Han-Qing, Yu. (2011). A simulation-based integrated approach to optimize the biological nutrient removal process in a full-scale wastewater treatment plant. Chem. Eng. J., 174, 635 – 643. https://doi.org/10.1016/j.cej.2011.09.079

Fernández, J.M. (2012). Técnicas numéricas en ingeniería de fluidos: Introducción a la dinámica de fluidos computacional (CFD) por el método de volúmenes finitos. (Numerical techniques in fluid engineering: Introduction to computational fluid dynamics (CFD) based on finite volumes method). Editorial Reverte, ISBN 978-84-291-2602-0 (in Spanish).

Food and Agriculture Organization of United Nations. (2011). The state of the world's land and water resources for food and agriculture. Managing systems at risk. Earthscan. ISBN 978-1-84971-326-9

Food and Agriculture Organization of United Nations. (2018). Water. Will there be enough for everyone and everything? The state of planet series.

Gualteri, C. (2008). Discussion on "Performance assessment of hydraulic efficiency indexes" by Edmison Costa Teixeira and Renato do Nascimento Siqueira. J. Environ. Eng. 136(9), 1006-1007. https://doi.org/10.1061/(ASCE)EE.1943-7870.0000088

Gualteri, C. (2009). Analysis of flow and concentration fields in a baffled circular storage tank. 33rd IAHR Congress: Water Engineering for a Sustainable Environment. ISBN 978-94-90365-01-1.

Gómez, C. (2010). Desarrollo y modelización de un sistema biopelícula para la eliminación de materia orgánica y nitrógeno (Development and modelling of a biofilm system for organic matter and nitrogen removal). Ph.D. diss., University of Cantabria, Santander (in Spanish)

Henze, M., Gujer, W., Mino, T. (2000) Activated Sludge Models ASM1, ASM2, ASM2d and ASM3. IWA Publishing, London, UK.

Hernández, A. (2015). Depuración y desinfección de aguas residuales, 6ª edición. (Wastewater treatment and disinfection, 6th edition). Colegio de Ingenieros de Caminos, Canales y Puertos. ISBN 978-84-380-0495-1 (in Spanish).

Holzmann, T. (2019). Mathematics, numerics, derivations and OpenFOAM®. Holzmann CFD, Release 7.0. DOI: 10.13140/RG.2.2.27193.36960.

Hu, B., Wheatley, A., Ishtchenko, V., Huddersman, K. (2012). Performance linked to residence time distribution by a novel woolbased bioreactor for tertiary sewage treatment. Appl. Microbiol. Biot. 94, 817–828. https://doi.org/10.1007/s00253-011-3659-7

Intergovernmental Panel on Climate Change. (2019). An IPCC special report on climate change, desertification, land degradation, sustainable land management, food security, and greenhouse gas fluxes in terrestrial ecosystems. https://www.ipcc.ch/srccl/

Intergovernmental Science-Policy Platform on Biodiversity and Ecosystem Services. (2019). Global assessment report on biodiversity and ecosystem services. https://ipbes.net/news/Media-Release-Global-Assessment

International Energy Agency. (2010). World Energy Outlook. https://www.iea.org/reports/world-energy-outlook-2010

Issa, R.I. (1982). Solution of the Implicitly Discretized Fluid Flow Equations by Operator-Splitting. J. Comput. Phys., 62, 40-65.

Jasak, H. (1996). Error analysis and estimation for the finite volume method with applications to fluid flows. PhD Diss., Imperial College of Science, Technology and Medicine, United Kingdom.

Jasak, H., Vukcevic, V., Gatin, I., Lalovic, I. (2019). CFD validation and grid sensitivity studies of full scale ship self propulsion, Int. J. Nav. Archit. Ocean Eng., 11, 33-43 https://doi.org/10.1016/j.ijnaoe.2017.12.004

Jeyanayagam, S.S. (2007). So, you want to remove phosphorus? Part 1: Enhanced Biological Phosphorus Removal. Buckeye Bull. 4(80), 22-29.

Ji, JY., Zheng, K., Xing, Y.J., Zheng, P. (2012). Hydraulic characteristics and their effects on working performance of compartmentalized anaerobic reactor. Bioresour. Technol. 116, 47–52 https://doi.org/10.1016/j.biortech.2012.04.026

Klusener, P.A.A., Jonkers,G., During, F., Hollander, E.D., Schellekens, C.J., Ploemen, I.H.J., Othman, A., Bos, A.N.R. (2007). Horizontal cross-flow bubble column reactors: CFD and validation by plant scale tracer experiments. Chem.Eng.Sci. 62(18–20), 5495–5502. https://doi.org/10.1016/j.ces.2007.03.044

Kwon, J.C., Park, H.S., An, J.Y., Shim, K.B., Kim, Y.H., Shin, H.S. (2005). Biological nutrient removal in simple dual sludge system with an UMBR (upflow multi-layer bio reactor) and aerobic biofilm reactor. Water. Sci. Technol. 52(10-11), 443-451. https://doi.org/10.2166/wst.2005.0722

Latrach, L., Ouazzani, N., Hejjaj, A., Zouhir, F., Mahi, M., Masunaga, T., Mandi, L. (2018). Optimization of hydraulic efficiency and wastewater treatment performances using a new design of vertical flow Multi-Soil-Layering (MSL) technology. Ecol. Eng. 117, 140-152. https://doi.org/10.1016/j.ecoleng.2018.04.003

Launder, B.E., Spalding, D.B., (1972). Lectures in Mathematical Models of Turbulence. Academic Press, London, England.

Levenspiel, O. (1999). Chemical Reaction Engineering. 3rd Edition. John Wiley & Sons, New York, 54.

Le Moullec, Y., Potier, O., Gentric, C., Leclerc, J.P. (2008). Flow field and residence time distribution simulation of a cross-flow gas-liquid wastewater treatment reactor using CFD. Chem. Eng. Sci., 63(9), 2436-2449. https://doi.org/10.1016/j.ces.2008.01.029

Liu, M., Yang, M., Chen, M., Yu, D., Zheng, J., Chang, J., Wang, X., Ji, C., Wei, Y. (2018). Numerical optimization of membrane module design and operation for a full-scale MBR by computational fluid dynamics. Bioresour. Technol. 269, 300-308. https://doi.org/10.1016/j.biortech.2018.08.089

Lopez, I., Borzacconi, L. (2010). UASB reactor hydrodynamics: residence time distribution and proposed modelling tools. Environ. Technol., 31:6, 591-600. https://doi.org/10.1080/09593331003646638

Losada, I.J., Lara, J.L., Del Jesus, M. (2016). Modeling the interaction of water waves with porous coastal structures. J.Waterway, Port, Coastal, Ocean Eng., Vol 142(6). https://doi.org/10.1061/(ASCE)WW.1943-5460.0000361

Makinia, J., Rosenwinkel, K.H., Spering, V. (2006). Comparison of Two Model Concepts for Simulation of Nitrogen Removal at a Full-Scale Biological Nutrient Removal Pilot Plant. J. Environ. Eng., Vol. 132, No. 4, 476-487. http://doi.org/10.1061/(ASCE)0733-9372(2006)132:4(476)

Martin-Dominguez, A., Tzatchkov, V.G., Martin-Dominguez, I.R., Lawler, D.F. (2005). An enhanced tanks-in-series model for interpretation of tracer tests. J. Water. Supply. Res. T. 54, 435-448. https://doi.org/10.2166/aqua.2005.0041

Martin, K.J., Nerenberg, R. (2012). The membrane biofilm reactor (MBfR) for water and istewater treatment: principles, applications, and recent developments. Bioresour. Technol. 122, 83–94. https://doi.org/10.1016/j.biortech.2012.02.110

Menter, F.R. (1994). Two-equations eddy-viscosity turbulence models for engineering applications. AIAA Journal, 32, 1598-1605. https://doi.org/10.2514/3.12149

Michalopoulos, I., Kamperidis, T., Seintis, G., Pashos, G., Lytras, C., Papadopulou, K., Boudouvis, A.G., Lyberatos, G. (2018). Experimental and numerical assessment of the hydraulic behaviour of a pilot-scale Periodic Anaerobic Baffled Reactor (PABR). Comp. Chem. Eng. 111, 278-287. https://doi.org/10.1016/j.compchemeng.2018.01.014

Mihovilovic, B. (2010). Optimización del proceso BLAS® en alta carga: Modelización del atascamiento (Optimization of BLAS® process for high loads: Modelling of binding). Ph.D Diss, University of Cantabria, Santander.

Narayanan, B., Johnhon, B., Baur, R., Mengelkoch, M. (2006). Critical role of aerobic uptake in biological phosphorus removal. Proceedings of the 79th Annual Water Environment Federation Technical Exposition and Conference; Dallas, Texas.

Nemade, P.D., Dutta, S.M., Shankar, H.S. (2010). Residence time distribution and oxygen transfer in a novel constructed soil filter. J Chem. Technol. Biot. 85, 77–84. https://doi.org/10.1002/jctb.2269

Olivet, D., Valls, J., Gordillo, M.A., Freixo, A., Sánchez, A. (2005). Application of residence time distribution technique to the study of the hydrodynamic behaviour of a full-scale wastewater treatment plant plug-flow bioreactor. J. Chem. Technol. Biotechnol. 80, 425–432. https://doi.org/10.1002/jctb.1201

Panepinto, D., Fiore, S., Zappone, M., Giussepe, G., Meucci, L. (2016). Evaluation of the energy efficiency of a large wastewater treatment plant in Italy. Appl. Energy, 161, 404-411. https://doi.org/10.1016/j.apenergy.2015.10.027

Patankar, S.V., Spalding, D.B. (1972). A calculation procedure for head, mass and momentum transfer in three-dimensional parabolic flows. Int. J. Heat Mass Transfer, 15, 1787-1806.

Pereira, J., Karpinska, A., Gomes, P., Martins, A., Dias, M.&Santos, R. (2011). Activated Sludge Models coupled to CFD simulations In: Single and two-Phase Flows on Chemical and Biomedical Engineering. Bentham Science Publishers, Dubai, U.A.E.

Persson, J., Somes, N.L.G, Wong, T.H.F. (1999). Hydraulics efficiency of constructed wetlands and ponds. Water Sci. Technol. 40, 291–300. http://dx.doi.org/10.1016/S0273-1223(99)00448-5

Plascencia-Jatomea, R., Almazán-Ruiz, F.J., Gómez J., Rivero, E.P., Monroy, O., Gonzalez, I. (2015). Hydrodynamic study of a novel membrane aerated bioflim reactor (MABR): tracer experiments and CFD simulation. Chem. Eng. Sci. 138, 324-332. https://doi.org/10.1016/j.ces.2015.08.004

Pons, M.N., Potier, O., Roche, N., Colin, F., Prost, C. (1993). Simulation of municipal wastewater treatment plants by activated sludge. Comput. Chem. Eng. 17, 227-232. https://doi.org/10.1016/0098-1354(93)80234-E

Qi, W., Guo, Y., Xue, M., Li,Y. (2013). Hydraulic analysis of an upflow sand filter: tracer experiments, mathematical model and CFD computation. Chem. Eng. Sci. 104, 460–472. https://doi.org/10.1016/j.ces.2013.09.035

Qi, W.K., Hojo, T., Li, Y.Y. (2013). Hydraulic characteristics simulation of an innovative self-agitation anaerobic baffled reactor (SA-ABR). Bioresour. Technol., Vol. 136, pp 94-101. https://doi.org/10.1016/j.biortech.2013.02.033

Rehman, U. (2016). Next generation bioreactor models for wastewater treatment systems by means of detailed combined modelling of mixing and biokinetics. Ph.D Diss, BioMath, Ghent University, Belgium.

Renade, V.V., (2002). Computational Flow Modeling for Chemical Reactor Engineering. (Academic Press, New York).

Rengers, E.E., Barbosa, J., Loureiro, P., Gerson, J. (2016). Hydraulic performance of a modified constructed wetland system through a CFD based approach. J. Hydro-Environ. Res. 12, 91-104. https://doi.org/10.1016/j.jher.2016.04.002

Roche, N. (1989). Influence de l'hydrodynamique des bassins d'aerations sur la decantabilite desboues activees. Ph.D Diss, INPL, Nancy, France.

Roeleveld, P.J., Van Loosdrecht, M.C. (2002). Experience with guidelines for wastewater characterisation in The Netherlands. Water. Sci. Technol. 45, 77-87. https://doi.org/10.2166/wst.2002.0095

Samstag, R.W., Ducoste, J.J., Griborio, A., Nopens, I., Batstone, D.J., Wicks, J.D., Saunders, S., Wicklein, E.A., Kenny, G., Laurent, J. (2016). CFD for wastewater treatment: an overview. Water Sci. Technol. 73(3), 549-563. https://doi.org/10.2166/wst.2016.249

Sarathai, Y., Koottatep, T., Morel, A. (2010). Hydraulic characteristics of an anaerobic baffled reactor as onsite istewater treatment system. J. Environ. Sci. 22(9), 1319–1326. https://doi.org/10.1016/S1001-0742(09)60257-6

Seb, B. (2017). Numerical characterisation of a ship propeller. Master Thesis, University of Zagreb.

Shih, T.H., Liou, W.W., Shabbir, A., Yang, Z., Zhu, J. (1995). A new k-e eddy-viscosity model for high Reynolds number turbulent flows. Model development and validation. Comput. Fluids, 24(3), 227-238.

Song, K.G., Cho, J., Ahn, K.H. (2009). Effects of internal recycling time mode and hydraulic retention time on biological nitrogen and phosphorus removal in a sequencing anoxic/anaerobic membrane bioreactor process. Bioprocess. Biosyst. Eng. 32. 135-142. https://doi.org/10.1007/s00449-008-0232-6

Song, K.G., Cho, J., Cho, K.W., Kim, S.D., Ahn, K.H. (2010). Characteristics of simultaneous nitrogen and phosphorus removal in a pilot-scale sequencing anoxic/anaerobic membrane bioreactor at various conditions. Desalination, 250(2), 801-804. https://doi.org/10.1016/j.desal.2008.11.045

Stensel, D. (1991). Principles of Biological Phosphorus Removal. Phosphorus and Nitrogen Removal for Municipal Wastewater-Principles and Practice, Sedlak, R., Ed.; Lewis Publishers: Boca Raton, Florida.

Tang, D., Jess, A., Ren, X., Bluemich, B., Stapf, S. (2004). Axial dispersion and wall effects in narrow fixed bed reactors: a comparative study based on RTD and NMR measurements. Chem. Eng. Technol. 27(8), 866-873. https://doi.org/10.1002/ceat.200402076

Tchobanoglous, G., Stensel, H.D., Tsuchihashi, R., Burton, F., Abu-Orf, Bowden, G., Pfrang, W. (2014). Wastewater Engineering. Treatment and resource recovery. Volume I, 5th edition. Metcalf & Eddy, McGraw-Hill, New York. ISBN 978-1-259-01079-8.

Teixeira, E.D., Siqueira, R.N. (2008). Performance assessment of hydraulic efficiency indexes. J. Environ. Eng. 134, 851-859. https://doi.org/10.1061/(ASCE)0733-9372(2008)134:10(851)

Tejero, I., Díez, R., Esteban, A.L., Lobo, A., Temprano, J., Rodríguez, L. (2010). Reactor biológico anóxico-anaerobio para la eliminación de nutrientes de aguas residuales. Spanish Patent ES2338979B2 (in Spanish).

Tejero, I., Eguía, E. (1991). Proceso de tratamiento biológico de aguas residuales basado en biopelícula desarrollada sobre un soporte permeable a gases. Spanish Patent ES2038556 (in Spanish).

Terashima, M., Goel, R., Komatsu, K., Yasui, H., Takahashi, H., Li, Y.Y., Noike, T. (2009). CFD simulation of mixing in anaerobic digesters. Bioresour. Technol., Vol 100, 2228-2233. https://doi.org/10.1016/j.biortech.2008.07.069

Tu., J., Yeoh, G.H., Liu, C. (2013). Computational Fluid Dynamics. A practical approach. Elsevier Ltd, 2nd edition. ISBN 978-0-08-098243-4.

Trad, Z., Vial, C., Fontaine, J.P., Larroche, C. (2015). Modelling of hydrodynamics and mixing in a submerged membrane bioreactor. Chem. Eng. J. 282, 77-90. https://doi.org/10.1016/j.cej.2015.04.119

United States Environmental Protection Agency (USEPA). (1991). Guidance manual for compliance with the filtration and disinfection requirements for public water system using surface water. Washington, DC: USEPA.

United States Environmental Protection Agency (USEPA). (2001). Disinfection profiling and benchmarking guidance manual: Appendix A. Rep. No. EPA 816-R-03-004. Washington, DC: USEPA.

United Nations Environment Programme. (2015). Economic Valuation of Wastewater - The Cost of Action and the Cost of No Action. ISBN 978-92-807-3474-4

United Nations. (2019). Sustainable Development Goals. https://sustainabledevelopment.un.org/

United Nations Educational, Scientific and Cultural Organization. (2017). The United Nations World Water Development Report 2017. Wastewater, the untapped resource. Paris, UNESCO, ISBN 978-92-3-100201-4

Valero, A., Valero, A. (2014). Thanatia. The destiny of the Earth's mineral resources. A thermodynamic Cradel-to-Cradel assessment. World Scientific Publishing Company, ISBN 978-98-142739-3-0.

Water Environment Federation. (2011). WEF Manual of Practice Nº 34: Nutrient Removal. WEF Press. ISBN 978-0-07-173709-8.

Water Environmental Federation. (2014). WEF Manual of Practice Nº31: Wastewater Treatment Process Modelling. WEF Press, 2nd edition. ISBN 978-0-07-179842-6

Wei. P., Mudde, R.F., Uittewaal, W., Spanjers, H., van Lier J.B., de Kreuk, M. (2019). Characterising the two-phase flow and mixing performance in a gas-mixed anaerobic digester: Importance for scale-up applications. Water Res. 149, 86-97. https://doi.org/10.1016/j.watres.2018.10.077

Weller, H.G., Tabor, G., Jasak, H., Fureby, C. (1998). A tensorial approach to computational continuum mechanics using object oriented techniques. Comput. Phys. 12, 620-631. https://doi.org/10.1063/1.168744

Wicklein, E., Batstone, D., Ducoste, J., Laurent, J., Griborio, A., Wicks, J., Saunders, S., Samstag, R., Potier, O., Nopens, I. (2015). Good modelling practice in applying computational fluid dynamics for WWTP modelling. Water Sci. Technol. 73(5), 969-982. https://doi.org/10.2166/wst.2015.565

Wilcox, D.C. (1988). Turbulence modelling for CFD. DCW Industries.

World Health Organization. (2014). Preventing Diarrhoea through Better Water, Sanitation and Hygiene: Exposures and Impacts in Low- and Middle-income Countries. https://bit.ly/2IYrEdO

Wu, B. (2009). CFD Analysis of mechanical mixing in anaerobic digesters. Structures & Environment Division of ASABE 52 (4), 1371–1382. https://doi.org/10.13031/2013.27786

Yakhot, V., Orszag, S.A., Thangam, S., Gatski, T.B., Speciale, C.G. (1992). Development of turbulence models for shear flows by a double expansion technique. Phys. Fluids, 4, 1510-1520. https://doi.org/10.1063/1.858424

Yan, X., Xiao, K., Liang, S., Lei, T., Liang, P., Xue, T., Yu, K., Guan, J., Huang, X. (2015). Hydraulic optimization of membrane bioreactor via baffle modification using computational fluid dynamics. Bioresour. Technol. 175, 633-637. https://doi.org/10.1016/j.biortech.2014.10.133

Yan, X., Wu, Q., Sun, J., Liang, P., Zhang, X., Xiao, K., Huang, X. (2016). Hydrodynamic optimization of membrane bioreactor by horizontal geometry modification using computational fluid dynamics. Biresour. Technol. 200, 328-334. https://doi.org/10.1016/j.biortech.2015.10.050

Yerushalmi, L., Ogilvie, M.J. (2010). Integrated multi-zone wastewater treatment system and method. US Patent 7820047.

Yerushalmi, L., Alimahmoodi, M., Mulligan, C.N. (2011). Performance evaluation of the BioCAST technology: a new multi-zone wastewater treatment system. Water. Sci. Technol. 64(10), 1967-1972. https://doi.org/10.2166/wst.2011.776

Yerushalmi, L., Alimahmoodi, M., Behzadian, F., Mulligan, C.N. (2013). Mixing characteristics and liquid circulation in a new multi-environment bioreactor. Bioprocess Biosyst. Eng. 36, 1339–1352. https://doi.org/10.1007/s00449-012-0836-8

Zeng, Y., Mu, S.J., Lou, S.J., Tartakovsky, B., Guiot, S.R., Wu, P. (2005). Hydraulic modelling and axial dispersion analysis of UASB reactor. Biochem. Eng. J. 25(2), 113–123. https://doi.org/10.1016/j.bej.2005.04.024

Zhang, J., Tejada-Martinez, A.E., Zhang Q. (2016). Rapid analysis of disinfection efficiency through computational fluid dynamics. J. Am. Water Works Assoc. 2018, E50-E59. https://doi.org/10.5942/jawwa.2016.108.0005

Zittel, W., Zerhusen, J., Zerta, M., Nikolaus, A. (2013). Fossil and Nuclear Fuels – the Supply Outlook. Energy Watch Group. https://bit.ly/2Unvqmm

Zlokarnik, M. (2002). Scale-up in Chemical Engineering. Wiley-VCH, ISBN 3-527-30266-2.

Annex A

Hydrodynamic validation with AMI and Overset grids

In this annex, the hydrodynamic validation of the AnoxAn reactor is carried out based on Arbitrary Mesh Interface (AMI) and Overset approaches for the impeller, both specially developed to simulate rotating physics.

The **AMI approach** (see Fig. A.1a-b) enables simulation for disconnected and adjacent mesh domains. Its main property is to couple the condition between a pair of patches with the same outer bounds but with different inner geometry or properties. In short, a rotating mesh (depicted in blue in Fig. A.1a-b) and a static mesh (depicted in black in Fig. A.1a-b) are defined independently, and only the domain of the first one is moving during the simulation.

The **Overset approach**, (see Fig. A.1c-d) is a generic implementation of overset meshes. In this case, a composite domain is created by means of cell-to-cell mapping between disconnected mesh regions. Within this approach, a rotating mesh (named M1 in Fig. A.1c-d) and a background mesh (named M2 in Fig. A.1c-d) are defined and, unlike the AMI, both meshes are overlapped (i.e. not defined independently) during the simulation.

To reduce the computational cost of the simulations, a simplified impeller (represented in purple in Fig. A.1) with six parallelepipedal blades and the same diameter of the original one is defined.
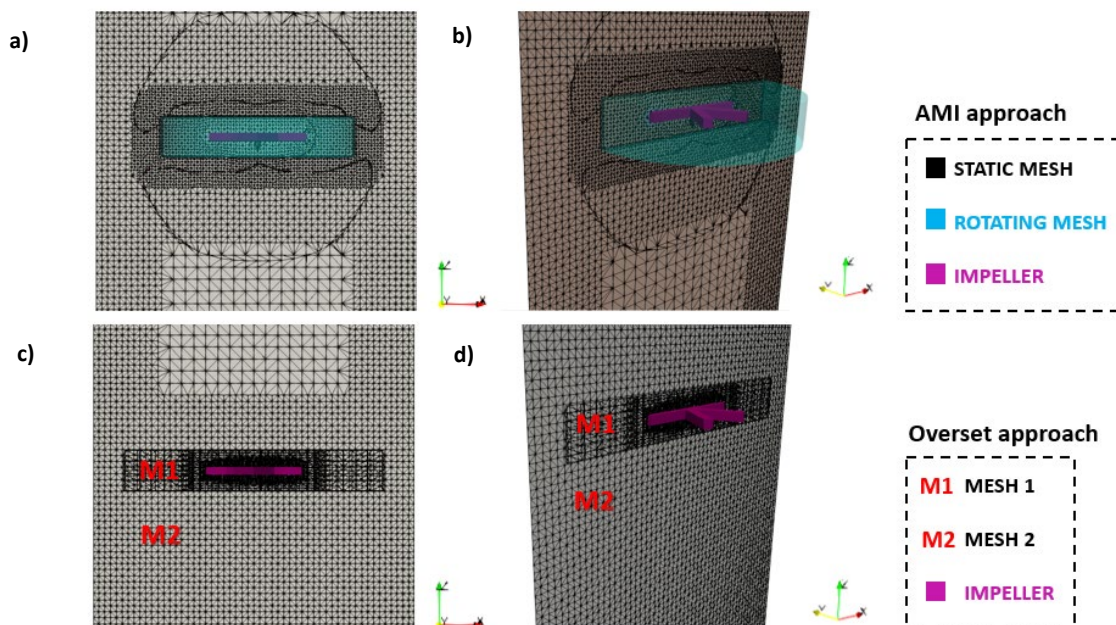
Figure A.1. (a) XZ plane for AMI approach, (b) perspective for AMI approach, (c) XZ plane for Overset approach and (d) perspective for Overset approach.

In Fig. A.2 results for the step RTD$_3$ tracer test (see Chapter 5) are shown for the three different approaches, i.e. AMI and Overset. As stated in the document, successful validation results are achieved for AMI and Overset approaches for the first-time steps, but they led to an excessive computational cost.
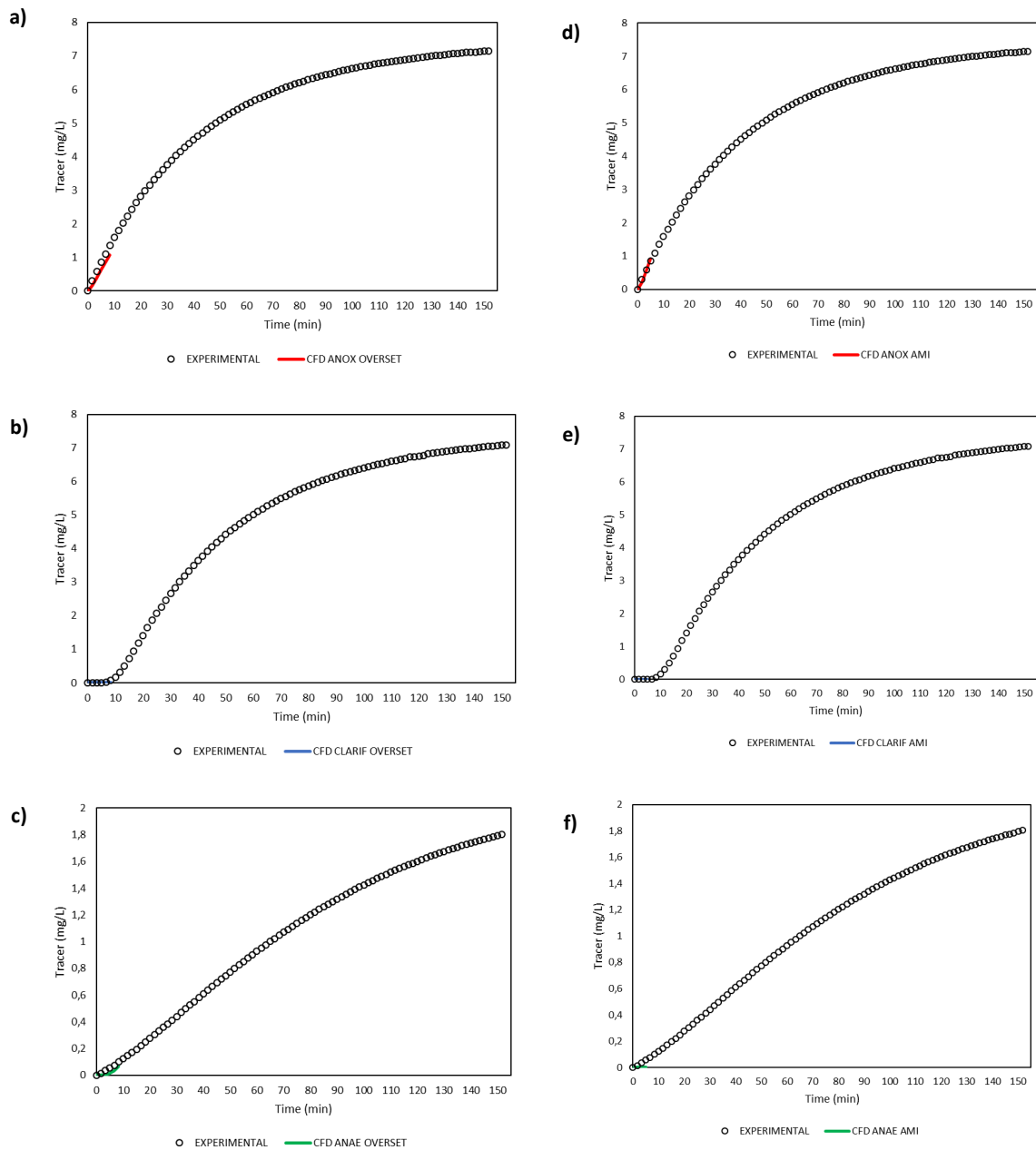
Figure A.2. Comparison of experimental (black circles) and simulated CFD (coloured lines) RTD$_3$ curves: (a) overset approach in the anoxic zone, (b) overset approach in the clarification zone, (c) overset approach in the anaerobic zone, (d) AMI approach in the anoxic zone, (e) AMI approach in the clarification zone and (f) AMI approach in the anaerobic zone.

Annex B

Compartment-based model of AnoxAn

In this annex the compartment-based model of AnoxAn reported in Chapter 5 for the obtention of dimensionless hydraulic indexes is presented.

To reproduce the complex hydraulic behaviour of AnoxAn a compartment-based model was built (Díez-Montero et al, 2015). This model is a combination of several approaches commonly used to describe non-ideal flow in reactors, such as Tank in Series (TIS) and Axial Dispersion Model (ADM) (Figure B.1).

- Anaerobic zone modelling

The anaerobic zone was modelled as a combination of three continuous stirred tanks reactors (CSTR) in series, dividing the hole zone into the hopper at the bottom (2.0 L), the main anaerobic zone (10.0 L) and the upper zone receiving the internal recycle (0.4 L) from the hopper. Internal recirculation was introduced setting a flow between the hopper and the upper zone.

- Anoxic and clarification zones

The anoxic zone was modelled as a single CSTR and the clarification zone as ADM in order to simulate a plug flow reactor (PFR) behaviour caused by the baffle between both zones.

Maintaining the global original volume, CSTR behaviour was applied to 28.8 L of the anoxic zone, and PFR with advective-diffusive behaviour to 7.2 L of the upper zone of AnoxAn, with the aim of modelling the entire clarification zone plus 1.2 L volume of the anoxic zone under the influence of the baffle.

The general expression of the tracer concentration for the PFR used is (Eq. B.1):

$$D_a \frac{\partial^2 C_T}{\partial z^2} - \frac{\partial (U C_T)}{\partial z} = \frac{\partial C_T}{\partial t} \qquad (B.1)$$

Being D_a the diffusion coefficient, C_T the tracer concentration and z references the location. The diffusion coefficient fitting the hydrodynamic behaviour was estimated to be $3.6 \cdot 10^{-6}$ m²/s. Thus, the Peclet number can be calculated using Eq. B.2:

$$Pe = \frac{UL}{D_a} \qquad (B.2)$$

being U the upflow velocity (m/s) and L the length of the compartment (m). A large Pe number indicates low back-mixing (recall that an ideal PFR corresponds with Pe=∞, while Pe=0 for a CSTR). Peclet number was equal to 15.2. Taking Pe≤5 as the criterion of greater back-mixing

(CSTR) and Pe≥50 as small back-mixing (PFR) (Levenspiel, 1999), the behavior is intermediate between PFR and CSTR.
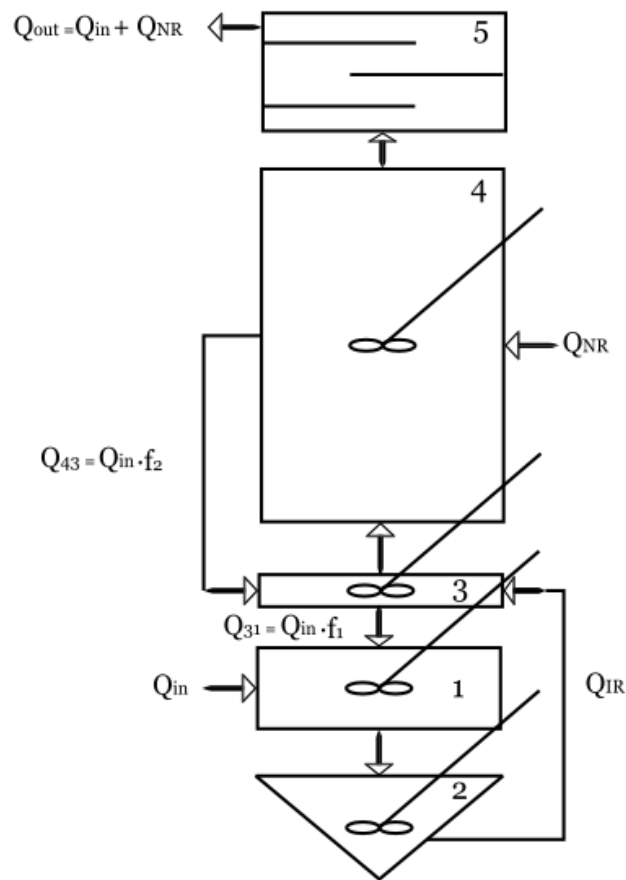
Figure B.1. Schematic diagram of the hydraulic compartment-based model of AnoxAn

References

Díez-Montero, R.; De Florio, L.; González-Viar, M.; Volcke, E.I.P.; Tejero, I. (2015). Feasibility of hydraulic separation in a novel anaerobic-anoxic upflow reactor for biological nuetrient removal. Bioprocess Biosyst. Eng. 38, 93-103. https://doi.org/10.1007/s00449-014-1247-9

Levenspiel, O. (1999) Chemical Reaction Engineering. 3rd Edition. John Wiley & Sons, New York, 54.

Annex C

Dimensional analysis of AnoxAn

In this annex the dimensional analysis of AnoxAn reported in Chapter 6 for the obtention of dimensionless hydraulic indexes is presented.

The most relevant variables intervening in the hydrodynamic of AnoxAn are shown in Table C.1:

Table **C.1.** Variables for the dimensional analysis of AnoxAn

	C_{anae}	C_{anox}	H_{imp}	a	b	HRT_{real}	HRT_{theo}	t_{90}	t_{10}	ρ
M	1	1	0	0	0	0	0	0	0	1
L	-3	-3	1	1	1	0	0	0	0	-3
T	0	0	0	0	0	1	1	1	1	0

Being the repeated variables of the physical problem are HRT_{theo}, b and ρ, the dimensionless numbers are deduced following Buckingham (1914):

- $\Pi_1 = C_{anae} \cdot HRT_{theo}^{\alpha} \cdot b^{\beta} \cdot \rho^{\gamma}$

$$\frac{M}{L^3} \cdot T^a \cdot L^b \cdot (\frac{M}{L^3})^c = M^0 \cdot L^0 \cdot T^0$$

$$a = 0,\ \beta = 0,\ \gamma = \text{-1}$$

$$\Pi_1 = \frac{C_{anae}}{\rho}$$

- $\Pi_2 = C_{anox}\ HRT_{theo}^{\alpha} \cdot b^{\beta} \cdot \rho^{\gamma}$

$$\frac{M}{L^3} \cdot T^a \cdot L^b \cdot (\frac{M}{L^3})^c = M^0 \cdot L^0 \cdot T^0$$

$$\alpha = 0,\ \beta = 0,\ \gamma = \text{-1}$$

$$\Pi_2 = \frac{C_{anox}}{\rho}$$

- $\Pi_3 = \text{H}_{\text{imp}} \ \text{HRT}_{\text{theo}}^{\alpha} \cdot b^{\beta} \cdot \rho^{\gamma}$

$$L^1 \cdot T^a \cdot L^b \cdot \left(\frac{M}{L^3}\right)^c = M^0 \cdot L^0 \cdot T^0$$

$$\alpha = 0, \ \beta = -1, \ \gamma = 0$$

$$\Pi_3 = \frac{H_{imp}}{b}$$

- $\Pi_4 = \text{a} \ \text{HRT}_{\text{theo}}^{\alpha} \cdot b^{\beta} \cdot \rho^{\gamma}$

$$L^1 \cdot T^a \cdot L^b \cdot \left(\frac{M}{L^3}\right)^c = M^0 \cdot L^0 \cdot T^0$$

$$\alpha = 0, \ \beta = -1, \ \gamma = 0$$

$$\Pi_4 = \frac{a}{b}$$

- $\Pi_5 = \text{HRT}_{\text{real}} \ \text{HRT}_{\text{theo}}^{\alpha} \cdot b^{\beta} \cdot \rho^{\gamma}$

$$L^1 \cdot T^a \cdot L^b \cdot \left(\frac{M}{L^3}\right)^c = M^0 \cdot L^0 \cdot T^0$$

$$\alpha = -1, \ \beta = 0, \ \gamma = 0$$

$$\Pi_4 = \frac{HRT_{real}}{HRT_{theo}} = \frac{V_{effective}}{V_{total}} = e$$

- $\Pi_5 = \text{t}_{90} \ \text{HRT}_{\text{theo}}^{\alpha} \cdot b^{\beta} \cdot \rho^{\gamma}$

$$T^1 \cdot T^a \cdot L^b \cdot \left(\frac{M}{L^3}\right)^c = M^0 \cdot L^0 \cdot T^0$$

$$\alpha = -1, \ \beta = 0, \ \gamma = 0$$

$$\Pi_5 = \frac{HRT_{theo}}{t_{90}} \rightarrow \Pi_5 = \frac{t_{90}}{HRT_{theo}} = \theta_{90}$$

- $\Pi_6 = \text{t}_{10} \ \text{HRT}_{\text{theo}}^{\alpha} \cdot b^{\beta} \cdot \rho^{\gamma}$

$$T^1 \cdot T^a \cdot L^b \cdot \left(\frac{M}{L^3}\right)^c = M^0 \cdot L^0 \cdot T^0$$

$$\alpha = -1, \ \beta = 0, \ \gamma = 0$$

$$\Pi_6 = \frac{HRT_{theo}}{t_{10}} \rightarrow \Pi_6 = \frac{t_{10}}{HRT_{theo}} = \theta_{10}$$

- $\Pi_7 = \text{HRT}_{\text{theo}} \, \text{HRT}_{\text{theo}}{}^{\alpha} \cdot b^{\beta} \cdot \rho^{\gamma}$

$$T^1 \cdot T^a \cdot L^b \cdot \left(\frac{M}{L^3}\right)^c = M^0 \cdot L^0 \cdot T^0$$

$$\alpha = -1, \; \beta = 0, \; \gamma = 0$$

$$\Pi_7 = \frac{HRT_{theo}}{HRT_{theo}} = \theta_m = 1$$

Combining obtained non-dimensional numbers, new expressions are developed:

$$\frac{\Pi_1}{\Pi_2} = \frac{\dfrac{C_{anae}}{\rho}}{\dfrac{C_{anox}}{\rho}} = \frac{C_{anae}}{C_{anox}} = HS$$

$$\frac{\Pi_5}{\Pi_6} = \frac{\dfrac{t_{90}}{HRT_{theo}}}{\dfrac{t_{10}}{HRT_{theo}}} = \frac{t_{90}}{t_{10}} = Mo$$

$$\frac{\Pi_5 - \Pi_7}{\Pi_7 - \Pi_6} = \frac{\theta_{90} - \theta_m}{\theta_m - \theta_{10}} = \frac{\theta_{90} - 1}{1 - \theta_{10}} = AD$$

References

Buckingham, E. (1914). On physically similar systems; Illustrations of the use of dimensional equations. Physical Review 4, 345-376. https://doi.org/10.1103/PhysRev.4.345

Epilogue

Epistemology of

Computational Fluid Dynamics

A theoretical approach from the Philosophy of Science

"When I meet God, I am going to ask him two questions:

Why relativity? And why turbulence?

I really believe he will have an answer for the first."

Unknown authorship, attributed to Werner Heisenberg.

"The philosophy without science is empty,

but the science without philosophy is blind."

Paraphrase of Immanuel Kant.

This epilogue is a result of a parallel (and complementary) research to the main theme of the doctoral thesis, and comes from the interest of the author in the philosophy, and particularly in that philosophy that discusses about the nature, characteristics, progress and limits of the human knowledge. The accelerated and (self)destructive one-way rhythm that imposes the contemporary academic world does not allow scientists to reflect about their scientific practice beyond the (over)production of papers, congresses and meetings. This text is a claim and a humble tribute to the slow science, which necessarily ought to incorporate a deliberate and conscious philosophical reflection.

All in all, based on the methodological framework provided by the philosophy of science, after a brief introduction, the first part of this document focusses on studying the nature and structure of the knowledge inferred from computational simulations. Next, conclusions obtained in that first part are used to analyse the specific case of Computational Fluid Dynamics.

1. <u>Science and philosophy of science: A desirable symbiosis</u>

The nature, characteristics and limits of the knowledge (known as epistemology) have been extensively studied all along the history of the humanity, and still remain as some of the greatest questions of the specie. At this respect, the review of the history shows that philosophers have shown the biggest interest and inquisitiveness about all these issues. In fact, Aristoteles is considered as one of the first scientists of Occident, and all the metaphysical and scientific theory he developed was valid until approximately the end of the Middle Age. Between the 16th and 18th centuries, rationalist and empirical philosophies reigned in Europe. The rationalist conception of knowledge priories the reason over the experience, and conversely, the empirical current priories the knowledge obtained by the experience over the reason. Descartes, Spinoza or Leibniz are considered rationalist philosophers, and Bacon, Hobbes, Locke, Berkley or Hume, empirical. Kant, meanwhile, with the publication of the masterly *Critic of Pure Reason* in 1781, tried to base all the achievements of the Newtonian mechanics in the structure

of the reason, and his work was considered a symbiotic approach between the philosophy of Leibniz and Newton. Anyway, it was not until the beginning of the 20ᵗʰ century with the appearance of the Theory of special (1905) and general (1916) relativity developed by Einstein, and the development of the Quantum Theory (1900-1927) by Planck, Einstein, Bohr, De Broglie and Heisenberg among many others, that many scientists and philosophers felt the need to rethink about the nature of the scientific progress and its theories.

Consequently, it can be considered that the Philosophy of Science as an autonomous discipline was born with the physical revolution of the very beginning of the last century. Since the 1930s with the creation of the Vienna Circle until the present, the philosophy of science has been concerned about giving answers to the following fundamental problems (Diéguez, 2005):

- What is Science? Concretely, what distinguishes Science from the pseudo-sciences?

- How is Science progressing? Is the scientific progress gradual and accumulative, or revolutionary and discontinuous? Is the scientific progress based on objective and neutral criteria, or is it based on social, economic and political factors?

- What is the objective of Science? Does its progress need to be interpreted as a unique goal more important than the rest? Which is that goal? What function do the scientific theories have? Are the scientific theories just conceptual tools to make predictions or do they pretend to give a realistic explanation about the natural phenomena?

- Which is the social authority of Science? Does it deserve that authority? How is it integrated with the rest of human social activities?

The clear relevance of the science in the contemporary world makes logic the interest of the philosophers in the scientific knowledge, the way it is produced and its effects on the society. Nevertheless, is it necessary for a scientist to know about philosophy of science?

Attending to the recent history of science, it is evident that to know about philosophy of science is not necessary to produce good scientific results, and consequently, scientists do not need to pay attention to these issues to successfully develop their work. However, it is also true that, despite of not being aware of it, every scientist has an inherent and implicit conception about the way of making science. At this respect, many of them think that only experiments can give true knowledge and that all the theories need to be constructed based on results obtained by the experience. The latter is a very empirical philosophy, which is close to the Vienna Circle's conception of scientific knowledge, known as logic positivism. Conversely, many scientists believe that experiments cannot be interpreted without a theory, and that theories do not come from a pure inference process born in the generalization of what observed in the experience. At this respect, they defend that the development process of a scientific theory is a creative and imaginative activity that then needs to be validated with experimentation. In fact, the history of science shows that many of the great scientific revolutionary ephemerides such as the innovations of Galileo, Newton, Darwin or Einstein came from this conception (Chalmers, 2015), which is mainly inspired in the work of Karl Popper or Thomas Kuhn.

Further, although it is commonly thought that the philosophy of science is made by people that ignore the practice of science, it must be mentioned that the most important philosophers of science of the past century were also scientists. For instance, Karl Popper, Thomas Kuhn and Paul Feyerabend were physicists, and Rudolf Carnap, Imre Lakatos and Bertrand Russel mathematicians.

All in all, it can be concluded that although to know about philosophy of science is not strictly necessary to make successful science, it helps to understand the nature of the discipline, to revise its goals and the conception of its progress, making explicit all the inherent and implicit beliefs among scientists. After all, the relation between science and philosophy of science can be conceived as a desirable symbiosis: the philosophy without science gets lost in the speculation without foundation, but the science without philosophy is empty and blind (Von Engelhardt et al., 2004).

2. <u>Epistemology of numerical simulations</u>

As described in the introduction, the philosophy of science has commonly been concerned about general questions such as the demarcation problem of the science, the conditions for the universality of the scientific theories and the nature of the scientific progress, just to name a few. In other words, the philosophy of science shows an upward epistemology where the main focus is placed in the most general issues of the field (located in the top of the hierarchical pyramid), defining the experiments and empirical observations (located in the base of the hierarchical pyramid) as simple tools for building up or confirm that universal theories. Therefore, traditional philosophy of science has assumed that once a good theoretical understanding of the phenomenon has been acquired, the philosophical interest is over (Winsberg, 2010). In this sense, philosophers have conceived computational simulations as a pure application of the theory, i.e. a process where no further knowledge is generated since all the results and conclusions are inferred from general, well established scientific theories.

However, along with the significative development of the computational capacities in the last decades, many scientists and philosophers have pointed out that the scientific practice of computational simulations implie challenging epistemological and methodological philosophical issues (Grüne-Yanoff et al., 2010; Schweber et al., 2000; Rohrlich, 1991; Humphreys, 2009). Concretely, the work carried out by Winsberg (1999, 2001, 2003, 2010) is of special interest since, influenced in a way by the New Experimentalism (Chalmers, 2015), it extensively justifies that the results of simulations are not that simple and do not have a so direct relation with their theoretical backgrounds as it is commonly believed. In short, simulations have appeared to be as complex as theorizing and experimenting. In the following sub-sections, this issue is clarified.

2.1. The epistemic process in numerical simulations

The main reason why the simulations have commonly been out of the interest of the philosophy of science is simple: they have a downward epistemological process instead of an upward one (Winsberg, 2001). At this respect, simulations have been supposed to be pure mathematical transformations based on the theory of the model: since it has been assumed that the epistemology of simulations is completely deductive, the justification is not necessary. However, as previously stated, this process is not as simple and straightforward as it apparently seems to be.

The process that goes from the general theory to the obtention of results in a numerical simulation (note the downward epistemic process, from the top to the base of the pyramid) can be described in the following chronological steps:

- **Theory.** Although a lot of literature and intense debates have been carried out around its definition, a scientific theory can be defined as a set of concepts and statements, including abstractions of observable phenomena and measurable properties, that along with scientific laws, state relations between the observations of these concepts. Every simulation starts with the selection of the theory (or set of theories) to be applied to the construction of the numerical model.

- **Theoretical model.** Previously to the construction of the computational model, the general governing equations of the phenomena aimed to simulate are defined based on a general theory or set of theories. This stage represents a pure mathematical model, e.g. a set of partial differential equations describing a fluid motion. Winsberg (1999) differenced two stages of the theoretical model: mechanical models (the general theory plus some general physical modelling assumptions to establish the governing equations) and dynamical models (mechanical models plus additional data such as initial conditions, boundary values and additional parameters).

- **Computational model.** In this stage appears the real epistemological interest and importance claimed by some contemporary philosophers and ignored by the traditional philosophy of science. The governing equations of many theoretical models do not have analytical solutions (e.g. Navier-Stokes equations of fluid mechanics). To overcome this issue, the continuous partial differential equations need to be transformed into discrete algebraic difference equations that approximate the solution. For that, the simulation domain is discretized into a finite number of elements, and the approximate difference equations are solved in every element. Many times, the physics aimed to simulate occur in so small length and time scales that the ideal grid must be so fine that becomes computationally intractable. In this situation, simulationists use modelling assumptions that usually include ad hoc models (simple mathematical relationship designed to approximately capture some physical effect), simplifications or removal of degrees of freedom (Winsberg, 2001) in order to turn the theoretical model not only mathematically tractable but also computationally affordable. Besides, many of those assumptions do not come neither from theory nor from even physical intuition: they

are just mathematical tricks to overcome the computational limits of the simulation. At this point, the reader should note how the computational model differs from the ideal theoretical model (numerical approximation of the solution, non-ideal size of the mesh, mathematical assumptions and simplifications, etc).

- **Solving procedure.** Once the computational model is developed, the final set of equations and assumptions that describe that models are solved by means of the execution of different algorithms.

- **Results.** Finally, results in form of a wide set of data are obtained. Winsberg (1999, 2010) defined the final result of this stage as a "model of the phenomena", and pointed out that it is also epistemically very relevant as creation of new knowledge is carried out, commonly out of the scope of theory and experimentation. Concretely, the model of the phenomena consists on a condensation of the relevant knowledge of the simulation and it is formed by mathematical relations and laws, images and textual descriptions. In contemporary modelling slang, it can be considered as the result of the post-processing stage, and consequently, the final objective of the simulation.

As just observed, the epistemic process in numerical simulations is not as straightforward as presumed. In fact, the significant difference that usually exists between the theoretical and the computational model evidences the complexity of the simulation process. First, the choice of the model and the final results are not completely determined by the original mathematical formulation of the theories, they are only guided by them. Additionally, physical intuition or experience of the modeller and model-building tricks or assumptions (usually revealed through trial and error) play an important role in the process. This ontological dissociation between the computational model (not only determined by theorical foundations) and the ideal theoretical model (only determined by theorical foundations) arises in the epistemology of numerical simulations some uncertainties that need to be managed.

2.2. The relation between numerical simulations and experiments

The previously described motley nature of the epistemology of computational simulations has given rise to the search of analogies to complete the understanding of their ontology. Concretely, the similarity with the experimental practice is of special interest and gives relevant insights about the nature of numerical simulations.

2.2.1. Complete analogy

One first view suggests that a computational simulation can be considered an experiment. In fact, the term numerical experiment is widely used as a synonym of computational simulation: concepts as precision, accuracy, error analysis, and calibration are both used in experimental and simulation practice, which evidences the similarity between both worlds (Winsberg, 2010). This complete analogy conception of the nature of the numerical simulation considers that the

simulation algorithm is literally mimicking the physical process aimed to be studied (Kaufmann et al. 1993). Hughes (1999) stated that simulations and experiments are conceptually inseparable. Concretely, he concluded that simulations are just experiments performed on computers that run algorithms to replicate complex physical systems. In this line, for Norton et al. (2001), the best way to understand the epistemology of simulations is to see them as experiments where the computer is the physical object being experimented on. In other words, a computational simulation is an experiment carried out on a computer as physical support. Winsberg (2010) also compared some experimental techniques analysed by Franklin (1986), and confirmed their analogy in the computational simulation practice.

Although the previous statements in favour of the complete analogy between both scientific practices are true, they suppose and assume that the computational simulations mimic the experiment, and consequently, avoids to answer or specify under what conditions the physical system of interest is reliably reproduced or simulated (Winsberg, 2010). Therefore, this conception does not perform a proper epistemological analysis since it only considers the final simulation properties, assuming that simulations results are always ideal and are able to faithfully reproduce the studied complex physical systems. In fact, it leaves a significant part of the epistemic process (e.g. the development of the computational model, which in the previous section has been observed to be complex and non-ideal) without explanation, behaving as a black-box.

At this respect, many scientist and philosophers have argued that it is precisely in the questioning of how the computer simulations become reliable where it must be found their ontological place. What is more, it is also important to note that experiments are always epistemologically prior to simulations, i.e. the knowledge needed to carry out a simulation depends on what learnt from a long history of experiment and observation (Winsberg, 2010). That is why, although having similarities, simulations seem to be something complementary, or even completely independent.

2.2.2.   A third mode

Although the epistemology of simulation has been observed to be very empirical, it cannot be forgotten that it is also logic-mathematical (guided by theory); but not only. At this respect, in order to overcome the epistemological issues of the complete analogy conception, many authors have defined the computational simulations as an entirely new scientific practice lying between theorizing and experimentation.

Concretely, Rorhrlich (1991) stated that computer simulations provide a novel methodology for the physical sciences, something intermediate between traditional theoretical physics and its empirical methods. Galison (1996) discussed that the simulation is a third mode that places physics somewhere between the experimental and theoretical domains. Further, Cartwright (1999) stated that theories themselves are not able to reproduce real, local states of affairs. Only computational models have the power *to "represent what happens, and in what circumstances"*, and this novelty nature makes the process of creating models from theory

complex and creative. For instance, in what Winsberg (1999, 2010) calls "model of the phenomena", i.e. all conclusions, results and graphic representations coming for post-processing, is clearly evidenced that computer simulations have an epistemic capability that is out of the scope of the theory and experimentation. Although it can be thought that all the results that conform the "model of the phenomena" are implicit in the theory, those could never be obtained without the creative, non-ideal and complex process of computational model building and post-processing already discussed in section 2.1.

Moreover, an important concept emerges in this third mode conception of computer simulations: their semi-autonomous nature (Hacking, 1983; Cartwright, 1999; Giere, 1999; Morgan et al., 1999). This comes from the evidence that although having a reliable theoretical knowledge in a particular field, there are still great difficulties to build reliable simulations. These difficulties emerge in the process of building the computational model, which as previously discussed, is not only based on theoretical knowledge but also on the aforementioned simplifications or tricks based on established model-building techniques developed over an extended tradition of employment, many times based on metaphors and intuition.

After all, Winsberg (2010) defended that only conceiving simulations as semi-autonomous and as a third mode partially separated from theorizing and experimentation, it is possible to describe and specify the main difference between computer simulations and experiments regarding the justification of the reliability of each scientific practice:

- On one hand, experiments are legitimated by their theoretical background and the previous practice regarding experimentation. Additionally, the legitimation of their reliability is internal: the object (physical system aimed to experiment) and the target (experimented physical system) are of the same kind (material) and consequently, the inferences and conclusions of the results do not need an external validation, i.e. the validation is internal as the object and the target are the same.

- On the other hand, simulations are legitimated by their theoretical background, their resemblance to the real world and by a special kind of argument based on previous knowledge and model-building practice. Further, for a numerical simulationist is not important if the object (computer) and the target (physical system simulated) are not of the same material. A simulationist is focused on building a model for the target and not for the object. Conversely, the experimental scientist builds a model (an experimental configuration) for the object. Thus, the legitimation of the reliability of the simulations is external (the target systems is what needs to be validated and justified) not internal (the object) as occurs for the experiment.

This metaphysical reasoning helps to further clarify the ontology of the computational simulation and define its epistemology as a third mode. Nevertheless, at this point, is still a fundamental question remaining: under what conditions is reliable the knowledge inferred from numerical simulations?

2.3. Reliability without truth

The first issue here is to clarify the notion of truth in this work. Although it is taken as a clear concept in the daily life (even in the scientific practice), the truth is a complex philosophical term that needs careful consideration (McCain, 2016). In fact, many contemporary philosophers and scientists think that humans just reproduce a filtrated version of the reality, i.e. the fact that our brain is able to walk across the world does not mean that we are able to capture its structure with faithfulness (Musser, 2019). To make search for the truth more unstable, even nature of mathematics is in doubt: are they invented (fiction) or discovered (real)? (Howston-Edwards, 2019). If fictional, are they really the most adequate tool to achieve the scientific truth? And what is that scientific truth?

Although all these metaphysical claims are necessary to question the nature and limits of the knowledge, the human being needs to progress and make science, at least in its own conception of reality and truth. That is why, in this text, the truth is considered relative (to the whole human species) since, for the moment, is impossible to know if our reality (relative) and the absolute reality (if exists) are the same. Consequently, the goal of the simulations is to get as close as possible to that human relative reality or truth. However, due to the observed difficulties and uncertainties that emerge in the development of computational models, the goal can be reformulated in order to achieve what Winsberg (2010) defined as *reliability without truth.*

As previously discussed, the difficulty of building reliable computational models, and consequently simulations, comes from their motley and diverse epistemology. At this respect, Winsberg (2010) (based on the work of Hacking (1992) for experiments) stated that the reliability of the computational simulations come in part from the history of their development (in his terms, simulations have "their own life"). Since simulations cannot be justified just on theories (they are not pure inferences and results of theories), they need to self-vindicate or self-validate. In most of the cases, part of this validation must come from their resemblance with the real-world data (conventional validation in science and engineering), but many times, data are sparse or even inaccessible as it happens for climate models, quantum mechanics models, complex fluid models or models describing extreme situations (fires, explosions…), just to name a few. Consequently, apart from the theory and the real-world data, based on their semi-autonomous epistemology, the reliability of computer simulation lies on their aforementioned history of development. In words of Winsberg (2010):

"Simulation practices have their own life: they evolve and mature over the course of a long period of use, and they are retooled as new applications demand more and more reliable and precise techniques and algorithms. We only have to think of simulations of the earth's climate, which have evolved over decades, to see that this claim is true. But simulations also, like experiments, gain their own credentials over time."

These credentials are based on the knowledge obtained during decades of modelling practice and, as already introduced in section 2.1, include assumptions about what parameters to use or neglect (and most common or best values for these parameters), rules about how to overcome computational difficulties such as model assumptions (ad hoc models, mathematical simplifications), differencing schemes or graphical techniques for the post-processing, among many others. All these tips or issues concerning the numerical simulations, as every numerical modeller can admit, are many times based on weak physical intuitions, experience or just on practical efficiency, but not just on theoretical foundations.

Additionally, every time these modelling practice techniques are used successfully, i.e. when they are validated reproducing real-world data and they are able to produce new knowledge predicting phenomena out of the scope of the theory and experimentation, their credibility as reliable assumptions increases. Consequently, when building a new computational model and carrying out a simulation, their credibility will be not only based on theory and real-world data validation, but also in a self-vindication or inner validation based on all these model-building techniques that define the semi-autonomy of numerical simulations.

As stated before, due to the nature of computational models and simulations, there is an evident distortion between them and the (relative to humans) reality. A distortion caused by the need of these models and simulations to be both mathematically-computationally affordable but, at the same time, as faithful as possible to the reality aiming to mimic. The success in the scientific practice of computational simulations is not that they are able to achieve the truth (for the moment, that is impossible or utopic by ontology), their success is that they are able to achieve reliability without (absolute) truth.

3. <u>Epistemology of Computational Fluid Dynamics</u>

Once defined the epistemology and ontology of computational simulations, an analysis of those features is carried out for the scientific practice of Computational Fluid Dynamics (CFD), and all the theorical concepts emerged in the previous section are try to be clarified with practical examples within the field.

As a general definition, CFD consists in the use of computers and numerical techniques to solve problems related with the fluid flow and, in addition, other associated physical phenomena such as heat transfer or chemical reactions. In this sense, CFD is being successfully applied from the pure research to a wide variety of industries and applications, e.g. automobile industry, aerospace and aeronautical engineering, naval industry, chemical engineering, electric engineering, nuclear industry, renewable energies, power generation or biomedical applications.

3.1. <u>Model uncertainty</u>

General equations of fluid mechanics, i.e. Navier-Stokes equations, do not admit general analytical solutions. What is more, that solution still remains as one of the millennium problems according to the Clay Mathematics Institute (https://www.claymath.org/millennium-problems). The inherent complexity of fluid dynamics, gives rise to different levels of uncertainty in computational model building and simulation as Winsberg (2010) described for models of climate: (i) structural model uncertainty, (ii) parameter uncertainty and (iii) data uncertainty. The epistemic process in CFD deals intensely with these uncertainties, and some clarifying examples are highlighted next.

3.1.1. Structural uncertainty

Structural uncertainty is referred to all those auxiliary assumptions, approximations and parametrizations that increase of uncertainty in the reliability of the model.

Since the fluid motion is described by a set of partial differential equations without analytical solution, the first structural uncertainty is represented by the need of dividing the physical domain into a finite number of elements (meshing) in order to discretize the Navier-Stokes equations in space (and in time if the problem is dynamic) to obtain an approximate solution. At this respect, a very fine mesh can result computationally unaffordable, but a very coarse mesh implies loss of precision. Although mesh independency tests are usually carried out, modellers usually do not perform them due to lack of resources, if similar geometries have been analysed before, or if reasonable previous engineering experience can be used in the development of the mesh (Wicklein et al., 2015). That previous experience usually involves structural modelling decisions relative to the computational domain (2D or 3D), symmetry planes or boundary conditions types among many others.

Another recurrent structural uncertainty is the turbulence modelling. To solve directly all the scales of the turbulent phenomena (Direct Numerical Simulation (DNS)) an extremely fine mesh (which is non-viable in most of the cases) is needed. A less restrictive alternative to DNS,

Large Eddy Simulation (LES), is able to solve through a coarser mesh the turbulent scales that transport the main amount of energy (approximately between the 50 and the 80%) and models the rest. Nevertheless, Reynolds Averaged Navier-Stokes (RANS) is the most used method to introduce the turbulence as all its scales are modelled. Although various turbulence models have been developed within this approach, is difficult to find a single turbulence model able to reproduce and model the different phenomena at micro and macro scales at the same time (Fernández, 2012), increasing the epistemic uncertainty.

Concretely, the numerical or eddy viscosity parameter that is found in RANS turbulence modelling represents an illustrative example of ad hoc modelling, mathematical simplification or trick to reach the computational and mathematical affordability of numerical simulations in CFD. As Winsberg (2010) brought up, Porter et al. (1998) clearly described its function in a computational simulation to analyse the convection in red giant stars:

"Viscous effects, which act only on tiny scales unresolvable by the computational grid, were approximated by a carefully formulated [eddy] viscosity. This viscosity of the numerical scheme dissipates kinetic energy of fluid motion into heat, like the real viscosity of the gas, but on the much larger scales of the computational grid. This [eddy] viscosity was carefully designed to restrict its dissipative effects to the shortest length scales possible, consistent with accurate representation of the nearly inviscid flow on the longer length scales."

In Winsberg (2010) is also mentioned the use of two more mathematical fictions in the field of CFD that contribute to the affordability of computational simulations: the artificial viscosity (do not mistake with eddy viscosity) and the vorticity confinement. At this respect, both parameters are examples of successful techniques used across a wide domain of fluid dynamical applications that do not rely on realistic principles of the nature of fluids (see Von Neumann et al., 1950 for artificial viscosity and Steinhoff et al., 1994 for vorticity confinement).

3.1.2.   Parameter uncertainty

Once built the structure of the computational model (meshing, discretization schemes, assumptions, turbulence model…) another level of uncertainty appears in the epistemic process of CFD. Concretely, CFD models deal with many parameters in which their most adequate value is uncertain or even unknown. This type of uncertainty is defined as parameter uncertainty.

For example, talking about a pure turbulent motion, the value of the Schmidt number (ratio between the kinematic viscosity and the diffusivity of the transported variable) represents a big uncertainty in modellers that obliges to try various values to validate the simulation. Constants appearing in turbulent models or values for sub-relaxation in solver algorithms are other examples or parameter uncertainty.

If additional physics are coupled to basic CFD, parameter uncertainty increases significantly. For instance, in wastewater application, biological models imply a large number of kinetic parameters and constants that are usually tested in every simulation to fit with real-world

data. At the end, this uncertainty can lead to an over-calibration of models, hiding problems related with structural uncertainty or mistaking with them.

3.1.3. Data uncertainty

Structural and parameter uncertainties are tested checking the correspondence between simulated results and experimental data However, many times, the availability of data for model and simulation validation can be sparse or of bad quality, emerging also a data uncertainty.

In that dealing with the data uncertainty emerges again the third mode nature of computational simulations defended in the section 2 of this text. In fact, when validation data are sparse, the self-vindicating of simulations and reliability of models must come from theoretical foundations and from what previously has been described as all those model-building techniques and weak physical intuitions taken from the experience. Some examples of the latter haven been already pointed out in the text: the aforementioned claim for previous engineering experience of Wicklein et al. (2015), or parameters like eddy viscosity, artificial viscosity and vorticity confinement (which have been demonstrated to be out of any fluid-dynamic theorical basis). At this respect, Darrigol (2013) stated that heuristics in the epistemic process of hydrodynamics required an *"unusual amount of creativity; they involved intuitions bound to personal styles of thinking. Such intuitions are tentative and may lead to erroneous guesses. (...) the impossibility of solving the fundamental equation and the evident complexity of observed flows sometimes forced engineers and even physicists to arbitrarily and drastically simplify aspects of the flow".*

Nevertheless, even when enough validation data is available, there is a question remaining: when is a model sufficiently validated? (Laurent et al., 2014; Nopens et al., 2019). This query refers in a way to a classical philosophical discussion between the logic positivism or inductivism (represented by the Vienna Circle) and the empirical falsification (represented by Karl Popper). According to the logic positivism, any theory to be considered as scientific must be validated in a wide variety of experimental or real conditions and observations. At that point, the question made by the empirical falsification is, how much is a wide variety? Even if thousands of validations are performed, there will be still an infinite number of cases left to validate, being the ratio between the validated conditions and the conditions left to validate always zero (Chalmers, 2015). In the specific case of computational simulations and also CFD, the problem is much the same, and in a practical sense, the solution is usually to claim for the experience gained by experts in the modelling practice along all these decades. As already discussed, this experience is not only based on theory or experimental validation, but also seems to be linked to properly non-epistemic reasoning.

Here appears a cyclic paradox. While it is obvious to think that, to build a reliable CFD simulation (and computational simulations in general), the main goal should be to minimize the dependence on the modelling experience; for that purpose, an infinite validation would be needed. As previously discussed, the latter is impossible, and that is why, actually, modelling experience or conventions are which determine when a model is sufficiently validated. But, even

if a CFD model could be validated for an infinite number of cases, all the difficulties that appear on the development of the computational model (meshing, approximations, ad hoc modelling, mathematical tricks) still make impossible to reduce the epistemic uncertainty. At this respect, when a computational simulation mimics the experimental data after a wide variety of assumptions and approximations, does not it seem a bit of luck or even a coincidence? What is more, how is it possible to speak in terms of truth or reality when fictional parameters as eddy viscosity or artificial viscosity are used to carry out simulations? All these issues are which make the expression "reliability without truth" adequate. As Chalmers (2015) stated, science probably has a stronger commitment with its progress than with the truth (as it seems unreachable).

3.2.   Added value

In the previous section the epistemic nature discussed for computational simulations has also been observed for CFD. Next, that third mode nature of simulations defended in the first part of this document and in the previous section for CFD, is further demonstrated with the added value that provides this technique.

In fact, CFD allows to obtain essential information regarding flow fields (velocity and flow patterns, pressure fields, fields for parameters related to turbulence or pollutant 3D distributions, among many others) can be obtained, being the level of detail of almost unlimited and unreachable by pure theory or experimentation. Besides, Fernández (2012) stated that this approach is also very adequate to study physical problems that are very difficult or impossible to reproduce experimentally such as hypersonic velocities, very high or low temperatures or dangerous systems (accidents, limit design of equipment).

Various practical examples can be found in this thesis. For instance, in Blanco-Aguilera et al. (2020) was concluded that CFD simulations provide a deeper understanding of the hydraulic behaviour of the fluid within the studied anaerobic-anoxic reactor, compared to previous analytical models and experimental work. This study allowed to detect not only the existence, but also the location and quantification of preferential flow channelling and dead volumes. In that work, a mixing level analysis of the reactor through the Uniformity Index (UI) (Terashima et al., 2009; Dapelo et al., 2018) was successfully carried out too, which only can be obtained through CFD techniques.

4. <u>Conclusions</u>

In this epilogue a theoretical introductory analysis of the epistemology of computational simulations, and concretely CFD, is carried out based on the framework provided by the philosophy of science.

This study has shown that the epistemology of numerical simulations seems to be semi--independent from theory and experimentation, constituting what some authors have defined as a third mode. At this respect, computational models and simulations are not pure theoretical deductions and applications as conventional philosophy of science has commonly thought: they are also a consequence of a creative and complex process of assumptions, ad hoc modelling and weak physical intuition that many times have nothing to do with theoretical fundamentals. That is why the validation of numerical simulations is not only based on its fidelity to the theory and resemblance to the real-world data, but also in the reliability of the aforementioned model-techniques that have gained credentials during decades of modelling practice and experience. The third mode epistemology of numerical simulations is also reflected on the results obtained in their application, since the knowledge created in the simulation process is mainly out of the scope of theory and experimentation.

All these epistemic and ontological features described for numerical simulations have also been observed in the specific practice of CFD techniques. For instance, in the development of CFD models emerges structural, parameter and data uncertainties that need to be overcome to perform reliable simulations. For that purpose, modellers' experience has appeared to be necessary, and at this respect, parameters like eddy viscosity, artificial viscosity and vorticity confinement (which are out of any fluid-dynamic theorical basis) have been successfully used in CFD simulations.

In the end, computational modelling and simulation, and science in general, are not perfect or idyllic. Many times, it seems that when searching into the deepest level of the nature of the scientific knowledge, it simply evaporates and fades away. This should remind us that human being is fallible, fragile and must be extremely humble. Nevertheless, the uncertainty that surrounds science does not mean that it is not the best and most successful tool that we have to understand the world around us: In the same way that Leibniz thought that we live in the best of all possible worlds, science is, surely, the best imaginable ally we could have. What is more, the uncertainty is necessary to avoid the scientific fundamentalism, to remind that scientific discoveries are not absolute, and should oblige us to keep science under permanent questioning and continuous movement.

> *"The empirical basis of objective science has thus nothing 'absolute' about it. Science does not rest upon solid bedrock. The bold structure of its theories rises, as it were, above a swamp. It is like a building erected on piles. The piles are driven down from above into the swamp, but not down to any natural or 'given' base; and if we stop driving the piles deeper, it is not because we have reached firm ground. We simply stop when we are satisfied that the piles are firm enough to carry the structure, at least for the time being."*

> *Karl Popper, The logic of scientific discovery (1959)*

5. <u>References</u>

Blanco-Aguilera, R., Lara, J.L., Barajas, G., Tejero. I., Díez-Montero, R. (2020). CFD simulation of a novel anaerobic-anoxic reactor for biological nutrient removal: Model construction, validation and hydrodynamic analysis based on OpenFOAM®. Chem. Eng. Sci. https://doi.org/10.1016/j.ces.2019.115390

Cartwright, N. (1983). How the laws of physics lie. Oxford University Press, ISBN 978-0198247043

Chalmers, A.F. (2015). ¿Qué es esa cosa llamada ciencia? (Spanish edition of "What is this thing called science?"). 4th edition, Siglo XXI editores, ISBN 978-84-323-1430-8.

Dapelo, D., Bridgeman, J. (2018). Assessment of mixing quality in full-scale, biogas-mixed anaerobic digestion using CFD. Bioresour. Technol., 265, pp 480-489. https://doi.org/10.1016/j.biortech.2018.06.036

Darrigol, O. (2013). For a philosophy of hydrodynamics. The Oxford Handbook of Philosophy of Physics. https://doi.org/10.1093/oxfordhb/9780195392043.013.0002

Diéguez, A. (2005). Filosofía de la ciencia. (Philosophy of science). Biblioteca Nueva Universidad de Málaga, ISBN 84-9742-404-2 (in Spanish).

Fernández, J.M. (2012). Técnicas numéricas en ingeniería de fluidos: Introducción a la dinámica de fluidos computacional (CFD) por el método de volúmenes finitos. (Numerical techniques in fluid engineering: Introduction to computational fluid dynamics (CFD) based on finite volumes method). Editorial Reverte, ISB 978-84-291-2602-0 (in Spanish).

Franklin, A. (1986). The neglect of experiment. Cambridge University Press.

Galison, P. (1996). Computer simulations and the trading zone. The disunity of science. Boundaries, contexts and power. Stanford University Press, ISBN 978-0804725620.

Giere, R. (1999). Science without laws. University of Chicago Press, ISBN 978-0226292083.

Grüne-Yanoff, T., Weirich, P. (2010). The philosophy and epistemology of simulation: A review. Simulation & Gaming, 41(1), 20-50. https://doi.org/10.1177/1046878109353470

Hacking, I. (1983). Representing and intervening: Introductory topics in the philosophy of science. Cambridge University Press, ISBN 978-0521238298.

Hacking, I. (1992). Do thought experiments have a life on their own? Proceedings of the biennial meeting of the Philosophy of Science Association, The Univesity of Chicago Press, 2, 302-308. https://www.jstor.org/stable/192844?seq=1

Howston-Edwards, K. (2019). Is the mathematical world real?. Scientific American, special issue about truth, lies and uncertainty, 321(3). https://www.scientificamerican.com/article/is-the-mathematical-world-real/

Hughes, R. (1999). The Ising model, computer simulation, and universal physics. Perspectives on natural and social science, 97-145. https://doi.org/10.1017/CBO9780511660108.006

Humphreys, P. (2009). The philosophical novelty of computer simulation methods. Synthese, 169, 615-626. https://doi.org/10.1007/s11229-008-9435-2

Kaufmann, W.J., Smarr., L.L. (1993). Supercomputing and the transformation of science. Scientific American Library, ISBN 978-0716750383.

Laurent, J., Samstag, R.W., Ducoste, J.M., Griborio, A., Nopens, I., Batstone, D.J., Wicks, J.D., Saunders, S., Potier, O. (2014). A protocol for the use of computaitonal fluid dynamics as a supportive tool for wastewater treatment plant modelling. Water Sci. Technol., 70(10), 1575-1584. https://doi.org/10.2166/wst.2014.425

McCain, K. (2016). The nature of scientific knowledge. Springer, ISBN 978-3-319-33403-5.

Morgan, M., Morrison, M. (1999). Models as mediators. Cambridge University Press. https://doi.org/10.1017/CBO9780511660108

Musser, G. (2019). The search for truth in physics. How close can physics bring us to a truly fundamental understanding of the world?. Scientific American, special issue about truth, lies and uncertainty, 321(3). https://www.scientificamerican.com/article/the-search-for-truth-in-physics/

Nopens, I., Sandrawska, D., Audenaert, W., Fernandes, D., Rehman, U. (2019). Water and wastewater CFD validation. Are we losing the balance?. Plenary session, Watermatex 2019, Copenhaguen (Denmark).

Norton, S., Suppe, F. (2001). Why atmospheric modeling is good science. Changing the atmosphere: expert knowledge and environmental governance. MIT Press, ISBN 978-0262632195.

Porter, D., Anderson, S., Woodward, P. (1998). Simulating a pulsating red giant star. Preprint. https://www.lcse.umn.edu/research/RedGiant/

Rohrlich, F. (1991). Computer simulation in the physical sciences. Biennial meeting of the Philosophy of Science Association, The University of Chicago Press, 507-518.

Steinhoff, J., Underhill, D. (1994). Modification of the Euler equations for vorticity confinement: Application to the computation of interacting vortex rings. Phys. Fluids, 6, 2738-2744. https://doi.org/10.1063/1.868164

Schweber, S., Waechter, M. (2000). Complex systems, modelling and simulation. Stud. Hist. Philos. M. P., 31(4), 583-609. https://doi.org/10.1016/S1355-2198(00)00030-7

Terashima, M., Goel, R., Komatsu, K., Yasui, H., Takahashi, H., Li, Y.Y., Noike, T. (2009). CFD simulation of mixing in anaerobic digesters. Bioresour. Technol., 100, 2228-2233. https://doi.org/10.1016/j.biortech.2008.07.069

Von Engelhardtm, D., Mainetti, J.A. (2004). Bioética y humanidades médidas. (Bioethics and medical humanities). Editorial Biblos, ISBN 987-9507864025 (in Spanish).

Von Neumann, J., Richtmyer, R.D. (1950). A method for the numerical calculation of hydrodynamical shocks. J. Appl. Phys., 21, 232-247. https://doi.org/10.1063/1.1699639

Wicklein, E., Batstone, D., Ducoste, J., Laurent, J., Griborio, A., Wicks, J., Saunders, S., Samstag, R., Potier, O., Nopens, I. (2015). Good modelling practice in applying computational fluid dynamics for WWTP modelling. Water Sci. Technol. 73(5), 969-982. https://doi.org/10.2166/wst.2015.565

Winsberg, E. (1999). Santioning models: The epistemology of simulation. Science in context, 12, 275-292. https://doi.org/10.1017/S0269889700003422

Winsberg, E. (2001). Simulations, models and theories: Complex physical systems and their representations. Philos. Sci. 68(3), 442-454. https://doi.org/10.1086/392927

Winsberg, E. (2003). Simulated experiments: Methodology for a virtual world. Philos. Sci. 70(1), 105-125. https://doi.org/10.1086/367872

Winsberg, E. (2010). Science in the age of computer simulation. The University of Chicago Press, ISBN 978-0-226-90204-3.